Engineering Direct Electrical Stimulation of Human Sensorimotor Cortex

David Caldwell

A dissertation
submitted in partial fulfillment of the
requirements for the degree of

Doctor of Philosophy

University of Washington

2019

Reading Committee:

Jeffrey G. Ojemann, Chair

Rajesh P.N. Rao, Chair

Azadeh Yazdan-Shahmorad

Program Authorized to Offer Degree:
Bioengineering

University of Washington

Abstract

Engineering Direct Electrical Stimulation of Human Sensorimotor Cortex

David Caldwell

Co-Chairs of the Supervisory Committee:
Professor Jeffrey G. Ojemann
Neurological Surgery

Professor Rajesh P.N. Rao
Computer Science and Engineering

Damage to the nervous system due to stroke, spinal cord injury, and limb loss leads to significant sensory and motor deficits. Despite the variety of reasons behind cortical injury, targeted direct electrical stimulation (DES) may be able to help restore both motor and sensory function in future neuroprosthetic applications.

Our research addresses fundamental barriers through a principled engineering approach for translation of DES to humans. We primarily focused on the physics of stimulation, the signal processing of these concurrent stimulation and recording signals, how sensory stimulation compares to natural touch, and how to induce plasticity to modify cortical connectivity through DES.

First, we modeled how electrical stimulation propagates through the tissue with analytic models, and found that analytic models with flat and spherical geometries fit the measured voltages on the surface well. We also discovered the importance of the assumptions about the overall geometry of the brain in these flat and spherical models and how these affect the subsequent interpretations of the resistivity of the brain tissue. These results have implications for the appropriate ways to make resistivity measurements in-vivo on the human

brain, and establishes benchmarks for comparisons with more computationally intensive finite-element models.

We subsequently developed novel unsupervised algorithms to extract the neural response to DES with concurrent stimulation validated on multiple human datasets, allowing for analyses of neural data contaminated by stimulation artifacts. This work will aid in the interpretation of data from experiments involving stimulation in humans, and we have made public all of the code and data for future algorithmic development and comparisons.

We discovered that humans respond more slowly to DES of sensory parts of the brain relative to natural peripheral touch, which may require future neuroprosthetic devices to account for this delay to allow for smooth and intuitive control. Concurrent DES of sensory parts of the brain and natural peripheral touch are perceived independently, which suggests that local cortical circuitry is not completely inhibited by DES and will allow for overlapping inputs in future neuroprosthetic devices. Furthermore, modified DES waveforms during sensory stimulation can modify percepts and reaction times, suggesting that better neuroprosthetic performance could be achieved by moving beyond the constant amplitude waveforms.

We tested two stimulation protocols to induce plasticity in human cortex, with potential applications in helping the brain heal after stroke. The first involved beta-oscillation driven stimulation, where we found short term (less than two seconds in duration) enhancement of cortically evoked potentials. This was driven by a dominant effect between the number of conditioning stimuli delivered and the size of the evoked potential following stimulation. Delivering stimuli during the depolarizing surface potential phase appeared to have an potentiating interaction effect during trains where the greatest number of conditioning stimuli were delivered.

The second was a paired pulse stimulation paradigm carried out intraoperatively in sub-

jects undergoing deep brain stimulator placement, where the optimal lag to induce plasticity as assessed through evoked potentials was longer than that predicted by the principles of spike timing dependent plasticity. We similar found that paired site stimulation was more effective than stimulation within the same site, suggesting that both the timing and location of stimulation are critical for the induction of plasticity. These two stimulation protocols lay the groundwork for future clinical trials in humans using these protocols to try and induce plasticity in damaged regions of cortex.

Our research in these areas of engineered stimulation of sensorimotor cortex in humans with implanted electrodes moves DES closer towards clinical rehabilitation use for sensory neuroprosthetics and neuromodulation to induce cortical plasticity.

TABLE OF CONTENTS

LIST OF FIGURES

LIST OF TABLES

GLOSSARY

ECOG: Electrocorticography. This refers to electrodes implanted subdurally, epidurally, or in deeper gray or whiter matter structures (depth electrodes), but in this thesis, all references refer to either subdural or depth electrodes.

IEEG: Intracranial electroencephalography. In thesis thesis, this is synonymous with ECoG, and refers to electrodes implanted subdurally, epidurally, or in deeper gray or whiter matter structures (depth electrodes).

EEG: Electroencephalography. This refers to the placement of electrodes on the scalp.

LFP: Local field potential. These are the composite signal from multiple neurons firing.

DES: Direct electrical stimulation. In this thesis, this refers to stimulation of any region of the brain, cortically or subcortically, through implanted electrodes.

DCS: Direct cortical stimulation. This refers to the electrical stimulation of the cortex through implanted electrodes.

DECS: Direct electrical cortical stimulation. In this thesis, this is synonymous with DCS.

CSF: Cerebrospinal fluid - clear fluid which provides cushioning, waste removal, and distribution of materials throughout the brain.

DURA: The outermost layer covering the brain and spinal cord. Subdural electrodes are implanted beneath the dura, and above the arachnoid and pia.

CRANIOTOMY: Surgical procedure in which bone is removed from the skull temporarily to gain access to the brain.

EPILEPSY: A disorder described by recurrent unprovoked seizures

DBS: Deep brain stimulation: a treatment using electrical stimulation to treat movement disorders (Parkinson's, Essential Tremor), and increasingly psychiatric disorders.

FEM: Finite element modeling. The use of a discretized mesh representing a surface, and the forward modeling of partial differential equations of interest (e.g. Laplace's equation for electrostatics).

CONTACT RESISTANCE: Total resistance of the electrode, electrode tissue interface, CSF, and brain.

SHEET RESISTANCE: Intrinsic resistance of the material of interest.

EP: Evoked potential. The cortical response due to DES, which is the recorded complex activity resulting from the superposition of numerous neuronal elements.

CEP: Cortically evoked potential. In this thesis, we refer to EP and CEP interchangeably.

EMG: Electromyography. The electrical recording of muscle activity.

SSEP: Somatosensory evoked potential. The signal in cortex following peripheral median nerve stimulation.

MEP: Motor evoked potential. A robust EMG in a peripheral muscle that occurs following DES of motor cortex regions.

DBSCAN: A density based clustering algorithm.

HDBSCAN: Hierarchical density based clustering.

UNSUPERVISED CLUSTERING: A machine learning method which discovers structure in the data without predefined user guidance.

CATHODAL STIMULATION: Electrical stimulation which causes electrons and negative ions to gather at the electrode, causing depolarization directly beneath the electrode.

ANODAL STIMULATION: Electrical stimulation which causes positive species to gather at the electrode, causing hyperpolarization directly beneath the electrode.

NMDA RECEPTOR: Receptor which binds NMDA, also functions as an ion channel, is one of the major excitatory neurotransmitters in the brain, and is important for cellular plasticity.

GABA RECEPTOR: Receptor which binds GABA, also functions as an ion channel, is one of the major inhibitory neurotransmitters in the brain, and is important for cellular plasticity.

FMRI: Functional magnetic resonance imaging. An non-invasive imaging method which allows for the indirect measurement of neuronal activity at a high spatial but low temporal resolution.

BOLD: Blood oxygen level dependent: The signal measured by fMRI, where decreases in blood oxygen locally correlate with neuronal activity.

S1: Primary somatosensory cortex.

M1: Primary motor cortex.

ACKNOWLEDGMENTS

I first and foremost appreciate the selfless generosity of our research participants, without whom this research would never be possible. I also express sincere appreciation to my committee members Jeffrey Ojemann, Rajesh Rao, Azadeh Yazdan-Shahmorad, Bingni Brunton, Eric Chudler, and my graduate school representative Jonathan Weinstein who stepped in at the last minute to ensure my thesis defense could proceed. I would particularly like to thank Jeff, for his guidance on both research and clinical practice, Raj for helping me along the entire PhD, and Bing for helping push along the signal processing aspects of my thesis.

I would also like to thank all the members of the GRID and Neural Systems laboratories, who have guided and shaped the research presented here. The long and incomplete list includes Kurt Weaver, Larry Sorensen, Jeneva (Jenny) Cronin, Jing (James) Wu, Kaitlyn Casimo, Nile Wilson, Courtnie Paschall, Alainna Brown, Gabriel Obregon, Chao-Hung (Clark) Kuo, Jared Olson, and Jeremiah Wander. Kurt helped over the years with mentorship and research guidance. Jenny worked with me along the whole way, and I am grateful for having been able to work with her for most of my PhD on all aspects of the research, but in particular the sensory and intraoperative DBS aspects. James was an invaluable technical resource for the entire PhD. I feel extremely fortunate that the other members of the lab have turned into great friends, and cannot imagine having gone through the PhD without their friendship and support. Jared and Miah helped me find my way at the beginning of my PhD, and were instrumental in helping me analyze the early plasticity work. Larry has provided support in all senses, ranging from mentorship and career guidance, to matters of physics, hardware, and data analysis.

Additional members not in the lab who have provided valuable feedback and guidance include Andrew Ko, Eberhard Fetz, Stavros Zanos, Steve Perlmutter, and Nathan Kutz. Andrew has been another clinical mentor for me, and without his allowing me to perform intraoperative experiments, much of the work would have not been possible. Eb and Stavros provided valuable conversation and feedback over the course of a number of years. Steve was invaluable in the planning and execution of the intraoperative plasticity work. Nathan helped jump start my interest in data analysis, and provided both mentorship and research feedback over the years.

Collaborators near and far have included Tonio Ball and Alexis Gkogkidis at the University of Freiburg, Dana Brooks, Kimia Shayestehfard, and Sumientra Rampersad at Northeastern University, and Rob Macleod, Chuck Dorval, Chantel Cherlebois, and Moritz Dannhauer at the University of Utah. My time over a summer working in the laboratory of Tonio Ball with Alexis Gkogkidis was a fantastic experience, and afforded me the opportunity to gain international experience and valuable skills outside of my domain.

I would would also like to thank my funding sources, which have included the the National Science Foundation (NSF) Center for Neurotechnology (CNT) (Award Number EEC-1028725), collaborative work through NSF Award Number IIS-1514790, the Big Data for Genomics & Neuroscience Training Grant under Grant Number 1T32CA206089-01A1, the ARCS Foundation, and a graduate fellowship through the University of Washington Institute for Neuroengineering (UWIN).

DEDICATION

I dedicate this thesis foremost to all of the patients who were so willing to participate in research. Without them none of this would be possible.

My friends in both the MD and PhD phases of training provide critical support and friendship, without which this would be a substantially less enjoyable journey. My family continues to support and encourage my interests and endeavours, for which I am eternally grateful. Their love and support is unwavering, and I am beyond fortunate to have the family that I do. My wife, Andrea, always stands with me, provides perspective when I am frustrated, and is a source of invaluable companionship and love.

Chapter 1
INTRODUCTION

1.1 Thesis

Use of direct electrical stimulation (DES) within a neural engineering context to restore sensation and enhance connectivity can be accomplished through in-dwelling intracranial electroencephalography (iEEG), also known as electrocorticography (ECoG) electrodes. Successful translation of human DES will require substantial gains in knowledge of its spread through cortex, interpretation of the underlying cortical dynamics in response to stimulation, how humans behaviorally respond to DES, and how it modulates neural plasticity. These elements are essential to properly engineer closed-loop functional neuroprosthetics for sensory restoration and plasticity enhancement.

1.2 Introduction

Damage to the nervous system due to stroke, spinal cord injury, and limb loss accounts for significant sensory and motor deficits. Despite the diversity of reasons behind cortical injury, targeted cortical stimulation may be able to help restore both motor and sensory function.

This thesis explores different aspects of engineered direct electrical stimulation (DES) of cortex, from understanding how it spreads through cortex, how to interpret neural signals during ongoing stimulation, the behavioral and neural effects of stimulation, and how different stimulation protocols work in humans (Figure 1.1). These studies may have future application in informing clinical trials and neuroprosthetic device design.

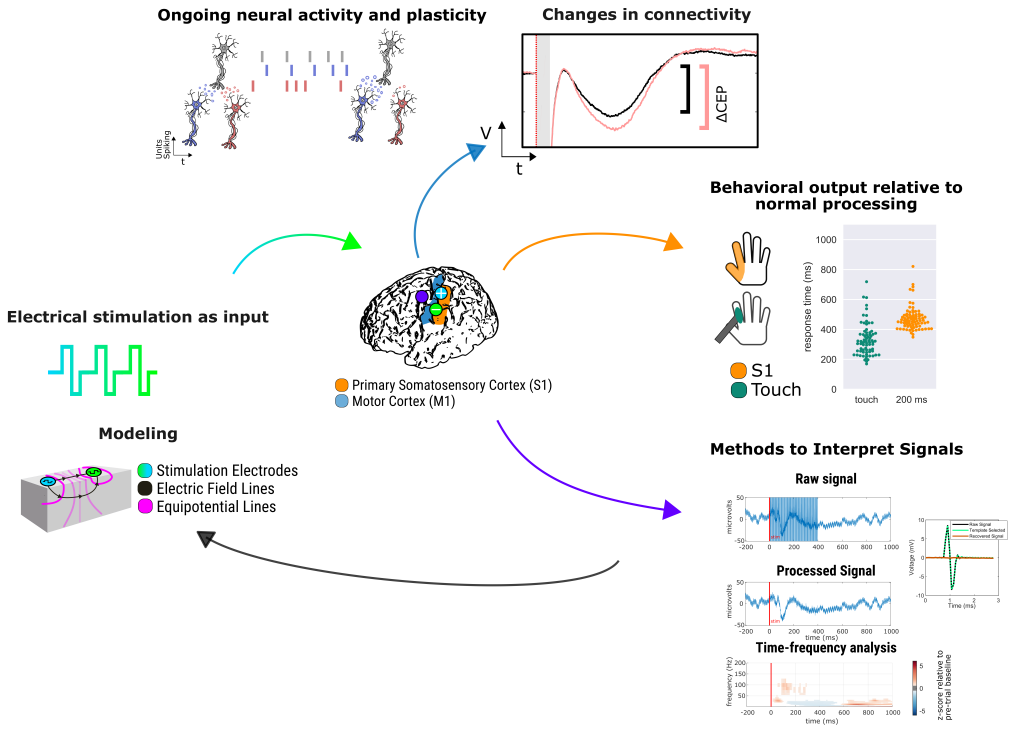

Figure 1.1: Thesis research overview. This thesis addresses a number of aspects of engineering direct electrical stimulation (DES) of the human brain for neuroprosthetic applications. The regions explored were primarily in sensorimotor cortex, but the principles may be extensible beyond this. The first part of our work was focused on understanding the physics of DES through analytic models to explore how well we can describe the flow of current in brain, and in particular how methods from other fields such as the characterization of semiconductors and geophysics apply to a system like the human brain. From here, we considered how to interpret brain data in the context of concurrent stimulation, which involved applying techniques from the field of unsupervised machine learning. We then focused on using DES sensorimotor parts of the brain, where the sensory and motor systems are tightly integrated. We worked on engineering stimulation of sensory cortex, and analyzed reaction time and temporal order judgment tasks to better understand the behavioral response to DES. Our work on engineering stimulation of motor cortex focused on the macroscale induction of plasticity, or the alteration of the strength of connections between neurons. One aspect focused on an beta-oscillation triggered paradigm in human epilepsy patients. The other focused on a paired-pulse paradigm intraoperatively with subjects undergoing DBS surgery.

1.3 Clinical Need

There are millions of individuals who are disabled due to stroke. It is estimated in the US alone for the year 2016, that healthcare and economic costs related to stroke disability totaled $34 billion, and that stroke is a leading cause of serious long-term disability [51]. 50-70% of stroke survivors reach functional independence, but 15-30% of survivors are permanently disabled [165]. Therapies using targeted activity dependent neuromodulation may be able to help restore motor recovery [107], but the biological effects of direct electrical stimulation (DES of cortex) are not well understood, and the parameters for potentially effective stimulation protocols need further development for implementation in a neuromodulation employing neuroprosthetic.

The motor output deficits associated with stroke are discussed more frequently than sensory deficits, but sensory feedback is critical for the planning and execution of voluntary movements [31]. Individuals suffering from somatosensory and visual deficits following stroke have worse motor recovery, highlighting the complex interplay between sensory and motor cortices. This motivates the exploration of techniques applicable to both regions. Somatosensory cortex is important for integrating sensory and motor signals and motor learning as well [34]. This integration of sensory and motor information, along with all of the connections between sensory and motor cortical regions [3], illustrates that engineering solutions should consider the complexities of the two highly interconnected regions.

Additionally, it is estimated that 5.4 million Americans are living with paralysis, with an estimated 41.8% of people living with paralysis unable to work [57]. The restoration of sensation is a priority for prosthetics users [28] as well as potential brain computer interface (BCI) end users such as individuals with paralysis [14,60]. Sensory feedback to cortex would enhance the efficacy of a prosthetic arm to aid with independent tasks, or help an individual better interpret data from body mounted sensors. The lack of sensory feedback in many BCIs may limit performance [23,71]. Indeed, integration of somatosensory feedback into BCIs has

been demonstrated to improve task performance with BCIs [65,137,220,247,264].This points to the importance of understanding how to appropriately engineer stimulation to restore sensation in BCI devices.

1.4 ECoG and DBS Background

Electrocorticography (ECoG) is used clinically as a recording modality for diagnosing specific spatial regions of focal epilepsy onset in individuals suffering from medically intractable epilepsy. By using invasive monitoring, the origins of seizures can be identified, and subsequent surgical removal of the seizure foci can reduce the frequency of or eliminate seizures. After surgical resection, approximately 50% or greater of patients experience significantly improved seizure control following surgical treatment [80]. For monitoring, patients are routinely implanted for 1 to 2 weeks with electrodes either directly on top of the dura (epidural), beneath the dura (subdural), or implanted in cortex (depth electrodes, or stereo electroencephalography (sEEG)). The term intracranial EEG, or iEEG, is often used to describe all implanted electrodes. We will use the term ECoG electrodes in this thesis to encompass surface as well as penetrating depth electrodes. Following electrode implantation, patients remain in the hospital under clinical monitoring by a team of neurologists and epilepsy technicians, until the clinical team has collected enough data to precisely localize the focal seizure zones for surgical resection.

To complement the passive recording of epileptic events, direct electrical stimulation (DES) [280] (or when applied particularly to cortex, known as direct cortical stimulation (DCS) [100], or direct electrical cortical stimulation (DECS) through ECoG electrodes is commonly performed for clinical mapping purposes, both intraoperatively and during the patients' clinical observation. For clinical mapping, the clinical team electrically stimulates different brain regions to delineate regions of cortex important for language, motor, and sensory function. By stimulating particular brain areas and observing the effects by querying

the patient, the clinical team can avoid resecting areas important for cognitive function and preserve these functions in an individual after surgical resection. The combination of recording and mapping through stimulation enables the clinical team to be best informed when making clinical decisions regarding reducing or eliminating seizures through resection, while maintaining cortical function. Clinical teams perform stimulation of both cortical and subcortical structures and pathways. We use the term DES here to refer to general electrical stimulation of any brain region through implanted electrodes, while we consider DCS a subcategory specifically describing stimulation of surface gray matter.

DES for clinical uses goes beyond delineating cortical regions of activity. For example, deep brain stimulation (DBS) is a therapy currently being used for therapeutic treatment of movement disorders. Electrodes similar to those used for sEEG are implanted into deep brain structures, and stimulation helps ameliorate clinical symptoms. The space of DBS research is vast, and this thesis does not exhaustively address DBS. I discuss stimulation through DBS as a demonstration of clinical stimulation through implanted electrodes, as well as draw from current research in this field for future directions of stimulation through all types implanted electrodes.

1.5 The Electrical-Neural Interface

1.5.1 Electrodes

Current clinically used ECoG electrodes are often embedded in a silicone sheet and are made of platinum or stainless steel. The electrodes are 1.5 mm diameter circular contacts contacts with 4 mm spacing ("micro"-ECoG electrodes), to 2.3-3 mm diameter contacts with 10 mm spacing ("macro"-ECoG electrodes) [53]. Depth electrodes are frequently comprised of platinum, with cylindrical contacts, and can be inserted with or without stereotactic guidance. These are commonly used to localize seizures coming from deep brain structures, such as the hippocampus. DBS electrodes are similar to depth electrodes in that they are

linear probes with cylindrical contacts, although they can be of smaller diameter, with tighter electrode spacing and fewer contacts.

1.5.2 Stimulation

Implanted electrodes can be used for direct modulation of neural activity through electrical stimulation. In order to better understand the underlying mechanisms of stimulation, we first consider the effects of stimulation on a single neuron. At the single neuron level, the redistribution of charge, and subsequent depolarization, where the inside of the cell becomes more positive relative to the extracellular fluid, can cause an action potential to be generated which propagates down the cell's axon. Hyperpolarization, which occurs when the inside of the cell becomes more negative relative to the outside of the cell, can inhibit action potentials. Electrical stimulation, through a redistribution of charge within an axon, can result either in hyperpolarization or depolarization. When sufficient depolarization is achieved, an action potential is generated through the diffusion of ions through sodium, potassium, and calcium channels [20]. Subthreshold intracellular stimulation, where an action potential is not generated, can result in the potentiation of synaptic strength with NMDA receptor mediation in the neuron's synapses [12].

In solutions, electrical stimulation results in the redistribution of ions through non-Faradaic reactions, and the transfer of electrons to electrolytes in the solution through Faradaic reactions [181]. There exist both reversible and irreversible Faradaic reactions: which one occurs depends on the rate of the electron transfers relative to the mass transport of the reactant. We discuss these reactions further and the impact of stimulation parameters on them in the "Limitations and Considerations" section. Through these mechanisms, charge is redistributed. When this redistribution of charge causes depolarization directly beneath the electrode, for the case of a single neuron, the stimulation is often referred to as cathodal stimulation, while electrical stimulation which causes hyperpolarization directly beneath the

electrode is referred to as anodal stimulation. (Figure 1.2(a)). On the scale of larger electrodes, such as with ECoG arrays, cathodal stimulation often refers to negative voltages and currents directly beneath the electrode, while anodal stimulation refers to positive voltages and currents.

Stimulation on a local scale can be achieved through intracortical microstimulation (ICMS), where electrical stimulation activates neurons primarily through their axons passing through the region of cortex stimulated [205, 271]. However, other regions of the cell such as the cell body and dendrites may also be activated depending on stimulus polarity and orientation. Anodal pulses best activate cell bodies and terminals, compared to cathodal pulses which best activate axons. In both cases, it is the outward flowing current at the axon initial segment or nodes of Ranvier along the axon that results in neuronal excitation [179, 271]. ICMS is thought to sparsely activate a population of cortical neurons, rather than just ones proximal to the stimulation electrode tip [120].

The distance of neuron elements from the stimulation source changes whether or not these elements will be hyperpolarized or depolarized by a corresponding cathodic or anodic stimulus. Directly beneath a cathode, a membrane will become depolarized, and hence can generate an action potential. During the case of anodal stimulation, the area directly beneath the electrode is hyperpolarized, but further away from the anode, action potentials may be generated, resulting in a "virtual cathode" [181] (Figure 1.2(a)). Stimulation beneath the anode can occur with surface anodal stimulation of neocortical cells, where current hyperpolarizes apical dendrites, and subsequently leaves through the axon resulting in depolarization [225](Figure 1.2(b)). For the case of bipolar stimulation, an axon is generally depolarized beneath the cathode and hyperpolarized beneath the anode. [225].

Physiologically, ICMS is thought to activate both inhibitory and excitatory populations of cells [43], and is not thought to evoke natural patterns of cortical activity [186]. Functional magnetic resonance imaging (fMRI) along with microstimulation has demonstrated that

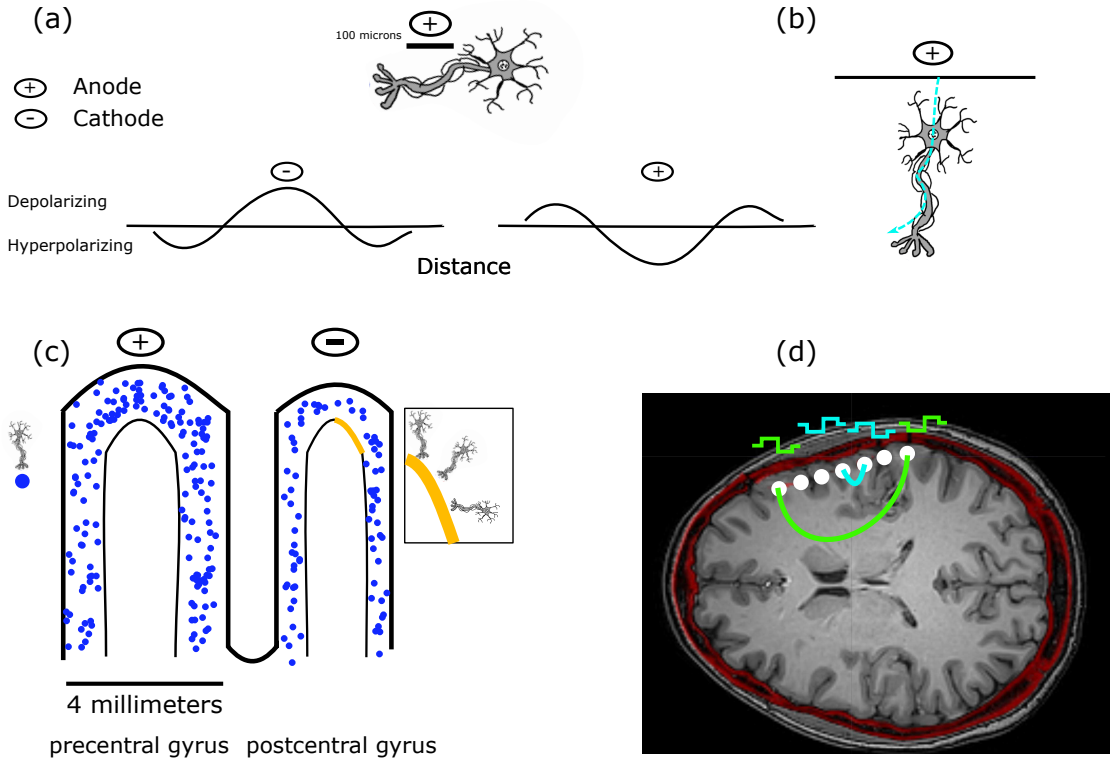

Figure 1.2: Effect of stimulation on a single neuron and a population of neurons. (a) Stimulation along a nerve fiber results in depolarization beneath a cathode, and hyperpolarization beneath an anode. (b) Single neurons can be stimulated by both anodal and cathodal stimulation depending on their orientation. In this example, anodal current enters the dendrites of the neuron and leaves through the axon, which results in depolarization of the axon and an action potential. (c) In the case of stimulation through ECoG electrodes, a large population of neurons can be activated by stimulation. Shown are approximate scales of an ECoG electrode relative to the precentral and postcentral gyrus, along with a representative mixed population of pyramidal neurons potentially depolarized by stimulation. In the zoomed-in region, we highlight the multiple orientations of neurons that could be activated. (d) An axial slice in a co-registered CT and MRI image following implantation with an ECoG array shows the potential current paths that different stimulation configurations would have to pass through, illustrating the large populations of neurons present within the potential current path.

microstimulation, at least in the visual cortical pathway, suppresses the output activity of neurons which have their afferents stimulated [166]. Further work in microstimulation of the visual cortex has demonstrated that microstimulation in V1 may locally activate cells, but silence neurons further downstream [140].

The frequency of ICMS also has an impact on whether neurons are excited or inhibited. High frequency stimulation (>10 Hz) is thought to potentiate neural activity (long-term potentiation) [30, 74], while low frequency stimulation (< 1 Hz) is thought to depress neural activity (long-term depression) [196].

Compared to ICMS, DES of human cortex using larger electrodes, such as ECoG or DBS electrodes, injects current over a larger surface area, and subsequently large amounts of current could lead to greater activation with the potential to spread to a larger area [280] (Figure 1.2(c,d)). Additionally, depending on the anatomic location of DES, stimulation can either evoke or inhibit neural activity [33]. For example, DES of language areas during a language task can disrupt speech production while DES of somatosensory cortex can evoke sensations and DES of motor cortex can evoke movements. In terms of subdural ECoG stimulation in humans, the patterns and types of cells activated are thought to depend on the intricate details of cortical geometry, cell fiber orientation [144], and whether the pulses are anodal or cathodal [251] ((Figure 1.2(c,d)). A finite element model model (FEM) of subdural cortical stimulation with integrated neuron models was used to demonstrate that neurons deeper in the bank (buried in cortex) are more activated during cathodal subdural stimulation, while those in the wider crown are activated during anodal stimulation [251]. DES through ECoG electrodes can result in both local effects, and effects remote to stimulation. The resultant signals recorded at other electrodes are often referred to as cortico-cortico evoked potentials (CCEP) [133]. These have been reviewed thoroughly by Keller et al. (see [133] (Keller, Honey, Mégevand, et al. 2014) for more details). We will therefore only review some of the relevant physiology here. Pyramidal cells, which are the

source of the majority of cortical output, and lie in cortical layers 2, 3, 5, and 6 can have their superficial dendritic trees depolarized. Layer 2/3 inhibitory GABA interneurons can be depolarized, which then synapse preferentially near the soma of pyramidal cells [37] and cause a decrease in pyramidal cell activity due to the inhibitory nature of GABA signaling. If there are axons passing through the region of stimulation, both orthodromic and antidromic stimulation can occur [133]. The measured surface potentials are therefore a combination of the initial monosynaptic connections, cortico-cortical pathways, and cortico-subcortical pathways which would explain the polymorphic response lasting hundreds of milliseconds [176].

In total, this speaks to the immense complexities of engineering stimulation in humans, and the work that remains to be done in understanding both its physical effects and resulting neural ones.

1.5.3 Sensing

A key part of a neuroprosthetic is the recording of neural activity to use as a control signal in order to successfully modulate the system using stimulation. The summed activity of many hundreds of thousands of neurons in the cortical tissue under an ECoG electrode contributes to the electric voltage recorded from the electrode. The increased firing rate of populations of neurons results in a broad increase in power across all frequencies, which is more easily separable in the broadband gamma band (above 50 Hz), rather than the lower frequency bands [188]. This is because other frequency bands modulate up and down independently during different tasks and brain states, masking the broadband increase in power. The higher frequency components are more asynchronous, and therefore are not as subject to this masking effect [114]. Lower frequency bands, such as the alpha (8-12 Hz) and beta (13-30 Hz) band, are thought to represent pulsed inhibition that serves to gate and coordinate neuronal firing [246]. Therefore, analysis of broadband gamma activity reveals the

local neuronal firing dynamics, while analysis of theta (4-8 Hz), alpha, and beta frequency regimes yields insight into the coordinating mechanisms across the brain.

The different oscillatory features discussed above have been explored for advancing our understanding of how different cortical regions function during motor movement and language function [36, 91]. Measurements of these signals during motor and speech imagery have been employed in ECoG brain-computer interfaces to drive end effectors such as computer cursors [156–158] and robotic arms [121]. Furthermore, non-motor regions can be used to drive ECoG-BCIs as well, illustrating the general utility of oscillatory band driven BCIs [224, 300].

1.6 Current Clinical Uses of Direct Electrical Stimulation

1.6.1 Functional Mapping for Epilepsy and Tumors

As detailed previously, DES is frequently used both intraoperatively and during a patient's stay at the hospital for functional mapping and identifying areas of cortex associated with important cognitive functions [25, 26, 209]. These mapping procedures are done both for epilepsy surgery and tumor resections [25, 26, 209]. Clinicians, using implanted ECoG electrodes or stimulators in the operating room, apply DES to various cortical and subcortical structures and pathways, and observe location dependent effects, including speech arrest in language regions, motor movements in motor cortex, and sensory percepts in somatosensory cortex. The results of these stimulation studies inform where the surgeons will plan to resect; for example, if the seizure focus is close to a language region, the surgeon and patient may decide the surgery is not worth the risk of a permanent language deficit.

1.6.2 Deep Brain Stimulation (DBS)

Deep brain stimulation (DBS) is a prominent example of electrical stimulation of the brain. It is currently being used for therapeutic treatment of movement disorders (Parkinson's

disease [38] and Essential Tremor [72]), and is also being explored for treating psychiatric illnesses (post-traumatic stress disorder, depression, obsessive compulsive disorder, Tourette syndrome [248]) and epilepsy treatment. Traditionally, linear probes of cylindrical contacts are inserted into deep brain structures such as the globus pallidus internus (GPi), subthalamic nucleus (STN), or ventral intermediate nucleus of the thalamus (VIM). Following implantation, clinicians may either be guided by intraoperative CT imaging, or wake the patient up intraoperatively to test for adverse effects of stimulation on different contacts, using a monopolar (one stimulating electrode and a distant return electrode), bipolar (two similarly sized electrodes), or multipolar arrangement of electrodes for the steering of current.

Advances in BCI related to deep brain stimulation (DBS) have explored the use of closed loop DBS to trigger stimulation of deep brain structures in response to signals recorded from the surface of the cortex [117]. Herron et al. used threshold crossing in the beta-band regime of recorded ECoG signals over motor cortex as a control decision to trigger DBS stimulation. This enables control of DBS stimulation solely through recorded neural signals. Besides potentially reducing the side-effects of open-loop stimulation, such closed-loop control of stimulation conserves power and helps extend the life of the DBS device, reducing the number of replacement surgeries needed over the life of a user. Adaptive DBS based on recordings in STN has been demonstrated to improve motor scores over traditional open-loop DBS [164]. In addition, primate models of Parkinson's disease demonstrate that closed-loop DBS has a greater effect than open-loop DBS on akinesia and on the neuronal output in both cortical and subcortical structures [239].

Finally, DBS is also being explored for the treatment of particular types of epilepsy. Partial onset seizures often spread through the circuitry of the basal ganglia, and therefore could be controlled using DBS strategies similar to those used for movement disorders [105, 151].

1.6.3 Closed Loop Stimulation for Epilepsy

Closed loop stimulation to control seizures is currently clinically available to epilepsy patients through the Neuropace RNS system [150, 193]. A neurosurgeon implants ECoG electrodes either on the cortical surface or in deeper structures near the putative seizure focus. If an impending seizure is detected, high frequency stimulation is triggered near the seizure focus to control the seizure. This is a demonstration of clinically effective and already implemented DES in an ECoG BCI, where neural control signals are acquired in real time from the brain and used to trigger stimulation.

1.7 Advantages of DES Relative to Other Stimulation Techniques

An advantage of DES relative to non-invasive electrical stimulation modalities is the delivery of much greater amounts of the applied current to neurons. During transcranial electrical stimulation (TES. We use this term to encompass transcranial direct current stimulation or tDCS and transcranial alternating current stimulation or tACS.), as much as 75% of the current is shunted through the scalp and the skull [284, 298]. This greatly blunts the efficacy of cortical stimulation, and suggests that some of the published results using TES are due to mechanisms other than direct neuronal excitation. In contrast, by directly stimulating the brain and bypassing the skull and scalp, DES delivers current to cortical structures more effectively. Although the currents applied during TES could be raised to a high enough level to reach a desired electric field strength at a target location in the brain, there would be potential off-target effects and skin damage due to the amount of current required, in contrast to DES through electrodes implanted precisely at the targeted site for this same electric field strength. This reinforces the large advantage of the DES relative to TES, i.e., the ability to place electrodes close to the target structures, and consequently minimize the amount of current passing through off-target structures.

Even with epidural and subdural stimulation, not all current reaches neurons in the

cortex. Epidural stimulation results in current shunting by the dura [304], while both epidural and subdural stimulation have some degree of cerebrospinal fluid (CSF) shunting depending on the characteristics of the CSF beneath or surrounding the electrodes [104, 304].

A factor in epidural and subdural stimulation is the presence of pain receptors within the dura which can be activated with dural stimulation [301]. However, previous clinical trials with epidural stimulation made no reports of dural pain with stimulation up to 6.5 mA and 250 μs pulse widths [159].

TMS has primarily been used to induce motor movements, rather than isolated sensory percepts (although phosphenes can often be produced via TMS, and tapping sensations and auditory clicks can accompany TMS) [260]. A method such as DES affords the ability to focally and specifically produce sensations that would not be achievable through TMS.

Additionally, traditional figure-8 TMS coils are currently unable to target cortical structures beyond 2-3 cm deep [240, 286]. DES electrodes, on the other hand, can be physically placed in deeper cortical regions of interest in order to elicit the desired stimulation effects. Another advantage of DES over TMS is the fact that the maximum of the electric field strength induced by TMS has to occur at the cortical surface, and not in deeper structures [111]. This means that off-target effects in cortical layers near the surface are possible when targeting deeper structures. Even with more sophisticated coils, such as the H-coil, the maximum stimulation strength still occurs at the surface and greater depth of stimulation (4-6 cm) is achieved with a loss of focality [286, 313]. Although the field strength is greatest at the cortical surface for TMS, the orientation of neurons is a critical component in the activation of neurons, as both experimental and modeling work has shown that electric fields tangential to the sulcal walls can activate neurons oriented perpendicularly to them [93, 253, 258]. Similarly, different layered pyramidal neurons are activated differently between the gyral crown and sulcus walls [253, 258]. This in total points to the complex physiologic effects of TMS, and the potential difficulties in activating groups of neurons both

on the crown of the gyrus and within the sulcus together. A further disadvantage of TMS is that with current hardware, use outside of the lab is limited due to the bulky hardware and the need to maintain a precise spatial relationship between the coil and the head for stimulation.

The fact that DES electrodes can be placed near the deeper structures of interest is vital for the treatment of Parkinson's and Essential Tremor through DBS. As these structures cannot currently be effectively stimulated through alternative methods such as TMS, effective clinical treatment relies upon DES via electrodes near the desired brain regions.

1.7.1 Financial, Translational, Regulatory, and Ethical Concerns for DES in future applications

We expect early applications of engineered direct electrical stimulation to leverage existing clinical devices. This has been a pathway forward for many prior medical devices. Advances in early DBS devices were based largely off of prior work in cardiac pacemaker and spinal cord stimulation devices [58]. We imagine a similar trajectory for DES in future neuroprosthetics. Preliminary use of DES has been enabled by investigational device exemptions [106]. Further iterations of Medtronic DBS devices, such as the PC+S device, have been granted an investigational device exemption in research studies, and are improvements upon an already clinically approved device [117].

Whenever new technology is implemented for clinical treatment, a question of cost efficacy is raised. However, we suggest that DES for sensory restoration and neuromodulation have the potential to be cost effective long-term devices if clinical efficacy is demonstrated, as illustrated by examples such as vagus nerve stimulators and DBS. Vagus nerve stimulation for epilepsy has been show to be effective long-term, and cost benefit analysis has shown that the cost of the treatment pays off within a 2 year period [32]. Although it is not universally the case, DBS in general is thought to be cost effective, when looking at studies across

European and North American centers [218]. It has been noted that during the adoption of DBS large-volume hospitals had lower prices and superior short-term outcomes, which is something to be aware of with future neuroprosthetic devices incorporating DES [83].

Ethical concerns are critical to address for any engineered device which is implanted in a patient. A previous review has explored some of the ethical concerns for BCIs [138], and we seek here to highlight some of the concerns which are particularly relevant to incorporating DES into future engineering devices.

Articulating the potential risks and long-term requirements devices interfacing with the brain, particularly employing DES, is essential for appropriate informed consent. Biologic risks such as infection, seizures, and tissue damage from stimulation [59] are accompanied by technological concerns such as repeated surgeries for battery replacements, heating due to potential wireless charging, and lifetime electrode wear from repeated stimulation [138].

Privacy and security are another key aspect in implantable medical devices, particularly with any BCIs that communicate signals wirelessly or can be programmed wirelessly. One can imagine situations where a stimulator could be set to either less than therapeutic levels or to unsafe levels, by malware transmitted to the device. Research efforts that build on current security and privacy protocols for medical devices are required to ensure neural signal security and protection against malevolent programming.

1.8 Research Directions for DES

We discuss various research directions for stimulation for neuroprosthetic applications. An existing review [289] has explored the use of brain-computer interfaces for investigating scientific questions in the nervous system. Further information on classical ECoG-BCIs and comparison to other types of BCIs can be found in [228].

1.8.1 Sensory Feedback through DES

Prior work has shown that humans can respond to direct DES of the surface of the primary somatosensory (S1) cortex [119, 129, 161, 230], which results in an artificial sensory percept organized according to the standard somatotopy of cortex. Cronin et al. demonstrated that DES of S1 could be used by an individual in the absence of visual feedback to perform a motor task [63]. Although these percepts would not be mistaken by the individuals for natural touch [61, 63, 129], they are useful for performing closed-loop BCI tasks. An open question is how using DES for feedback compares to a normal somatosensory pathway. Another key consideration for neuroprosthetic use is the embodiment of the prosthetic device. DES through ECoG has been shown to induce prosthetic hand ownership, suggesting that prostheses could be made to feel more natural as a result of DES [61].

With recent advances in materials and manufacturing, spatially smaller microECoG arrays are able to target smaller volumes of cortex. More targeted DES through microECoG grids allows higher spatial selectivity relative to larger clinical electrode grids [119, 149], opening up the possibility of encoding more complex percepts compared to larger electrodes.

Although short term studies have demonstrated that these percepts induced by DES do not feel natural, the principles of neuroplasticity, which are prevalent in somatosensory cortex and other associated regions, and adaptation within the cortex [189, 273, 294] will be relevant in the long-term implementation of DES for sensory restoration.

A neuroprosthetic focused on sensory restoration through DES (Figure 1.3) could use signals from motor cortex to drive a sensorized prosthetic arm, which could provide feedback about the task via DES of primary somatosensory cortex (Figure 1.2(a)). Depending on the potential parameter space of discernible stimulation percepts, a user could learn to map physical contact locations on the prosthetic arm to distinct stimulation percepts (Figure 1.3(b)), providing feedback from external sensors directly to the brain brain. The recent demonstrations of usable sensory signals in humans via DES brings us a step closer to such

closed-loop human devices.

1.8.2 Quantification of Cortical Connectivity

An additional application of DES is in quantifying cortical connectivity. DES of a cortical site can produce a cortico-cortical evoked potential (CCEP) at local and remote sites depending on the cortical area stimulated and the intensity of stimulation [133]. Studies have explored CCEPs in the context of different cortical networks, including language [177] and motor regions [176]. The connections probed with CCEPs correspond well with known functional networks observed through fMRI as well as white matter pathways confirmed by diffusion tensor imaging (DTI) [132]. Such evoked potentials could have utility in engineered applications where depending on the presence or modulation of these CCEPs, an algorithmic decision could be made.

1.8.3 Modification of Cortical Excitability and Induction of Plasticity

Another use for DES currently being explored is the induction of cortical plasticity. This refers to enhancement or other modification of connectivity between different cortical regions, which could aid in the recovery of individuals suffering from disrupted neuronal communication due to injuries such as stroke.

A persistent theme in cortical connectivity is the idea of Hebbian plasticity, a type of synaptic plasticity first proposed by Donald Hebb in 1949 [109]: presynaptic firing of one neuron (site A) can strengthen the connection between it and a postsynaptic neuron (site B) that fires soon after A. Bi and Poo demonstrated a version of this plasticity rule, known as spike timing dependent plasticity (STDP), in rat hippocampal slice cells: consistent firing of a presynaptic cell (site A) within a time window of 20-30 ms before another postsynaptic cell (site B) led to a strengthened connection (LTP) from A to B, while B firing in a time window of 20-30 ms before A led to a weakened connection (LTD) [27]. Both of these mechanisms

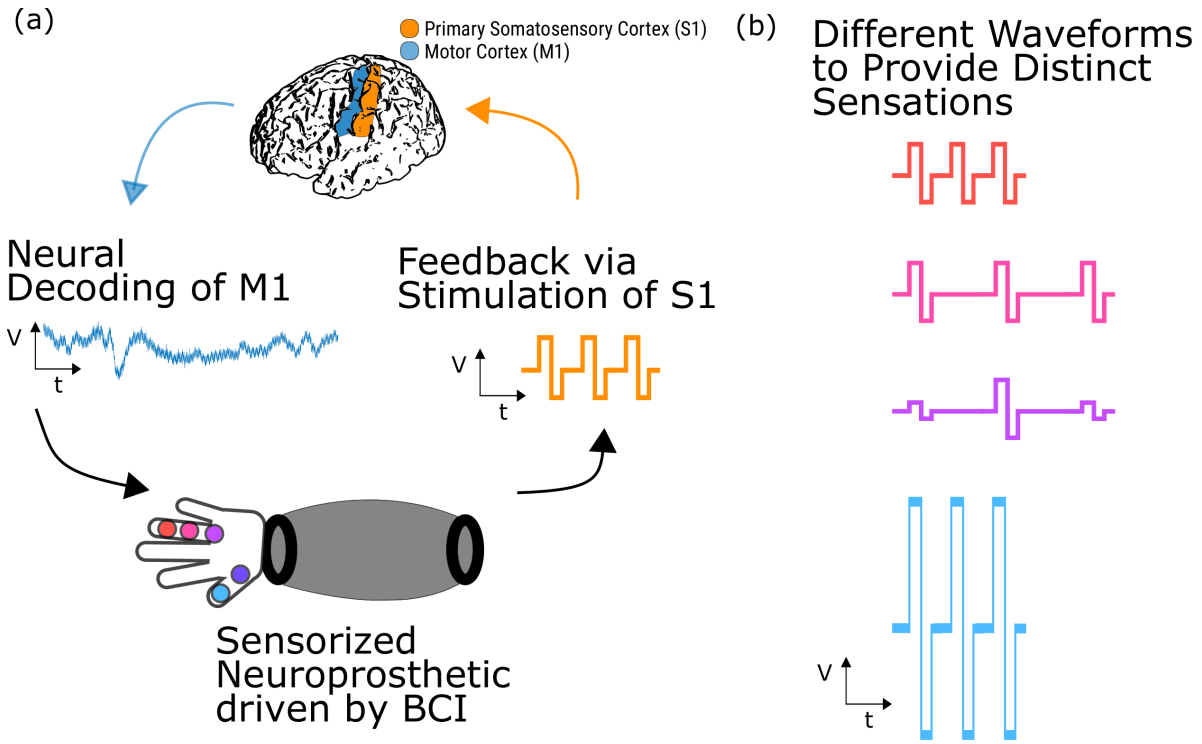

Figure 1.3: Somatosensory neuroprosthetic with closed-loop stimulation. (a) Neural signals recorded from cortical regions such as primary motor cortex could be used to drive a sensorized prosthetic arm. Feedback about task performance or object manipulation could then be conveyed to the user by DES of primary somatosensory cortex. (b) Different stimulation parameters, such as amplitude, frequency, and carrier frequency shape, could convey different percepts which a user could learn to map to locations on the neuroprosthetic arm.

were determined to be dependent on NMDA receptors.

We know that active participation in skill training can shape neurological recovery and lead to improved functional outcomes [303]. We also know that not using impaired limbs (learned nonuse) inhibits neurological recovery [77]. The various mechanisms that underlie functional recovery are complex [293], but hinge on concepts of neural plasticity. A number of studies in animals and humans support the theory that neurological recovery can be enhanced by stimulating brain tissue. In these studies, repetitive stimulation changed the motor representation in cortex after lesioning in rats [206], led to dendritic changes [6], and ultimately improved functional outcomes [4, 5]. Based on these findings, clinical researchers aimed to excite neural tissue with continuous epidural stimulation with implanted devices, essentially to increase brain activity during tasks and therefore enhance the recovery process in humans when coupled with traditional therapy [106]. Although a promising Phase II clinical trial demonstrated some improvement of functional outcomes with epidural cortical stimulation in stroke patients with impaired upper limb function [122], the Northstar Neuroscience Phase III EVEREST clinical trial to improve hand and arm function in stroke survivors did not meet the primary efficacy endpoint of clinically meaningful improvements in the upper extremity Fugl-Meyer scale and Arm Motor Ability Test 4 weeks postrehabilitation; thus, it was discontinued. We discuss the limitations of the EVEREST trial and the resultant hypotheses in a subsequent "Limitations and Considerations" subsection.

In contrast to these "open-loop" stimulation techniques, it is possible that brain stimulation may have to be coupled with neural activity to effectively modulate neural connections, as discussed by Edwardson et al. [75].

These principles of the importance of stimulation timing have been applied to induce plasticity in nonhuman primate (NHP) motor cortex [125] and rodent rehabilitation experiments, where triggering stimulation in somatosensory cortex several milliseconds after premotor cortex firing in rats that suffered from damage to motor cortex resulted in increased

functional performance [103]. Other work has explored the use of paired-pulse paradigms in NHPs to induce plasticity: where concurrent surface to depth stimulation at one site was consistently followed by stimulation at another site with a fixed time lag [250]. The optimal time lag for potentiation was found to be between 10-30 ms, with longer delays not resulting in potentiation. Only a fraction of the sites in this study were potentiated, and effects were often seen globally, illustrating the complex factors influencing cortical plasticity.

To highlight potential functional changes in connectivity and brain function from neural activity dependent stimulation, a recent study highlights the use of delta (1-4 Hz) oscillation triggered stimulation during slow wave sleep to improve learning a brain computer interface task [233]. A recent study in NHPs examined the timing of DES relative to the aggregate activity of neurons: DES delivered during beta oscillations during the depolarizing potential (negative peak as recorded through LFPs) caused potentiation of cortical connectivity, while DES delivered during the hyperpolarizing potential caused depression of cortical connectivity as assessed through cortically evoked potentials [314]. The authors also observed a dose dependent effect regarding the number of conditioning pulses delivered.

Beyond work in animals, and importantly, for applications such as stroke rehabilitation, recent work has reported improvements in physiological measures of motor function with non-invasive stimulation such as movement triggered TMS compared to random TMS stimulation [42]. Adding further support to the importance of brain state dependent stimulation for rehabilitation is a recent study that demonstrated TMS delivery during movement-related beta-band (16-22 Hz) desynchronization caused a significant increase in corticospinal excitability, as evaluated through motor evoked potentials, lasting beyond the period of stimulation [142]. Another study employed peripheral stimulation of the peroneal nerve timed to arrive at the peak negative phase of electroencephalography (EEG) detected movement-related cortical potentials compared to random stimulation, and found significantly increased Fugl-meyer scores, 10-m walking speed, motor-evoked potentials, and foot/hand tapping fre-

quency [195]. From these recent studies, it is clear that various central and peripheral nervous system stimulation paradigms are enhanced by neural activity coupled stimulation.

Keller et al. demonstrated that repetitive 10 Hz DES using subdural electrodes induced both potentiation and suppression in different cortical sites, depending on the baseline network characteristics [134]. This suggests that plasticity can indeed be modulated through DES in humans, and that individual patient models of connectivity may inform the optimal sites to target to either enhance or decrease connection strength.

An neuromodulation focused neuroprosthetic (Figure 1.4) could include an oscillatory feature at a surface electrode, such as activity in the beta band or high gamma activity representing coordinated neuronal firing, driving stimulation at a damaged cortical region to enhance cortical connectivity and help restore motor function. This activity dependent stimulation could be similar to the activity-dependent DBS paradigms being explored [117]. A more sophisticated approach, based on the concept of neural co-processors [229], could utilize artificial neural networks to map complex ECoG activity patterns at multiple recording sites to stimulation patterns at multiple stimulation sites to achieve goal-directed stimulation.

The combination of theoretical, animal, and human data discussed above suggests that activity-dependent DES is a promising approach to enhance and modify connectivity in humans, offering a new type of therapy for targeted restoration of function after neural injury. Intracranial electrodes are well-suited to acquiring and decoding appropriate control signals and when coupled with DES, can be used to influence cortical activity and induce activity-dependent plasticity.

1.9 Limitations and Considerations

While ECoG based neuroprosthetics offer several advantages over other types of neuroprosthetics, there are limitations and considerations that must be taken into account. For either subdural or epidural electrodes, neurosurgery is required. The size of the electrodes, relative

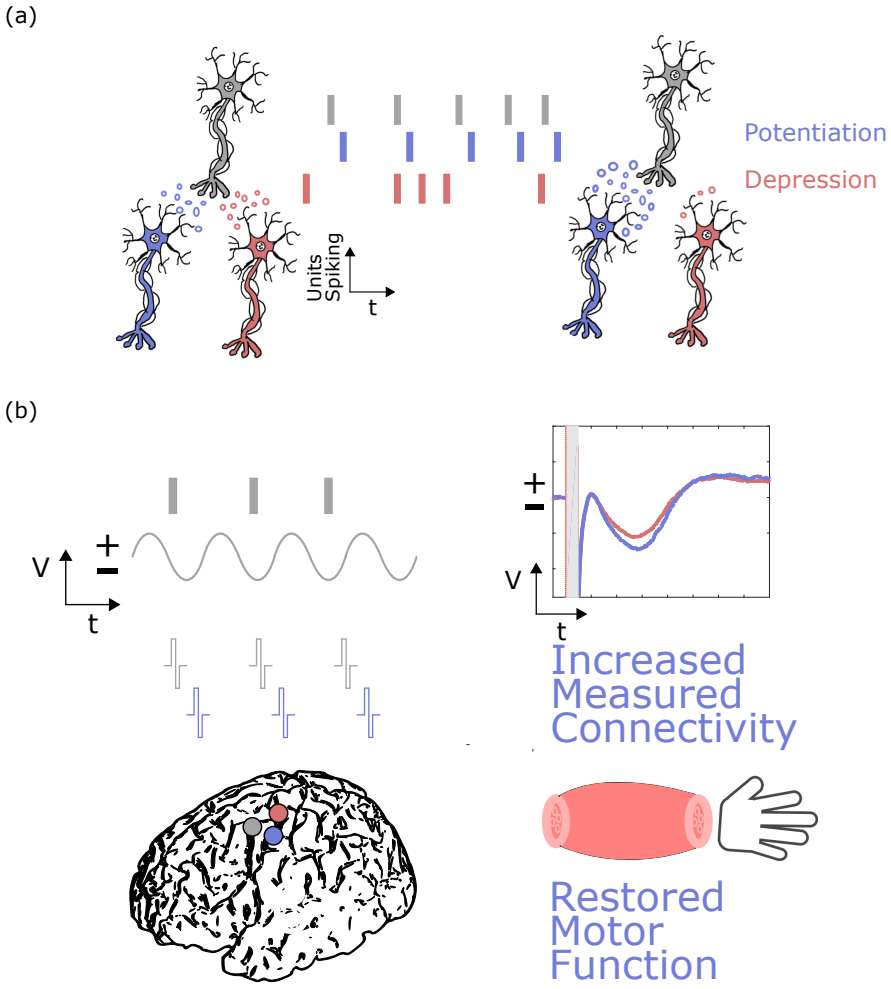

Figure 1.4: Neural plasticity induction through neuromodulation via DES. (a) The basic principles of neural plasticity involve the timing of activity between neurons resulting in the strengthening of connections, where potentiation occurs if the neurons fire with the appropriate timing in a causal manner, and depression occurs if neurons do not fire with the appropriate timing. (b) These principles could be used for neuromodulation through DES by stimulating near a particular damaged cortical region (purple), based on activity at a spared cortical region (gray). This activity could be a marker of neuronal firing, or a local field potential representing when neurons are more likely to be firing synchronously. Appropriately timed stimulation could then result in increased connectivity, measured through markers such as evoked potentials, and restored motor function relative to baseline. A damaged region not undergoing neuromodulation is shown in red, where evoked potentials are not positively modulated and motor function is not restored.

to other invasive methods such as ICMS, results in larger population of neurons being targeted. Furthermore, there is no ability to target specific types of cells. Additionally, larger neurons with larger diameter axons are more likely to be activated by electrical stimulation [271].

The developing field of optogenetics [69,311] describes the use of genetic modification and optical methods to either activate or inactivate specific neurons in-vivo. Optogenetics has been demonstrated to change functional connectivity in sensorimotor cortex in NHPs [310]. Although optogenetics may offer a more targeted approach to activating neurons, progress to humans may be slow due to the technique's reliance on genetic modification of neurons.

Another current consideration when developing technologies and protocols to induce plasticity is our current lack of understanding of the mechanisms of plasticity induction [85]. Beyond the single neuron spiking level, plasticity is a complex phenomenon as discussed above, and in a human brain, the potential factors influencing plasticity can be complex and numerous. Optogenetics, with its ability to selectively target different populations of neurons will help provide critical insight into the mechanisms of plasticity.

Although DES may offer a promising approach to inducing plasticity, it has yet to be demonstrated to be unequivocally effective in a stroke model. Limited subgroups of stroke patients who had motor thresholds reached with stimulation were shown to benefit from open-loop DES in the EVEREST trial, but other groups showed no benefit at 4 weeks [160]. However, the investigational group did show significant benefits at 24 weeks.

Several hypotheses surround the mixed results of these trials [160, 221]. One drawback of the EVEREST trial was the primary use of fMRI to localize the location for stimulation. Using techniques such as somatosensory evoked potential mapping and motor mapping [221] would enable more fine-grained localization of different functional anatomic regions. In the phase I and phase II parts of the clinical trial, motor thresholds (MT) were reached with stimulation in 75% and 42% of patients, respectively, while only 14% of subjects reached

MT in the phase III trial. The subset of subjects able to have MT reached in the EVEREST trial were the ones who benefited significantly from stimulation [160]. Furthermore, the MT subgroup had smaller stroke lesion volumes, which were more isolated to the basal ganglia and internal capsule, and less corticospinal tract damage [160]. However, lesion size alone does not predict residual motor function [213]. This in total demonstrates the importance of cortical and descending pathway function for stroke recovery, and suggests that residual motor function as confirmed through motor mapping or functional localization may be important for beneficial neuromodulatory effects.

The issue of particular patient subgroup benefit as discussed above speaks to the broader issue of patient variability. Due to anatomic or surgical variations, results from one group of subjects may not necessarily apply to another. Careful consideration of these individual factors will be important for future neuroprosthetic devices.

As better animal models of stroke are developed [261], one can hope to gain a better mechanistic understanding of how DES can be used for stroke rehabilitation, leading to optimized therapies for maximizing functional recovery following cortical injury.

An additional consideration is the durability of electrodes with repeated stimulation. As mentioned in the section on the mechanisms of neural activation through stimulation, charge transfer can occur through irreversible Faradaic reactions, where electrolysis occurs, and depending on the polarity of stimulation, either hydrogen gas or oxygen gas are the by-products [181]. In this electrolytic window, accelerated corrosion and electrode damage can occur. Even below the voltage required for the electrolysis of water, detrimental byproducts such as the formation of metal chloride and hydrogen peroxide can occur, leading to electrode corrosion. Therefore, long-term use of stimulating ECoG electrodes will require careful selection of stimulation parameters and materials to minimize adverse effects. Relative to monophasic pulses, both charge balanced and imbalanced biphasic waveforms result in less electrode potential shift and accumulation of charge. Accumulation of charge during

monophasic stimulation can result in additional undesirable Faradaic reactions, and the formation of reactive oxygen species which can cause tissue damage [181]. When comparing charge balanced and charge imbalanced biphasic waveforms, charge imbalanced waveforms have the advantage that at the end of each stimulation pulse, the electrode potential is closer to that of the open-circuit potential, resulting in less charge going to irreversible oxidation reactions [181].

Beyond electrode damage, tissue damage induced by stimulation is a key consideration for long-term use of DES. The study of electrical stimulation through platinum electrodes in cats [178] was used to define the Shannon equation [254], which has been used frequently for assessing safe stimulation levels. Earlier research established a 30 $\frac{\mu C}{cm^2}$ limit on the charge per phase of stimulation for macro-scale electrodes (in particular, DBS electrodes) [145], but tissue damage can occur above and below this threshold [59]. There are factors influencing whether or not tissue damage occurs that are not included in the Shannon equation, for example, the scale of the electrode (macro vs. micro), the current density, duty cycle, pulse frequency, and the uniformity of current distribution [59]. These complex factors will require further modeling and laboratory testing to establish what the appropriate stimulation parameters are to minimize tissue damage, particularly with the use of novel materials and stimulation patterns.

With penetrating microelectrodes (such as with the Utah array), there is a significant change in the electrode-tissue interface over time [299]. In addition, stimulation can change the characteristics of the electrode-tissue interface. A recent study analyzing the impedance characteristics of DBS electrodes following implantation and stimulation has shown that DBS electrode impedance increases after implantation and decreases with clinically relevant stimulation [153]. Other work has shown that the stimulation parameters used affect the impedance measured for DBS electrodes [295]. ECoG electrode impedance measurements from 191 persons implanted with the Neuropace RNS system, over a median time period

of 802 days, did not reveal significant differences between stimulating and non-stimulating electrodes in peri-implant changes in impedance or impedance stability [242]. In this study, while there were statistically significant short-term changes in impedance following implantation, long-term impedances were stable. These results suggest that neuroprosthetics with concurrent DES may prove viable as chronic implants.

In any closed-loop application involving concurrent stimulation and recording, the electrical artifact due to stimulation is many orders of magnitude greater than the neural signals being recorded. Disentangling the volume conduction of the stimulation pulse from the neural responses is a topic of active research [316]. Different approaches have been used for handling artifacts, ranging from hardware approaches to mitigate artifacts before signal acquisition to post-processing techniques to minimize artifacts after the signals have been acquired.

1.10 Relevant Neural System Physiology

As this thesis is considered primarily with stimulation of upper limb motor and somatosensation systems, we will review their basic physiology. These two systems are also of particular interest in the case of a neuroprosthetic device driven by motor signals using DES for feedback, as in Figure 1.3. For a complicated task such as dexterous manipulation of an object, the coordinated function of the sensory and motor systems is essential. The intricacies will not be discussed here, and further information can be found elsewhere [130] for both motor and sensory systems, and in [3, 70, 294]

The brain transforms sensory inputs, which include intrinsic information like body position and motion, and extrinsic information, like where an object is in space, into motor outputs through sensorimotor transformations. In the scheme of feedforward control, sensory feedback is not used to correct the movement, as would be done in the initial parts of a rapid reach. Sensory feedback is critical for feedback control, where errors are conveyed through

sensory feedback and modify the motor command [130].

These two systems are integrally related through sensorimotor integration, where motor output is modified by sensory input [3]. For instance, during active hand movement, motor neuron activity in primary motor cortex is influenced by touch on the hand, and sensory feedback provides information about the error during a movement, allowing for feedback corrections [130]. Similarly, in the process of active touch, which refers to consciously exploring the world around us, involves the integration of proprioceptive information and motor signals about the movements we intend to perform to aid in the perception of objects [243].

Furthermore, the principles of plasticity apply broadly to both sensory and motor systems. Motor cortex exhibits plasticity in response to motor-skill learning, cognitive motor actions, and in response to cortical damage [244]. Sensory cortices also exhibit plasticity, where following neurological damage, adjacent regions undergo remapping to process sensory signals from the lost regions [39]. Similarly, extensive cutaneous stimulation to a particular region can enhance the size of cortical receptive fields and reorganize somatosensory cortex [67]. An additional example of this is that the cortical representation of fingers can be reorganized in Braille readers [67].

Both primary motor cortex and primary sensory cortex are in close proximity, as motor cortex is within the precentral gyrus anterior to the central sulcus, while primary sensory cortex is posterior to the central sulcus in the postcentral gyrus. Both receive and send off ipsilateral contributions, but traditionally most activity occurs for external body parts on the contralateral side. Both the primary motor cortex and primary sensory cortex are organized somatopically, where body parts are arranged in a stereotyped map, known as the homunculus. Areas such as the face and upper limbs have a disproportionate area relative to their physical size in both the sensory and motor homunculus, which represents their large degree of innervation. An interesting difference between sensory and motor cortex is that cortical columns are a prominent feature of sensory cortex, but not motor cortex [130].

1.10.1 Motor System

How do we volitionally reach out and interact with the world around us? Our motor systems are responsible for translating intent into physical action. Here we primarily focus on primary motor cortex, although successful motor execution and feedback involves contributions from the cerebellum, basal ganglia, and thalamus.

Once a decision and plan to move is made, which involves premotor, supplementary motor areas, the cerebellum, the basal ganglia, and motor cortex itself, the motor cortex is largely responsible for converting the sensory information and intended motor output into the desired motor command. Neurons in motor cortex encode both the kinematics and kinetics of movement, and are thought to use a population-coding mechanism.

The most well understood path of motor output is the pyramidal tract, originating in layer V of the cortex. Between 30–40% of the neurons of the corticospinal tract originate in primary motor cortex, with other neuron in areas such as supplementary motor and promoter areas. From motor cortex, these neurons decussate, or cross over, at the pyramid in the medulla, and project axons onto the spinal cord. The entire projection is sometimes referred to as the pyramidal tract.

A particular type of neuron in the motor cortex known as the corticomotoneuron projects monosynaptically from the brain to the spinal motor neurons, and these are important for skillful hand and finger movements [130]. Motor commands are not sent exclusively through the corticospinal tract, as other tracts including the corticobulbar, colliculospinal, rubrospinal, vestibulospinal, and reticulospinal tracts play roles in motor activity.

Once these descending signals reach the spinal cord, the motor neurons in the spinal motor circuits generate movement patterns, which can also be generated by reflexes and pattern generators in the spinal cord. A large part of the corticospinal tract originating from primary motor cortex terminate in the ventral horn of the spinal cord. The ventral horn of the spinal cord is also referred to as the "final common pathway" [130], as here is where

all the upstream processing is fully incorporated and conveyed to the motor neurons. From here, α and γ motor neurons innervate muscles. A motor unit is referred to as a single α motor neuron and the striated muscles that it innervates.

The motor cortex is also crucial for motor skill learning, where motor cortex changes its activity patterns and motor mapping to accomplish its desired goal in the presence of perturbations.

1.10.2 Somatosensory System

How do we acquire information about world around us? The human somatosensory system acquires information about ourselves and our surrounding environment, and results in perception, which includes the senses of pain, temperature, vision, hearing, proprioception, and touch. [130]. In this thesis, we discuss primarily the sense of touch on the hand, and subsequently, the examples we discuss will be focused on this. There are other important receptors and afferents for touch and object manipulation, which include muscle spindle afferents which provide information about position and velocity, and Golgi tendon organs which signal muscle tension during activity [294].

Once we make contact with an object, as during objection manipulation with our hands, mechanoreceptors in our hand translate this contact into nerve impulses in primary afferent neurons. We have four kinds of mechanoreceptors in our hands, which include Meissner corpuscles, merkel cells, ruffini endings, and pacinian corpuscles. These are subsequently innervated by slowly adapting (SA) or rapidly adapting (RA) fibers, which are types of large and medium diameter cutaneous nerve fibers (Aα and Aβ respectively). SA fibers respond primarily to consistent object contact, while RA fires respond to contact onset and offset. There are subsequently two kinds of each of these fibers (SA1, SA2, RA1, RA2). SA1 fibers innervate Merkel cells, which respond well to edges and points of objects. RA1 fibers innervate Meissner corpuscles, and respond to lateral motion primarily. SA2

fibers transmit information from Ruffini endings, which signal skin stretch, while RA2 fibers innervate Pacinian corpuscles and signal vibration.

As an example, in the case of a grasping and lifting task of an object, SA1 fibers provide information about the force used for gripping an object, while SA2 fibers inform the hand position. RA1 fibers provide information about hand motion and force rate, while RA2 fibers sense vibrations, which include when an object is first touched, lifted off of a table, and released [128, 130].

The central axons from these peripheral nerves, specifically the the cluster of neurons known as the dorsal root ganglion, converge on the spinal cord, where they split and form projections onto neurons which ascend to the brainstem, or locally project to the spinal cord. The neural microcircuitry in the dorsal horn allows for the integration of intra- and inter-modality somatosensory information, such as temperature and pain inputs, and top down, descending drive, which all can influence the touch input relayed from the periphery [3].The dorsal column on each side of the spinal cord contains these afferents as they go to the medulla. The upper limb tactile and proprioceptive information is integrated in the cuneate nuclei, while lower limb information is integrated in the gracillis nuclei. The second order fibers originating in the nuclei of the dorsal column decussate in the medulla, become part of the medial lemniscus, and finally synapse in the medial and lateral ventral posterior nuclei of the thalamus. Additional somatosensory and proprioceptive information is carried in the spinocerebellar tracts, which synapse in the cerebellum and help regulate motor output [294]. The spinothalamic tract, primarily response for transmitting the sensation of pain, also conveys temperature and crude touch [294].

Once somatosensory signals reach the ventral posterior lateral nucleus, they are sent to areas responsible for sensory perception. In somatosensory cortex, these include Brodmann areas 3a, 3b, 1, and 2. Area 3b is considered primary somatosensory cortex, while proprioceptive information travels to area 3a and area 2. Areas 1 and 2 also receive tactile

cutaneous input. Up through area 3b, the particular sensory images encoded by the touch receptors in the skin are maintained, but as information flows to higher-order cortical areas. For instance, secondary somatosensory cortex, which is located in the parietal operculum, and posterior parietal cortex, uses sensory information to inform cognitive (what object is this?) and motor activities (how should I manipulate this object?). Additional cortical areas activated during touch include BA5 and BA7 in the posterior parietal cortex and insular cortex, which are important for integration and multisensory processing [3]. Orbitofrontal cortex, important for reward and emotion pathways, is activated as well during touch of the hand, highlighting the multifaceted downstream processing of touch [3].

In summary, the cortical circuitry required for effective sensory and motor function is multifaceted and spans many cortical regions.

1.11 Related publications and presentations

Caldwell DJ, Ojemann JG, Rao RPN, "Direct Electrical Stimulation in Electrocorticographic Brain-Computer Interfaces: Enabling Technologies for Input to Cortex", Frontiers in Neuroscience, Neuroprosthetics, In revision, 2019.

Chapter 2

GENERAL METHODS AND BACKGROUND USED THROUGHOUT THE DISSERTATION

For all subdural grid electrode work, human subjects were implanted at Harborview Medical Center (Seattle, WA), with electrocorticographic (ECoG) grids (platinum contacts, 2.3 mm exposed diameter, 10 mm spacing, Ad-tech Medical, Racine, WI, USA) for acute clinical monitoring of intractable epilepsy prior to surgical resection (Figure 2.1). ECoG grid placement were determined solely based on clinical needs without consideration of research benefits. We conducted all stimulation studies after subjects were back on their anti-epileptic medications, after approximately one week of clinical monitoring. All patients gave informed consent under a protocol approved by the University of Washington Institutional Review Board.

For work involving deep brain stimulator patients, human subjects were chronically implanted at the University of Washington Medical Center (Seattle, WA), with Medtronic, St. Jude, or Boston Scientific leads for treatment of Parkinson's disease, Dystonia, or Essential Tremor. During the course of our intraoperative work, they were implanted with 8 contact subdural strip electrodes (1.8-2.3 mm exposed diameter, 10 mm spacing). A Cadwell clinical system (Cadwell, Kennewick, WA, USA) was used for somatosensory evoked potential (SSEP) and motor evoked potential (MEP) testing, as the TDT system was not capable of generating the required output current to consistently elicit responses.

2.1 Cortical Reconstructions

We performed cortical reconstructions (e.g. Figure 2.1) using previously described techniques [29,113,290]. In brief, we co-registered the electrode locations as localized by a post-operative CT scan with a preoperative MRI of the brain to build patient specific models.

2.2 Data Acquisition and Stimulation

Neural data were acquired using a Tucker Davis Technologies (TDT) System 3 with the RZ5D and PZ5 Neurodigitizer (Tucker Davis Technologies, Alachua, Florida, USA). The particular sampling frequency depended on the experiment, ranging from 1227 Hz to 48828 Hz. The highest sampling rates possible given then number of recorded channels and hardware limitations were used for any experiment involving stimulation to best capture the artifact pulses. We delivered stimulation through the TDT IZ2H-16 stimulator and LZ48-400 battery pack (Tucker Davis Technologies) with biphasic, bipolar, constant current stimulation trains for epilepsy patients, and monophasic bipolar constant current or constant voltage trains for DBS patients.

2.3 Determination of Sensory Cortex in Epilepsy Patients

In order to localize sensory cortical regions in epilepsy patients, we first consulted the clinical notes of the epilepsy monitoring team at the hospital. Based off of any prior clinical sensory mapping, we decided on a subset of the cortical electrodes to test for sensory percepts.

2.4 Determination of Sensory and Motor Cortex in DBS patients

In order to localize sensory cortical regions in DBS patients, we performed SSEP screening using a Cadwell clinical system. Once the electrode strip was placed, we used the phase reversal technique during median nerve stimulation to locate the central sulcus [52], from which we have knowledge of the different cortical regions covered by particular strip electrodes.

2.5 Haptic Stimulation

We applied haptic feedback with digital touch probes (Karolinska Institute, [61]), and our own custom analog touch probes, that time stamped the deflection, and touched the cutaneous region where subjects localized the DES percepts. Characterization of the digital touch probes is discussed in Chapter 5, and analog probe characterization is discussed in Chapter 6. An audio signal presented to the researcher via headphones but which is inaudible to the subject, cues the experimenter to apply the haptic feedback. During experiments where we conduct both DES and haptic stimuli, the subjects are blindfolded to avoid any confounders from simultaneous visual processing.

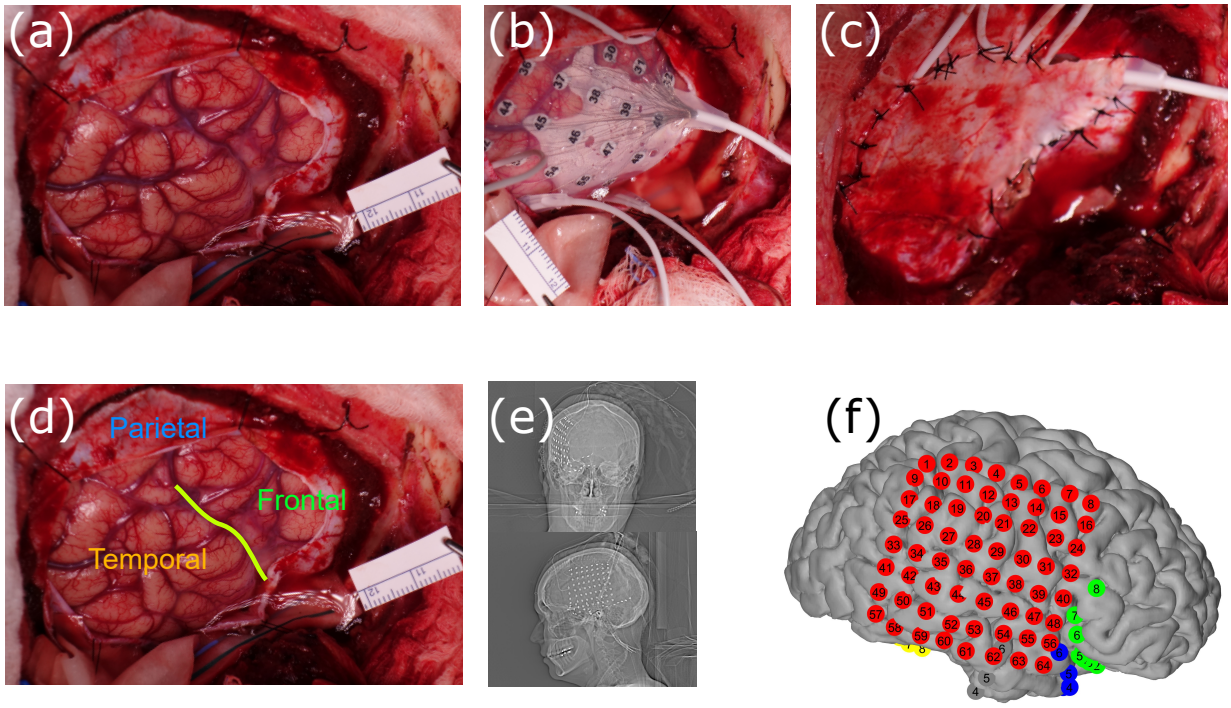

Figure 2.1: Subject implanation, cortical reconstruction, and electrode registration. (a) Craniotomy window prior to electrode implantation. The dura has visibly been cut, and the cortical surface is covered by the arachnoid and pia mater. (b) 64 contact electrode grid placed subdurally. (c) Dura sewn (d) Cortical regions, as well as the approximate location of the central sulcus indicated. (e) CT image illustrating the electrode grid after implantation. (f) 3D Reconstructed cortical surface with electrode locations, using preoperative MRI scans and the postoperative CT images.

Chapter 3

THE MACROSCOPIC RESISTIVITY OF THE HUMAN BRAIN

Current flow in the brain is controlled both by the anatomy, and by the associated electrical resistivity of its three components: cerebrospinal fluid (CSF), gray matter, and white matter. This is called volume conduction. Volume conduction applies both to the current flow due to neural activity and to the current flow from electrical brain stimulation. Comprehending it is essential for understanding how the neural sources inside the brain are observed through measurement techniques such as EEG, ECoG, and MEG. An understanding of volume conduction is also essential for modeling stimulation the brain using internal and external (transcranial) electrodes and using pulsed magnetic fields.

We report here measurements of the propagation of bipolar current pulses from DES made using clinical ECoG grids in humans being monitored for epilepsy. We stimulated between a pair of electrodes in an ECoG grid and recorded the resulting voltage waveforms across the entire grid. Because the resistivity values of the three components are different, the value of the resistivity that you measure will depend on the electrode locations. For example, if the electrodes are very small and very close together and inside a single component of the brain, then you will measure the resistivity of that component. In the case of separations on our clinical electrode scale, the apparent resistivity is measured, which summarizes the resistivity with contributions from all of individual constituents. For two-point measurements, the apparent resistivity is dominated by the spatial region near the stimulation electrodes. Such two-point measurements have been called spreading resistance, constriction resistance, and contact resistance. Our two-point measurements yield a single resistivity value for each pair of stimulation electrodes, with contributions from both the sample resistance between the

electrodes and the contact resistance. For three-point measurements, the apparent resistivity contains contributions from the spatial regions near all three electrodes. For four-point measurements, the apparent resistivity contains contributions from the spatial regions near all four electrodes and from the regions joining them where current flows. Our four-point measurements yield a distribution of resistivity values that depend on the locations of the stimulation electrodes and the recording electrodes.

We find our measurements are described qualitatively very well by two simple analytical models for a volume conductor with an apparent resistivity. We compare our measurements with two simple models and find qualitative agreement with both. The first model is a flat semi-infinite homogeneous isotropic resistivity half space. The second is a homogeneous isotropic resistivity sphere. Both models are simplifications of the brain's geometry, but by studying simpler geometries we can gain insight into the principles of volume conduction in the brain. We additionally compared our two models with resistivity values calculated using the two-point method, and find that the two-point method fails to accurately measure the resistivity of the brain. As far as we know, our measurements are the first direct macroscopic measurements that show the brain can be qualitatively modeled as a simple volume conductor without considering the detailed anatomy. They are also the first measurements in humans with two-point, three-point, and four-point measurements.

3.1 Introduction

How does current flow in the brain? This is an essential question for the analysis of both current injection through stimulation as well the currents resulting from neural activity. The macroscopic constituents of the brain: cerebrospinal fluid (CSF), gray matter, and white matter, as well as the anatomy affect this flow of current which is called volume conduction. The resistivity of the medium between the neural sources of interest and our recording modalities, such as ECoG, EEG, MEG, and penetrating arrays of electrodes, affects the signal

we measure and the corresponding source modeling problem. Our methods of stimulating the brain, which include DES of the brain using internal electrodes, stimulation through external (transcranial) electrodes, as well pulsed magnetic fields (transcranial magnetic stimulation, or TMS), also involve current flow through a resistive medium. Neuroscientists and engineers across many spatial scales and modalities are therefore concerned with the resistivity of the brain and its various layers.

Despite the importance of the resistivity, there are a range of measurements in the literature for CSF, gray matter, and white matter. For instance, CSF at room temperature has been measured to have a resistivity of 0.690 ohm-m, but 0.559 ohm-m at body temperature using current injection and voltage measurements between 10 Hz-10 kHz [19]. In-vivo measurements with a monopolar needle electrode suggest a value of 0.8 ohm-m [148]. Using finite-difference time-domain simulations, CSF, gray matter, and white matter were calculated to have resistivites of 0.479, 1.92, and 3.33 respectively [283]. The same study, using electric properties tomography determined CSF, gray matter, and white matter to have resistivities of 0.5714, 1.449, and 2.564 ohm-m respectively [283]. Using implanted depth electrodes, focal electrical current injection using 50 kHz signals found gray matter with a resistivity of 3.85 ohm-m, and white matter with a resistivity of 5.88 ohm-m [141]. A compilation of values in Paul Nunez's book on electric fields in the brain lists CSF with a resistivity of 0.64 ohm-m, gray-matter with 2.3 ohm-m at 5 kHz, 3.5 ohm-m at 5 hz, and white matter on average with 6.5 ohm-m [207]. White matter is known to demonstrate anistropy, where measurements made in cats illustrate white matter to have a $5-9\times$ greater resistivity in the transverse direction relative to the longitudinal direction [215, 226]. This in total points to the variety of values obtained using different measurement techniques, and motivates exploration in-vivo with humans.

Using a variety of techniques, such as two-point and four-point measurements, which are commonly used in the semi-conductor [184] and geophysics fields, the resistivity of a material

of interest can be probed. There are many factors which affect the measured resistivity, including the geometry of the sample, the arrangement of the probes, and the layering of materials with different resistivities. In our case, because the resistivity values of the three brain components are different, the value of the resistivity that you measure will depend on the electrode locations. For example, if the electrodes are very small and very close together and inside a single component of the brain, then you will measure the resistivity of that component. However, we have been unable find any published measurements that satisfy these conditions. This means that all such measurements will report an apparent resistivity which is a weighted average over the regions where the stimulation current flows.

We are interested in using the commonly used tool of DES through implanted intracranial electrodes to directly interrogate the cortical surface and the layers beneath.

Accurate characterization of different tissue resistivity parameters could also have implications for delineating epileptic from non-epileptic gray-matter tissue [141]. Similarly, the resistance of cortical tissue through has been characterized implanted depth electrodes (sEEG) [50]. Stimulation through depth electrodes with simultaneous scalp electroencephalography recording has also been performed to address the relative effect to which the brain has frequency dependent filtering characteristics [227].

We present our analysis of the data that we have collected on the DES of human brains in-vivo with the goal of providing insight into the apparent resistivity on the macroscopic scale. The volume of resistive material that is probed depends on the geometry of the electrodes used. As our minimum electrode spacing is one centimeter, we probe the resistivity on the centimeter and larger length scale. Due to the size of our electrode arrays compared to the size of the brain, our measurements probe the apparent resistivity rather than the true resistivity. This is because the brain is not a simple homogeneous medium. Because of this, the apparent resistivity that we measure, and that all previous in vivo studies have measured, depends on the anatomy and on the resistivity of the three components (cerebrospinal fluid

(CSF), gray matter, and white matter). We here focus on analyses considering the brain as a medium with an apparent resistivity (Figure 3.1(a)). As shown in panel (b) of Figure 3.1, current flows between our two stimulation electrodes, and we measure the voltages on the surface. We pursue two models. The first model is a flat semi-infinite homogeneous isotropic resistivity half space. The first model neglects finite size and shape corrections. The second model includes them. The second is a homogeneous isotropic resistivity sphere. The brain is neither flat nor a perfect sphere, but insights gained by studying the brain under simplifying assumptions help us understand the flow of current in the brain.

The geometry of the brain is inherently very complex (Figure 3.2), with sulci and gyri that result in a compicated geometry across which current must pass in cortical stimulation. For stimulation between electrodes with narrow spacing (Figure 3.2(c), blue lines) the majority of the current will flow through a simple geometric structure, while for larger spacings, the current flow path may be more complex (Figure 3.2(c), green lines).

3.2 Theory

This section summarizes the theory underlying resistivity measurements made using bulk samples. It contains the equations that we used to calculate our two-point resistivity values, three-point, and our four-point resistivity distributions from our measured voltages.

3.2.1 DC Flow Assumption

All of our analyses regarding three and four-point measurements are assuming a DC flow model [171], where the voltage at our measured time points is not changing. This allows us to ignore the time varying components of Maxwell's equations, and allows us to consider simple relations such as Ohm's law ($V = IR$).

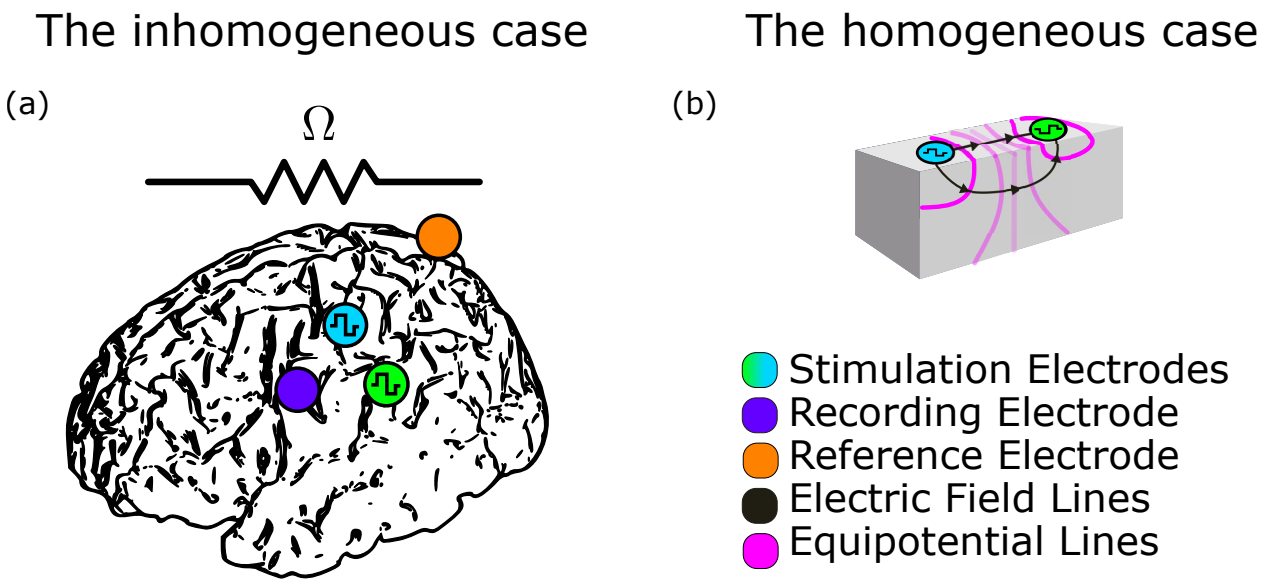

Figure 3.1: What is the resistivity of the human brain? (a) We here consider the simple case of where the brain is a resistive medium, with current injected at two electrode locations. Electrical stimulation of cortex results in charge injection which flows between a source and a sink electrode. Given how much current we inject, and the voltages we measure, what can we learn about the resistivity of the brain knowing that it has a complicated geometry and components of different resistivity? What we calculate is the apparent resistivity, which describes what the resitivity of the material measured would be if it were a homogeneous sample, and captures the geometry and composition of the various layers. (b) In the case of bipolar electrodes, all of the current flows between two electrodes. The electric field lines are everywhere perpendicular to the equipotential lines. We measure voltages all of the other electrodes in the array. The current follows the path of least resistance. Because the structure of the brain is inhomogenous and the conductivities of the components are different, the current flow is tortuous. (See Figure 3.2 for example flows overlaid on a patient's brain).

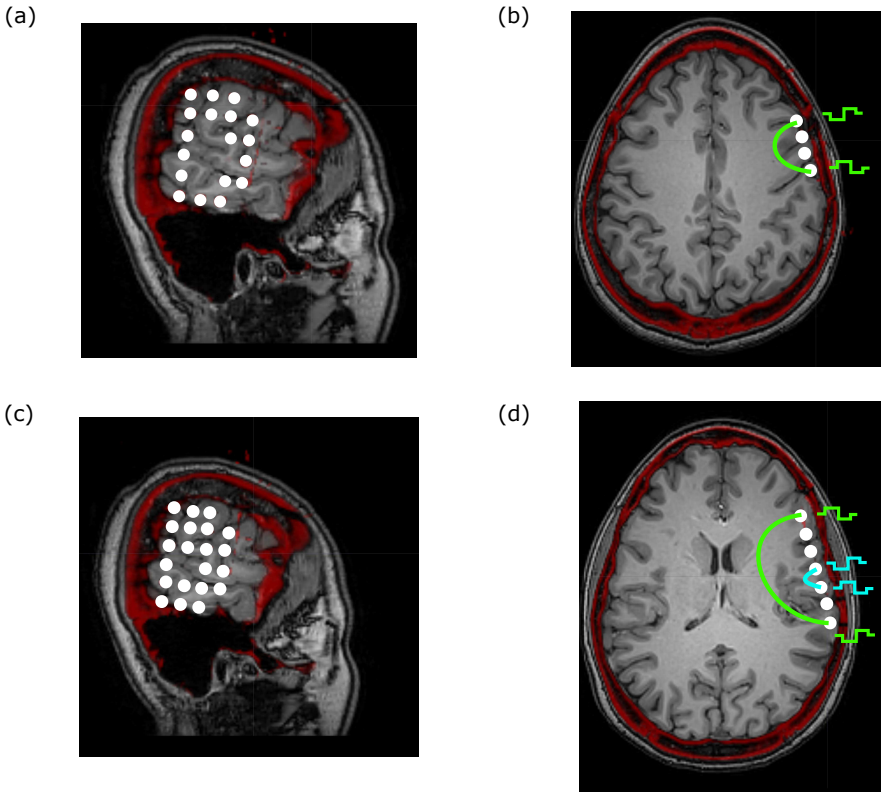

Figure 3.2: Example co-registered patient CT and MRI with current flow paths. Here we show one of our patients with their posteroperative CT and preoperative MRI co-registered, and highlight the complicated geometry that current must flow through between the two electrodes. Panels (a) and (c) highlight a sagittal view through the brain. White dots represent electrode locations as visualized in the CT. Panels (b) and (d) are the corresponding axial planes for panels (a and (c). Of note is that the overall shape brain on the larger scale could be considered spherical or ellipsoidal, while on a local scale there are the complicated folds of the gyri and sulci. In panels (b) and (d) we highlight two potential current paths through the cortex, depending on the separation of the stimulating electrodes. With greater separations, the depth of penetration increases, and there are varying layers of gray, CSF, and white matter depending on the path. In panel (d), it appears as if this set of electrodes lies on a flat line. Therefore, one could question what the best geometric model would be for these electrodes. A flat half-space fits the electrode positions well, but ignores the global geometry of the brain. However, the electrodes would not lie perfectly on any sphere. Therefore, we consider both spherical and flat models to test how assumptions about geometry affect our results.

3.2.2 Point, Constant Voltage, and Constant Current Electrodes

The principles of superposition hold generally for point electrodes and constant voltage electrodes [171]. They do not hold for constant voltage electrodes. The analytic solution to Laplace's equation for multiple constant voltage electrodes on the surface of a half-space of uniform resistivity material is extremely complicated. The boundary conditions are mixed: constant voltage boundary conditions apply under the two electrodes and constant normal derivative (zero current) boundary conditions apply everywhere else on the surface. However, a pair of circular constant voltage electrodes separated by a center-to-center distance d that is large compared to their radius a can be well approximated by the standard formula of $R_2 = \frac{\rho}{2a}$, with an error of less than 0.1% for our application. [143]. We use constant current stimulation, but we assume due the excellent electrical conductivity of platinum that the voltages are close to constant across the electrode during our long stimulation pulses (1.2 ms/phase).

Using previously published formulas for constant current electrodes on a homogenous semi-infinite substrate [222], constant current electrodes [171], and point electrodes [302], we calculated the theoretical voltages on the surface of a uniform half-space as a function of distance from the stimulating electrodes (Figure 3.3). At a distance of 2 electrode radii away, the models become indistinguishable, and all decay with an A/d, where d is the distance from the electrode, with the same value of the constant A. All of our arrays have electrodes with separations of 8.6 electrode radii, and therefore, we use point electrode models for all of our analytic models for computational simplicity with minimal error.

During our long stimulation pulses, we assume that the current density is no longer sharply peaked, as we are on the order of one time constant for the electrode-tissue interface. [21]. To estimate the time constant τ for our stimulation electrodes, we assume a conductivity of 1.5625 $\frac{S}{m}$ for CSF in contact with the platinum electrode, a disk of radius 0.00115 m, and a conservative γ of 2.1 $\frac{F}{m^2}$ for the pseudocapacitance of platinum [181]. The access resistance

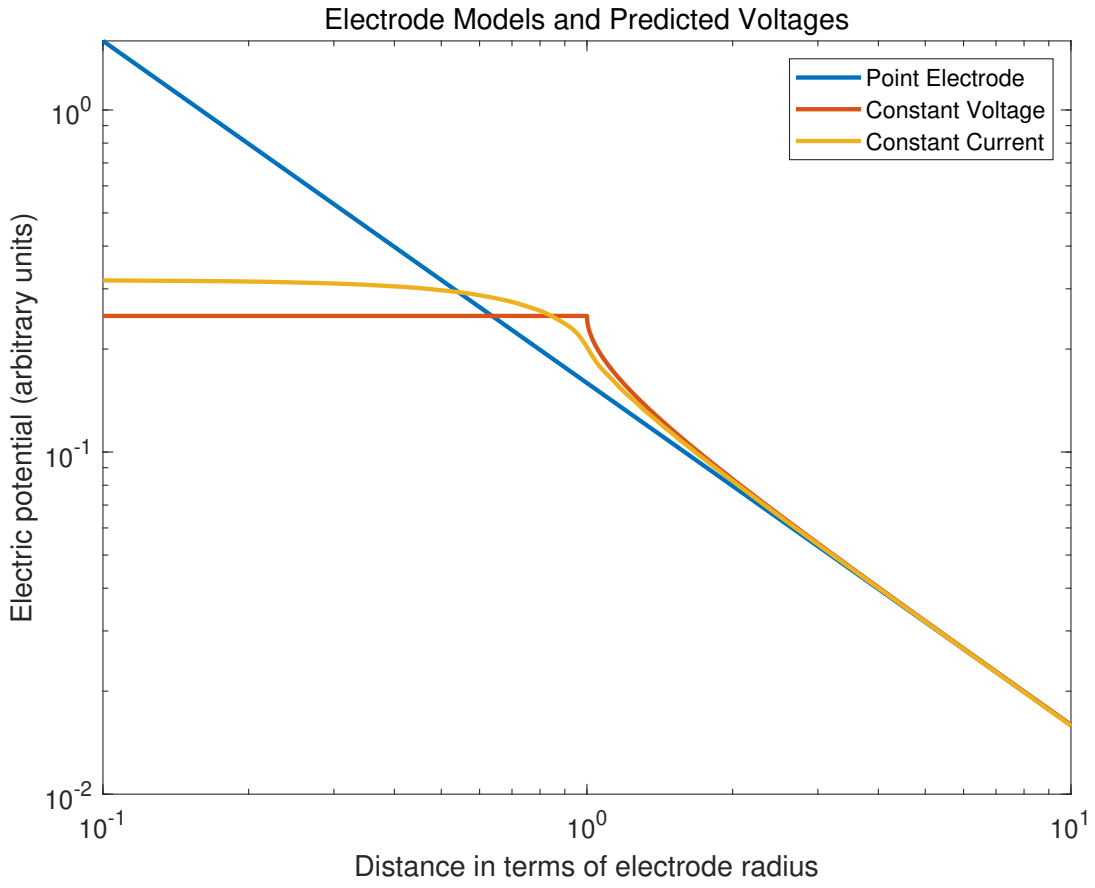

Figure 3.3: Point, constant voltage, and constant current electrodes. We calculated the theoretical voltage on the surface of a uniform half-space for all three cases. There are substantial differences within the electrode radius, but after approximately 2 electrode radii, the models predict similar voltages. They all fall off like A/d, where d is the distance from the electrode, with the same value of the constant A. As all of our data points are acquired more than 8.6 radii away, we have point electrode models in our analysis.

$R_s = \frac{1}{4\kappa a}$ is then 139.1304, and the double layer capacitance $C = \gamma\pi a^2 = 8.7250\text{e-}06$ [21]. This yields $\tau = 0.0012$. Therefore, for a pulse phase width of 1.2 ms, we are on the order of one time constant.

3.2.3 Resistance Measurements Made on Bulk Samples

In resistance measurements on bulk samples, a voltage is applied to two contacts on the sample and the resulting current is measured, or vice versa [76]. To convert the measured resistance into the resistivity of a homogeneous isotropic resistive sample, or into the apparent resistivity of an inhomogeneous isotropic resistive sample, requires the detailed spatial structure of the sample and the location of the electrodes. In the next sections, we first discuss the apparent resistivity, as well as the necessary equations for converting resistance measurements made on semi-infinite bulk samples and on spherical samples using two point (only for the semi-infinite bulk samples), three-point, and four-point measurements and four-point measurements (both semi-infinite and spherical).

3.3 The Apparent Resistivity

For a half space composed of any number of uniform thickness and uniform resistivity layers, the equation for the voltage on the surface has the same form as that for the same electrode configuration on a uniform resistivity substrate with the value of the resistivity ρ for the uniform resistivity substrate replaced by an apparent resistivity ρ_a. The apparent resistivity depends on the paths that the current takes, which depend on both the geometry and the resistivities of the various layers. It is the appropriate average over all paths.

Apparent resistivity is the basis for geological resistivity prospecting [302]. For example, for a two-layer earth, when the electrodes are very close together, the current penetration is very shallow and the apparent resistivity is equal to the resistivity of the top layer. When the electrodes are very far apart, the current penetration is very deep and the apparent

resistivity is equal to the resistivity of the bottom layer. In between, it is the appropriate average over the paths. In general, for a uniform resistivity substrate, the 50% penetration depth is about one half of the spacing between the two stimulation electrodes. [302] For geological resistivity prospecting, the separation between the current electrodes is varied and the apparent resistivity is measured. From these measurements, the composition versus depth can be determined.

Because the brain is layered, any measurements of the resistivity of an intact living brain will measure an apparent resistivity unless the electrodes are very close together. In humans, the thickness of the gray matter is about 3.5 mm, so to measure the resistivity of the gray matter without seeing the white matter using a four-point probe would require the entire electrode array to be sub-millimeter in size. Our clinical ECoG grids have an electrode spacing of 1 cm. Consequently, the focus of this paper is on determining the apparent resistivity of the human brain on the macroscopic scale. In our measurements, there is an additional issue due to the presence of CSF with unknown thickness between the clinical grid and the surface of the cortex during our measurements.

3.4 Flat vs. Spherical Models

The brain is often modeled as a spherical object [200], but on the scale of an array of ECoG electrodes, what is the local topography? We analyzed our data using two models (Figure 3.4(a,b)). The first model is a flat semi-infinite homogeneous isotropic resistivity half space, which neglects finite size and shape corrections. The second is a homogeneous isotropic resistivity sphere, which includes is both a finite size and takes into account the problem's geometry. Of course, the brain is neither flat nor a perfect sphere. However, by studying the predicted voltages and calculated resistivities under different simplifying assumptions, we can better understand the macroscopic characteristics of the brain.

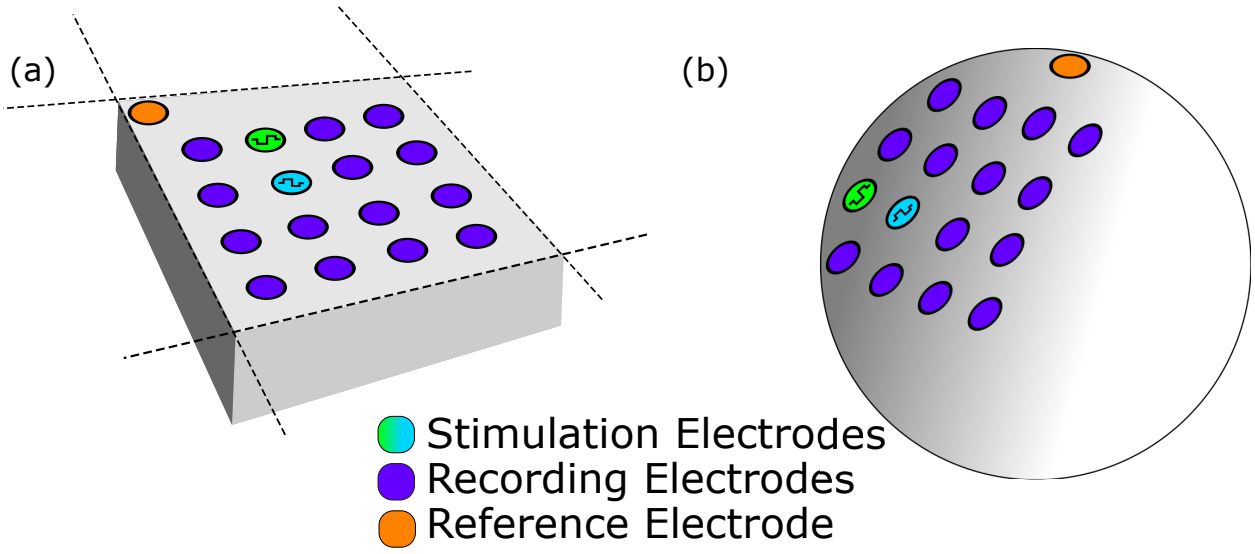

Figure 3.4: Flat and spherical models. We analyzed the data using two models. We applied current controlled bipolar stimulation pulses between two electrodes and measured the resulting voltages between all of the recording electrodes an a "distant" reference electrode. For our electrode diameters and separations, the voltages can be described well using point electrodes, as shown in Figure 3.3. (a) The first model is a semi-infinite homogeneous isotropic resistivity half space. (b) The second model is a homogeneous isotropic resistivity sphere. Here, there is an additional parameter which is the radius of curvature for a sphere, which we estimated from the subjects' individual brains. We found that these two models produced different apparent resistivity values despite both fitting the measured data well, which means that the global geometry of the problem has significant effects in interpreting the resistivity values calculated.

3.4.1 Two-point Measurements and Electrode Resistance

For a constant-voltage ohmic electrode on the surface of half-space of uniform resistivity material (with infinity held at zero potential), the steady-state voltage and current are related by Ohm's law $V = IR$ and the electrode resistance is defined to be $R = V/I$. For circular electrodes with radius a, the resistance is related to the resistivity of the material by $R = \frac{\rho}{4a}$ [76, 204]. For two identical well separated electrodes, the resistance between them is twice that for a single electrode $R_2 = \frac{\rho}{2a}$ [76]. These equations are routinely used to measure the resistivity of bulk semiconductors. This measurement technique is subject to contributions from both the contact resistance and resistance of the material between the probes [184], and hence careful consideration of the electrode properties are required.

However, because of the capacitance of metallic electrodes on the surface of the brain, the above relation does not apply under steady state conditions due to the time-dependent charging of the double-layer capacitance. However, it does apply under constant current pulse conditions before the electrodes start to charge. We determined the electrode resistances by extracting the voltage jump at the onset of the stimulation and dividing it by the applied current [124].

We calculated the apparent resistivity values for each subject using our measured electrode resistances by solving for ρ, yielding $\rho = 2aR$.

In order to extract the two-point resistivity, we first have to calculate the jump voltage, which is the first part of the curve in Figure 3.5(b). This jump voltage represents the voltage required to drive the constant current stimulation through the electrode-tissue interface resistance.

3.4.2 Three-Point Measurements Made on Homogeneous Flat Bulk Samples

For a pair of constant current point electrodes on the surface of a half space with uniform resistivity, the voltage everywhere on the surface is given by superposition

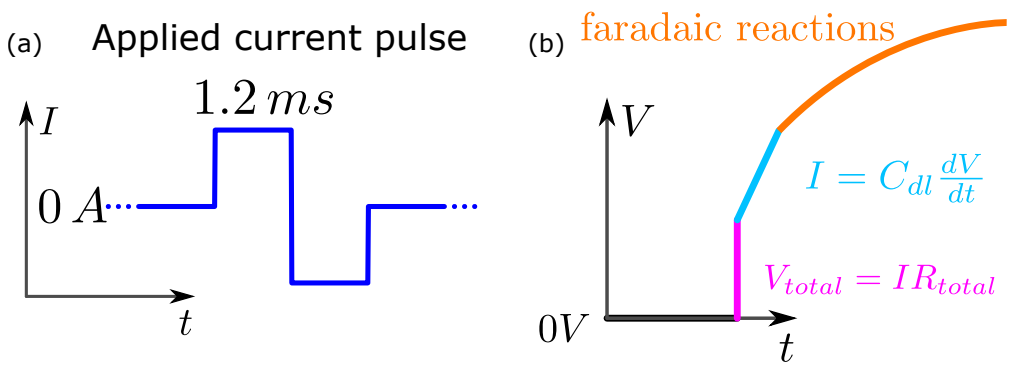

Figure 3.5: Constant current stimulation and resultant stimulation voltage waveform. (a) We apply a constant current biphasic, bipolar stimulation pulse, with an example pulse width of 1.2 ms (b) The voltage applied to drive a constant current stimulation pulse has three primary components, which include an immediate electrode jump resistance, charging of the double layer capacitance, and Faradaic reactions. In an ideal world, we can determine the total resistance of the sample beneath the electrode from the initial voltage jump, and subsequently the 2-point resistivity. However, as outlined in the results, the 2-point method with clinical ECoG electrodes does not result in the correct resistivity as assessed through a saline phantom.

$$V(r) = \left(\frac{\rho\, I}{2\pi}\right)\left[\frac{1}{r_a} - \frac{1}{r_b}\right]$$

here V is the measured voltage, I is the applied current, r_b is the distance between the first current source and the point where the voltage is measured, and r_a is the distance between the second current source and the point where the voltage is measured. Again this voltage is measured relative to infinity. For the one-layer case with point-electrodes, the apparent resistivity ρ_a is equal to the true resistivity ρ.

3.4.3 Three-Point Measurements Made on Homogeneous Homogeneous Spherical Samples

The relationship between the voltage measured between two sense electrodes on the surface of a sphere and the current imposed between two source electrodes on the surface of the sphere was first worked out in a remarkable, now classic paper by Helmholtz in 1859 [92]. It is given by [94]

$$V = \frac{I\rho}{4\pi}\Big[\frac{2}{r_b} - \frac{2}{r_a} + \frac{1}{R}\ln\frac{r_a + R - a\cos(\beta)}{r_b + R - b\cos(\theta)}\Big]$$

Here I is the applied current

V is the measured voltage

r_b is the distance from the sense electrode to the first stimulation electrode

r_a is the distance from the sense electrode to the other stimulation electrode

R is the radius of the spherical surface fit

β is the angle between the sense electrode and the first stimulation electrode, and

θ is the angle between the sense electrode and the second stimulation electrode.

We calculated the radius of the sphere to be the sphere that best fit the outer cortical surface for each subject, via linear least-squares fitting. In order to calculate the angles β and θ, we use the arc length formula

$$\beta = \frac{r_b}{R}$$
$$\theta = \frac{r_a}{R}$$

3.5 Distance Binning

In geoelectric prospecting and semiconductor characterization, the resistivity versus depth is determined by making measurements as the recording electrode spacing is increased [302]. Larger recording electrode separations probe deeper. This motivated us to extract the apparent resistivity versus electrode separation.

We divided the electrode separations into bins. Each bin was 1 cm wide. We calculated the distance from each recording electrode to the center of the stimulation dipole. The centers of the bins were at 1.5, 2.5, 3.5, 4.5, and 5.5 cm. We then fit all of the electrodes within each bin to determine the apparent resistivity, as described in the three-point homogeneous flat and spherical sections.

3.5.1 Four-Point Measurements Made on Homogeneous Flat Bulk Samples

The four-electrode method is the gold standard for making resistivity measurements. Its main advantage is that it is insensitive to inevitable variations in the contacts. For example, since our surfaces are not flat, the effective contact area can be smaller than the actual area of the contact. When this happens or the region under the contact is inhomogeneous, the contact resistivity will not be equal to $2aR$. However, by using constant current stimulation and measuring away from the stimulation electrodes, the voltages on the recording electrodes will be correct. They do not depend on the contact area. This is why the four-point electrode method works better for our measurements. Similarly to three-point measurements on a flat substrate, the voltage measured is a function of the applied current, resistivity, and distances

to each of the stimulation electrodes. The additional consideration here is the distance to two recording electrodes, rather than a single electrode. For four-point measurements on homogeneous isotropic flat bulk samples, the resistivity is related to the measured voltage difference between the two sense electrodes in terms of the current imposed between the two source electrodes by [184].

$$V = \frac{I\rho}{2\pi}\Big[\big(\frac{1}{r_1} - \frac{1}{r_2}\big) - \big(\frac{1}{r_3} - \frac{1}{r_4}\big)\Big]$$

where r_1 is the distance from the first source electrode to the first sense electrode,$r_2$is the distance from the second source electrode to the first sense electrode, r_3 is the distance from the first source electrode to the second sense electrode, r_4 is the distance from the second source electrode to the second sense electrode, I is the current, and ρ is the resistivity.

The most often used electrode configurations are linear and square. For finite size samples, there are correction factors that depend on the electrode configuration, spacing, and location and on the size and shape of the sample. In addition to the bulk equation above, there are well known results in the literature for parallelepipeds, disks, and cylinders that include the size and shape factors [184].

3.5.2 Four-Point Measurements Made on Homogeneous Spherical Samples

As mentioned in the section on three-point measurements on homogeneous spherical samples, the simple equation for spherical models can also be used for four-point measurements. The voltage at two points V_1 and V_2, where [1,2] represent two different points in space, is calculated

$$V_1 = \frac{I\rho}{4\pi}\Big[\frac{2}{r_{b1}} - \frac{2}{r_{a1}} + \frac{1}{R}\ln\frac{r_{a1} + R - a1\cos(\beta_1)}{r_{b1} + R - b1\cos(\theta_1)}\Big]$$

$$V_2 = \frac{I\rho}{4\pi}\Big[\frac{2}{r_{b2}} - \frac{2}{r_{a2}} + \frac{1}{R}\ln\frac{r_{a2} + R - a2\cos(\beta_2)}{r_{b2} + R - b2\cos(\theta_2)}\Big]$$

The difference between the voltage values V_1 and V_2 is used to generate a distribution of resistivities.

3.5.3 Three and Four-Point Measurements Made on Inhomogeneous Flat Bulk Samples

For the special case of three and four-point measurements on inhomogeneous isotropic flat bulk samples composed of parallel layers with constant resistivity values, the apparent resistivity that will be measured can be calculated in terms of the resistivity values, the thicknesses, and the arrangement of the layers. This relationship is the basis of vertical electrical sounding used to determine the geological layering underneath the surface of the earth [279] and of the three-point and four-point characterization of the layering of semiconductor materials [1, 2, 76]. The apparent resistivity is the ratio of the measured resistivity divided by the resistivity that would be measured for the same structure if it were homogeneous and isotropic with a resistivity equal to unity. However, the structure of the brain under our clinical ECoG grids does not consist of parallel layers with constant resistivity values so we simply present the distribution of apparent resistivity values that we measure.

3.5.4 Three and Four-Point Measurements Made on Inhomogeneous Spherical Samples

There have been many models of the brain made using concentric spheres with constant resistivity values. However, the structure of the brain under our clinical ECoG grids does not consist of concentric spheres with constant resistivity values so we simply present the distribution of apparent resistivity values that we measure.

3.6 Experimental Methods

3.6.1 Patient Characteristics for First Seven Patients

Our first seven subjects are summarized in Table 3.1, including the stimulation amplitudes used, the bipolar pairs used, the total number of stimuli during the session, and the duration

Subject	Stimulation Amps. (mA)	Pairs stimulated (-/+)	total # stimuli	Duration of session (minutes)
1	1.75	22/30	3001	16.43
2	0.75	13/14	10000	24.24
3	3.5	11/12	10005	45.14
4	0.75	59/60	7014	38.39
5	3	56/55	10590	44.17
6	2.5	54/62	7000	42.49
7	1.75	64/56	10000	37.00

Table 3.1: First seven subject characteristics. Table showing the subject number, the stimulation current, which were the pairs of electrodes stimulated (-, cathodal first, + anodal first), how many total stimuli were delivered, and the length of the session during which stimuli were delivered (minutes)

of the session. Our total stimulation durations ranged from 16.43 to 45.14 minutes. The locations of their stimulation electrode pairs are summarized in Figure 3.6. The general overlap of the electrodes is the same anatomic area (sensorimotor cortex). The individual stimulation and recording electrodes are shown in Figure 3.7. We have measurements from both hemispheres.

3.7 Eighth Subject Characteristics

For our eighth subject, we stimulated different sets of bipolar pairs with various separations. The electrode separations, stimulation currents, number of stimuli, and length of in each session are shown in Table 3.2, including the stimulation amplitudes used, the bipolar pairs used, the total number of stimuli during the session, and the duration of the session. The locations of the recording and stimulation electrodes are summarized in Figure 3.8.

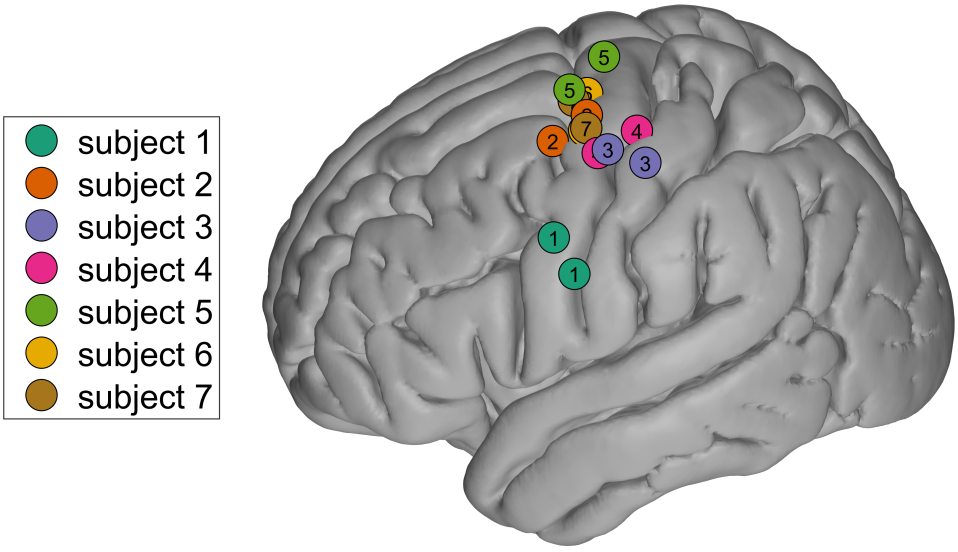

Figure 3.6: Subjects 1-7 stimulation electrode locations projected onto a common MNI brain. The locations of the stimulation electrodes are shown projected in common MNI coordinates onto the left hemisphere. Due to both post-operative brain shift and reconstruction error, these electrode locations are not exact. The electrodes are situated over sensorimotor cortex due to experimental design for a motor stimulation induced plasticity experiment.

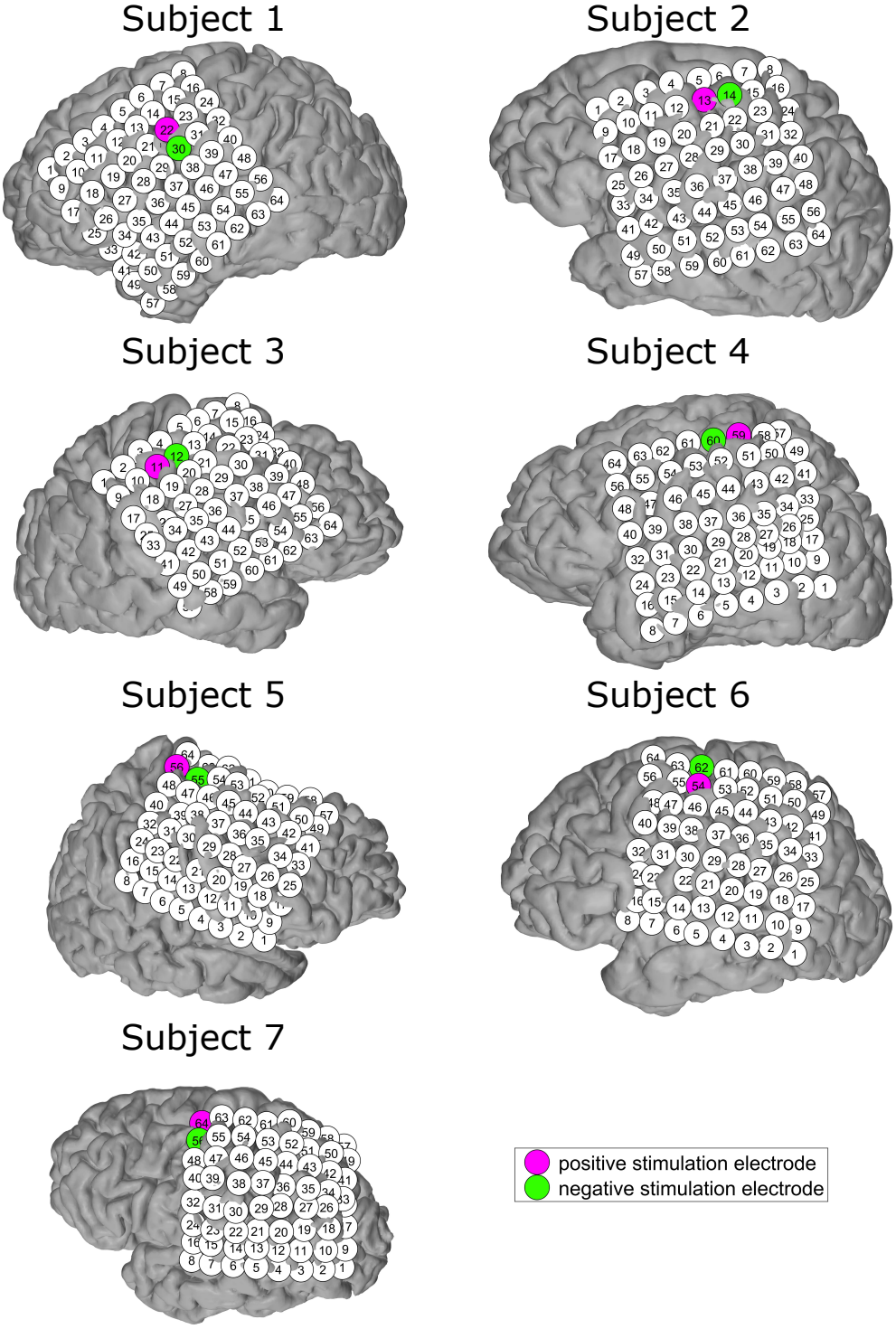

Figure 3.7: Individual stimulation electrode locations in subject specific space. The locations of the stimulation and recording electrodes in subject specific space following cortical reconstruction and CT/MRI co-localization are shown. Due to both post-operative brain shift and reconstruction error, the electrode locations are not exact.

Pairs stimulated (-/+)	Stimulation (mA)	Amps. total # stimuli	Duration of session (minutes)
3/4	0.5	10	0.11
4/3	0.5	10	0.11
4/12	0.5	10	0.11
12/4	0.5	10	0.11
5/7	0.5	10	0.11
7/5	0.5	10	0.11
12/13	0.5	10	0.11
13/12	0.5	10	0.11
11/14	0.5	10	0.11
14/11	0.5	10	0.11
10/15	0.5	10	0.11
15/10	0.5	10	0.11
9/16	0.5	10	0.11
16/9	0.5	10	0.11

Table 3.2: Characteristics of the eighth subject. Table showing the pairs of electrodes, the electrode separation the stimulation current, which were the pairs of electrodes stimulated (-, cathodal first, + anodal first), how many total stimuli were delivered, and the length of the session during which stimuli were delivered (minutes)

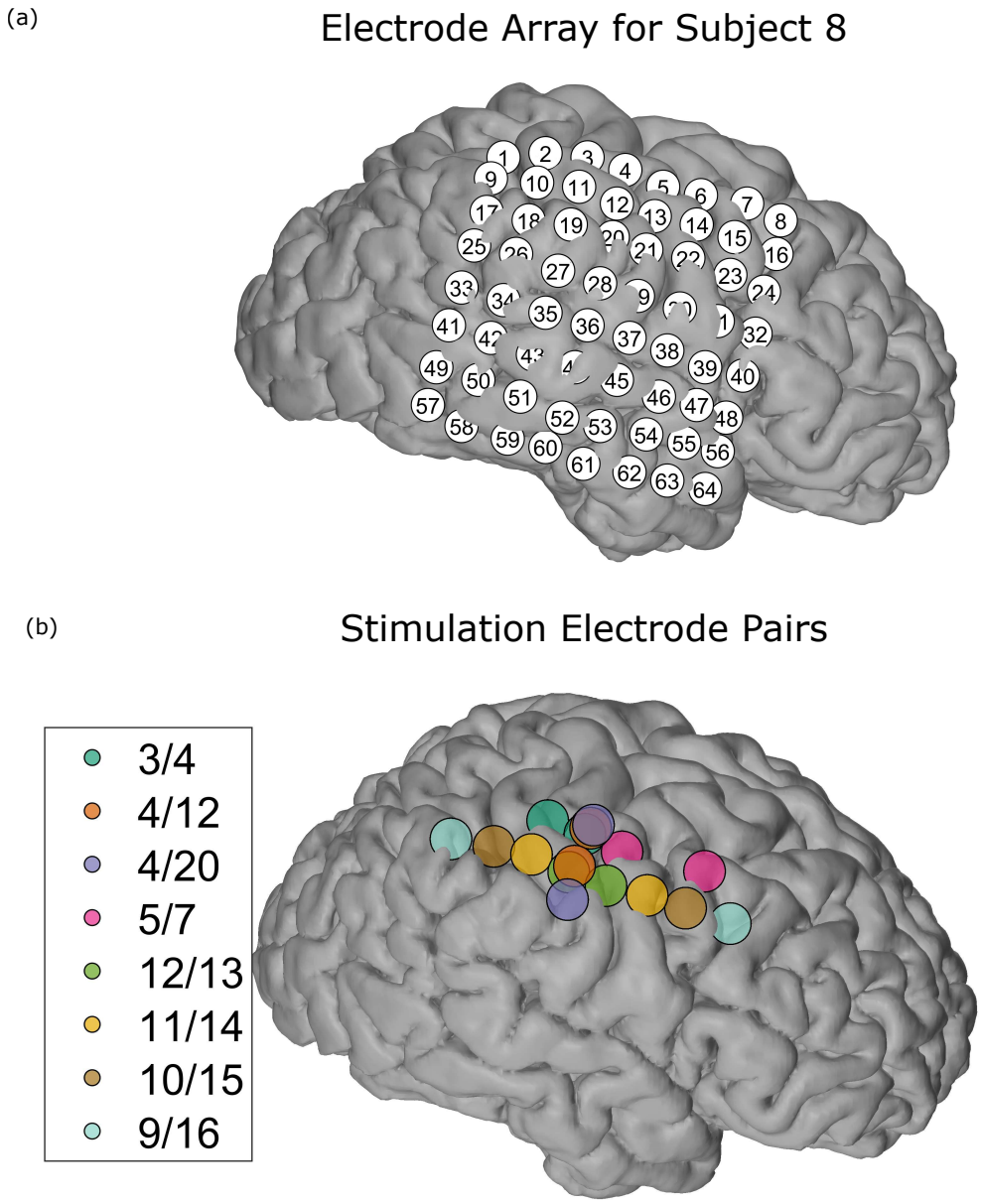

Figure 3.8: Eighth subject recording and stimulation electrode locations. (a) The 64 contact electrode array for subject eight covers the right hemisphere, shown here in subject specific space. (b) The locations of the stimulation electrodes for different pairs and separations are shown projected in subject specific space. There has been slight jitter added to show the overlapping pairs of electrodes. Due to both post-operative brain shift and reconstruction error, these electrode locations are not exact. We have varying separations of stimulation electrodes, which results in varying amounts of current penetration to different depths.

3.8 Data Acquisition

Our data was acquired at 12 kHz. We delivered biphasic, bipolar, constant current stimulation stimulation pulses. The length of each phase was 1.2 milliseconds (ms). The voltage delivered to the stimulation electrodes during constant current stimulation was also measured using the TDT.

During each stimulation pulse, the stimulation artifact voltages were measured for all of the electrodes that were not stimulated. These "artifacts" are our signals. For example, Figure 3.9 shows what they look like for subject 3, with each channel scaled individually. In Figure 3.10, we show the signals with the same scale to highlight the falloff in the recorded voltage as the distance from the stimulation electrodes increases.

See the Section A, Figures A.1– A.6, A.8 for additional subjects, including an example (Figure A.8) from one of stimulation electrode pairs for subject eight. We do not discard any channels from analysis based on the waveform shape for the results in the body of this work, but removing waveforms which do not look like they match the expected fall off in voltage or switch in polarity does not substantially change our results for the first seven subjects (See Appendix Table A.2). For the first seven subjects, we removed any local, time varying DC offset by subtracting the average time period from 25 ms to 5 ms before the stimulation pulse begins. Due to the lower stimulation frequency (1 Hz) of the eighth subject, rather than the first seven subjects which ranged from 2 to 20 Hz, we performed no DC offset correction, as the signal reliably returned to near zero between each stimulus.

To calculate the resistivity values, we developed an algorithm to extract the flat section of the voltage pulses, under which our DC flow conditions hold. Briefly, we average all of the recorded pulses, and then use Z-score thresholding of the entire averaged epoch to detect the onset and offset of each stimulus pulse. We then detect the transition point as the stimulus waveform switches polarity, and subsequently shift our start and end indices by a fixed number of samples to ensure we are inside the flat waveform regime. We then use

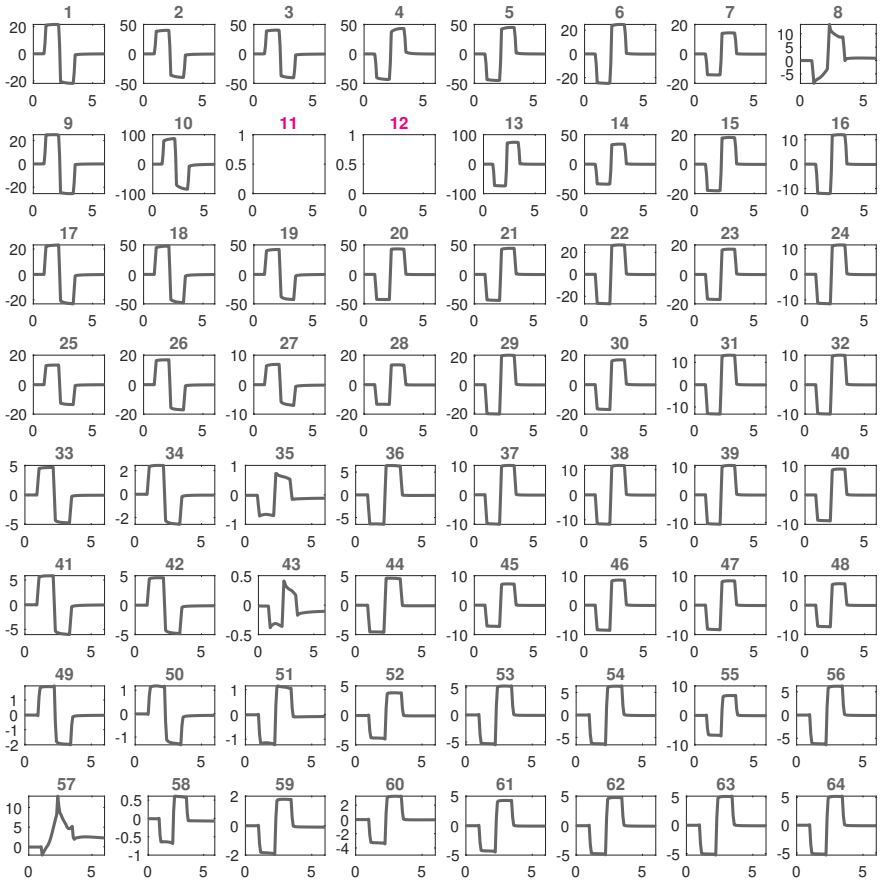

Figure 3.9: Average recorded waveforms for subject 3. We see fast rise times to generally flat voltages across the majority of the array, which indicates that the effects are dominated by the resistance of the sample, rather than capacitive effects. It is from these flat voltages that we extract our signals for the resistivity calculations. A subset of channels, including channel 8, 43, and 57, demonstrate unexpected shapes, with edge transients that are suggestive of a phenomena such as capacitive coupling. The x-axis units are in milliseconds, while the y-axis units are in millivolts. The stimulation channels are represented by the blank channels. The channels not included in supplementary analysis (57) are shown in Table A.1. Discarding this did not change the resistivity values appreciably, as shown in Table A.2.

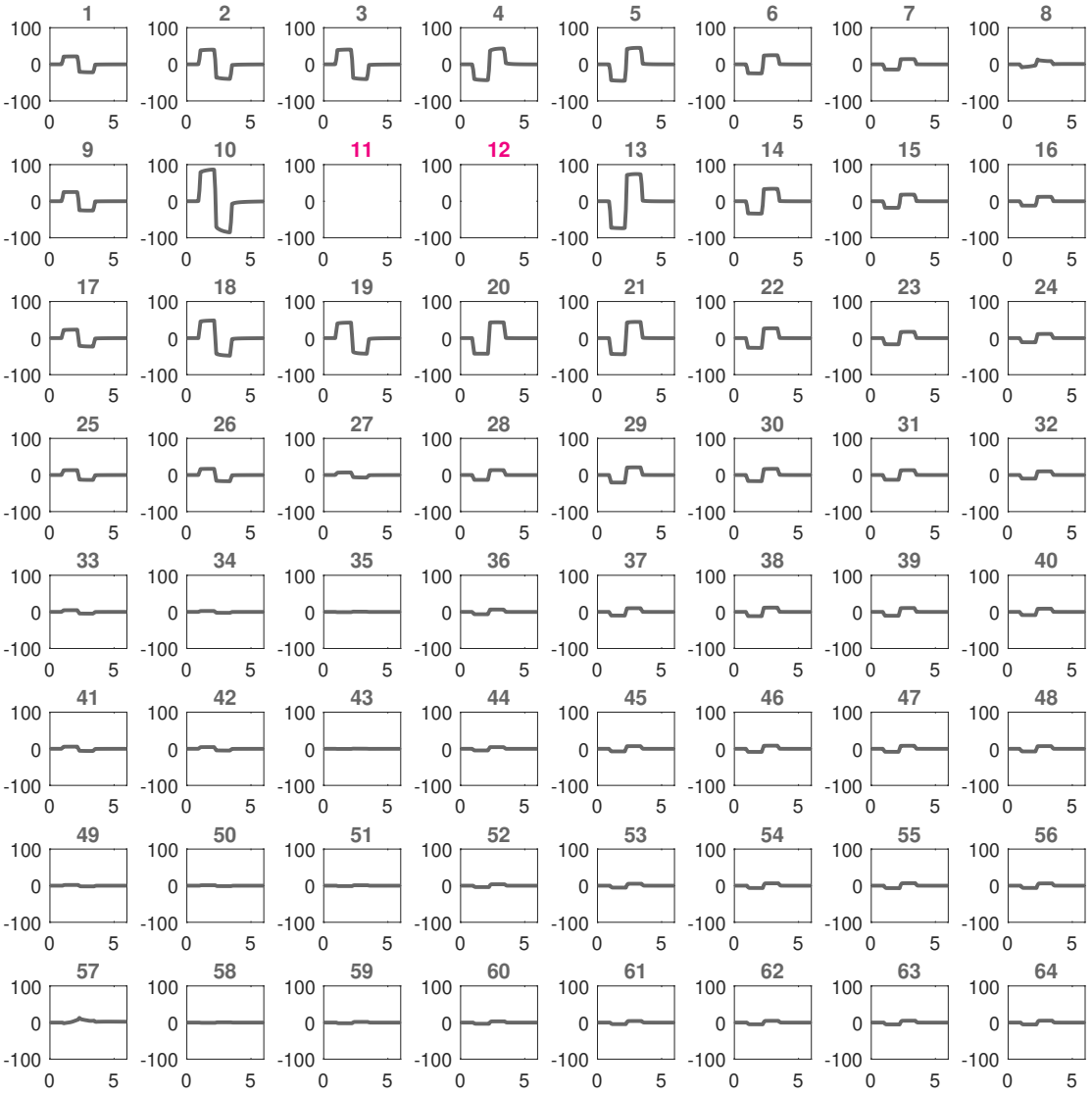

Figure 3.10: Average recorded waveforms for subject 3 with the same y-scale. We note a drop off in the recorded amplitude as the distance increases from the stimulation electrodes, indicative of current propagation in a resistive medium from bipolar stimulation.

these start and end indices on a single trial basis to extract a subset of points over which the voltage changes little. We then average across each trial to calculate the mean voltage, and calculate the standard deviation across these mean voltages for each trial (Figure 3.11).

The means and standard deviations for the recorded voltages for our subjects during stimulation are highly reproducible (Figure 3.12 shows the data for the first seven subjects). Qualitatively, the voltages are highest near the stimulation electrodes, and smaller further away. In the appendix, we show the means and standard deviations for the eighth subject (Figure A.7). Both polarities of stimulation agree well with one another, which is expected.

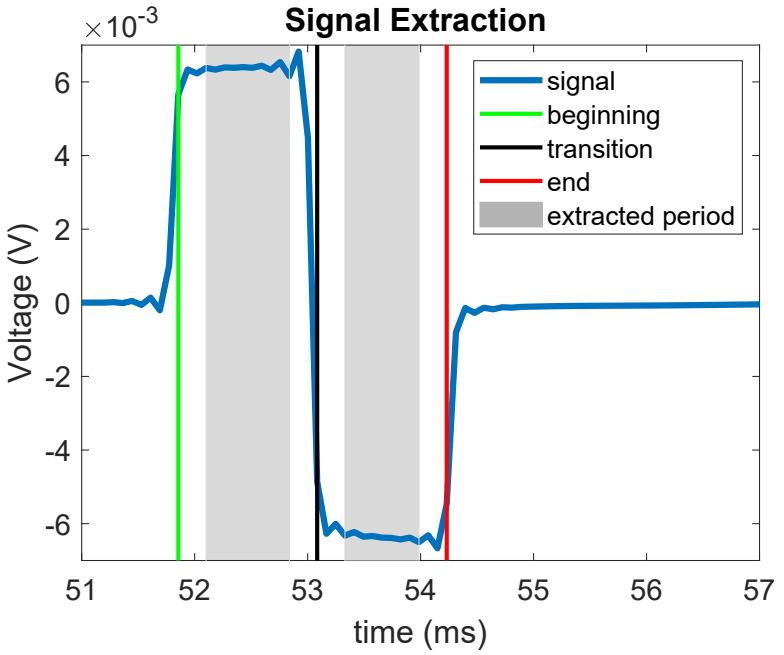

Figure 3.11: Algorithm for data extraction. In order to extract a voltage value that we could use for our DC flow model, we needed to ensure that we were extracting values over a relatively unchanging period in the middle of each phase. We calculated the magnitude of the stimulation artifact by determining the onset and offset times of each phase of stimulation, and avoided the edge transients to obtain a reliable voltage measurement. By excluding the variable regions during changes in the applied current, we extracted flat, consistent voltage values.

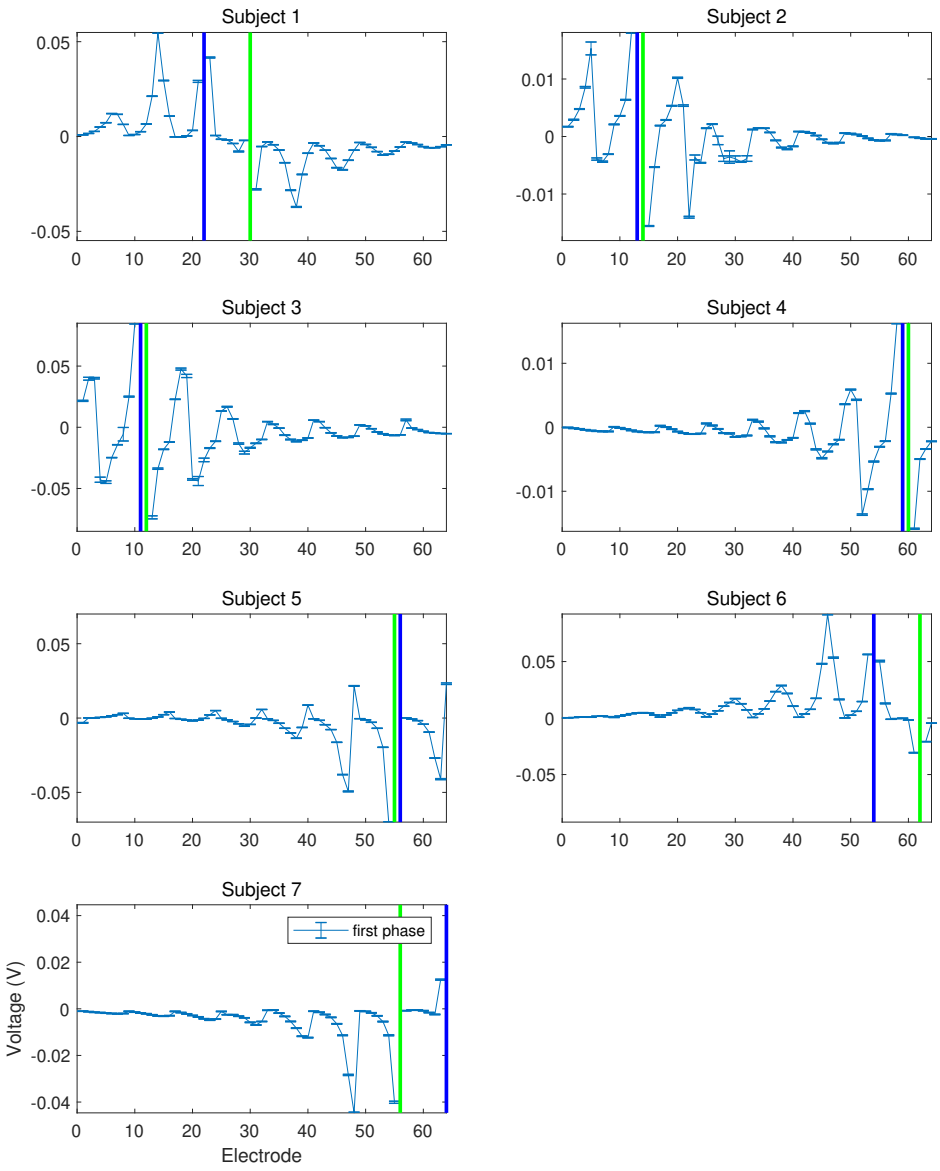

Figure 3.12: The means and standard deviations of the data for the first seven subjects. The means and the standard deviations of the magnitudes of the stimulation artifacts for the first seven subjects following our signal extraction algorithm are plotted versus the electrode number. The mean is the mean voltage across all trials within the extracted region illustrated in Figure 3.11. The standard deviation is the standard deviation of the means

3.9 Experimental Results for the Statics and Dynamics of ECoG Electrodes

3.9.1 Saline Phantom Measurements

We found that our 2-point measurements using saline solutions with known resistivities did not produce reliable results, but our 3-point measurements did. The failure of 2-point methods has been reported previously [184], as is one of the primary motivations for the 3- and 4- point measurements.

Using our same data extraction and analysis strategy as outlined in the methods, we compared our results with ECoG grids to a commercial conductivity meter using a sodium chloride saline phantom model to serve as validation. We created two solutions of 0.511 and 3.44 ohm-m NaCl solutions. We highlight four examples from 3 separate electrodes sets at a 1 mA stimulation current level, although different current levels and stimulation electrode pairs yielded similar results. The four sets were a 28/29 stimulation pair in 3.44 ohm-m saline, a 36/37 stimulation pair in 3.44 ohm-m saline, and a 28/36 stimulation pair in both 3.44 ohm-m and 0.51 ohm-m saline.

By using the TDT, we determined the jump resistances to be 1.97, 1.93, 1.97, and 0.51 V for the conditions described above. This yields resistances of 1987, 1926, 1971, and 583 ohm respectively. Therefore, the solution resistivities are 4.57, 4.43, 4.53, and 1.34 ohm-m respectively. This highlights that naive application of the two-point method includes both the electrode resistance in series with the bulk resistance. Back calculating the two-point resistances we would expect from our two solutions, we calculate solution resistances of 221 and 1496 ohm. The electrode and bulk resistances are in series, so this yields electrode resistances on the order of 362 ohm and 491, 430, or 475 ohm for the 0.511 and 3.44 ohm-m solutions. Since these resistances can vary by the particular electrodes and electrode-tissue interface characteristics, we do not perform any correction of our reported two-point values, but rather highlight that there is a meaningful contribution of the electrode resistance.

We used the TDT and the three-point measurement technique with a homogeneous half-space model, we determined the solution resistivities to be 3.44, 0.54, 3.38, and 3.45 ohm-m respectively (Figure 3.13) with the same 1 mA stimulation pulses we used for the two-point measurements. We excluded one channel (channel 27) from this array, and it had unreliable measurements. This concordance between the three-point measured values and the commercial resistivity meter serves as validation that using a uniform solution of known resistivity, we are able to accurately calculate the resistivity using a three-point measurement technique, a homogeneous flat point source model, and our clinical ECoG electrodes.

We subsequently used the four-point measurement technique and excluded any values less than 0 ohm-m or greater than 10 ohm-m. We then determined the mean solution resistivities to be 3.42, 3.38, 3.44, and 0.59 ohm-m, respectively. The median solution resistivities were 3.40, 3.44, 3.43, and 0.56 ohm-m, respectively (Figure 3.14). The four-point measurement technique is therefore a valid technique to determine the resistivity of a material using our electrode arrays. Additionally, the ability to calculate the amount of spread in the distribution, through either the standard deviation or median absolute deviation, gives an idea of how uniform the resistivities throughout the entire material are.

3.9.2 Two-point Measurements

Despite calculating resistivity values that were too high from the two-point measurements, we proceeded to calculate the two-point resistivities for all eight subjects.

We use constant current bipolar biphasic stimulation. At low currents, the voltage required to produce pulsed constant current stimulation depends on the resistance and the double-layer capacitance. At intermediate currents, it depends on the pseudo-capacitance associated with the reversible oxidation and reduction of the electrodes (Figure 3.5). At high currents, it depends on the electrolysis of the water [124].

As described in the methods, we extracted all time windows around when the stimulator

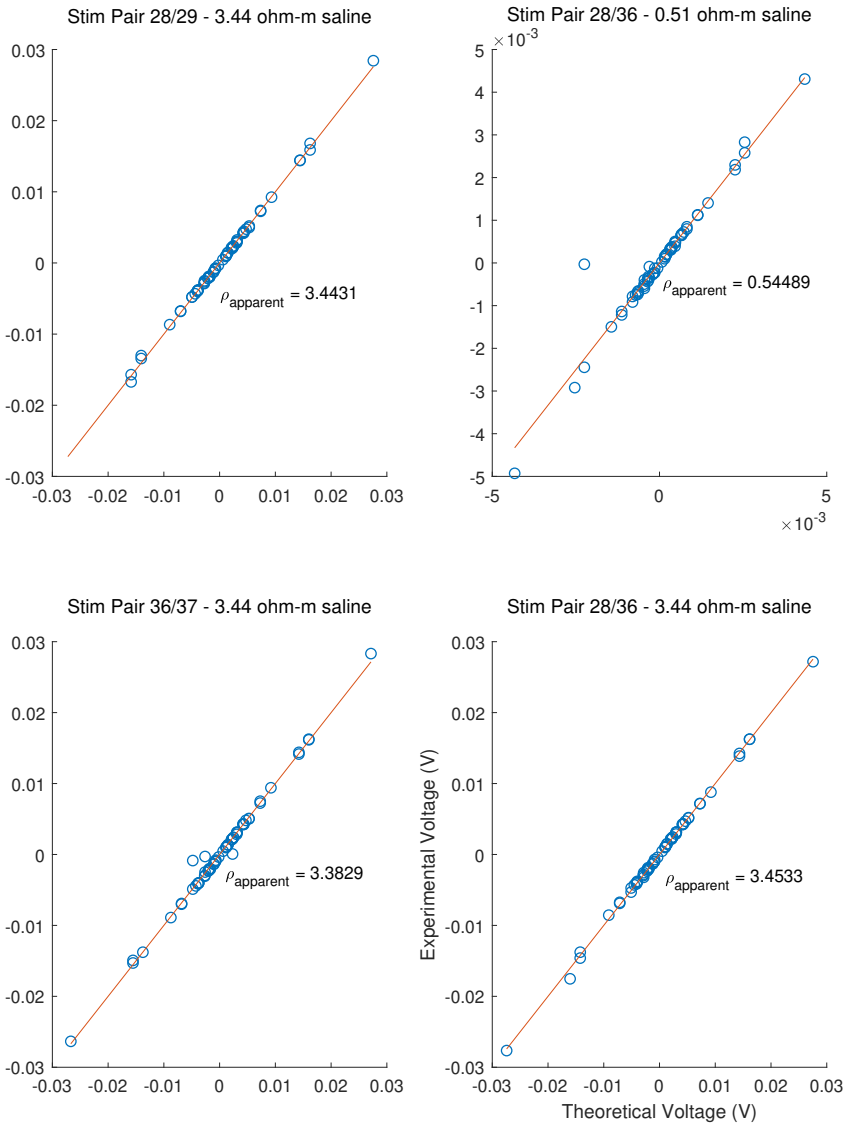

Figure 3.13: Three-point saline validation with a clinical ECoG array and solutions of two resistivities. We used saline solutions with resistivities of 3.44 and 0.51 ohm-m, and accurately calculated the resistivity of the solution with the three-point technique the recording channels in an ECoG array. We used multiple sets of adjacent stimulation contacts were used for these plots, indicating that the results are not specific to a single stimulation pair. This serves as validation for our use of the three measurement techniques in human patients with our clinical ECoG arrays, and stimulation and recording hardware.

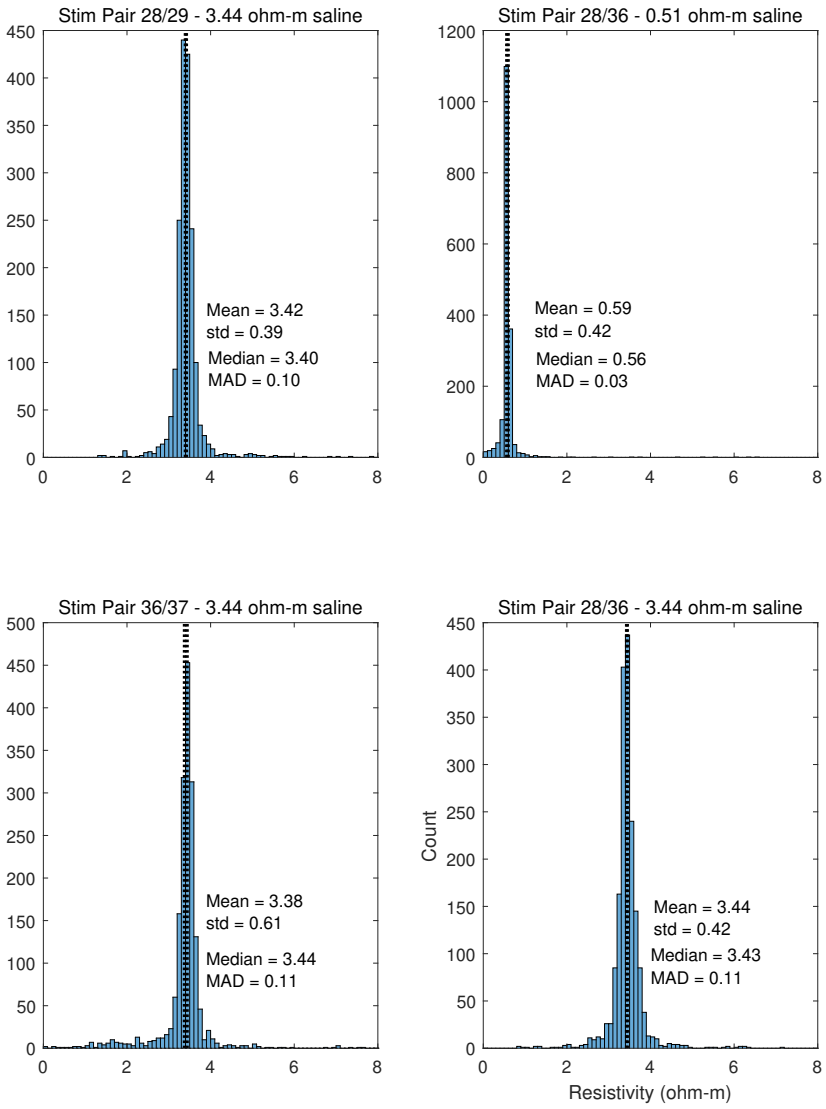

Figure 3.14: Four-point saline validation with a clinical ECoG array and solutions of two resistivities. We used saline solutions with resistivities of 3.44 and 0.51 ohm-m, and accurately calculated the resistivity of the solution using the recording channels in an ECoG array. We used multiple sets of adjacent stimulation contacts were used for these plots, indicating that the results are not specific to a single stimulation pair. We calculated the mean, median, standard deviation (std) and median absolute deviation (MAD) to describe the distributions. This serves as validation for our use of the four-point measurement techniques for our data.

was set to deliver a bipolar, biphasic pulse, and discarded any pulses where the stimulator incorrectly delivered stimulation, which we defined as being greater than 1.5 times, or 0.5 times the median maximum peak voltage delivered (We excluded 534/10590 trials for subject 5, and 139/7000 trials for subject 6). We consider the first phase of stimulation, in order to avoid analyzing where the stimulator failed to deliver a proper biphasic waveform during the second phase of stimulation at high currents.

All of measured stimulation voltage pulses required to produce the experimental current levels are shown in Figure 3.15. The waveform shapes are similar between all of the subjects, with an immediate voltage jump, followed by a curved section with contributions from the double layer capacitance, and Faradaic reactions. The average of these curves is shown in figure 3.16. The plot of the averages masks the variation for some of the subjects (Subject 5 in particular).

The time dependence of the voltage curves is shown in Figure 3.17. It is clear from these plots that there is not a consistent nor predictable pattern of jump voltages over the course of a stimulation session, suggesting that two-point measurements in our stimulation setup are subject to potential changes in the electrode-tissue interface, or stimulator performance over time that may systematically affect resistivities calculated through two-point measurements.

The same data for the first seven subjects is shown again in figure 3.18(a-c)normalized by dividing by the stimulation current. We have additionally added in the results for the eighth subject (Figure 3.18)(d-f). In this form the data has units of ohms and is the dynamic impedance of the sample in response to our applied stimulation. Properly engineered stimulators must be able to drive these dynamic impedances. We calculated the resistance, and subsequently apparent resistisvities. The apparent resistivity values are shown in Table 3.3 for the first seven subjects, and Table 3.4 for the eighth subject, along with all of the other calculated apparent resistivity values. As noted in the section on two-point validation, these values have contributions from the electrode resistance. As each pair of consecutive

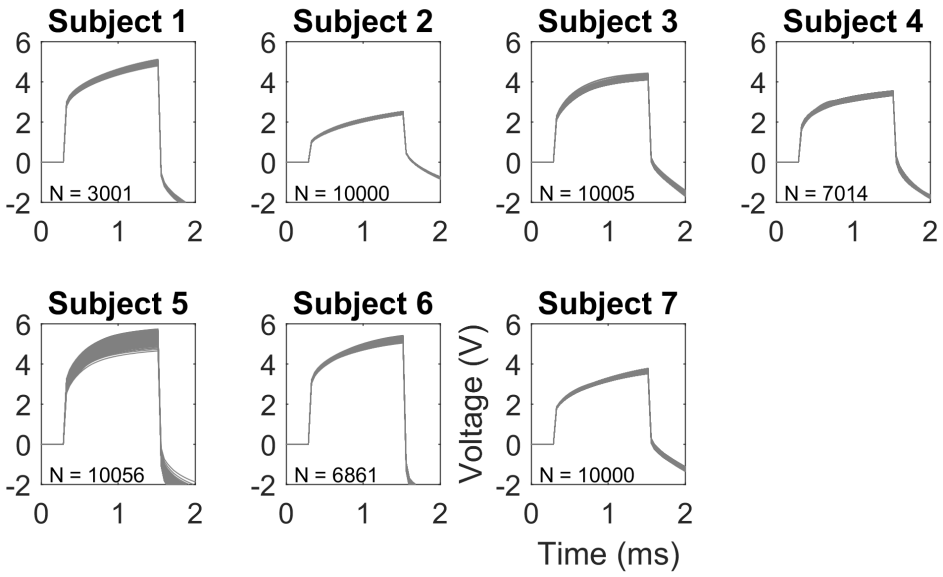

Figure 3.15: Individual subject stimulation monitor output for the first seven subjects. Individual trials of the first phase of the monitored voltage on the stimulator output are plotted. N represents the number of trials plotted, as well as used for further analyses. See Table 3.1 for the duration of the stimulation session, which ranged from 16.43 for subject 1 to 45.14 minutes for subject 3.

data sets for the eight subject had both polarities of stimulation (e.g 1/2, 3/4, were sets of the same contact pairs but with opposite polarities), we can see that both polarities resulted in similar jump voltages (Figure 3.18, Table 3.4).

3.10 Flat vs. Spherical Models

In order to address the question of the validity of flat and spherical models, we plotted our reconstructed electrode grids, and calculated Gaussian curvatures on the triangulated surface representing the grid between our electrodes [183]. We used a MATLAB implementation of the aforementioned method [68]. We found that all of our electrode arrays, despite variations

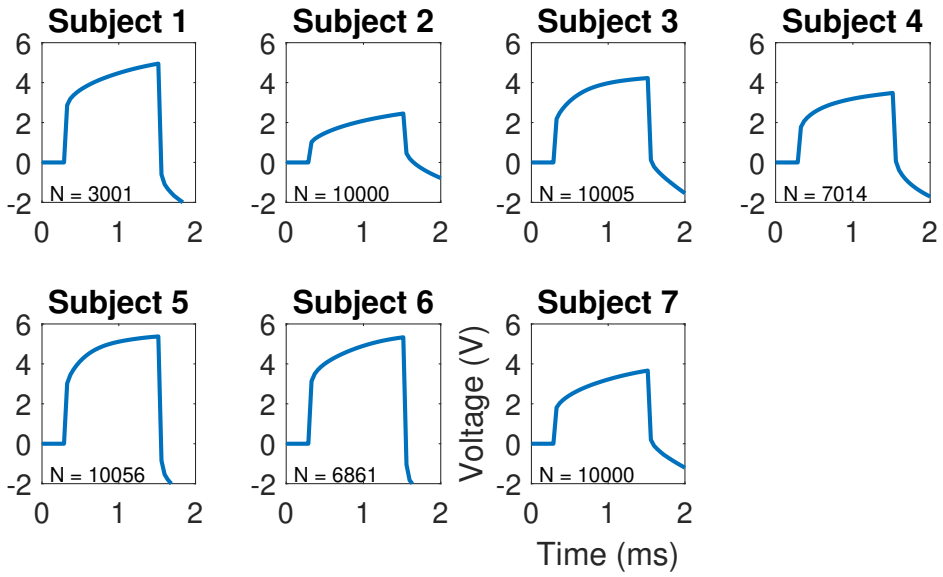

Figure 3.16: Average stimulation monitor output for each subject. The average initial voltage jump was used for the two-point measurement of the resistivity. N represents the number of trials over which the average was calculated. Table 3.1 illustrates the length over which these stimuli were delivered, which ranged from 16.43 for subject 1 to 45.14 minutes for subject 3. We extracted the voltage jump from these mean waveforms for the two-point analyses.

in the magnitude and sign of the Gaussian curvature were locally flat, as the small values of the calculated Gaussian curvatures correspond to a very large radius of curvature, far greater than the radius of the brain. as shown in Figure 3.19.

Additionally, there exist sections of both positive and negative curvature, which illustrate bending in both away and towards the brain in the electrode array.

By fitting a sphere to the outer surface of the cortical reconstructions for each subject, we estimated the radius of curvature for the individual subject brains, and make the assumption that this is a reasonable curvature to use for our spherical model (Figure 3.20), as this is a subject derived measure of the brain radius and subsequent global geometry.

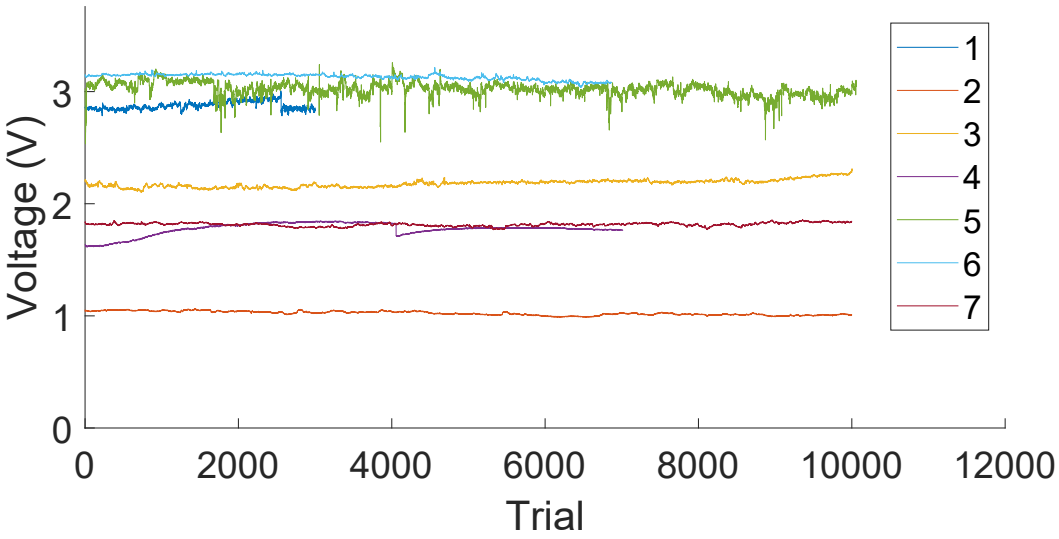

Figure 3.17: Jump voltages over time all subjects. The initial jump voltages for all subjects to illustrate the time dependence and large voltage jumps intermittently throughout the stimulation session (Subject 4 in particular).

The local flat nature of the electrode grid, as well as the global spherical geometry, motivates the simple models we used for the coordinates of the flat brain model (which were euclidean distance from the 3D CT coordinates) and of the spherical brain model (angles computed from arc lengths of the CT coordinates).

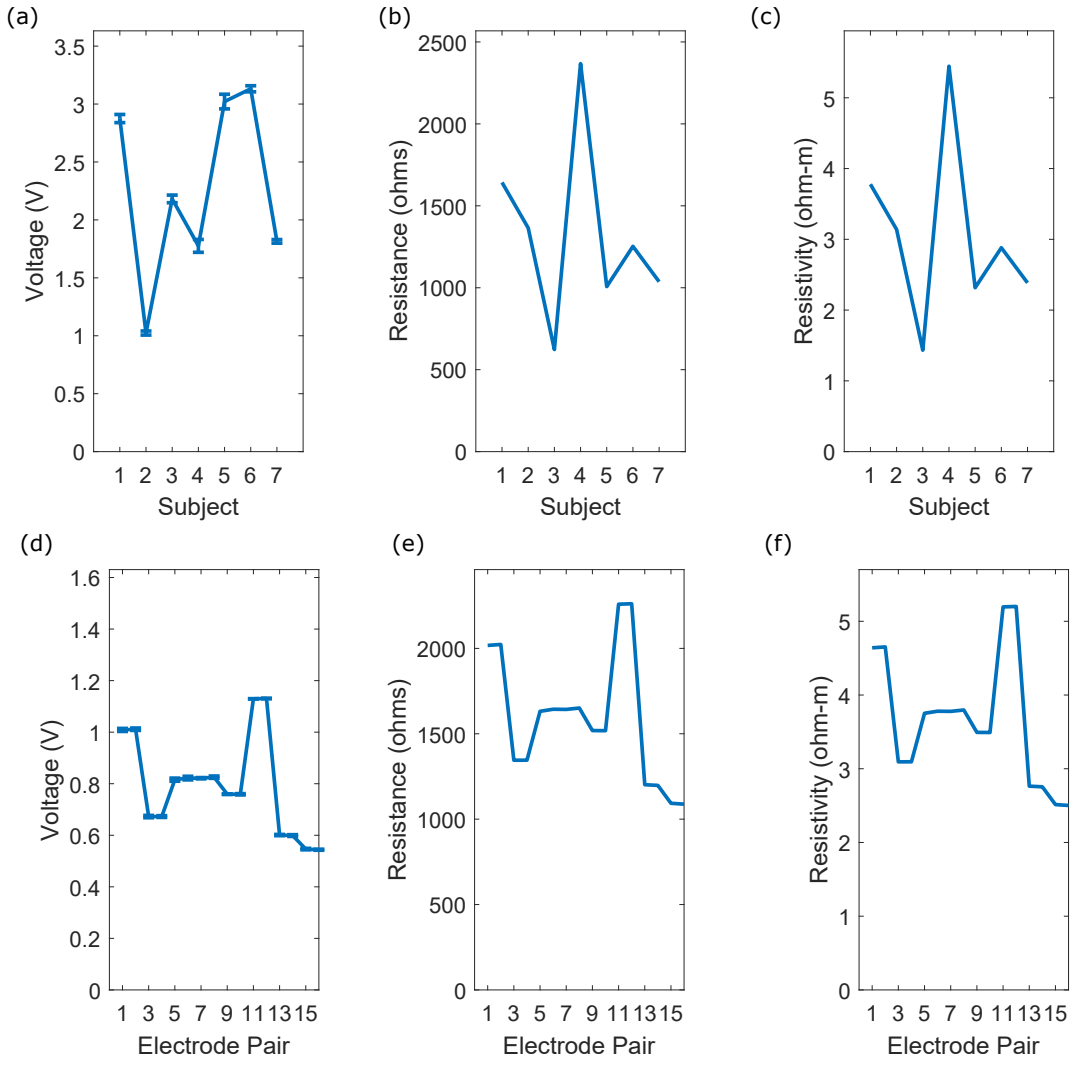

Figure 3.18: Two-point results for all eight subjects. (a) The mean jump voltage (+/- standard deviation) is plotted for each of the first seven subjects. (b) This is subsequently divided by the applied current to calculate the resistance, and (c) appropriately converted into resistivity values. Due to the inability of two-point measurements to accurately capture the resistivity of a saline phantom, these values are not accurate reflections of the underlying resistivity. (d) As in panel (a), we show the mean jump voltage (+/- standard deviation) for each of the electrode pairs for the eight subject. Consecutive electrode pairs (e.g. 1/2, 3/4) were opposite polarities of the same contacts. We see that both polarities of stimulation result in similar jump voltages. (e) After dividing the jump voltages by the applied current (0.5 mA for all of these contact pairs), we calculate the resistance (c) and subsequently the resistivity.

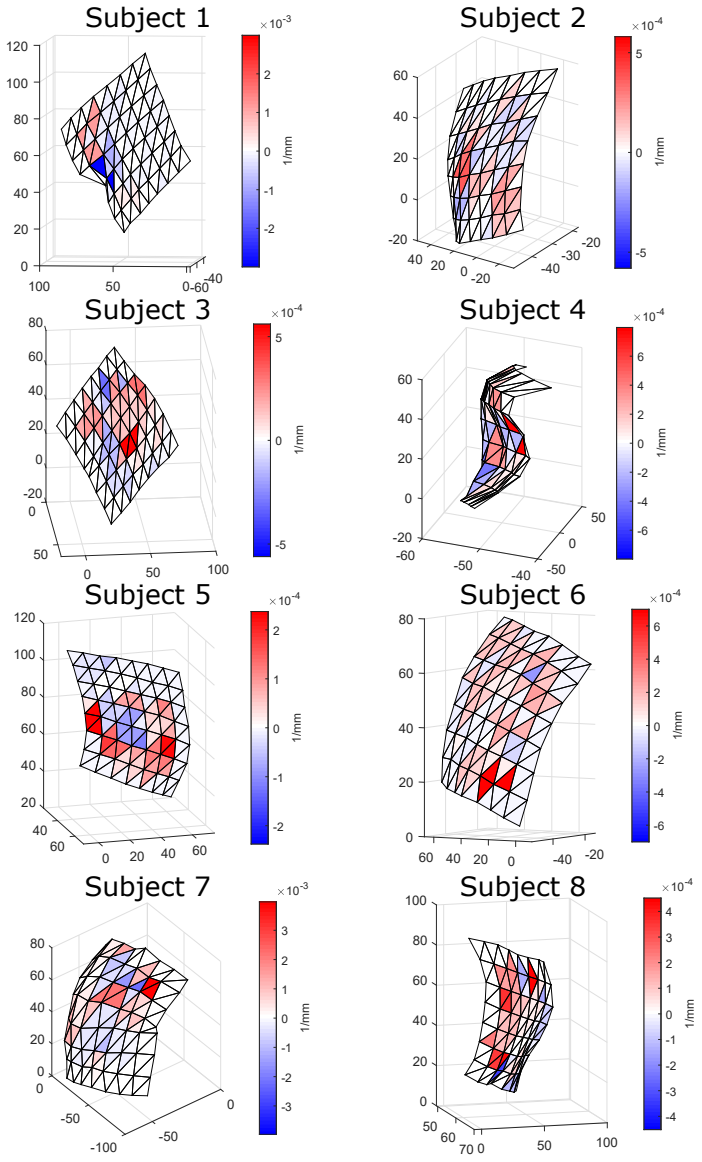

Figure 3.19: Gaussian curvatures for electrode arrays for 8 subjects. In order to understand the topography of the electrode arrays, we created a delaunay triangulation of the 64 array points, and calculated the the Gaussian curvature for each one of these. Large swaths of the arrays have very little Gaussian curvature (Subject 1 in particular illustrates this), which means these arrays can be considered to be locally flat in those regions. Even where the Gaussian curvature is higher in magnitude, as in approximately 3e-3 (1/mm) for Subject 7, this yields a radius of curvature of approximately 333 mm, which is around 5 times too large. This tells us that the curvature of the electrode arrays does not reveal the global geometry of the brain, and they can be considered to be locally flat.

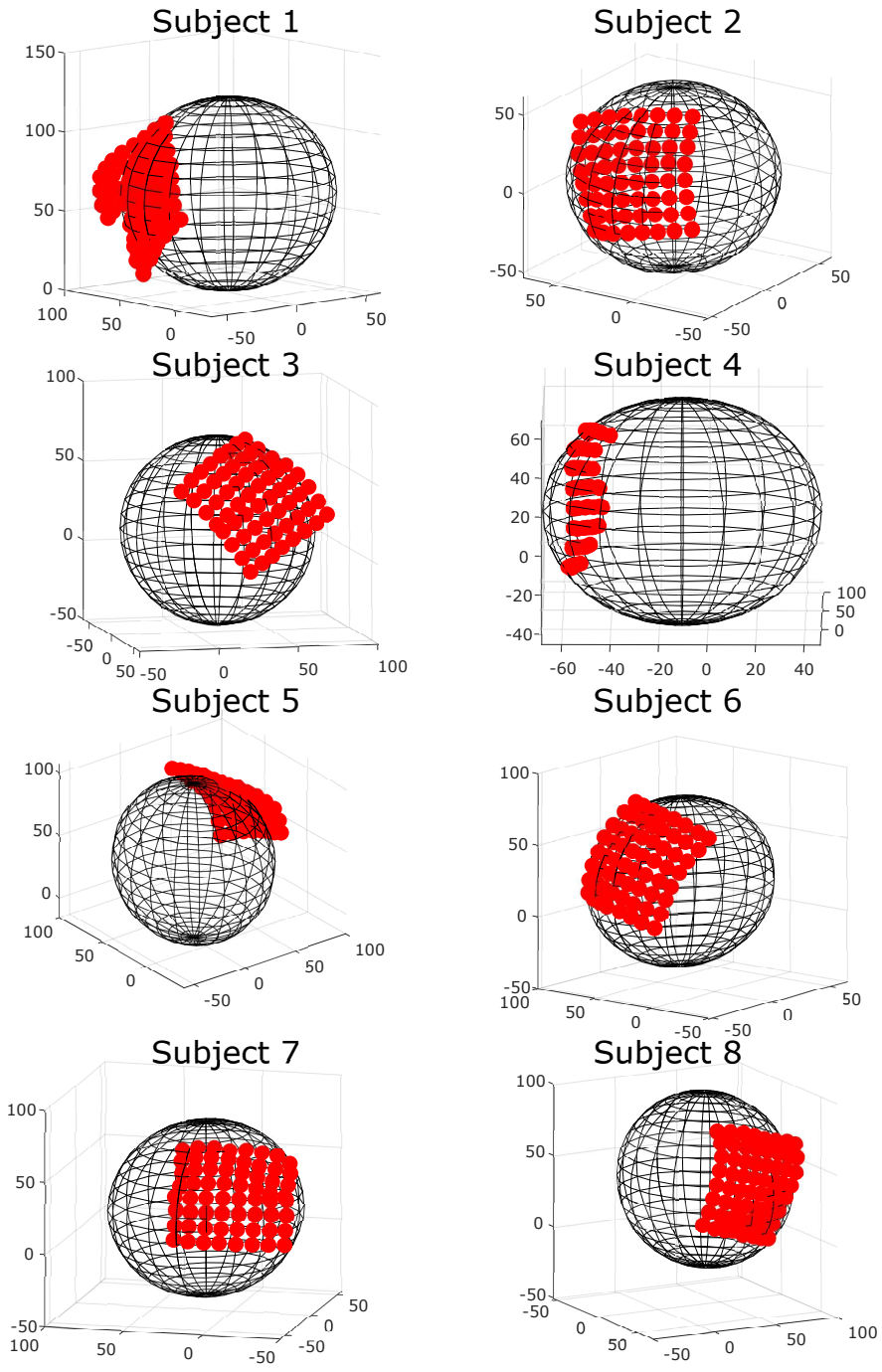

Figure 3.20: Sphere fits to subject cortices with overlaid electrodes. We fit a sphere using linear least squares fitting to the outer surface of the subjects' cortical reconstructions to estimate the radii of their cortices. We then overlaid the CT coordinates before transformation on top of the best fit sphere. Some subjects (subjects 1,4) illustrate distortion of the electrode arrays and subsequently are not as well described by a spherical model as other subjects (2,5,7, for example).

3.10.1 Voltage over Time

To determine whether our measured resistivities depended on time, and to compare the reliability of the recorded waveform voltage over time to that of the stimulation waveform, we compared the mean voltages over time to the jump voltages over time (Figure 3.21). As an example, the jump voltages from the stimulation waveforms demonstrated clear drifts and shifts over time. The coefficient of variation (standard deviation/mean) for both the recorded waveforms (7.26e-3), and for the jump voltages between trial 2200 and 3900 in this example (2.87e-3), were similar. However, the coefficient of variation for the jump voltages over the entire waveform was 3.13e-2. Therefore, the entire stimulation jump waveform is subject to more errors. This suggests that using data from the recording channels is more reliable than the measured stimulation voltage during constant current stimulation, and subsequently the two-point measurements are subject to more errors.

3.11 Three-Electrode Measurement - Flat Model & Spherical Model

Comparisons with the experimental data for the first seven subjects in the global fit can be seen for the flat and spherical models in Figure 3.22, with the calculated apparent resistivity values in Table 3.3. In Figure 3.22, we see that both models predict the measured voltages well. The apparent resistivity values for the spherical fit are in general lower than the corresponding ones for the flat semi-infinite model. Depending on the subject, the root mean square error (RMSE) may be lower for either model.

Comparisons with the experimental data for the eight subject subjects in the global fit can be seen for the flat and spherical models in Figure 3.23, with the calculated apparent resistivity values in Table 3.3. Of note from Figure 3.22 is that both models predict the measured voltages well. The apparent resistivity values for the spherical fit are in general lower than the corresponding ones for the flat semi-infinite model. Depending on the subject, either the root mean square error (RMSE) may be lower for either model. We show both

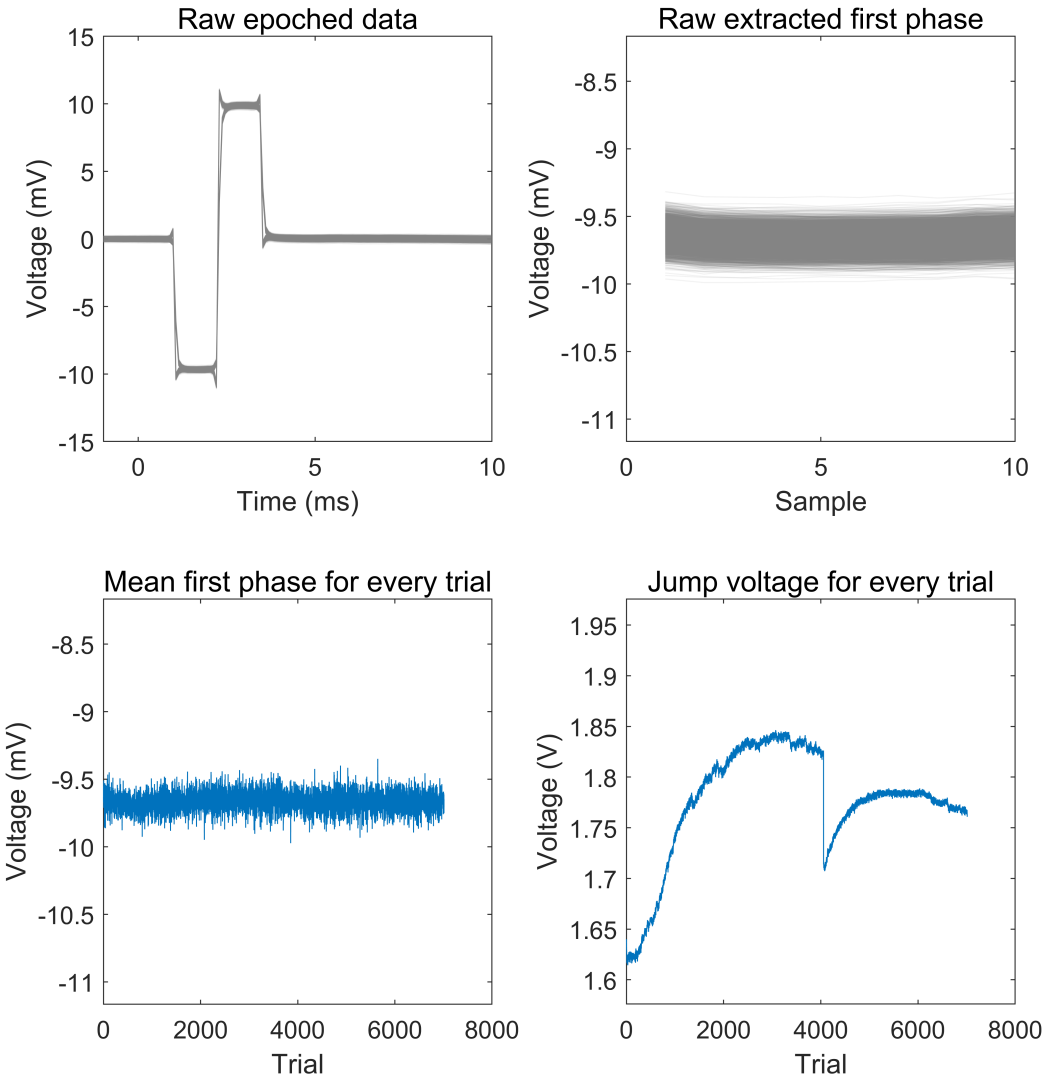

Figure 3.21: Comparison of recorded voltage and the stimulation jump voltage. We extract the flat part of the the raw waveform for an example channel (53), as illustrated in Figure 3.11. We then compare this over each individual trial to the jump voltage for each trial. The coefficient of variation (standard deviation/mean) for both the recorded waveforms (7.26e-3), and for the jump voltages between trial 2200 and 3900 in this example (2.87e-3), were similar. However, the coefficient of variation for the jump voltages over the entire waveform was 3.13e-2. Therefore, the entire stimulation jump waveform is subject to more errors. The jump voltage is subject to greater shifts and drifts over time than the recorded waveform.

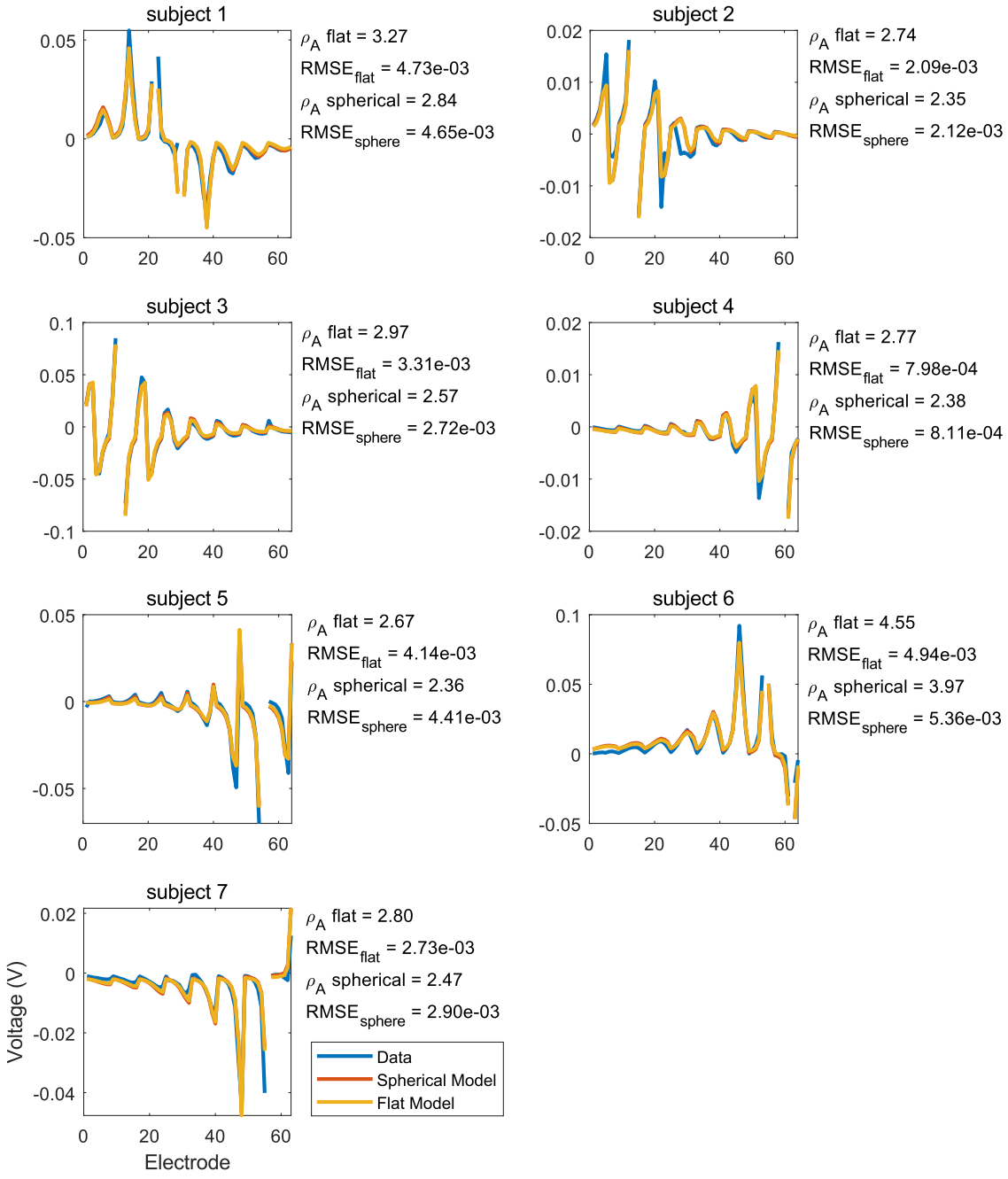

Figure 3.22: Data and global model fits for the first seven subjects. The experimental data for each subject is plotted, as well as the model predicted values for the flat and spherical models with a global ρ_a for each subject. We also show the $\rho_{apparent}$ values, as well as the root mean square error (RMSE) for the models. Depending on the subject, the root mean square error (RMSE) may be lower for either model.

polarities of stimulation that we performed to illustrate the between session reproducibility of a given bipolar pair, as well as no visible influence of different polarities within a pair.

3.12 Distance Binning

Comparisons with the experimental data for the first seven subjects in the distance binned fit can be seen for the flat and spherical models in Figure 3.24. As there are additional free parameters, with a resistivity value for each distance bin, the model fit is even better than the global fits, as shown by the corresponding lower RMSE values for every subject and both models compared to the global fits. Depending on the subject, the root mean square error (RMSE) may be lower for either the spherical or half-space model.

The binned apparent resistivity values with distance binning are shown in Figure 3.25 for the flat and spherical models for the first seven subjects. We see an apparent increase in apparent resistivity with distance for the flat model, a generally greater apparent resistivity for each comparable point for the flat model relative to the spherical model, as well as flat trends for the apparent resistivity for the spherical bin case. We see flat trends for the spherical model, which suggests that the increase seen in the apparent resistivity for the flat model is due to the assumed geometry of the half-space model.

Comparisons with the experimental data for the eighth subject in the distance binned fit can be seen for the flat and spherical models in Figure 3.26. Similarly to the first seven subjects, the model fit for the distance binned fit is better as assessed through the RMSE for each stimulation pair.

The binned apparent resistivity values with distance binning are shown in Figure 3.27 for the flat and spherical model for each stimulation electrode pair for the eighth subject. We see an apparent increase in apparent resistivity with distance for the flat model, a generally greater apparent resistivity for each comparable point in the spherical fit, as well as flat trends for the apparent resistivity for the spherical bin case (except for the 4/12 and 12/4

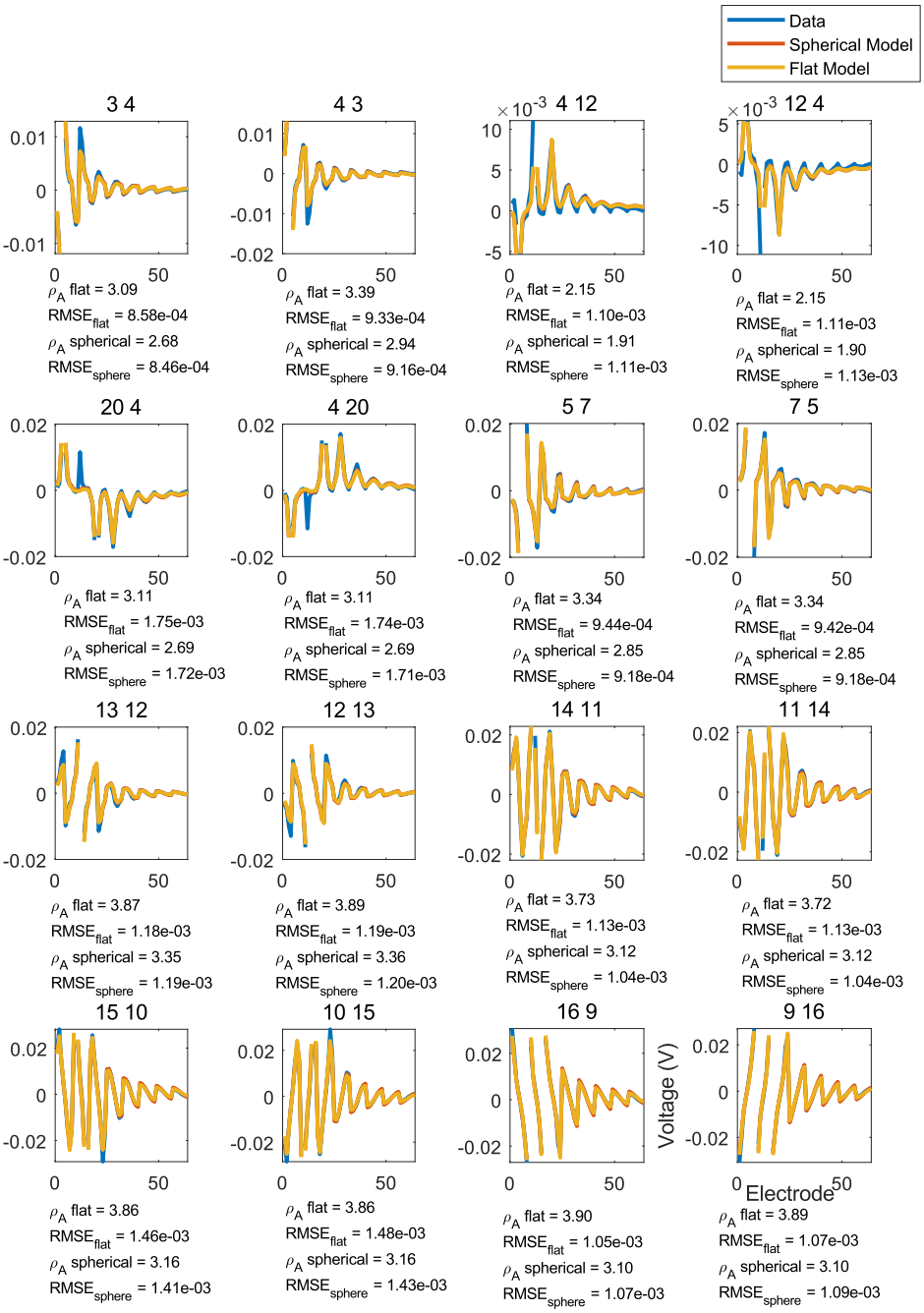

Figure 3.23: Data and global model fits for the eighth subject. The experimental data for each electrode pair for the eight subject is plotted, as well as the model predicted values for the flat and spherical models with a global ρ_a for each stimulation pair. We also show the $\rho_{apparent}$ values, as well as the root mean square error (RMSE) for the models. Depending on the electrode pair, the root mean square error (RMSE) may be lower for either model.

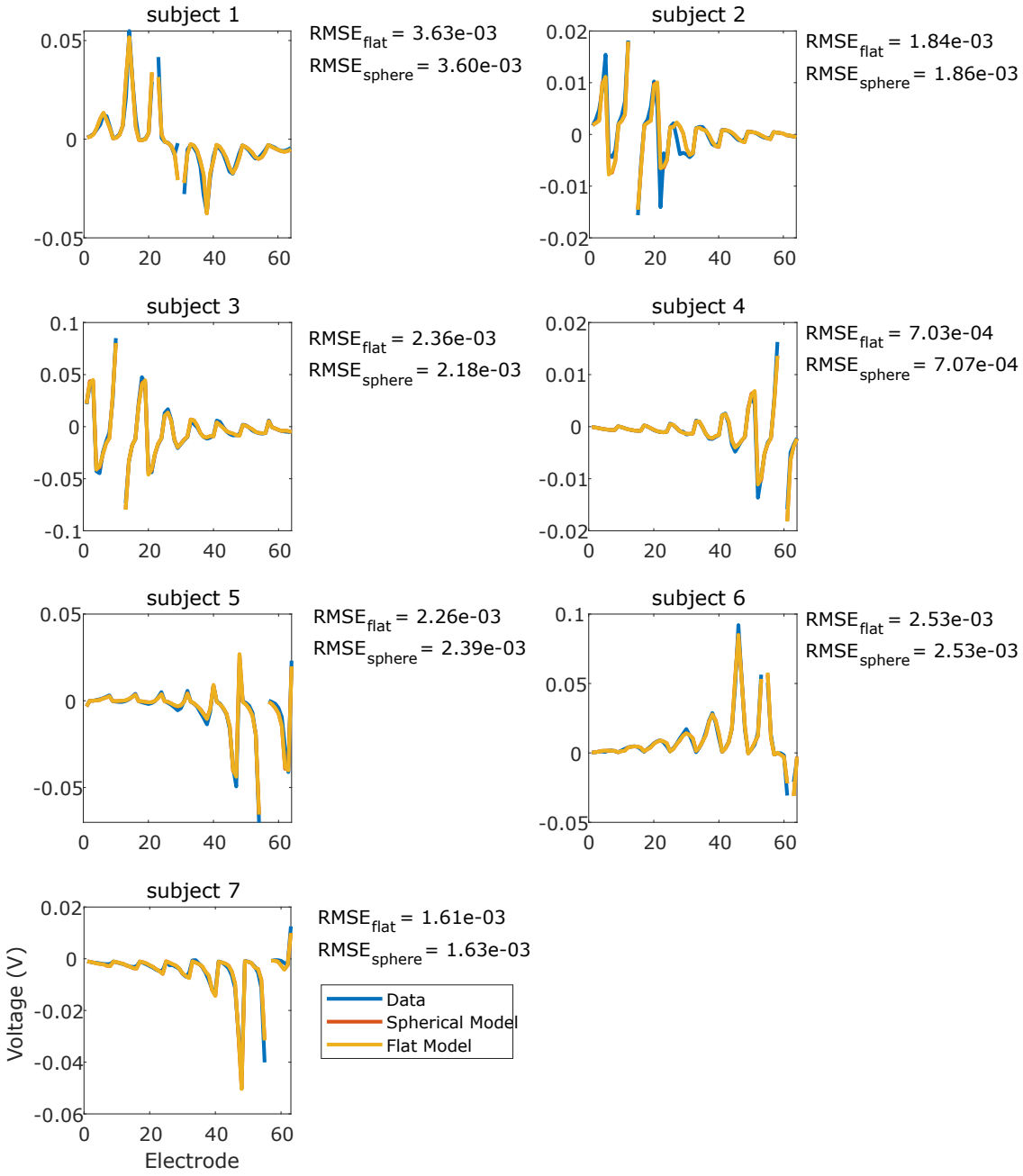

Figure 3.24: Data and binned model fits for the first seven subjects. The experimental data for each subject is plotted, as well as the model predicted values for the flat and spherical models with binned ρ_a for each set of electrodes within the distance bins of 1-2, 2-3, 3-4, 4-5, and 5-6 cm. As there are additional fitting parameters relative to the global model case, the RMSE errors are lower for all of the subjects. Depending on the subject, the root mean square error (RMSE) may be lower for either model.

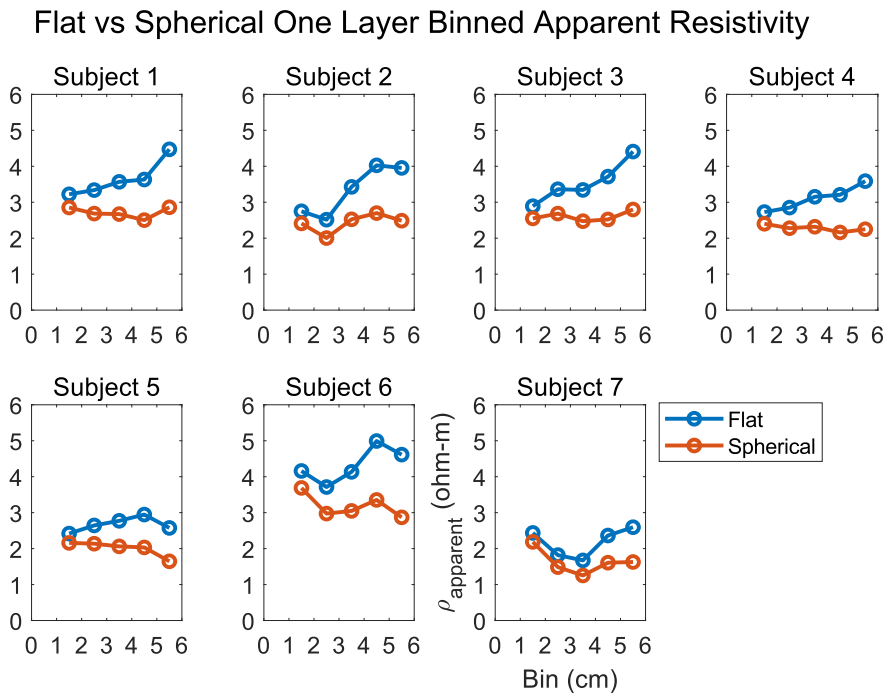

Figure 3.25: Binned distance apparent resistivity values for the first seven subjects. We calculated apparent resistivity within bins by using the best linear least-squares fit for the measured voltages for electrodes within the distance bins of 1-2, 2-3, 3-4, 4-5, and 5-6 cm. As the binned distance increases for the flat model, we see an increase in the apparent resistivity. Relative to the spherical model at each bin point, the flat model has a higher apparent resistivity. The trends for the spherical model are flat, suggesting that the increase seen in the apparent resistivity with the flat model is due to the assumed geometry of the half-space model, where as the spherical model is for a closed space, which reflects the geometry of the brain.

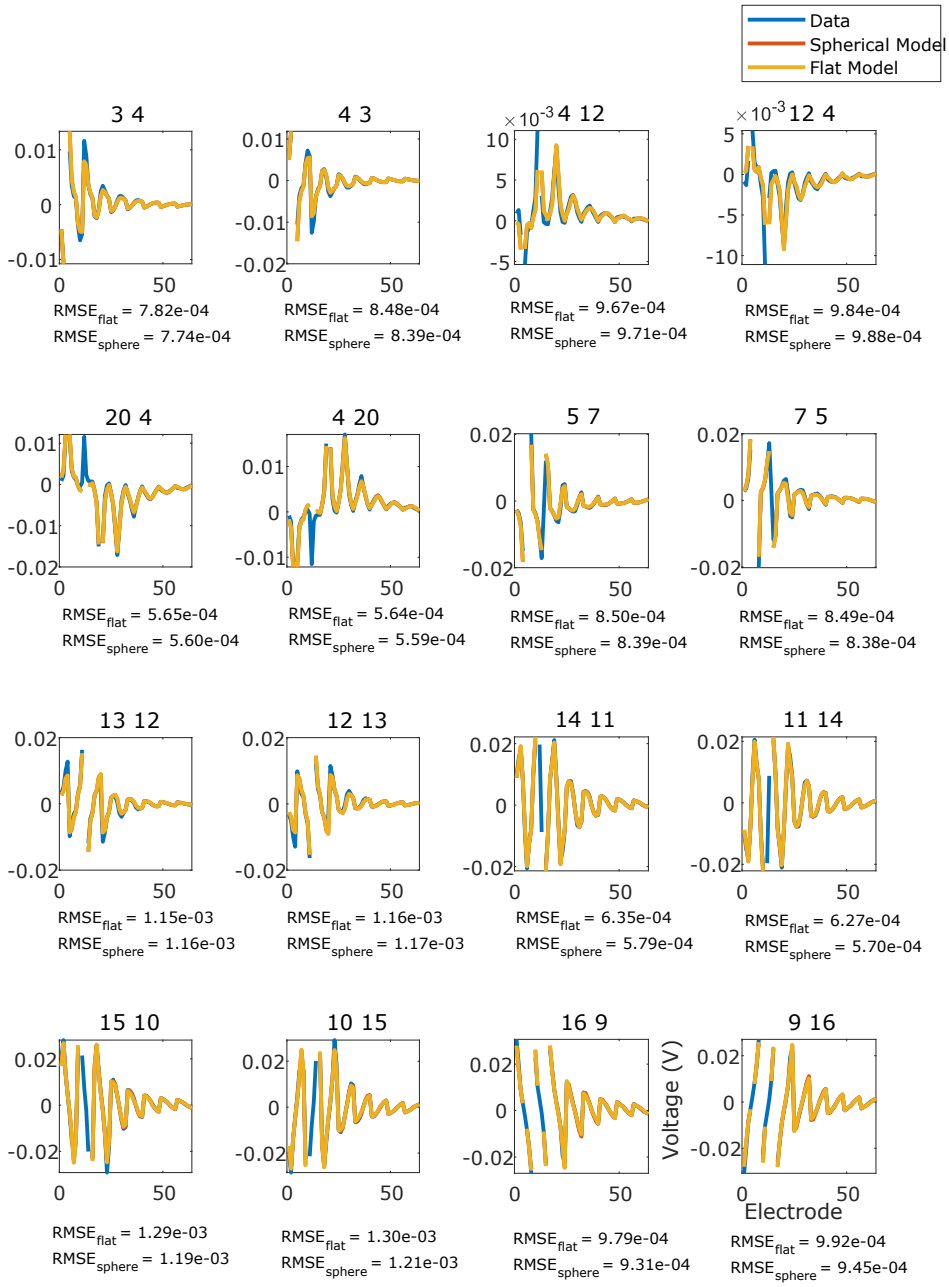

Figure 3.26: Data and binned model fits for the eighth subject. The experimental data for each stimulation electrode pair is plotted, as well as the model predicted values for the flat and spherical models with binned ρ_a for each set of electrodes within the distance bins of 1-2, 2-3, 3-4, 4-5, and 5-6 cm. As there are additional fitting parameters relative to the global model case, the RMSE errors are lower for all of the subjects. Depending on the subject, the root mean square error (RMSE) may be lower for either model.

electrode pair). We see flat trends for the spherical model, which suggests that the increase seen in the apparent resistivity for the flat model is due to the assumed geometry of the half-space model.

3.13 Four-Electrode Measurements - Flat & Spherical Model

Two of the four electrodes are stimulation electrodes and two are recording electrodes for a four-point measurement. There are many (62 choose 2=1891) choices for the recording electrode pairs, and subsequently the following histograms have these number of calculated values. Figure 3.28 shows the four-point histograms for the half-space and spherical models for the first seven subjects. There is a shift towards lower resistivity values in the four-point distributions for the spherical distributions, as evidenced by the lower median values, mirroring what was seen in both the global three-point and binned three-point fits. We excluded any resistivities that were greater than 10 ohm-m or less than 0 ohm-m.

The mean, standard deviation, median, absolute median deviation (MAD), and apparent resistivity values from these distributions for the first seven subjects are shown in Table 3.3.

We similarly calculated the four-point histograms for the eighth subject for each stimulation electrode pair. Figure 3.29 shows the four-point histograms for the half-space and spherical models. Similar to the trends seen in the first seven subjects, there is a shift towards lower resistivity values in the four-point distributions for the spherical distributions, as evidenced by the lower median values, mirroring what was seen in both the global three-point and binned three-point fits.

The mean, standard deviation, median, absolute median deviation (MAD), and apparent resistivity values from these distributions for the eight subject are shown in Table 3.4.

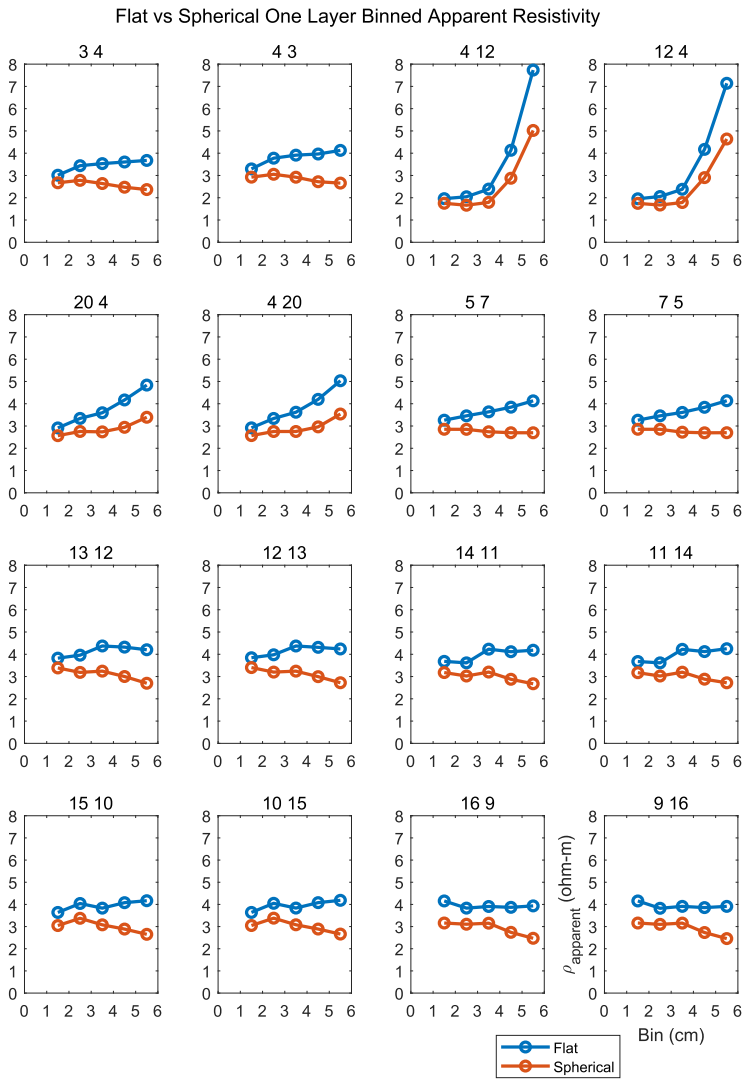

Figure 3.27: Binned distance apparent resistivity values for the eighth subject. We calculated apparent resistivity within bins by using the best linear least-squares fit for the measured voltages for electrodes within the distance bins of 1-2, 2-3, 3-4, 4-5, and 5-6 cm from the center of the stimulation dipole. As the binned distance increases for the flat model, we see an increase in the apparent resistivity. Relative to the spherical model at each bin point, the flat model has a higher apparent resistivity. The trends for the spherical model are flat (except for electrode pair 4/12 and 12/4), suggesting that the increase seen in the apparent resistivity with the flat model is due to the assumed geometry of the half-space model, where as the spherical model is for a closed space, which reflects the geometry of the brain.

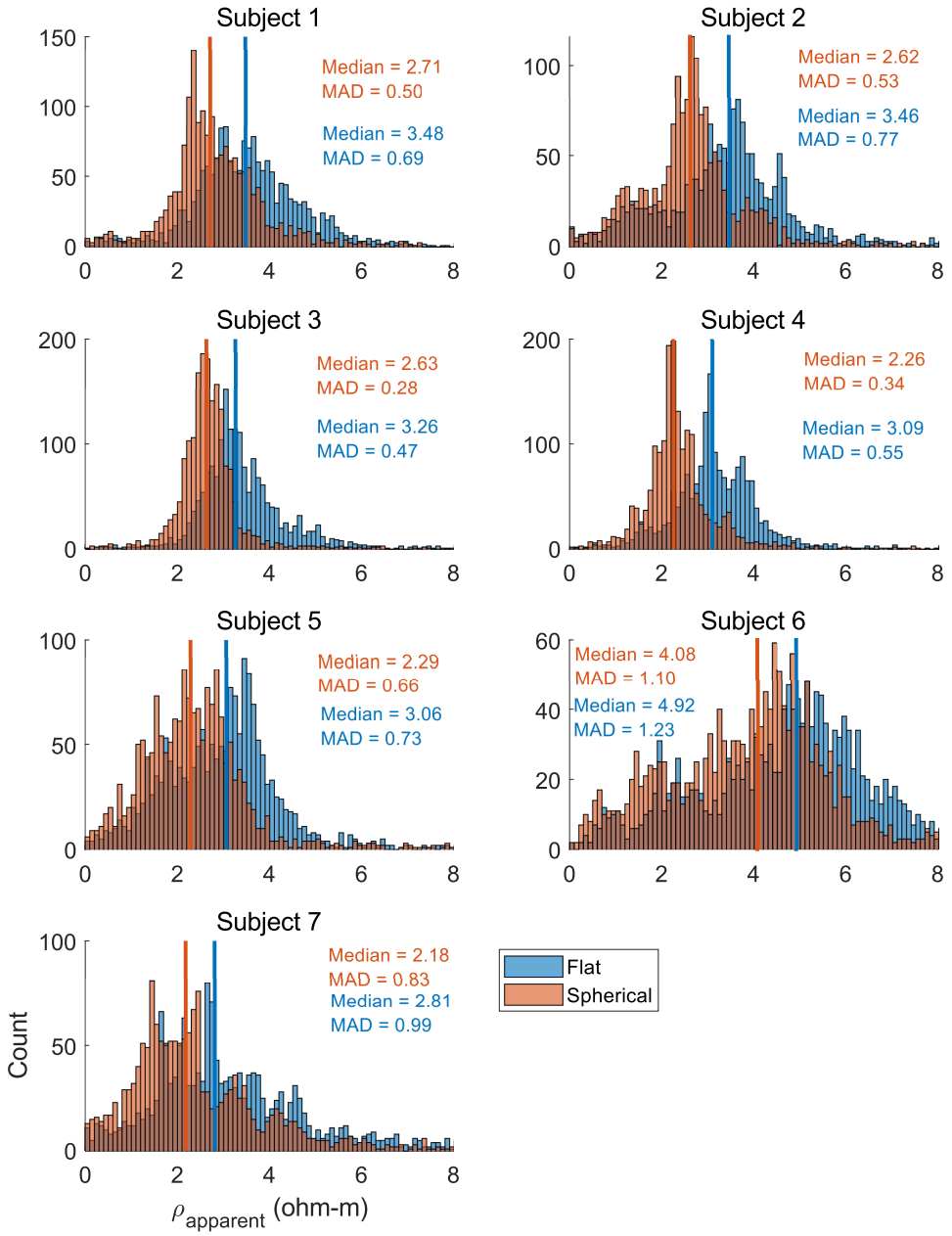

Figure 3.28: Four-point histograms for the first seven subjects. We show for each subject the four-point histograms for both the flat and spherical models, as well as the median and median absolute deviation (MAD) for each distribution. Similar to the trends shown in the global and binned fits, we see a lower median for each subject for the spherical model relative to the flat model. The spherical model shows a lower MAD as well for each distribution.

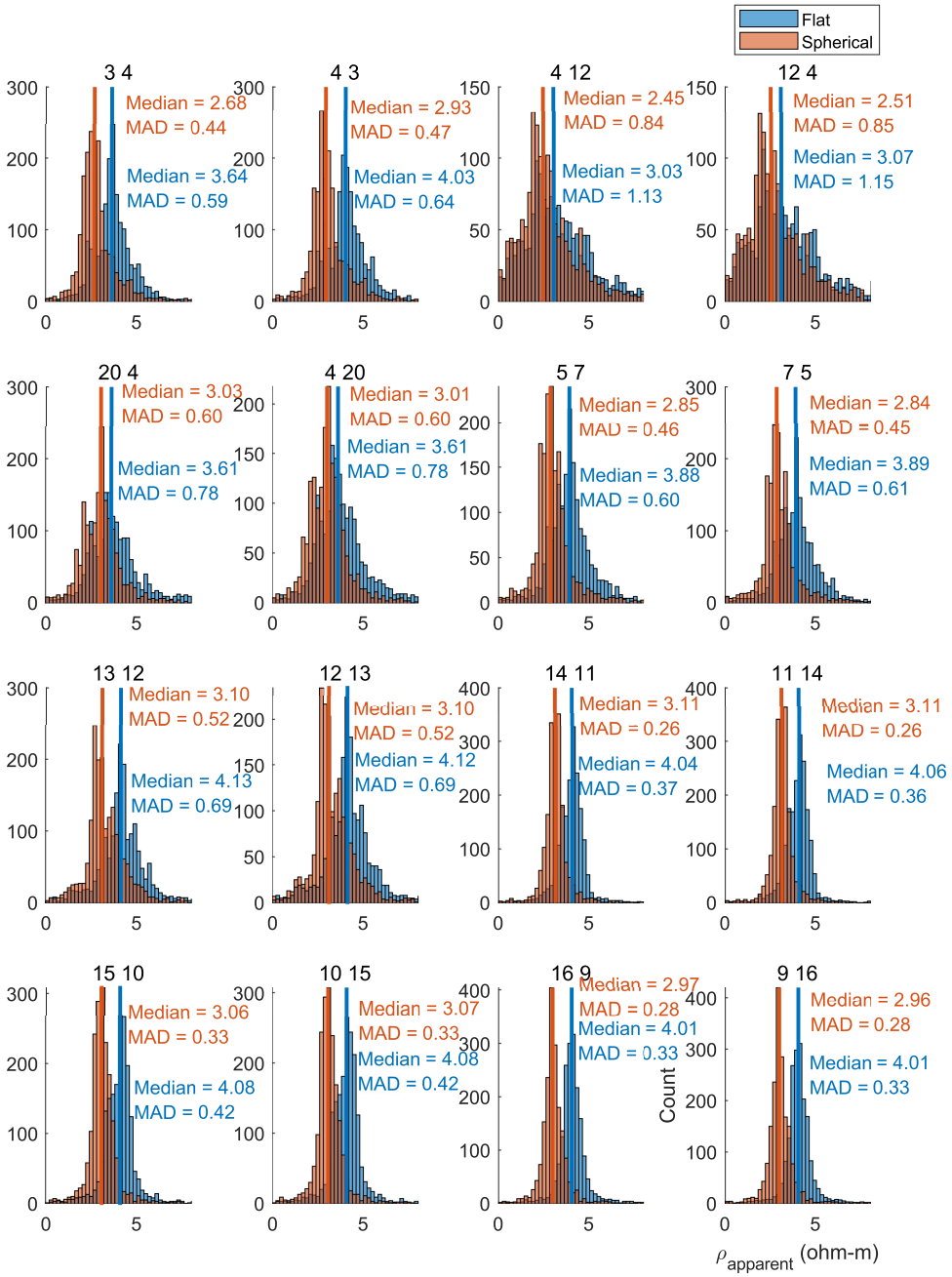

Figure 3.29: Four point histograms for the eighth subject. We show for each stimulation pair for the eighth subject the four-point histograms for both the flat and spherical models, as well as the median and median absolute deviation (MAD) for each distribution. Similar to the trends shown in the global and binned fits, we see a lower median for each subject for the spherical model relative to the flat model. The spherical model shows a lower MAD as well for each distribution.

Subject #	Two-Point	Flat Three-Point	Spherical Three-Point	Flat Four-Point Mean	Flat Four-Point Standard Deviation	Flat Four-Point Median	Flat Four-Point MAD	Spherical Four-Point Mean	Spherical Four-Point Standard Deviation	Spherical Four-Point Median	Spherical Four-Point MAD
1	3.78	3.27	3.01	3.56	1.26	3.48	0.69	2.87	1.12	2.71	0.50
2	3.14	2.74	2.32	3.41	1.50	3.46	0.77	2.67	1.23	2.62	0.53
3	1.43	2.97	2.62	3.46	1.07	3.26	0.47	2.69	0.75	2.63	0.28
4	5.45	2.76	2.42	3.20	1.04	3.09	0.55	2.4	0.89	2.26	0.34
5	2.32	2.67	2.48	3.00	1.36	3.06	0.73	2.38	1.24	2.29	0.66
6	2.88	4.55	4.07	4.80	1.98	4.92	1.23	3.92	1.81	4.08	1.1
7	2.39	2.44	2.52	3.21	1.79	2.81	0.99	2.54	1.67	2.18	0.83

Table 3.3: Compilation of two-point, three-point, and four-point resistivities for the first seven subjects. All of these values are in ohm-m. For the four-point measurements, we report the mean, median, standard deviation, and median absolute deviation (MAD).

3.14 Discussion

3.14.1 Relation to Other Human Measurements

Using the three and four-point measurement techniques in humans, we find that our average measured apparent resistivities fall within the bounds of a combination of CSF, white matter, and gray matter. This complements other work performed in humans, where Carvallo et al. used two-point measurement techniques to measure the resistance of cortical tissue through sEEG electrodes [50].

3.14.2 Tissue Capacitance

There has been considerable interest in, and controversy about, whether neural signals propagate without frequency-dependent absorption or dispersion [185]. This was not a primary objective of our study, but we our recorded waveforms inform us qualitatively about the tissue capacitance. To zeroth order, the square wave like current pulses we inject at the

Electrode Pair (-/+)	Two-Point	Flat Three-Point	Spherical Three-Point	Flat Four-Point Mean	Flat Four-Point Standard Deviation	Flat Four-Point Median	Flat Four-Point MAD	Spherical Four-Point Mean	Spherical Four-Point Standard Deviation	Spherical Four-Point Median	Spherical Four-Point MAD
3/4	4.64	3.09	2.68	3.71	1.13	3.64	0.59	2.85	1.07	2.68	0.44
4/3	4.65	3.39	2.94	4.09	1.24	4.03	0.64	3.14	1.18	2.93	0.47
4/12	3.09	2.15	1.91	3.37	1.98	3.03	1.13	2.79	1.68	2.45	0.84
12/4	3.09	2.15	1.9	3.45	2.05	3.07	1.15	2.86	1.72	2.51	0.85
20/4	3.75	3.11	2.69	3.81	1.45	3.61	0.78	3.07	1.21	3.03	0.6
4/20	3.78	3.11	2.69	3.83	1.47	3.61	0.78	3.07	1.19	3.01	0.6
5/7	3.78	3.34	2.85	3.98	1.25	3.88	0.6	3.04	1.16	2.85	0.46
7/5	3.80	3.34	2.85	3.98	1.26	3.89	0.61	3.02	1.15	2.84	0.45
13/12	3.49	3.87	3.35	4.17	1.3	4.13	0.69	3.31	1.16	3.1	0.52
12/13	3.49	3.89	3.36	4.17	1.3	4.12	0.69	3.32	1.16	3.1	0.52
14/11	5.20	3.73	3.12	4	0.84	4.04	0.37	3.14	0.73	3.11	0.26
11/14	5.20	3.72	3.12	4	0.83	4.06	0.36	3.15	0.74	3.11	0.26
15/10	2.76	3.86	3.16	4.06	0.95	4.08	0.42	3.14	0.84	3.06	0.33
10/15	2.75	3.86	3.16	4.06	0.94	4.08	0.42	3.15	0.85	3.07	0.33
16/9	2.51	3.9	3.1	4.05	0.8	4.01	0.33	3.04	0.81	2.97	0.28
9/16	2.50	3.89	3.1	4.05	0.81	4.01	0.33	3.03	0.8	2.96	0.28

Table 3.4: Compilation of the two-point, three-point, and four-point resistivities for the eighth subject. All of these values are in ohm-m. For the four-point measurements, we report the mean, median, standard deviation, and median absolute deviation (MAD).

stimulation electrodes propagate without any obvious absorption or dispersion: the voltages we measure using the recording electrodes exhibit little dispersion over the frequencies in the pulses (they remain square-wave like out to the most distant recording electrodes). Due to the fact that we are sampling at 12207 Hz, we do not see significant capacitive effects up to this frequency. The recorded pulses also do not exhibit any excess attenuation (they have the 1/r decay, where r is the distance from the stimulation electrode, expected for a resistive medium). This is in line with recent work in humans with simultaneous depth electrode stimulation and surface EEG recording, where no significant frequency dependent effects were found [227].

3.14.3 Curvature

As shown by Figures 3.19 and 3.20, the electrode grids exhibit varying degrees of curvature locally, depending on the topography of the cortical surface. The radius of curvature calculated from these Gaussian curvatures is at least 300 mm, illustrating the the local curvature of the electrode array does not capture the real radius of curvature of the brain.

The lack of an increase in the apparent resistivity for the eight subjects, regardless of the separation of the stimulation electrode pair, suggests that the increases seen in the apparent resistivity for the flat model are due to the assumed geometry of the half space-model. If they were present in the spherical model, this would suggest that this would be a real trend, but instead, the lack of consistency suggests The trends for the spherical model are flat, suggesting that the increase seen in the apparent resistivity with the flat model is due to the assumed geometry of the half-space model, where as the spherical model is for a closed space, which reflects the geometry of the brain.

3.14.4 Distance Binning

For the flat model, the apparent resistivity values tend to increase as the recording electrode separation increases (Figures 3.25,3.27). This is the expected behavior if the resistivity of the white matter is larger than that of the gray matter because larger recording electrode separations include larger contributions from the white matter. As discussed in the introduction, white matter tracts in humans demonstrate complex morphologies, and depending on the orientation, have different resistivity values. Depending on the geometry assumed, as we increase the electrode separation, there are contributions from both parallel (lower/equal resistivity to gray matter), and perpendicular white matter (higher resistivity than gray matter) tracts. However, the spherical model in general does not illustrate this increase in the apparent resistivity with increasing distance bins. This informs us that we are probing all three layers, rather than exclusively CSF or gray matter, with the various distance bins.

3.14.5 Electrode Separation

For the eighth subject where we moved apart the stimulation electrodes, we probed deeper layers of cortex with further apart separations. The lack of systematic changes in the apparent resistivity as a function of electrode separation (See Figure 3.8 for visual illustrations of the electrode separations, Figure 3.23 for the global fits, and Figure 3.27) indicates that at 1 cm, the apparent resistivity we measure has substantial contributions from all the cortical layers, and is not restricted exclusively to CSF or gray matter.

3.14.6 Two vs. Three vs. Four-Point Measurements

As shown in the section on two-point measurements, the voltage exhibits drifts over time (Figure 3.17), which affects the calculated resistivities. The recorded voltages on the recording electrodes are more uniform (Figure 3.21), illustrating the benefits of the three and four-point techniques over the two-point technique when possible. Most critically, the two-point measurements in saline were unable to accurately calculate the resistivity of the saline solution, whereas the three-point saline validation did accurately calculate the resistivity. This, along with the spread in values for the two-point measurements in Table 3.3 highlights that the two point measurement techniques are both susceptible to contributions from the contact resistance, which can artificially increase the apparent resistivity, as well as local material properties, where increased amounts of CSF beneath the stimulation electrodes, but not elsewhere, could decrease the measured apparent resistivity relative to the three and four-point techniques.

3.14.7 Four-point Measurement for Saline Phantoms vs. Brain

The MAD for the saline solution was on the order of 0.10 ohm-m for the 3.44 ohm-m solution, and 0.03 for the 0.51 ohm-m solution. For the first seven subjects, the half-space model had MAD values ranging from 0.47 to 1.23 ohm-m. This indicates there is a larger spread of

resistivity values throughout the whole distribution, which is what we would expect for a non-homogeneous, layered substrate, where the distribution is comprised of the voltage differences between all possible recording electrodes.

3.14.8 CSF Considerations

A parameter we do not explicitly explore is the depth of the CSF. CSF, as a better conductor than the underlying brain tissue, is capable of shunting current away from the cortex in DES [202], and decreases the apparent resistivity seen at particularly close electrode separators. The fact that we see apparent resistivity values closer to that of gray and white matter than CSF leads us to conclude that there is a relatively thin layer of CSF beneath the majority of the electrodes in the array. For some of the two-point measurements, where the two-point value is far below the three or four-point measurements, we believe there to be more CSF than for the other subjects.

3.14.9 Implications for Source Modeling

An understanding of the global geometry of the surface, as well as the local paths through which current passes between electrodes, is important for both understanding how current applied will propagate, as well as understanding how signals at a neural source would propagate and attenuate at a distant location. Therefore, the principles of this resistivity modeling and important for anyone seeking to understand how the neural activity they measure reflects the neural signal source.

3.14.10 Future Directions

This research points to the applicability of simple analytic models to accurately depict the voltages measured on the surface of the cortex. The applicability to 3D geometries with implanted electrodes will be further studied as implanted depth electrodes become more

common for epilepsy monitoring.

To accurately characterize the resistivity of the gray matter would require electrodes with tighter spacing. For instance, assuming a gray matter thickness of 3.5 mm, a spacing of 7 mm between electrodes would be required to ensure that 50% of the current passes through the gray matter, and a spacing of 2.9 mm to ensure that 75% of the current passes through the gray matter [302].

Comparison and integration with FEM models will allow for enhanced understanding of current spread and cortical activation through tissue. The analytic models may serve as a simple benchmark for FEM models to be compared against. These analytic models do not replace FEM models, as on the smaller (less than electrode radius) scale the errors increase for the analytic model without correction factors or more complicated structuring. For studies with Utah arrays and μECoG arrays, FEM models would be of tremendous benefit. However, as we have experimentally acquired data which has been validated in a saline phantom, any FEM model should match the. Therefore the data contained within this work should serve as a benchmark for FEM models, where good agreement should be achieved between the FEM model and the measured data.

We cannot comment on the differences in voltages at the top or bottom of sulci and gyri purely from our model [251, 252], and similarly, the electric field vectors at any component would depend heavily on the geometry of the interface between materials of different resistivities in cortex.

The effect of DES on neuronal populations is complex [33], with excitatory and inhibitory effects depending on the stimulation parameters and parameters used. Work is being done to model the effect of DES through ECoG electrodes on the cellular population level [144]. A better understanding of how the current flows through the cortex, coupled with an understanding of how neurons respond to these currents, will enable a better understanding of DES.

3.15 Conclusions

We find in eight subjects that the voltage distributions across cortex due to bipolar, constant current stimulation are well described by both a simple homogeneous half-space model, and a homogeneous spherical model. The effect of the geometry of the problem affects the interpretation of the results with distance binned fitting, as a distance dependent effect is evident with the flat half-space model and not with the spherical model. This suggests that we are probing all three cortical layers (CSF, gray, and white matter) with our stimulation, and that measurement electrodes further apart do not receive substantially greater contributions from higher resistivity layers. In our eight subject, further apart stimulation probe separation did not systematically increase the apparent resistivity measured, further underscoring the idea that all three cortical layers are being probed, regardless of whether the electrode separation is 1 cm or 8 cm. We find that the two-point measurement technique through clinical ECoG electrodes is unable to accurately measure the the resistivity of saline phantom, unlike the three-point technique, which suggests that two-point measurements using bipolar, current controlled pulses in our arrays have resistance contributions from not just the bulk material. The four-point method, resulting in a distribution of apparent resistivity values, minimizes the effect of any particular choice of electrode for the reference electrode. These results illustrate the applicability of different resistivity measurement techniques on human brains through implanted electrodes and reveal the utility of simple analytic models for understanding volume conduction.

3.16 Code and Data Availability

The code to recreate our analyses and extensive figures for all seven subjects, as well as modeling analysis, is available from the following repository

https://github.com/davidjuliancaldwell/ElectrodeModeling.

The curated data is available publicly via a link in the github repository.

3.17 Related Publications and Presentations

Caldwell DJ, Cronin JA, Rao RPN, Ko AL, Ojemann JG, Sorensen LB, "What is the resistivity of the human brain? Insights from direct electrical stimulation, electrocorticographic recordings of the human cortex, and analytic models", BMC Neuroscience 2018, CNS 2018

Caldwell DJ, Cronin JA, Rao RPN, Ko AL, Ojemann JG, Sorensen LB, "What is the resistivity of the human brain? Insights from direct electrical stimulation, electrocorticographic recordings of the human cortex, and analytic models", Computational Neuroscience Meeting 2018, Seattle, WA, July 2018

Chapter 4

SIGNAL RECOVERY FROM STIMULATION ARTIFACTS IN INTRACRANIAL RECORDINGS WITH DICTIONARY LEARNING

Electrical stimulation of the human brain is commonly used for eliciting and inhibiting neural activity for clinical diagnostics, modifying abnormal neural circuit function for therapeutics, and interrogating cortical connectivity. However, recording electrical signals with concurrent stimulation results in dominant electrical artifacts that mask the neural signals of interest. Here we develop a method to reproducibly and robustly recover neural activity during concurrent stimulation. We concentrate on signal recovery across an array of electrodes without channel-wise fine-tuning of the algorithm, especially with trains of stimulation pulses that have varying parameters. We have made all of our code and data publicly available. We developed an algorithm that automatically detects templates of artifacts across many channels of recording, creating a dictionary of learned templates using unsupervised clustering. The artifact template that best matches each individual artifact pulse is subtracted to recover the underlying activity. To assess the success of our method, we focus on whether it extracts physiologically interpretable signals from real recordings. We demonstrate our signal recovery approach on invasive electrophysiologic recordings from human subjects during stimulation. We show the recover of meaningful neural signatures in both electrocorticographic (ECoG) arrays and deep brain stimulation (DBS) recordings. In addition, we compared cortical responses induced by the stimulation of primary somatosensory (S1) to natural peripheral touch, as well as motor cortex activity with and without concurrent S1 stimulation. Our work will enable future advances in neural engineering with

simultaneous stimulation and recording.

4.1 Introduction

Direct electrical stimulation of the brain is a powerful tool in both clinical and basic neuroscience; it is useful for probing neural circuitry [132, 177], modifying cortical connections [134, 314], as well as providing direct feedback to brain regions [45, 61, 63]. Importantly, electrical stimulation has promise to advance the emerging field of neuroprosthetics. However, the interpretation of neural activity during concurrent electrical stimulation is a substantial challenge. The recorded stimulus artifact induced by electrical stimulation is often orders-of-magnitude greater than the neural signals of interest, confounding traditional analytic techniques, such as time-frequency and time-series analyses [316]. Both hardware and analytic approaches have been developed to minimize the impact of electrical artifacts on neural recordings. Emerging front-end hardware solutions are promising [296, 316], but they will likely continue to work in concert with further processing after signal acquisition.

There is a wealth of work in the literature developing computational methodology to process recordings with concurrent electrical stimulation. These methods can be summarized as taking one of five different approaches to manage the stimulation artifact: *simple interpolation*, *template subtraction*, *biophysical modeling of the artifact*, *frequency-based filtering of the signal*, and *modal decomposition of the artifact from the signal*. Fortunately, an increasing number of these methods have been made available through toolboxes with code and data for rapid dissemination and evaluation of the results [82, 115]. Interpolation and curve fitting through the artifact window is a simple but often effective approach for short-duration artifacts, especially when the neural responses during these short artifacts are not the focus of the study [110, 282, 285]. Beyond interpolation, a variety of methods have instead subtracted an averaged template of the artifact window to estimate the underlying signal [108, 265]. Interestingly, these approaches have been extended for real-time closed-

loop stimulation in humans implanted with ECoG electrodes [308]. The template extraction method has been extended with a variation using unsupervised manifold learning [10]. An alternative approach is to make simplifying assumptions and construct biophysical models of the interactions between the electrical stimulation and the tissue to isolate the neural signals [275, 288]. Nevertheless, it is challenging to balance adequate recovery of the neural signal with complete artifact elimination in these time-domain subtraction methods.

The stimulation artifact can also be processed in the frequency domain. A variety of filters have been developed to match the characteristics of the artifact, including band-stop filters [126, 266], a Hampel filter [11], and a recursive Wiener filter [194], to name a few. Even with these advanced filtering methods, it remains difficult to isolate the neural signal when the frequency spectra of the signal and the artifact are overlapping [163, 201].

By leveraging correlations across multiple, simultaneously-recorded channels, much progress has been made using modal decomposition techniques to separate the neural signals from the artifacts. Commonly used methods have included independent component analysis (ICA, [99, 167]) and empirical mode decomposition (EMD, [9]). Another recent study has modeled the spatial and temporal correlations among a large array of electrical recordings as structured Gaussian processes [180]. Modal decomposition has also been used to generate artifact templates by sequential principal component regression (PCR), which are subsequently subtracted from the recordings [212].

In this paper, we develop a data-driven method based upon dictionary learning to recover neural signals from recordings with concurrent electrical stimulation. The method proposed here is a type of template subtraction; our innovation lies in using unsupervised machine learning to learn a dictionary of artifact templates. In particular, our method is designed to perform well with ongoing trains of stimulation across many channels in human intracranial recordings. Trains of stimulation are required to provide therapeutic benefit through modalities such as DBS [192] and to serve as feedback in neuroprosthetic applications with DES

of primary somatosensory cortex [63]. When many stimulation trains are used, pulses may have varying stimulation parameters, the recorded waveforms may differ depending on the sampling, and their proximity to each other may lead to ambiguity in separation from the neural signals.

We demonstrate the performance of our method on several different human intracranial experiments, including stimulation of S1 and DBS. For the S1 stimulations, we also compare the neural responses across the array of recording electrodes for DES and natural haptic touch. In addition, we show that our method extracts adjacent motor cortical activity with concurrent S1 stimulation. Such signal extraction is important in the design and analysis of future stimulation and protocols. We have made all of the code and data publicly available, which will serve as a resource to accelerate future research in neural engineering with concurrent stimulation and recording. Our dataset includes five different subjects performing five different tasks; we hope that these datasets may be used as common testbeds for others who contribute further algorithmic developments.

4.1.1 Data Acquisition and Stimulation

Neural data were acquired at 1221, 12207 or 48828 Hz using a Tucker Davis Technologies (TDT) System 3 with the RZ5D and PZ5 Neurodigitizer (Tucker Davis Technologies, Alachua, Florida, USA). We delivered stimulation through the TDT IZ2H-16 stimulator and LZ48-400 battery pack (Tucker Davis Technologies).

4.1.2 Haptic Touch Dataset

The neural data acquired for comparisons between stimulation of S1 and natural haptic touch are from experiments previously described [45], in which subjects received S1 stimulation and peripheral haptic touch to the same localized spot during a response timing task. We used 200 Hz, biphasic(200 μs pulse width), bipolar, 2 mA constant current stimulation trains

of 400 ms duration.

4.1.3 Non-uniform Train Dataset

The neural data acquired for the non-uniform train set were sampled at 12207 Hz. Stimulation waveforms consisted of two, 3 mA pulses followed by 38, 1.5 mA pulses at 200 Hz, for a total of 200 ms of bipolar, biphasic (200 μs pulse width) stimulation.

4.1.4 Button Press Dataset

The neural data acquired for extracting motor behavior with stimulation of sensory cortex was acquired with a subject performing a self-paced motor button pressing task with and without concurrent, random stimulation of S1. The subject was instructed to press the button firmly and consistently, while an experimenter randomly stimulated S1 during the activity. The subject was told not to respond differently based on the stimulation, and was able to complete the button pressing task both with and without stimulation. We used 200 Hz, 200 μs pulse width, biphasic, bipolar, 1.5 mA constant current stimulation trains of 200 ms duration.

4.1.5 DBS Dataset

The neural data acquired for the DBS set were acquired intraoperatively during DBS lead placement, with stimulation and recording through the TDT system on a four-contact implanted Medtronic lead. Subjects received 15 epochs of 4 different stimulation amplitudes (1.5, 2, 2.5, 3V, all of 500 ms duration) with 185 Hz, bipolar, monophasic (60 μs pulse width) constant voltage stimulation, for a total of 60 epochs.

4.1.6 Rubber Hand Illusion Dataset

The neural data to illustrate inadequate sampling for stimulation epoch processing were sampled at 1221 Hz and were previously described in Collins et al. 2017 [61]. 100 Hz, 2.2 mA constant current, biphasic (200 μs pulse width), bipolar stimulation was used.

4.2 Signal Recovery Algorithm

Our goal was to develop an algorithmic approach to recover neural signals recorded concurrently with electrical stimulation. We have designed our algorithm with a number of key assumptions of the neural data. First, we assume that the data are acquired by recording amplifiers that do not saturate during stimulation, are capable of oversampling, and are synchronized between recording and stimulation devices. Second, we assume that the timing of artifact windows may be extracted in all channels by the stimulation onset from a single channel; this assumption draws on knowledge that volume conduction is much faster than neural signal propagation. Our software includes options to recover stimulation pulse-evoked potentials, and to dynamically detect the offset of stimuli pulses on a channel and pulse-wise basis.

Figure 4.1 illustrates the overall algorithm; each step in the pipeline is elaborated in the subsequent sections. Briefly, raw recorded data during stimulation epochs from many channels are taken as input; these typically include trains of concurrent stimulation (Figure 4.1(a)). Individual pulses within each of these epochs are detected (Figures 4.1(b), 3) and clustered using a density-based algorithm (HDBSCAN, or (hierarchical density-based spatial clustering of applications with noise) [47]) to learn a dictionary of artifact templates. Since this step is crucial for the success of our signal recovery, it is shown in more detail in Figure 4.3. Next, each individual pulse is compared to this dictionary, and the closest template (Figure 4.1(c)) is subtracted from the raw pulse. After subtraction, subsequent analyses in the time and frequency domains may be performed on the recovered signals

directly (Figure 4.1(d)).

4.2.1 Detection of Artifact Windows

We begin with e epochs of data that are each t time snapshots by c channels, so the size of the input is $(t \times c \times e)$. Instead of relying on alignment to stimulation pulses, we detect artifact windows by leveraging timing information on the channel with the largest electrical artifact magnitude. To estimate artifact onset and offset, we use a Savitzky-Golay filter [245] to reduce high frequency noise (3rd order, 7 samples, or 0.57 ms at 12207 Hz). We have empirically found an absolute Z-score threshold of 1.5 to successfully detect the onset of the artifacts, but this parameter can be modified by the user.

We then define a set window size (an example is below) around each single pulse and align the start of these windows to extract pulses from all epochs (Figure 4.1(b) and Figure 4.3(a)). For the data shown for the first data set (Figures 4.1–4.5), we used a time window of 0.8 ms before the detected onset of stimulation. We subsequently used a Z-score threshold on both the raw voltage and differentiated smoothed signal (75% cutoff) to select the end of each stimulation pulse. This estimate was computed for each pulse, in each epoch, and in each channel. An extra 1 ms was added after the end of each artifact to ensure that the entire artifact had been adequately sampled. In this way, we transform the $t \times c \times e$ input data to be a cell of size $(t_p \times c \times (e \times p))$, where t_p is an index for the time window for each pulse on each channel and p is the number of pulses. The smoothed signal is not used further in the signal recovery pipeline.

To make these extracted individual pulses suitable for unsupervised clustering, we equalized the pulse lengths by zero-padding the end of each pulse within a channel, so that they are all the same length (Figure 4.3(a)). In order to normalize the onset baseline of the artifact window, a user defined number of samples is used to define a period over which an average is calculated, and this average is subtracted from the entire pulse to normalize it. In

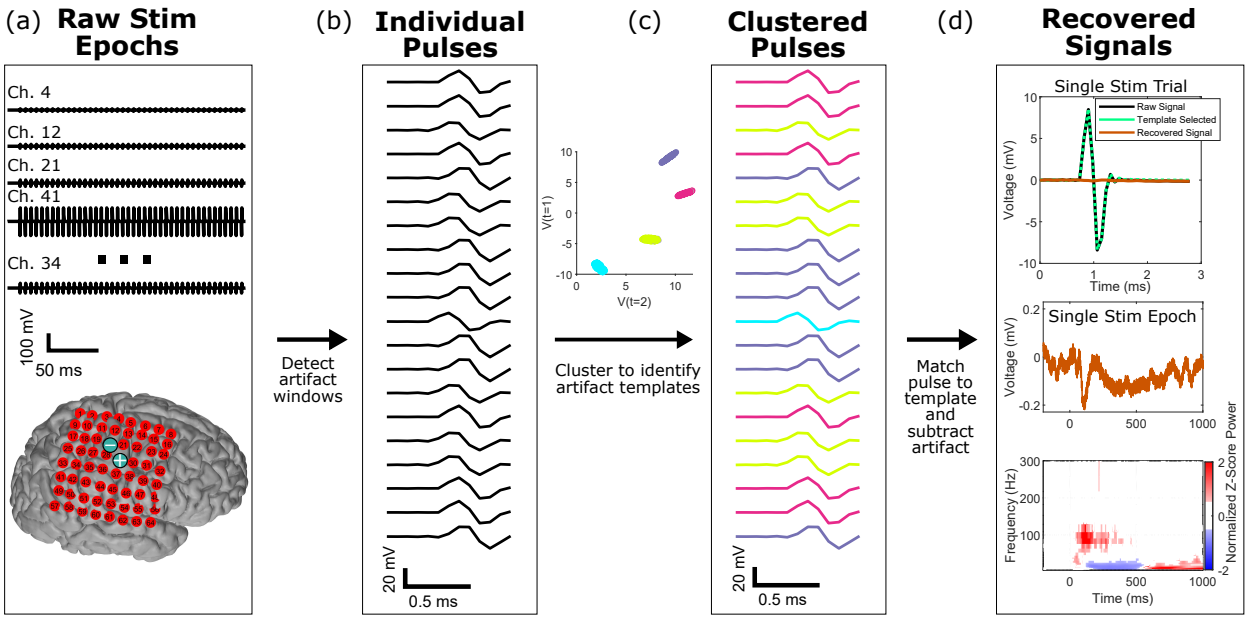

Figure 4.1: Schematic overview of our method for signal recovery with stimulation artifacts. (a) Raw stimulation signal epochs (time × channel × epoch) are recorded across an array of electrodes, as shown on a cortical reconstruction of one patient. The two electrode locations indicated by blue $\oplus$ and $\ominus$ signs were the sites of the electrical stimulation. These are the input for our algorithm. (b) Individual pulses are identified and extracted within each of these stimulation epoch time periods across all the channels in the array. A small random subset are visualized here. (c) An unsupervised hierarchical density-based clustering technique (HDBSCAN) is used to cluster the individual pulses. Each pulse is colored by the artifact template to which it clustered. (d) Signals are recovered by subtraction of the closest artifact template for each pulse. Subsequent analyses can then be performed directly on the output signals, which are the same size as the input data.

this work, we have used the first 3 samples of the artifact window, as this is empirically what has worked well with our data sets, but longer time periods, as well as mean of each window could be used. These onset times, offset times, percentage thresholds, and normalization duration are all parameters in the algorithm and are tunable by the user to the particular nuances of their data.

4.2.2 Comparison to Recovery by Alternative Methods

Once each stimulus pulse has been isolated, the next step aims to reduce the artifact present within this window. The electrical artifact is typically many orders-of-magnitude larger in amplitude than the underlying neural signals (Figure 4.2(a)), making this task particularly challenging. Additionally, the effect of the artifact extends into frequencies other than just the stimulation frequency and its harmonics.

One strategy is an interpolation scheme that ignores the artifact itself, filling in the data between the endpoints of the stimulus artifact. As noted, variants of these have been used for electrophysiologic recordings with concurrent stimulation. Figure 4.2(c) shows the results of a shape-preserving piece-wise cubic interpolation scheme using data points adjacent to the stimulus artifact. Code to perform this interpolation is provided in our repository. While the recovered signal in the time domain is continuous and in the right order-of-magnitude in voltage, Figure 4.2(c) shows that the interpolation scheme has introduced large, undesirable signals in the frequency domain.

Another common approach is low pass filtering, which as shown in Figure 4.2(d,e) overly smooths the time-domain signal and either eliminates neural signal in the time-frequency domain (Figure 4.2(d), or fails to remove the stimulation artifact (Figure 4.2(e)). Although the time-series signal may look smooth, the normalization to baseline time periods without artifact, as commonly done in neural analyses, still introduces spectral artifacts.

Another approach is ICA. Here, an ICA implementation which selectively removed ICA

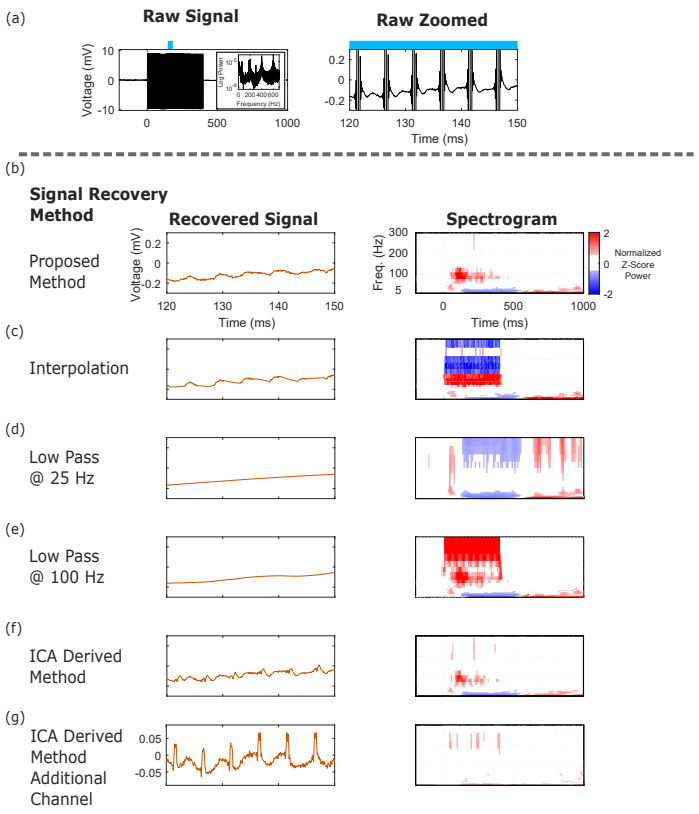

Figure 4.2: Comparisons between artifact rejection with our dictionary learning method and alternative methods as illustrated with a single channel. (a) A raw stimulation epoch, from concurrent stimulation and recording. The broad spectral nature of these artifact reveals significant overlap between spectral features of interest and the stimulation frequency. (b) Signal recovery by our method has leveraged the data to account for variable artifacts in the raw voltage and timing across different channels. Our approach captures both time-series and time-frequency information well. (c) Piece-wise cubic spline interpolation locally reduces the time-domain artifact, but the time-frequency plot illustrates how large, undesirable signals have been introduced, highlighting how similar time-series traces can have significantly different spectral content. (d) Low pass filtering at 25 Hz with a 4th order acausal butterworth filter eliminates the high frequency artifact at 200 Hz, but flattens the time-series signal and eliminates the 100 Hz activity recovered in panel (b). (e) Low pass filtering at 100 Hz fails to eliminate the high frequency artifact at 200 Hz, and flattens the time-series signal. (f) An ICA derived method that selectively removes components with a dominant 200 Hz spectral component removes the 200 Hz artifact, but also attenuates the time-varying spectral information in panel (b). (g) The same ICA derived method results in incomplete signal separation on other channels within the array, leaving large residual artifacts.

components with a 200 Hz spectral peak was used to attempt to eliminate the stimulus artifacts. This resulted in reasonable performance in the time-frequency domain (Figure 4.2(f)) for the same channel as panels (a–f), but there were residual artifacts present in the time-series signal. Most importantly, other channels (Figure 4.2(g)) had large residual artifacts. This points to the difficulty in blind source separation using ICA even with domain-specific optimization for signals that have artifact components orders-of-magnitude greater than the neural signals of interest, that are not consistent in shape across channels.

4.2.3 Dictionary Learning with Unsupervised Clustering to Extract Artifact Templates

Electrical artifacts recorded at each pulse on each channel have different waveforms. Consequently, the mean artifact waveform is a poor representation of individual artifacts. Differences in artifact morphology arise from a few different sources, including slight temporal offsets due to windowing, fine differences in timing of sampling, different stimulation parameters during and across epochs, as well as varying factors at each electrode-tissue interface. Nevertheless, there are stereotypes of artifact waveforms, and here we have implemented a data-driven strategy for learning these templates. In particular, we created a dictionary of artifact waveforms from all pulses and all epochs of each channel using unsupervised clustering.

Our algorithm uses a modified HDBSCAN algorithm for clustering [47], which is in turn a variant of the classic DBSCAN algorithm [84]. We use a MATLAB implementation of HDBSCAN openly distributed on GitHub [262]. This algorithm discovers dense regions (clusters) within a noisy dataset; the algorithm determines the number of clusters that explain the data, given three key parameters that must be chosen by the user. The first parameter is the minimum cluster size n, which is to say, the minimum number of data points considered a cluster. The second parameter is the number of neighbors k used in the density computation; increasing this parameter restricts clusters to increasingly dense areas.

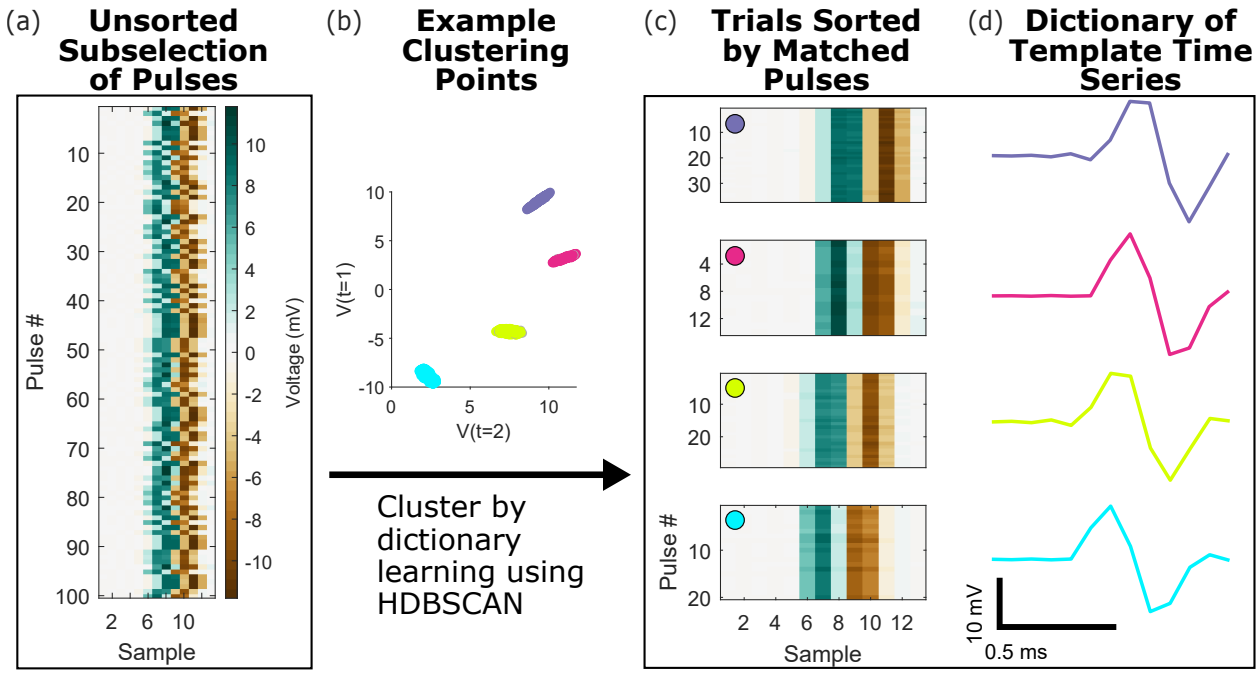

Figure 4.3: Clustering, dictionary learning, and template matching. (a) The input to clustering is a matrix of mean-subtracted raw voltages following artifact onset and offset detection, shown here as a heatmap for a small subset of trials. The sampling rate for this data is 12207 Hz. (b) Example voltages at two time features used for clustering, which are input into an HDBSCAN clustering algorithm. (c) The voltage data sorted by matched templates, color coded to match the clusters in panel (b). (d) The four extracted artifact template clusters for the raw traces in panel (a).

The third parameter is the outlier score threshold $\theta = [0, 1]$, above which an observation is considered to be noise. In our haptic touch, variable stimulus amplitude, and DBS datasets, we specified $n = 2$, $k = 3$, and $\theta = 0.9$. For our button press dataset, we used $n = 15$, $k = 10$, and $\theta = 0.95$.

All the pulses for each channel are clustered together. Figure 4.3(a) illustrates the input data matrix for the clustering; 12 features were used in the clustering, taken as 6 samples (0.5 ms) on either side of the time at which the maximum absolute value voltage occurred. The number of features is able to be defined by the user depending on how many informative data points are contained within a given artifact pulse. This number of features is independent of the window length, and allows for selection of the maximally separable number of points by the user for any arbitrary window length. We chose this part of the artifact to manage the dimensionality of the clustering task, focusing on the time-point features that are most informative about the separability of stimulus artifacts. Two of these time-point features are shown in as axes in Figure 4.3(b), which shows the clustering of artifacts into 4 distinct regions in this example.

4.2.4 Signal Recovery by Template Matching and Artifact Subtraction

The mean waveform of every cluster form the dictionary of artifact templates (Figure 4.3(c) and (d)). The correlation of each individual pulse in the signal with each of the templates in the dictionary is calculated, and the maximally correlated template is chosen. We use correlation to minimize the impact of scaling and normalization in our template selection. Once the best template has been selected, it is subsequently scaled by ratio of the template's range to the individual pulse's range. This is to adjust for slight changes in stimulation pulse amplitude across pulses. Finally, the scaled template is linearly subtracted from the time window for that pulse to recover the neural signal (Figure 4.3(c,d)). We also implement for comparison an average within epoch template subtraction scheme, as well as an average

across all stimulation pulses for each channel (data not shown). Under simple cases, these methods may perform as well as the more complex method detailed above, but for varying amplitude waveforms, large exponential recovery components of the signal, and stimulation pulses with different sampling times, our more advanced method outperforms these other approaches (Figure 4.7,4.8).

4.2.5 Post-processing and Visualization

Following signal recovery, we performed averaging of the epochs to obtain the average time-series visualized in this paper. For Figure 4.6, we performed common average rereferencing against the non-stimulation channels to remove common noise. On each epoch, we use non-analytic Morlet wavelets [41, 290] to calculate amplitude in time and frequency bins. We used 10 ms bins as our time resolution for the wavelet processing. We visualized the 5-300 Hz region to avoid including lower frequencies where edge effects from the wavelet processing may exist, and to focus on signals such as broadband gamma [188]. We considered broadband gamma to be an aggregate of local neuronal activity and to be more easily separated from lower frequency oscillations above 50 Hz. The time-frequency plots for the haptic touch datasets were Z-scored relative to a baseline period from 800 ms to 5 ms before stimulation or before touch onset within each frequency band. In the button press datasets, the plots were normalized relative to the trial for -900 ms before button press to 900 ms after button press, as there was no consistent baseline period before each trial.

4.3 Results

Our unsupervised clustering approach to learning artifact templates is reproducible and robust, recovering underlying neural signals recorded concurrently with electrical stimulation. We demonstrate that the signals recovered in a variety of different human intracranial recording datasets are interpretable and physiologically valid. Importantly, our method preserves

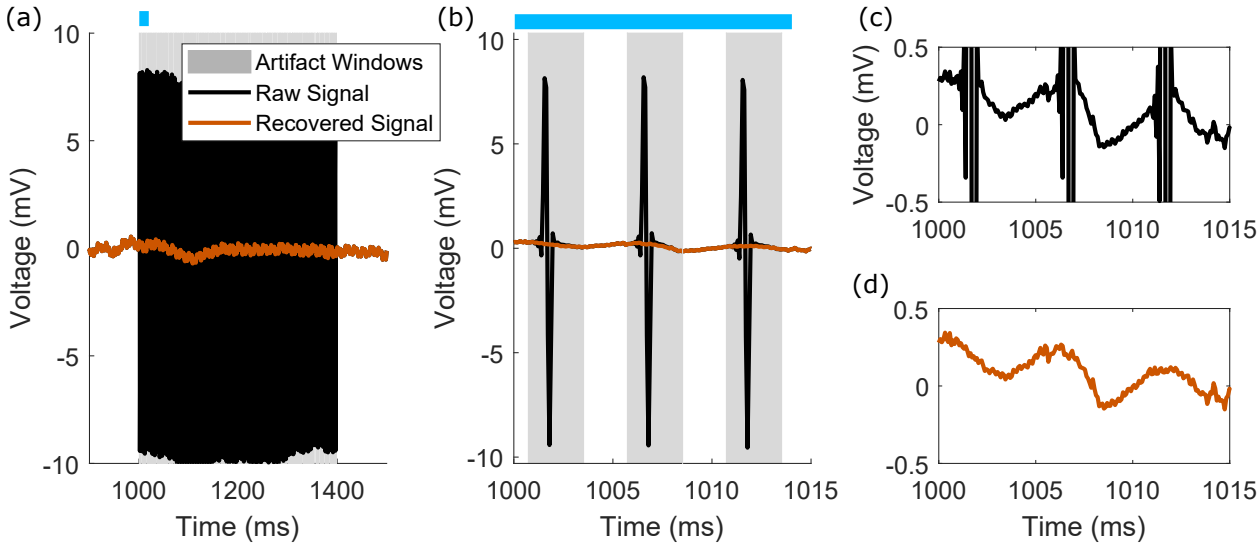

Figure 4.4: Details of the raw and recovered time-series signals. (a) The raw (black) and recovered (orange) time-series data for one epoch, with gray windows indicating the artifact windows. The channel highlighted is channel 28 in Figures. B.1–B.2. The blue bar indicates the period of time shown as zoomed in time in panel (b). (b) Zoomed-in region of panel (a), highlighting the onset and offset for each individual artifact, and the recovered signal. (c) and (d) Corresponding raw and recovered signals at a smaller voltage scale for panel (b), highlighting the preservation of signal outside of the artifact window. Signal recovery within the artifact window has no obvious discontinuities.

time-points outside the stimulation epochs from further processing, which mitigate any adverse effects of the signal recovering algorithm on data without artifacts. Figure 4.4 compares the raw and recovered signals for one stimulation train epoch of one channel from an array of intracranial recordings; results from the rest of the channels for this subject and a second subject are shown in Figures. B.1–B.2.

4.3.1 Comparison between Direct Electrical Stimulation of S1 and Natural Haptic Touch

To demonstrate that the recovered neural activity is physiologically meaningful and valid, we highlight results comparing neural recordings from direct electrical stimulation of S1 to those from peripheral haptic touch. As illustrated in Figure 4.5(d), the haptic touch was localized to the same region where the stimulation sensation was localized. Figure 4.5(a) and (e) show the raw signals recorded on the same channel, one adjacent to the stimulation electrode, where the 200 Hz stimulation train dominates the recording. Despite these large-amplitude stimulation train artifacts present in the raw signal, we observe that the overall structure of the neural response in the time domain of the recovery signal (Figure 4.5(b)) closely resembles the raw signal from the haptic touch (Figure 4.5(e)). Crucially, the S1 stimulation and natural haptic touch signals show strong similarities in the time-frequency domain (Figure 4.5(c) and (f)). In addition, there is no evidence of aliasing in the spectrogram at the stimulation frequency band (200 Hz).

4.3.2 Comparison between Motor Activity with and without DES of S1

In a related experiment, we analyzed neural responses at an electrode that showed motor activity during a self-paced button pressing task; we compared epochs with and without concurrent stimulation of the ipsilateral hand S1 cortex. In Figure 4.6, the data were aligned and averaged using the timing of the self-paced button presses. We observed a striking overlap in both the time-series and time-frequency domain between epochs with and without stimulation, as well as no evidence of residual power in the stimulation frequency band of 200 Hz. The size of the artifacts in the averaged signal before processing is smaller than in Figure 4.5 because the epochs here are aligned not on stimulation onset, but rather on button press, resulting in the stimulation pulses being averaged out across trials.

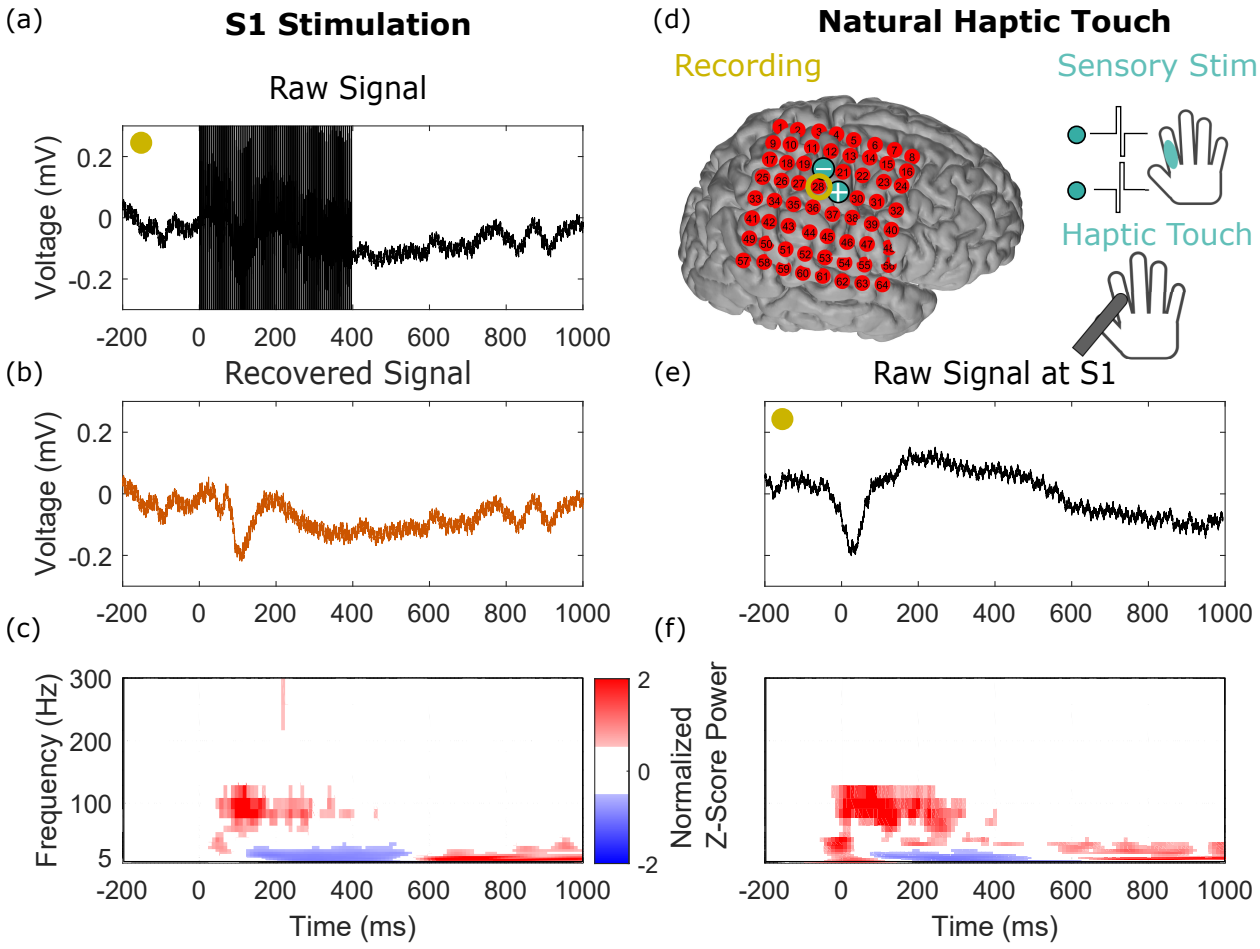

Figure 4.5: Signal recovery shows meaningful neural activity after artifact subtraction in a comparison of electrical stimulation with peripheral haptic touch. We compared responses at an electrode (yellow circle) that showed robust responses to both haptic and direct S1 stimulation. The site of the touch was matched to where the stimulation sensation was localized, as illustrated in (d). (a) The raw time-series trace, averaged over all stimulation epochs, aligned on stimulation train onset at time t = 0 ms, showing prominent stimulation artifacts (a train of pulses at 200 Hz applied for 400 ms). (b) The average of the recovered signal. (c) The time-frequency plot of the signal in panel (b). (d) The experimental paradigm. (e) and (f) The mean time-series and time-frequency plots of the haptic touch experiment aligned on touch onset, which occurs at time t = 0 ms.

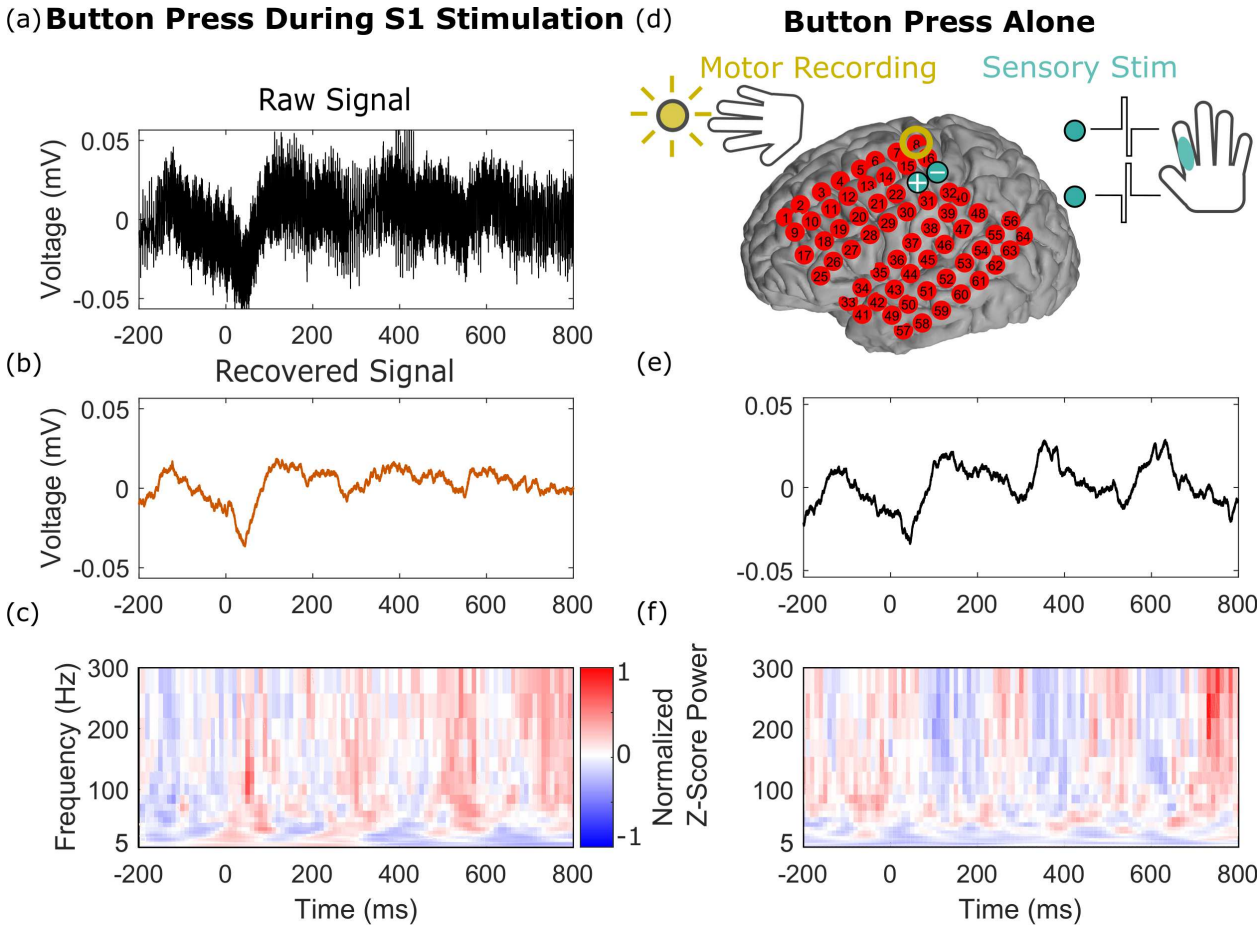

Figure 4.6: Signal recovered during a self-paced button pressing task with and without concurrent stimulation are comparable. We analyzed responses at one electrode (yellow circle in panel (d)) in motor cortex. (a) Raw time-series trace during S1 stimulation (200 Hz trains at turquoise electrodes in (d)), aligned to time of button presses. (b) and (c) The recovered signal, shown as time-series and time-frequency plots. (d) The experimental paradigm, where the subject perform a self-timed button pressing task and received electrical stimulation in S1 of the same hand on some of the trials. (e) and (f) The time-series and time-frequency plots of the stimulation-free conditions.

4.3.3 Recovery with Non-uniform Stimulation Trains

A key feature of our algorithm is its ability to adapt to time-varying stimulation pulse amplitudes (Figure 4.7). In this scenario, an approach where the template is computed as an average within stimulation epoch would fail. Non-uniform stimulation trains are useful because neural activity is frequently non-uniform in amplitude over time. For instance, object contact onset and offset is coded by neurons in S1 primarily through the highest firing rate during touch onset and offset, and decrease their firing during the maintenance of touch [216]. Therefore, stimulation with trains that mimic the natural firing patterns of neurons may be more effective for neuroprosthetic applications to encode contact with an object [268]. When using a non-uniform stimulation train, we are able to recover rapid evoked potentials after the onset of each stimulation pulse which occur within 2 ms of the stimulus, which would be missed if the artifact windows were not carefully selected (Figure 4.7(c,d)). In addition, the time-frequency representation of the processed signal appears to have an artifact in the frequency band of stimulation (200 Hz), but we believe this to be a real response driven by the rapid onset evoked potentials triggered from the 200 Hz stimulation (Figure 4.7(b)). We emphasize that we have used one set of parameters for all of the channels within this ECoG array and have been able to achieve good results across the array without detailed fine tuning (Figures B.3–B.4 show the time-series and time-frequency responses for the entire array).

4.3.4 Extraction of Early-Evoked Potentials in DBS Recordings and Concurrent ECoG Recordings with DBS stimulation

In some stimulation paradigms, signals are known to exhibit long exponential recovery to baseline. We isolated early, rapid evoked potentials in deep brain stimulation (DBS) electrodes with concurrent stimulation (Figure 4.8(a)), where Figure 4.8(b),(d) show the recovered evoked potentials. In addition, using the same parameters for an ECoG strip concurrently recording results in good performance in acquiring the resultant surface cortical

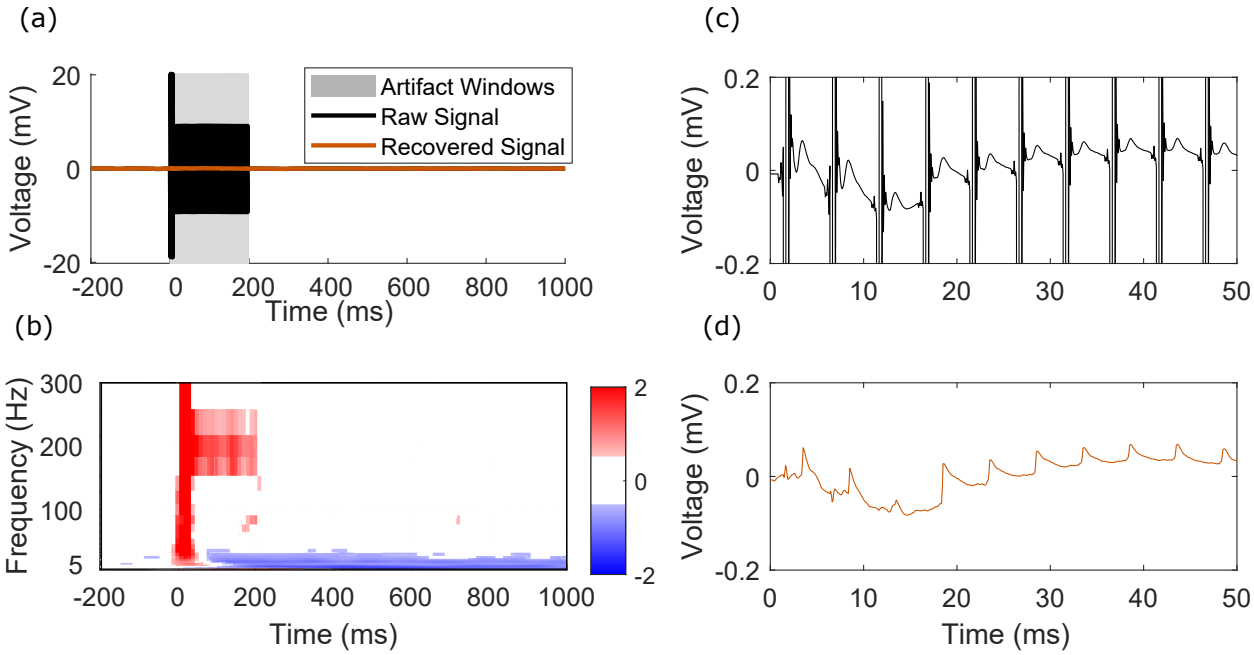

Figure 4.7: Recovery of signals from non-uniform stimulation trains and recovery of rapid evoked potentials. (a) Overlaid raw and processed signal for channel 15 in Figures B.3–B.4, highlighting initial two high amplitude pulses, followed by a train of lower amplitude pulses. Average epoched template subtraction would fail to recover the correct signal here. (b) Time-frequency plot of the recovered signal, highlighting the representation of the reproducible rapid evoked potentials in the time-frequency domain. The units are normalized Z-Score power as in other figures. (c) Zoomed-in raw signal highlighting rapid evoked potentials following each stimulation pulse. (d) Recovered signal highlighting the preservation of these early evoked potentials.

activity (Figure 4.8(f)).

4.3.5 Limitation of the Algorithm

Despite meaningful signal recovery in a number of circumstances, there are conditions under which the algorithms presented here are unable to recover the neural signal. One example of this failure is show in Figure 4.9, which shows a dataset acquired at a lower sampling rate (1221 Hz) and previously described in [61]. In particular, when the stimulation waveforms are not well resolved, such as when the signal is under-sampled, our algorithm performs poorly in discovering clusters and artifact templates (Figure 4.9(a)). Since the template learning procedure failed, our method was unsuccessful in recovering the neural signals (Figure 4.9(e)). We define unsuccessful signal recovery here as residual artifacts on the scale of the original signal, as well as no additional insight to the underlying neural activity (Figure 4.9(e)).

4.4 Discussion

Analyzing signals acquired with concurrent exogenous stimulation and recording is complicated, in large part because both the physics of direct electrical stimulation and subsequent neural responses are not well understood [33]. Therefore, there is no true ground truth on which to train and evaluate signal recovery algorithms. Previous work have made use of synthetic datasets to validate signal recovery. While simulations offer the advantage of knowing precisely what ought to be recovered, synthetic data do not accurately recapitulate key features of real data [308]. Artifacts can be different across individual channels and over time during the recordings, and may not be fully described by simple analytic models. For instance, past work have assumed constant voltage stimulation, where in our experiments we use constant current stimulation [275]. Beyond a simple RC circuit for the electrode-tissue interface, there are additional considerations from Faradaic and non-Faradaic reactions [181].

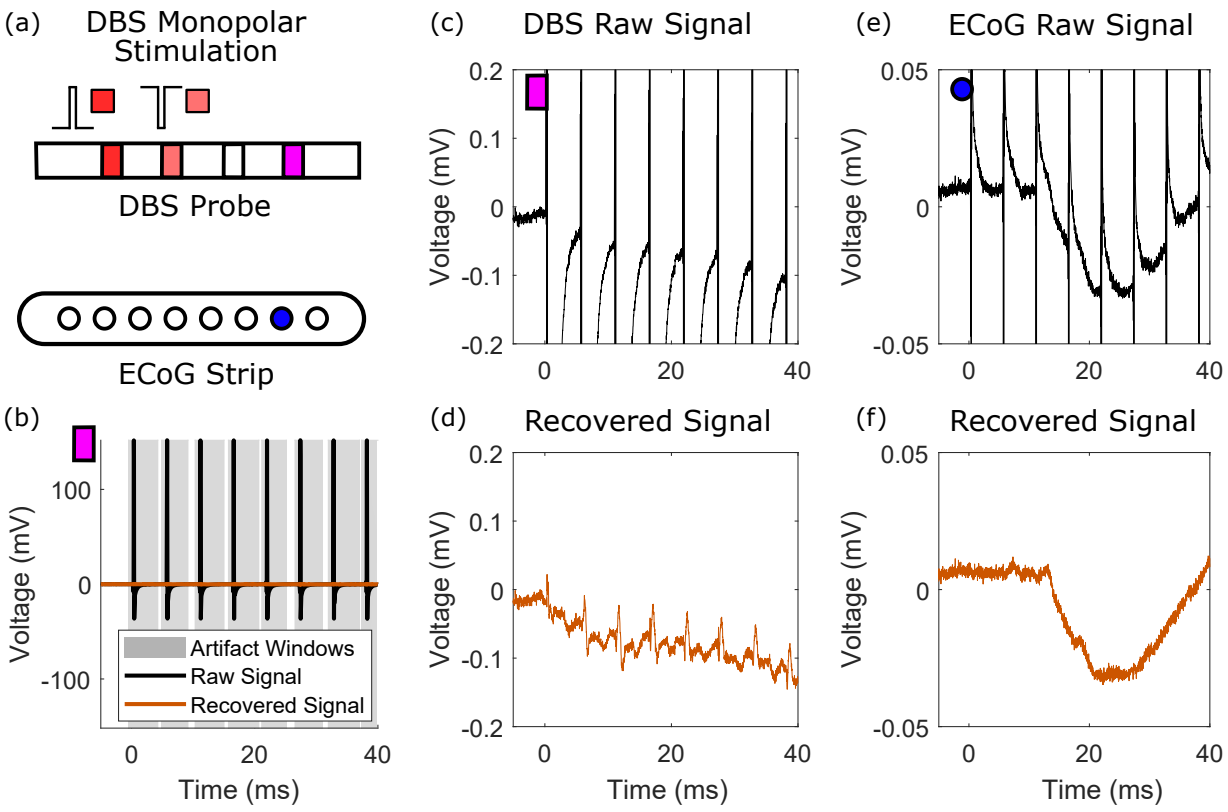

Figure 4.8: Recovery of early evoked potentials on DBS electrodes. (a) Bipolar, monophasic stimulation through DBS electrodes, with concurrent recording on the other channels. The example DBS and ECoG recordings are show by the purple rectangle and blue circle. (b) Raw and recovered example epoch, with the artifact windows highlighted. (c) Raw average signal on a DBS channel within the same probe as the stimulation electrodes. (d) Recovered average signal after template matching on the corresponding signal shown in (c), illustrating an early evoked potential. (e) Raw average signal on ECoG electrode during stimulation through the DBS electrode. (f) Recovered signal corresponding to (e).

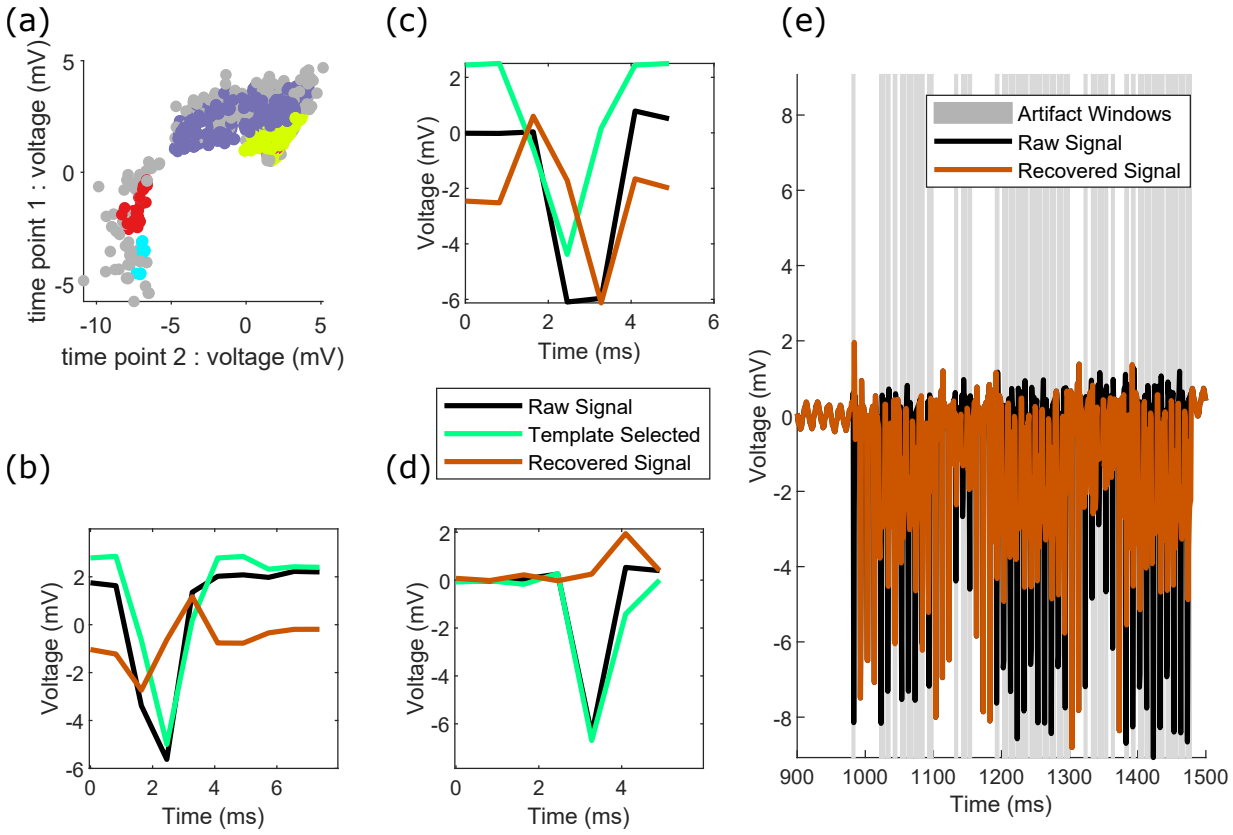

Figure 4.9: An illustration of failure to recover signal where the S1 stimulation data had been acquired at a lower sampling rate (1221 Hz) [61]. Partly due to the lower sampling rate, there were a number of failure modes. (a) The density-based clustering method did not produce distinct clusters (compare to Figure 4.3). Gray points represent individual trials which were classified as outliers and were not part of a cluster. (b) The template selected was not an ideal match and was imperfectly scaled. (c) The wrong template was selected. (d) The end of the template was not accurately calculated. (e) The result of these mismatches was unsuccessful separation of neural signal from the stimulation artifacts. We define unsuccessful signal recovery here as residual artifacts on the scale of the original signal, as well as no additional insight to the underlying neural activity.

Therefore, we highlight here examples with meaningful recovery of biologically interpretable signals as the goal. In Figure 4.6, we recovered patterns of decreases in low frequency power followed by increases in high frequency power. This pattern of cortical responses during over motor control is a well established phenomenon, having been observed throughout the systems electrophysiological literature [187], and the cyclic nature of the pattern observed is illustrative of the rapid, self timed nature of the task for this subject. Similarly, the overlap in the time-series and time-frequency plots in Figure 4.5 supports that we have extracted biologically grounded signals from our stimulation case.

Signals that are similar in the time domain may be quite different in the frequency domain (Figure 4.2). This discrepancy points to the importance of examination of the data in both the time and frequency domains following processing. Simple filtering approaches can either overly attenuate the frequency components of interest (Figure 4.2(d)) or fail to eliminate artifact components in the frequency domain (Figure 4.2(e)). Modal decomposition techniques, such as our ICA implementation in Figure 4.2(f,g), can exhibit superior performance to interpolation and filtering approaches, but it is difficult to ensure satisfactory performance across the entire array of electrodes (Figure 4.2(g)).

In our time-frequency plots (Figures B.2, B.4), we do not see aliased power at frequencies lower than the stimulation frequency, which is a potential issue with template approaches on epoched data without sufficient oversampling and artifact removal [163]. The extent of our oversampling is visible in Figure 4.1, where the maximum and minimum values for each of the stimuli within a stimulation epoch do not vary greatly. We acknowledge that our approach is not appropriate for all instances of human electrophysiologic data. In our experience, 200 Hz stimulation trains with pulse widths of 200 μs, sampled at 1221 Hz (Figure 4.9) were too under-sampled for use with our algorithm.

There has been much progress in the past decades with other template subtraction approaches [108], and the methods described here are an extension of these ideas. Our algorithm

leverages information across many channels at once, on a pulse-wise, channel-wise basis, by determining the likely window of the artifacts, and by clustering templates even in the presence of noisy outlier trials. The results shown in Figure 4.4 may be captured by a simpler approach where templates are computed as means within each epoch. However, in the case of more complex waveforms with varying parameters within a stimulation train (Figure 4.7), an average template during a train would be unsuccessful in recovering the underlying neural signal. Even so, our use of unsupervised clustering for template learning inherits some of the limitations of density-based methods [8]. Specifically, artifacts with many points require clustering in higher dimensions, which is both less computationally efficient and requires more densely sampled data.

The code provided includes default parameters that perform reasonably well for the included datasets. A key point is that all channels within a given dataset were processed with the same parameters. Better performance could be achieved with tuning of parameters for different channels. Without adequate oversampling, alternative approaches using upsampling [265] may be appropriate, or in a worst case, interpolation could be performed to estimate the time course of lower frequency signals. Where residual low frequency aliasing occurs, a Hampel filter, which has been successfully used for concurrent DBS/EEG stimulation and recording, could be used [163].

The analysis of electrical recordings with concurrent stimulation may benefit from future developments driven by modern methods in simulation and machine learning. A combination of model-based and data driven approaches would help construct a more principled set of templates to separate neural activity from electrical artifacts. Deep learning, which has begun to find applications in signal processing [312] and ECoG processing [291], could also benefit the artifact processing community if enough training data were available.

4.5 Conclusions

Electrical stimulation applied concurrently with recording results in signals that contain both neural activity and electrical artifacts. Here we developed a novel algorithm that automatically detects electrical artifacts across many channels of recording, constructs a dictionary of learned templates using unsupervised clustering, and performs pattern matching to best extract the underlying neural activity. Rather than evaluate our method on synthetic data, we demonstrated the efficacy of our approach on real human stimulation data in both ECoG arrays and DBS recordings. Further, we showed that the signals recovered have physiologically meaningful neural signatures in two datasets, providing good ecological validity for our method. In the first dataset, we showed that responses to stimulation of S1 and natural peripheral touch elicited similar responses. In the second, we showed that motor cortex activity in a button pressing task was similar with and without S1 stimulation. All of the code we developed and data sets we used have been made openly and publicly available.

4.6 Code and Data Availability

Full MATLAB code and a link to the data is available at https://github.com/davidjuliancaldwell/artifactRe

We hope these datasets may serve as benchmark datasets for future algorithm development and testing.

4.7 Related Publications and Presentations

Caldwell DJ, Cronin JA, Rao RPN, Collins KL, Weaver KE, Ko AL, Ojemann JG, Kutz JN, Brunton BW, "Signal recovery from stimulation artifacts in intracranial recordings with dictionary learning", Journal of Neural Engineering, in-preparation, 2019

Caldwell DJ, "Understanding the Neural Response to Direct Cortical Stimulation", UW Data Science Summit, April 2018

Caldwell DJ, "Engineering direct cortical stimulation in humans", UW Neural Computation and Engineering Connection, January 2018

Chapter 5

DIRECT STIMULATION OF SOMATOSENSORY CORTEX RESULTS IN SLOWER REACTION TIMES COMPARED TO PERIPHERAL TOUCH IN HUMANS

DES of S1 could help restore sensation and provide task-relevant feedback in a neuroprosthesis. However, the psychophysics of S1 DES is poorly studied, including any comparison to cutaneous haptic stimulation. We compare the response times to DES of human hand somatosensory cortex through electrocorticographic grids with response times to haptic stimuli delivered to the hand in four subjects. We found that subjects respond significantly slower to S1 DES than to natural, haptic stimuli for a range of DES train duration. Median response times for haptic stimulation varied from 198ms to 313ms, while median responses to reliably perceived DES ranged from 254ms for one subject, all the way to 528ms for another. We discern no significant impact of learning or habituation through the analysis of blocked trials, and find no significant impact of cortical stimulation train duration on response times. Our results provide a realistic set of expectations for latencies with somatosensory DES feedback for future neuroprosthetic applications and motivate the study of neural mechanisms underlying human perception of somatosensation via DES.

5.1 Introduction

While prior work suggests that the integration of somatosensory feedback into a BCI is possible and enhances performance relative to a task without somatosensory feedback, the comparison of human S1 DES to haptic stimulation has not been well explored. Specifically, given that S1 DES completely circumvents ascending dorsal column pathways, how human

subjects' response times to DES differ from response times to natural haptic stimulation has not been examined. This is an important consideration for effective BCI development aiming to integrate cortical stimulation as a method of sensory feedback as response latency invariably constrains feedback loop architecture.

We asked four subjects to press a button as soon as they perceived either a cutaneous haptic touch to the hand or a percept from S1 DES via ECoG grids covering the surface of the hand somatosensory cortex (see Figure 5.1 for general overview, Figure 5.2 for subject specific experimental progression). We initially hypothesized that direct cortical stimulation, by bypassing the ascending peripheral circuitry, would result in faster reaction times than peripheral haptic stimulation. We additionally hypothesized that subjects would become faster over multiple blocks of DES as they learned to interpret the signal, and that subjects' response times to DES would decrease with longer, sustained train durations relative to shorter trains with a constant stimulation current amplitude.

Remarkably, all four subjects were significantly slower to respond to the S1 DES than to haptic touch. Additionally, with our two blocks of testing we saw no significant differences between trial types and blocks, suggesting that on a short time scale, appreciable learning was not occurring. In three subjects we tested the train duration hypothesis and found that train lengths as short as 100 ms and up to 800 ms did not significantly affect the response times to the cortical stimulation. We performed off-target testing to serve as a control for the possibility that subjects were responding to stimulation that was applied anywhere in the cortex, rather than directly in somatosensory cortex. This reinforces our testing of electrical stimulation and subsequent activation of primary somatosensory cortex compared to natural ascending peripheral pathways activated through touch, converging on S1. We also included null trials without any stimuli to control for subject suggestibility and response anticipation. Our results shed new light on human perceptual processing of S1 DES and may direct future studies regarding the application and mechanisms of DES for both basic neuroscience

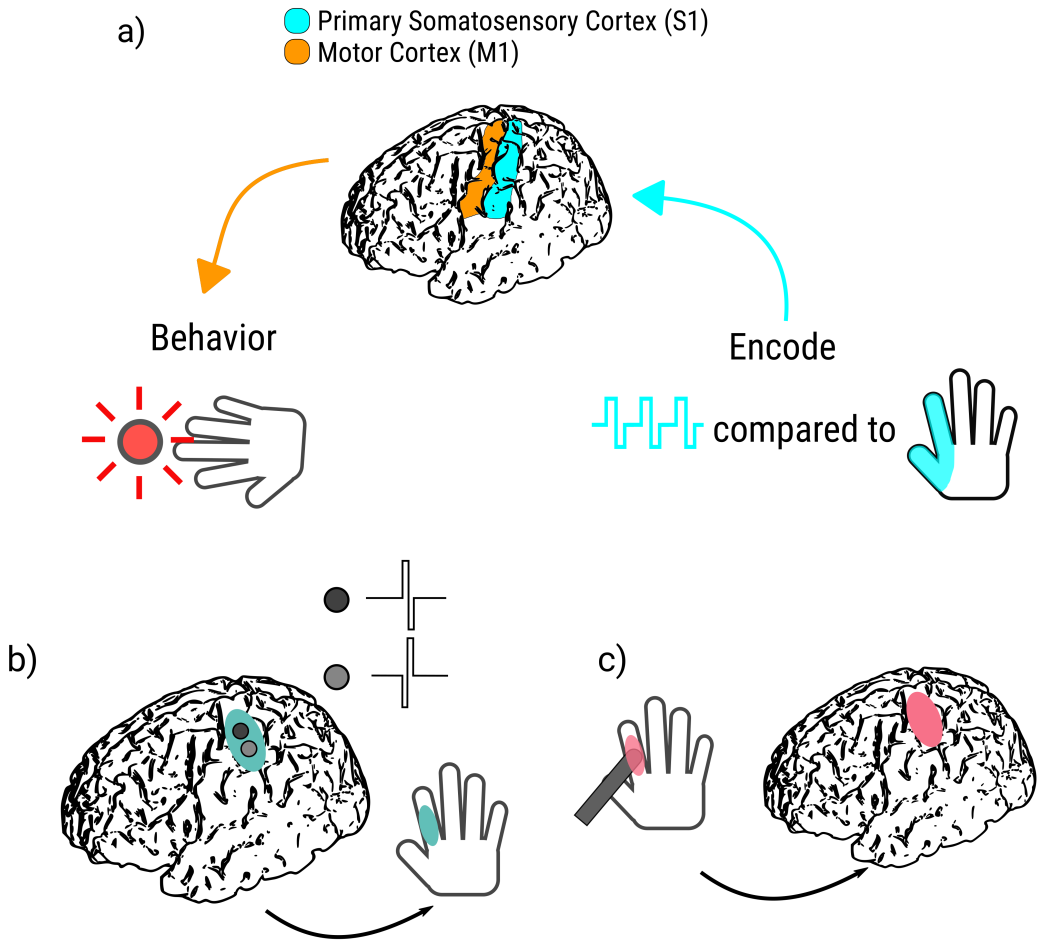

Figure 5.1: Response timing experimental protocol. a) Here, we test the impact on behavioral performance for native cortical input (haptic touch) compared to artificial feedback (bipolar direct cortical stimulation of primary somatosensory cortex via ECoG electrodes). (b-c) Schematic overview of experimental paradigm. b) DES to S1 hand cortex results in a sensory percept over a specific, consistent location on the hand. c) An experimenter uses a digital touch probe to provide haptic feedback to the same hand location. The subject then responds in both cases as soon as he or she feels sensation in the hand region, using a button held in the opposite hand to perceived sensation.

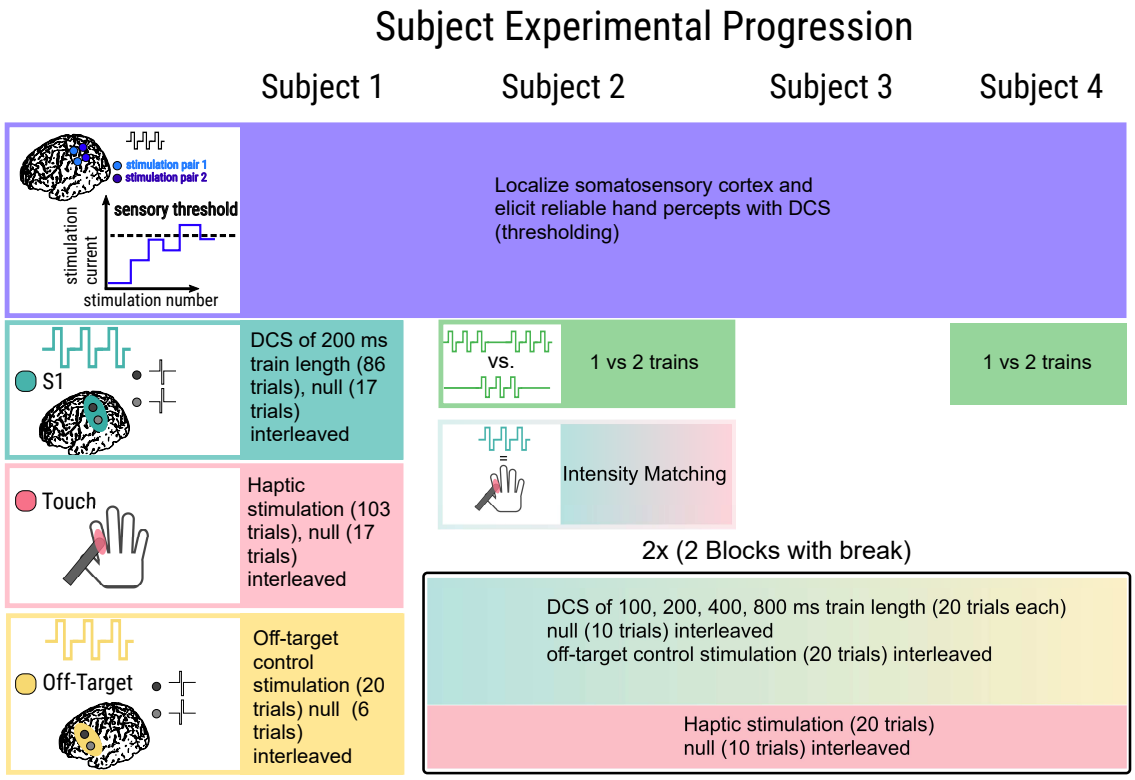

Figure 5.2: Response timing experimental progression by subject. Each column represents the experimental progression for our four subjects from top to bottom. In all subjects, we localized electrodes which elicited a reliable percept on the hand upon stimulation. We then found a threshold level of stimulation where sensations were elicited, and used stimulation currents above this to ensure reliable perception with 200 ms trains. Subjects 2 and 4 both performed a two-alternative forced choice task of discriminating between one and two trains to confirm our test amplitudes were suprathreshold. Subject 2 then performed an intensity matching experiment in which we identified stimulation levels that elicited approximately the same strength of response as the haptic touch provided by the experimenter. All subjects completed experimental trials after we established the suprathreshold current to use. Subjects 2-4 all had two blocks consisting of 100, 200, 400, and 800 ms trains, interleaved with 20 off-target and 10 null trials, followed by 20 haptic stimuli trials interleaved with 10 null trials.

research and neural engineering applications.

5.2 Methods

5.2.1 Subjects

Individual patient demographics (n=4), including side of electrode implantation and subject handedness, can be found in Table 5.2, with their corresponding cortical reconstructions and DES electrode positions shown in Figure 5.3. Epileptic foci are also identified in Table 5.2, to illustrate that we expected neurotypical somatosensory cortical processing for our reaction time task.

5.2.2 Stimulation waveform and hardware

DES trains consisted of 200 Hz biphasic pulses with 200 μs per phase, as such DES trains were previously found to elicit percepts during S1 stimulation [63].

5.2.3 Cortical stimulation

Subjects' perceptual thresholds for DES were determined by incrementally increasing the current amplitude of a 200 ms DES train in steps of 250 μA from a starting amplitude of 500 μA (Subjects 1 and 2), 1000 μA (Subject 3), or 200 μA (Subject 4) until the subject could perceive the stimulation as indicated by verbal report (Figure 5.2). In two subjects (Subjects 2 and 3), the first pair of DES electrodes that we tried did not elicit a consistent perceptual experience, so we tried a different pair of electrodes and again found the perceptual threshold (Figure 5.2). Due to experimental time constraints, we only comprehensively tested one pair of stimulation electrodes. During our screening tests we swept through different electrode pairs to choose the pair and stimulation polarity that most reliably produced recognizable percepts localized to the hand. Once we found this pair of electrodes for a given polarity, we

conducted all remaining experiments for the day with that bipolar configuration to maximize the number of trials we were able to acquire.

We first determined subjects' stimulation electrodes and perceptual current thresholds as described above, and then used a suprathreshold current amplitude during the experiment for all DES conditions (Table 5.2). To ascertain a suprathreshold stimulation current amplitude, we required two subjects (Subjects 2 and 4) to correctly identify, in ten sequential two-alternative forced choice (2AFC) trials, whether one or two 200 ms DES trains with a suprathreshold current amplitude were delivered before proceeding from the perceptual thresholding to the response timing experiment (Figure 5.2)). This demonstrated that the subjects could reliably perceive the 200 ms DES trains at that current amplitude. For the other subjects (Subjects 1 and 3), we achieved reliable discernment of stimulation with a suprathreshold amplitude (250-500 μA above their perceptual threshold) and proceeded with the response timing experiment without conducting the ten sequential 2AFC trials due to time limitations.

For Subject 2, after successfully completing the ten 2AFC trials, we attempted to match perceived intensity between the haptic feedback condition and the 200 ms DES train condition by increasing the DES current amplitude until the subject felt that the two stimuli were of qualitatively equal strength (Figure 5.2). We did not attempt intensity matching in Subjects 1 or 4 due to time constraints and patient fatigue. In Subject 3, we did not attempt intensity matching because DES elicited relatively weak percepts and raising the current amplitude high enough to match its perceived intensity to that of the haptic stimuli would increase the risk of afterdischarges.

5.2.4 Haptic Stimulation

We applied haptic feedback with digital touch probes (Karolinska Institute) that time stamped the deflection, and touched the cutaneous region where subjects localized the DES percepts

(Figures 5.1, 5.2). An audio signal presented to the researcher via headphones but which was inaudible to the subject, cued the experimenter to apply the haptic feedback. We used the digital touch probes previously [61] in conjunction with cortical stimulation, and at the time of manufacturing they were calculated to have a touch onset with an average delay of 1.04 ± 0.48 ms (mean ± standard deviation). To account for experimenter variability, and possible hardware changes over time, we measured them again and found them to have a touch onset with a delay of mean 5.24 ± 3.26 ms (mean ± standard deviation) and median 6.45 ms relative to an electrical short circuit (Appendix, Figures C.1, C.1). The small difference in registered touch onset, if added onto the digital touch probe latencies, does not change our significant effects in total (Appendix, Table C.1).

5.2.5 Experimental protocol

After determining DES current amplitudes, we completed one (for Subject 1) or two (for Subjects 2-4) blocks of response timing trials, each separated into a DES set and a haptic stimulation set (Figure 5.2). During the DES set we delivered DES train lengths of 200 ms for Subject 1, and train lengths of 100, 200, 400 and 800 ms in the subsequent three subjects (Subjects 2-4). Intertrial intervals of both DES and haptic feedback were jittered (ranging from 2.5 to 3.5 seconds) to minimize anticipatory effects or rhythmic perception by the subjects. We broke up the DES and haptic stimulation conditions into separate sets to allow subjects to anticipate and focus on one method of stimulation at a time. We reasoned that interleaving haptic and cortical stimulation within one block would result in a greater degree of uncertainty and error due to perceptual differences between modalities, rather than allowing a comparison between conditions where the subject was acclimated to either stimulation type.

All subjects were instructed to respond as quickly as possible by pressing a button held in their hand contralateral to sensation when they perceived the DES or haptic sensation. The

first subject was instructed not to look at the stimulated hand, while the subsequent three subjects (Subjects 2-4) were blindfolded to reduce potential confounds of visual distraction.

5.2.6 Off-target control stimulation

As a control, we also delivered off-target stimulation to a region outside of S1 during the DES experimental set. This was to ensure that the responses were specific to DES of S1, rather than a response to general, non-targeted DES. For the off-target stimulation electrodes, we chose two electrodes that would be safe for bipolar stimulation based on prior clinical mapping and knowledge of the subjects' epileptic foci. We used a 200 ms DES train length and the same suprathreshold current amplitude for off-target stimulation as we used for S1 stimulation. As detailed below and in Figure 5.2, Subject 1 completed a third set after the DES and haptic sets with this off-target control stimulation. For Subjects 2-4, we interleaved off-target stimulation with the on-target, S1 stimulation during the DES sets.

5.2.7 Subject 1 trial progression

In Subject 1 during the DES set, we delivered 86 trials of 200 ms trains of stimuli with 17 trials of null stimuli (i.e., no stimulation as a control) interleaved in a random order. In the haptic set, we delivered 103 trials of haptic touch, again with 17 interleaved null trials. During the third and final set, we delivered 20 trials of off-target stimulation, interleaved with 6 null trials (Figure 5.2).

5.2.8 Subjects 2-4 trial progression

For Subjects 2-4, we first delivered a DES stimulation set based on stimuli timing and conditions from a pre-generated file that randomly interleaved 20 trials each of 100, 200, 400, and 800 ms train-length S1 DES trials with 10 null trials and 20 off-target DES trials, for a total of 80 S1 DES trials and 30 control trials. Next during the haptic set, we provided

20 trials of haptic stimulation through the digital touch probes, with 10 null control trials randomly interleaved. After a brief rest period (5-10 minutes), we proceeded to a second block of cortical and haptic stimulation sets (Figure 5.2).

5.2.9 Data analysis

We performed all data post processing and analysis in MATLAB and Python with custom scripts. To calculate the response times in the DES conditions we took the temporal difference between the onset of the stimulation train and the subject's button press, while for response times in the haptic feedback condition, we calculated the difference between the registered timing of the deflection of the digital touch probe and the subject's button press. We identified and excluded outliers as trials with reaction times slower than 1 second and faster than 150 ms from further analysis, as faster responses are unlikely for untrained human subjects [152], and slower ones more likely represented a decrease in attention to the task rather than a true response time Additionally, we did not consider trials where either the button did not respond appropriately to the subject's press, or the digital touch probe did not register deflection. Table C.1 includes how many trials were analyzed for each subject and condition.

Anderson-Darling tests for normality confirmed that the data was not consistently well described by a normal distribution, therefore we proceeded with non-parametric testing. We corrected for multiple comparisons by dividing an alpha value of 0.05 by the number of conditions tested within each subject. Specifically, both conditions for Subject 1 were not normally distributed ($p = 2.725e\text{-}4$ and $1.888e\text{-}8$ for haptic and 200 ms DES conditions, respectively). For Subject 2 the 100 ms DES, 800 ms DES, and haptic conditions were not normally distributed ($p = 9.631e\text{-}5$, 0.0096, and $1.399e\text{-}16$, respectively), while the 200 and 400 ms DES condition failed to reject the null hypothesis of being normally distributed ($p = 0.046$, 0.194, respectively). For Subject 3 the 800 ms DES and the haptic conditions were not

normally distributed (p = 0.006 and 3.502e-4, respectively), while the 200 and 400 ms DES conditions failed to reject the null hypothesis of being normally distributed (p = 0.235 and 0.165, respectively). For Subject 4 the 800 ms DES and haptic feedback conditions were not normally distributed (p = 0.006 and 1.186e-6, respectively), while the 200 and 400 ms DES conditions failed to reject the null hypothesis of being normally distributed (p = 0.401 and 0.087, respectively). Due to the presence of non-normally distributed groups, we proceeded with non-parametric testing for all subjects, using the non-parametric Wilcoxon Rank Sum and Kruskal-Wallis tests (with Dunn-Sidák corrections for post-hoc comparisons for mean ranks [73, 257] to assess differences between conditions with an alpha significance level of 0.05. To assess blockwise differences, we used Rank Sum tests with Bonferroni corrections, and a base alpha critical level of 0.05.

Further, we tested for equal variances between groups using the Brown-Forsythe test [40]. For Subjects 2 and 4, testing revealed no significant differences in variances between groups, whereas for Subjects 1 and 3, there were significant differences in variances (critical value of 0.05; not significant- Subject 2: p = 0.094, Subject 4: p = 0.0873; significant- Subject 1: p = 0.0113; Subject 3: p = 5.662e-4). Thus, for Subjects 2 and 4 statistically significant differences between conditions from the Kruskal-Wallis and post-hoc tests were interpreted as differences in medians with haptic stimulation being significantly faster than cortical stimulation, while for Subjects 1 and 3, statistically significant differences were interpreted as differences in stochastic dominance of one sample over another [73].

5.3 Results

5.3.1 Response times

In Subject 1, we compared haptic stimulation to 200 ms trains of S1 DES with a suprathreshold current amplitude. Haptic feedback elicited a significantly different reaction time as compared to the 200 ms DES trains (p = 6.105e-16, Fig 5.3). The median response time

for the S1 DES trains was 459 ms, while the median response time for the haptic feedback condition was 313 ms (Table 5.1), consistent with classic tactile reaction times [152, 306]. Minimum, 25% and 75% quartile ranges, and maximum response times for all subjects are reported in Table 1. This subject did not perceive off-target DES, and responded to a single null stimulation trial. In light of the results from Subject 1, we subsequently chose to consider possible effects of S1 DES train length on reaction times, acquiring and comparing haptic responses to train lengths of 100, 200, 400 and 800 ms with suprathreshold currents in Subjects 2-4.

In addition to testing four DES train lengths for Subjects 2-4, we additionally inserted a rest condition in between two blocks to test for habituation or adaptation (Fig 5.4). There were no significant differences between blocks for Subjects 2-4, so we combined them for further statistical analyses. Specifically, for Subject 2, there were no significant blockwise differences between the conditions ($p = 0.811$, $p = 0.715$, $p = 0.675$, and $p = 0.0962$ for the 100, 200, 400, and 800 ms DES train conditions, respectively; $p = 0.579$ for the haptic condition, critical threshold of $p = 0.01$). For Subject 3, we excluded the 100 ms condition from statistical analyses due to only a single response within one block. Blockwise differences were not significant for any of the other conditions for Subject 3 ($p = 0.064$, $p = 0.087$, and $p = 0.155$ for the 200, 400, and 800 ms DES train conditions, respectively; $p = 0.519$ for the haptic condition, critical threshold of $p = 0.0125$). Similarly, for Subject 4, we excluded the 100 ms condition because of a single response on one block, and two responses on another block. Again, blockwise differences were not significant for any of the other conditions for Subject 4 ($p = 0.035$, $p = 0.669$, and $p = 0.109$ for the 200, 400, and 800 ms DES train conditions, respectively; $p = 0.316$ for the haptic condition, critical threshold of $p = 0.0125$).

For Subject 2, all S1 DES response times were found to be significantly different than the haptic response times due to statistical differences in medians ($p = 3.654e\text{-}8$ for the 100 ms, $p = 7.000e\text{-}5$ for the 200 ms, $p = 2.064e\text{-}6$ for the 400 ms, and $p = 1.866e\text{-}6$ for the

Subject	Experimental Condition	Minimum (ms)	25% quartile (ms)	Median (ms)	75% quartile (ms)	Maximum (ms)	Number of trials responded to within response time bounds
1	200 ms	348	422	459	495	821	81/86
	touch	169	254	313	374	719	73/103
	null	N/A	N/A	724	N/A	N/A	1/40
	off-target						0/20
2	100 ms	182	232	277	314	551	36/40
	200 ms	188	235	254	276	372	40/40
	400 ms	169	244	261	288	380	40/40
	800 ms	180	234	265	291	488	40/40
	touch	151	189	198	228	726	38/40
	null	N/A	N/A	449	N/A	N/A	1/40
	off-target						0/40
3	100 ms	N/A	514	N/A	N/A	N/A	1/40
	200 ms	403	409	442	494	553	9/40
	400 ms	383	455	515	603	747	26/40
	800 ms	348	466	528	806	994	31/40
	touch	151	169	222	318	507	30/40
	null						0/40
	off-target			484			1/40
4	100 ms	218	219	220	503	786	3/40
	200 ms	213	347	408	595	754	13/40
	400 ms	305	371	423	588	857	17/40
	800 ms	240	334	400	624	882	22/40
	touch	153	178	201	234	556	19/40
	null						0/40
	off-target						0/40

Table 5.1: Reaction times for each subject and each condition. In all subjects, cortical stimulation resulted in significantly different reactions times than haptic stimulation (assessed through non-parametric Wilcoxon Rank Sum and Kruskal-Wallis tests). Final column reports the number of trials responded to by each subject across both blocks for each of the trial types given our response time limits of 150-1000 ms, and appropriate signal detection. Response times outside of this range were considered outliers based on expected human performance (see Methods, Data Analysis for details). Blank boxes indicate trial types with no responses.

800 ms DES train, adjusted p-value threshold = 0.05), while no S1 DES conditions differed significantly from each other (Figure 5.3). The median response times for the 100, 200, 400, and 800 ms DES trains were 277, 254, 261, and 265 ms, respectively, while the median response time for the haptic feedback condition was 198 ms (Table 5.1). For this subject we chose off-target stimulation electrodes that had been safely tested during clinical language mapping but used much lower current amplitudes than tested clinically (Figure 3, Subject 2, off-target electrodes). The subject perceived the off-target stimulation as a vague, non-tactile, and non-localized sensation, and described it as distinct from the DES sensation. Although he could perceive the off-target DES, he was able to volitionally choose to not respond to these trial types and did not respond to any of the off-target stimuli within our 150-1000 ms response time window. The subject responded within our time window to a single null stimulus.

For Subject 3 the 200, 400, and 800 ms DES response times were found to be significantly different than the haptic feedback response times, due to haptic feedback stochastically dominating the reaction times ($p = 0.029$, $p = 5.971e\text{-}8$, $p = 1.290e\text{-}10$, respectively), while no S1 DES conditions differed significantly from each other. Subject 3 only responded in one trial with 100 ms S1 DES trains with a response time of 514 ms, so we excluded statistical comparisons with the other conditions. Median S1 DES response times were 442, 515, and 528 ms for the 200, 400, and 800 ms DES trains, respectively, while the median haptic feedback response time was 222 ms (Figure 5.33, Table 5.1). This large difference in medians provides convincing evidence that the cortical stimulation resulted in significantly slower reactions than haptic stimulation. This subject responded within our 150-1000 ms response window once to off-target stimulation, although they did not report being able to perceive the off-target stimulation. The subject did not respond to the null-condition.

For Subject 4 the 200, 400, and 800 ms S1 DES response times were found to be significantly different than the haptic response times due to a significant difference in medians (p

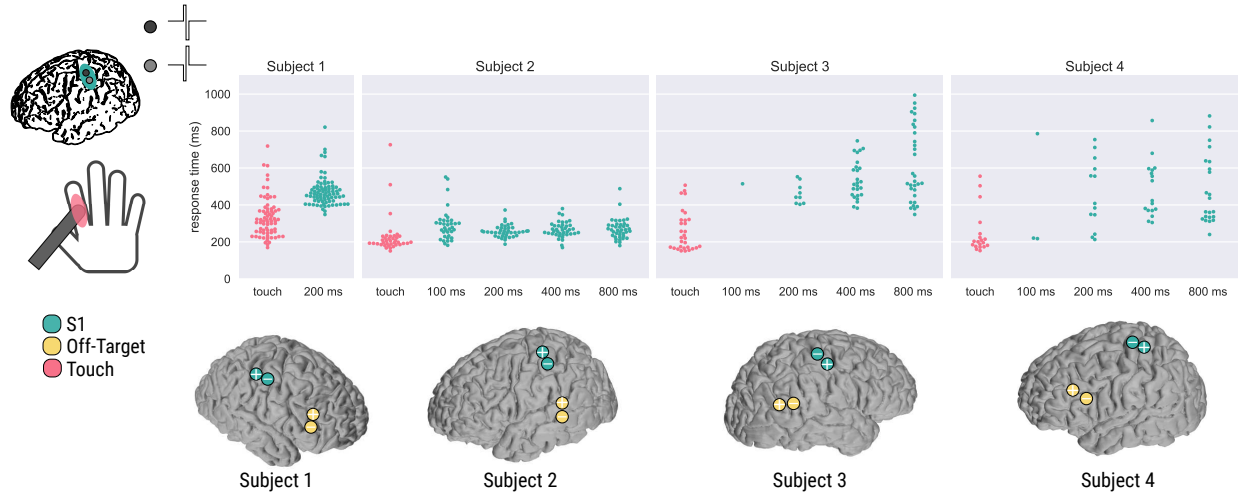

Figure 5.3: Comparison of reaction times for four subjects and their DES electrodes. Each dot represents a response time for a given trial, colored by condition. Pink indicates the haptic test condition, while turquoise indicates S1 DES conditions and electrodes over hand sensory cortex. Subject 1 only received the 200 ms DES and haptic stimulation conditions, while Subjects 2, 3, and 4 had 100, 200, 400, and 800 ms trains of stimulation applied. The two separate blocks for Subjects 2, 3, and 4 were pooled together for each subject. Off-target DES control electrodes are indicated in yellow. Electrode locations are based on cortical surface reconstructions for each subject as described in the Methods. Electrodes with a plus symbol (+) indicate anodal-first stimulation, while electrodes with a minus symbol (-) indicate cathodal-first stimulation.

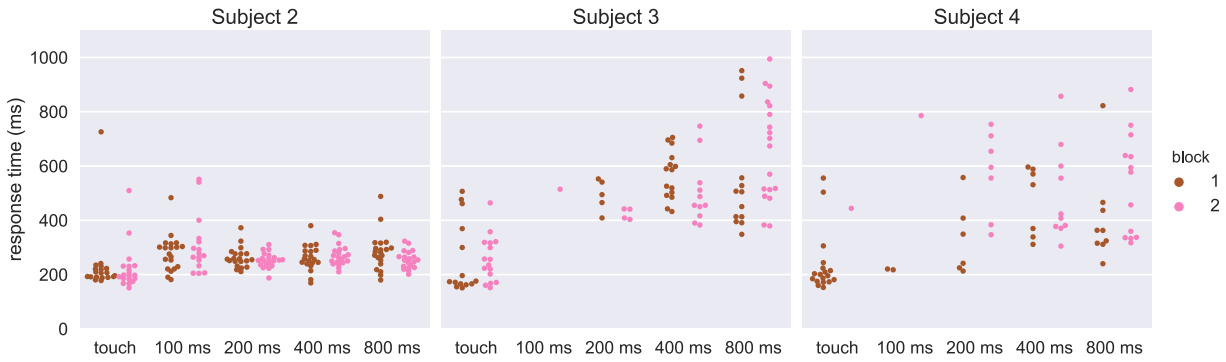

Figure 5.4: Comparison of the two blocked sessions for three subjects. Each dot represents a response time for a given trial, colored by block. Of note is the non-normality of some of the response timings for different conditions. Additionally, the paucity of responses for Subject 3 to the 100 ms and 200 ms conditions, and for Subject 4 to the 100 ms condition suggests the stimulation level was at or near their perceptual thresholds.

= 1.161e-3, p = 8.803e-5, p = 1.107e-4, respectively), while no S1 DES conditions differed significantly from each other. Subject 4 responded on only three trials with 100 ms S1 DES trains with a median reaction time of 220 ms, so we excluded the 100 ms DES condition from further statistical analysis. Median DES response times were 408, 423, and 400 ms for the 200, 400, and 800 ms DES trains, respectively, while the median haptic response time was 201 ms (Figure 5.33, Table 5.1). This subject did not perceive the off-target stimulation or the null stimulation.

For Subjects 1 – 3, there was no indication of adaptation, nor reported description of the stimulus intensity as weakening and changing throughout the DES sets. After the first block with Subject 4, however, he verbally described a noticeable decrease in stimulation intensity as the trials proceeded. Therefore on the subsequent block we increased the DES current amplitude from 1.0 mA to 1.2 mA. The subject again verbally described a decrease

in perceived intensity as the trials proceeded during the second block despite the increased current amplitude. This suggests individual differences in adaptation to cortical stimulation, perhaps dependent on parameters such as the electrode location, medication status, subject attentiveness, or amount of cerebrospinal fluid underneath the electrodes.

5.3.2 Qualitative assessment

The subjects described the S1 DES as non-painful, using descriptions such as a "pins and needles" like sensation (Subject 1), a "buzz", or the feeling of "something brushing" against the skin (Subject 2), "tingling" (Subject 3), and "pulse" or "throb" (Subject 4). These subjective descriptions are in line with previous reports for S1 DES10,11,18. The subjects reliably localized the percept from S1 DES during the experiment and across blocks (see Table 5.2 for percept localization). However, the pair of electrodes initially chosen for Subject 2 were not reliably localized, with the subject localizing the percepts from some stimuli to the proximal thumb and some to the proximal palmar area of the fifth finger. Therefore, prior to any experimentation, we selected a different pair of electrodes for Subject 2 that generated a percept which the subject reliably localized to the third finger.

For Subject 2 we attempted to match the perceived intensity of the 200 ms DES train to that of the haptic stimulation (see Methods, Figure 5.2), and although we were able to make their intensities more similar to one another, we were not able to match them completely. As we increased the DES current amplitude, Subject 2 felt that the percept he experienced both increased in intensity and in the size of the localized area. As a result, during the experiment his perceived intensity of the S1 DES was slightly less than the perceived intensity of the haptic stimulation in order to keep the localized areas of the sensation similar. Despite matching the sensation intensities as well as possible, Subject 2 described the haptic and cortical stimulation as very distinct from one another. The S1 DES percept was initially localized to the same region as the haptic stimulation (dorsal side of third finger), but then

Subject	Gender	Age	Experiments	Stimulation Current	Coverage and DES percept localization	Handedness	Seizure Etiology
1	Female	21	Cortical Stimulation Digital touch probe Off Target	2500 μA	Right grid Distal phalange of digit 2	Right	Complex partial epilepsy with multifocal ictal onset and at least 2 distinct epileptogenic areas with seizures arising from right frontal and right temporal regions. No resection / no pathology, VNS implant.
2	Male	37	**Block 1:** Cortical/Off Target interleaved Digital touch probe **Block 2:** Cortical/Off Target interleaved Digital touch probe	1500 μA	Left grid All of digit 3	Right	Focal epilepsy isolated to a left parietal calcified lesion (widespread calcifications eliciting diffuse and severe reactive changes including astrogliosis and microgliosis with unknown origin). Seizures originating from left lateral parietal cortical lesion.
3	Male	26	**Block 1:** Cortical/Off Target interleaved Digital touch probe **Block 2:** Cortical/Off Target interleaved Digital touch probe	2000 μA	Right grid Distal phalanges of digits 3-5	Right	Focal epilepsy isolated to a left parietal calcified lesion (widespread calcifications eliciting diffuse and severe reactive changes including astrogliosis and microgliosis with unknown origin). Seizures originating from left lateral parietal cortical lesion.
4	Male	34	**Block 1:** Cortical/Off Target interleaved Digital touch probe **Block 2:** Cortical/Off Target interleaved Digital touch probe	1000 μA 1200 μA	Right grid Palmar area near base of digit 1	Right	MRI negative, partial seizures originating from the left mesial temporal area including the anterior temporal pole and hippocampus. Pathology included mild gliosis with leptomeningeal and subpial reactive changes.

Table 5.2: Response timing subject demographics. This table shows the demographics for all the patients in this study, including experiments completed, stimulation currents used, and the localization of subjects' percepts, electrode locations, and seizure etiology.

radiated across the skin.

5.4 Discussion

Our study characterized reaction time differences between cortical and haptic stimulation in four human subjects. Our results demonstrate that response times to cortical stimulation are significantly slower than to haptic stimulation. We additionally demonstrate that cortical stimulation trains of varying lengths do not significantly affect the reaction times for suprathreshold cortical stimulation parameters.

Our results are consistent with a previous observation in non-human primates that intracortical microstimulation of area 1 in primary somatosensory cortex results in significantly slower response times than peripheral stimulation [101]. This delayed response for DES is counterintuitive at first, as one may suspect that bypassing the ascending peripheral afferents through DES would reduce the distance traversed by the sensory volley and consequently result in faster reaction times. However, as previously suggested [101], electrical stimulation may be exciting both inhibitory and excitatory connections in unnatural combinations, driving slower behavioral responses.

In human neocortex, approximately 20% of neurons are interneurons, many of which are inhibitory and contribute to local inhibitory neural circuits [16]. Similarly, in rodent neocortex, approximately 20-30% of neurons are interneurons [173]. This is important when considering the neural response to electrical stimulation, as microstimulation in rodents has been demonstrated to result in a spatiotemporal smear of activity, due to the evoked activity consisting of a combination of fast excitatory responses and inhibitory responses [43]. In addition to an unnatural spatial cortical activation, electrical microstimulation in rodents yields different trends in trial-to-trial variability relative to natural sensory stimuli [186]. Thalamocortical simulations suggest that high levels of synchrony generated by electrical stimuli, which are not seen in natural stimuli, are responsible for this difference in the shape

of the trial-to-trial variability curves [186].

Additionally, electrical microstimulation, as used in the intracortical microstimulation experiments, activates neurons primarily through their axons [225, 271], although other regions of the cell such as the cell body and dendrites may also be activated depending on stimulus polarity and orientation. Non-human primate work using microstimulation combined with fMRI has shown that electrical stimulation may disrupt cortico-cortical signal propagation by silencing output of areas where the afferents are electrically stimulated [166]. This supports the idea that electrical stimulation results in a distinctly different activation pattern, which may explain a less optimal (and longer response time) reaction to electrical stimuli compared to natural haptic stimulation. Other hypotheses for the delayed response to S1 DES include the possible need for downstream amplification, from a region such as the thalamus, that is initially skipped via S1 stimulation [101], or the possibility that surface stimulation is unable to directly stimulate deeper primary somatosensory areas, including area 3b where direct intracortical microstimulation has been shown to elicit similar reaction times to haptic stimulation during a discrimination task in non-human primates [237].

Recent work in computational modeling regarding subdural cortical stimulation in humans suggests that bipolar stimulation at our current levels is unlikely to activate pyramidal neurons directly in the deeper areas of the sulci, and rather, the primary activation of neurons occurs in Brodmann area (BA) 1 on the surface of the cortex [251,252], and possibly the superficial aspects (towards the crown of the gyrus) of BA3b. Area 3b, where the majority of thalamocortical connections are thought to project30, is likely sparsely activated, while Area 3a is in the deepest part of the sulcus [97], and is activated even less. Therefore, the lack of our ability to effectively target BA3 may partly explain the delayed reaction times to DES relative to natural haptic touch.

Early cortical stimulation work in elderly dyskinetic patients [161] suggested a 500 ms stimulation train was required for consistent perception of DES with a liminal, or near-

threshold, current amplitude. Later work in epileptic patients demonstrated that a 250 ms stimulation train could elicit conscious perception with near-threshold current amplitudes [230]. Furthermore, Ray et al. illustrated the inverse relationship between DES train duration and the current amplitude required for perception, with current thresholds increasing as the train durations decreased [230]. We observed a similar phenomenon in Subjects 3 and 4, where for a fixed current, shorter train lengths did not elicit conscious percepts. These two subjects' inability to reliably respond to the 100 ms train duration condition, suggests that we may have been using a stimulation current amplitude that was too low to reliably discern trains lengths under 200 ms (the train length used for perceptual thresholding) at a fixed amplitude. Additionally, Subject 3 perceived fewer of the 200 ms DES trials than the 400 ms or 800 ms DES trials, suggesting that we were stimulating close to the threshold train duration and intensity parameters.

In contrast to Subjects 3 and 4, Subject 2 reliably discerned all of the stimulation trains and had much faster reaction times. In this case we seemed to be operating far above the minimum current threshold necessary for the various DES train lengths tested. As Subject 2 was the only subject for whom we attempted DES/haptic stimuli intensity matching (see Methods), we used a current amplitude that was notably greater than the subject's perceptual threshold (roughly 750 μA greater). The other subjects completed the task with current amplitudes that were only roughly 250-500 μA above their perceptual thresholds. Stronger intensity stimuli are known to produce faster response times [306], and it is possible that, to a degree, more suprathreshold DES currents may lead to faster response times, but further experimentation is necessary to examine this hypothesis.

Human tactile, perceptual mean reaction times from one study in untrained, healthy volunteers have been found to vary between 210 and 400 ms [152], but can range down to 140-150 ms with practice for certain individuals [306] . Reaction times for individuals tend to stay relatively constant between ages 25 and 60 [306]. As our patients' ages (21, 37, 26,

34) are close to within this range, we expect little influence of age on the reaction times. With this as a basis for normal comparisons for our untrained subjects, we similarly find a range of different response times to cortical and haptic stimulation, speaking to individual variability. This suggests that for future BCI implementation, an individual's innate response time may need to be considered in light of variable latencies. That is, if one subject requires on average 500 ms to respond to cortical stimulation, while another subject requires 300 ms, this requires design considerations on the BCI side to account for time differences in the feedback loop.

Response times are also modulated by non-somatosensory features such as visual feedback, arousal, motivation, and attention [306]. In well-practiced healthy subjects, response times based purely on visual feedback are slower than those based on tactile stimuli for a simple reaction time task (approximately 180 ms on average compared to 140 ms, respectively) [306]. The combination of haptic and visual feedback has been shown to result in faster reaction times relative to visual feedback alone for computer-based tasks in healthy human subjects [281]. We controlled for potential effects of visual feedback by having Subjects 2-4 wear a blindfold, and asking Subject 1 to close her eyes. Subjects' attention may have also affected their response times, but we did not attempt to quantify their attentiveness. Experimenter observation suggests that Subject 2, who had the fastest response times, was the most engaged in the task and approached it with a competitive, game-like attitude. However, we cannot ascertain that Subject 2's attentiveness affected his response times, and have presented other possible explanations for his faster responses including use of a higher suprathreshold stimulation amplitude compared to those for the other three subjects. Mere observation suggests that Subject 1 was the groggiest and least engaged in the task, correlating with their slowest haptic reaction times. Future studies may consider including a comparison of response times to S1 DES and haptic stimuli with visual feedback (i.e., eyes open without a blindfold as would be likely in a future application) to understand how visual

feedback may modulate response times. As we increase task complexity and move away from a simple reaction time task as performed here, the benefits from additional feedback beyond only visual feedback may become even more apparent.

An additional factor to be explored in the future is the impact of the polarity of the bipolar stimulation used. Due to experimental time constraints we were unable to comprehensively test the effect of anodic relative to cathodic first stimulation at each electrode, but due to the different cortical activation due to the polarity of stimulation, there could be an effect on reaction times and perception. [272, 309]

Each of our blocks lasted on the order of 10 minutes, with 5-10 minutes of rest between the blocks. The lack of a consistent, discernible habituation or learning effect suggests that either the sessions were not long enough or frequent enough to elicit learning or habituation, or that subjects were already reacting close to their fastest possible reaction times. We do not claim that repeated training over multiple sessions and days would not show a decrease in reaction time, but rather we are unable with our acute ECoG epilepsy experiments to address this particular question.

In Subjects 1, 3, and 4, the frontal and temporal electrodes used for the off-target stimulation elicited no sensation and were only responded to once by Subject 3. However, in Subject 2 whose off-target stimulation site was over a language area, the subject perceived a vague, non-localizable, sensation of the stimulation. These off-target electrodes had been safely tested during clinical mapping and avoided possible seizure foci. We used current amplitudes much lower than those tested clinically to further avoid afterdischarges and match the suprathreshold stimulation used in the other S1 DES conditions. Subject 2 described the off-target DES as distinct from the S1 stimulation conditions, and had no difficulties in responding only to S1 stimulation. This suggests that humans can receive stimulation in multiple cortical regions and distinguish them within short temporal intervals.In Subjects 1, 3, and 4, the frontal and temporal electrodes used for the off-target stimulation elicited

no sensation and were only responded to once by Subject 3. However, in Subject 2 whose off-target stimulation site was over a language area, the subject perceived a vague, non-localizable, sensation of the stimulation. These off-target electrodes had been safely tested during clinical mapping and avoided possible seizure foci. We used current amplitudes much lower than those tested clinically to further avoid afterdischarges and match the suprathreshold stimulation used in the other S1 DES conditions. Subject 2 described the off-target DES as distinct from the S1 stimulation conditions, and had no difficulties in responding only to S1 stimulation. This suggests that humans can receive stimulation in multiple cortical regions and distinguish them within short temporal intervals.

An unknown factor in the work presented here is the extent to which DES of S1 is also impacting ipsilateral M1, and through connections to contralateral M1, motor output. Our subjects are able to perform motor tasks with the hand being stimulated concurrently, suggesting that there is not grossly visible motor disruption on the ipsilateral or contralateral side. Our subjects also are able to perceive temporally overlapping natural haptic stimulation and DES at the same spatial location, suggesting that there is not global inhibition or cortical jamming. However, we do acknowledge that some of the delay observed could indeed be due to some potential motor disruption from charge spread. This study does not serve to address this, but rather, presents data revealing significant delays in the timed response to S1 DES with respect to natural touch. This effect may possibly be due to a delay in conscious perception of the DES or in the motor output pathway, which has implications for neuroprosthetic and closed loop BCI design.

5.4.1 Outlook

Our results, while elucidating aspects of human perceptual processing of S1 DES, demonstrate a need for further exploration of the neural mechanisms underlying the reaction time differences between S1 DES and haptic stimulation. We found, in four human subjects, that

response times to cortical stimulation are significantly different than to haptic stimulation. The fact that there appears to be a significant delay in cortical processing and subsequent response after DES does not preclude ECoG stimulation from being a promising modality for feedback in a neuroprosthetic application. Rather, this highlights the importance of understanding variables such as human reaction time for neuroprosthetic applications and appropriately designing devices to account for these temporal delays. Our ongoing studies are aimed at understanding and potentially speeding up the temporal response to ECoG stimulation by varying stimulation parameters, regions targeted, and waveform shape.

5.4.2 Data availability

Data required to recreate the above analyses are in the following repository.

`https://github.com/davidjuliancaldwell/responseTimingPaper.git`

5.4.3 Code availability

Code required to recreate the above analyses are in the following repository.

`https://github.com/davidjuliancaldwell/responseTimingPaper.git`

MATLAB and Python are required to generate the full set of figures and analyses.

5.5 Related Publications and Presentations

5.5.1 Publications

Caldwell DJ*, Cronin JA*, Wu J, Weaver K, Ko AL, Rao RPN, Ojemann JG, "Direct stimulation of somatosensory cortex results in slower reaction times compared to peripheral touch in humans" *These authors contributed equally, Scientific Reports, 9(1), pp. 3292, 2019, doi: 10.1038/s41598-019-38619-2

5.5.2 Presentations

Caldwell DJ, "Behavioral and neural differences between haptic stimulation and direct cortical stimulation in humans: implications for neuroprosthetics", 7th International BCI Meeting, Workshop: Perception of Sensation Restored through Neural Interfaces, Asilomar, CA, May 2018

Caldwell DJ, Cronin JA, Wu J, Kutz JN, Brunton BW, Weaver K, Rao RPN, Ojemann JG, "Spectrotemporal analysis of direct cortical stimulation compared to haptic stimulation in a response timing task in humans", Society for Neuroscience – Annual Meeting, Washington DC, District of Columbia, November 2017

Caldwell DJ, Cronin JA, Wu J, Weaver K, Rao RPN, Ojemann JG, "Direct Cortical Stimulation Results in Slower Reaction Times Compared to Peripheral Touch in Humans", OHBM 2017, Vancouver, Canada, June 2017

Chapter 6

THE EFFECT OF CONCURRENT DES AND HAPTIC STIMULI AND MODIFIED STIMULATION WAVEFORMS ON RESPONSE TIMES AND PERCEPTION

DES of S1 elicits a somatotopically localized artificial percept. Consequently, S1 DES provides the ability to close the loop in a bidirectional BCI by restoring lost sensation and providing real-time feedback. However, previous work has revealed delays in the processing of DES relative to natural haptic touch. Similarly, the behavioral impact of DES on ongoing natural sensory processing in cortical areas adjacent to S1 DES is not well explored. More biomimetic waveforms may need to be engineered to improve performance in response to DES. We compare the response times to DES with non-uniform waveforms, which may be more biomimetic, of human hand somatosensory cortex through ECoG arrays to haptic touch stimuli on the hand in three subjects. We found that modified waveforms with higher amplitude initial pulses of only two pulses, both with and without continuing trains of stimulation, are able to modify response times and the quality and strength of induced percepts. Concurrently overlapping DES and haptic stimuli are able to be perceived independently, and the point of subjective simultaneity between the two modalities reinforces the delays seen during the response timing task. Our results provide support that the engineering of optimized waveforms may improve sensory neuroprosthetic performance, and that the brain is capable of concurrently and independently processing both direct artificial feedback and natural sensory processing.

6.1 Introduction

The effect of DES on S1 on ongoing processes in humans is not yet understood, nor are there reports detailing optimal design parameters in human S1 DES aiming to improve psychophysical outcomes. What will happen when DES and haptic feedback are applied concurrently? This is of critical importance for neuroprosthetics in the real world where continuous natural and artificial feedback will arrive concurrently. DES and natural sensory input are processed differently in cortex [186], but does DES impact the perception of other overlapping stimuli and interfere with normal function? One way to assess these interactions is through a temporal order judgment (TOJ) task, where two stimuli are presented in close temporal relation to one another, and subjects are asked to judge which arrived first [190]. Combinations of stimuli modalities can be presented, such as audio, visual, and tactile stimuli. This task lends insight into the processing related, nearly simultaneous events, a necessary ability to functionally register multiple streams of continuously-arriving sensory information from a changing world. Temporal order judgment experiments are currently being explored for peripheral nerve interface devices, where visual and tactile (both natural and peripherally stimulated) stimuli are combined [56]. We have implemented an experiment where humans received tactile information simultaneously from the two overlapping, yet different, modalities of DES and haptic touch in order to see if DES modifies normal sensory processing and to confirm the previously measured delayed responses to DES.

Complex sensorimotor behavior such as picking up an object is characterized by unique bottom-up, response profiles of different neuronal pools [22, 268]. The onset of touch is marked by a burst of activity in subsets of S1 neurons relaying information from rapidly-acting peripheral fibers, while a lower, tonic level activity is reflects slowly adapting peripheral fibers. In total, populations (rather than the responses of single neurons) of somatosensory cortical neurons encode transient contact events, more so than constant pressure [46]. Stimulating in a manner that captures this natural pattern of neural activity is referred

to as biomimetic stimulation to restore sensation. To this end, we modified our constant amplitude train waveforms to include two initial high "priming" pulses, in order to better match the initial onset of activity in S1. To address engineering stimulation for enhanced neuroprosthetic performance, with faster response times and more natural sensations, we hypothesize better mimicking the cortical response in different populations of neurons in S1 to picking up an object will yield improved behavioral metrics to S1 DES.

Our results demonstrate that manipulation of charge within the initial components of DES significantly improve reaction times over constant trains, without becoming overly intense as would be constant trains of the same amplitude, in individuals with ECoG arrays implanted over primary somatosensory cortex. Furthermore, we show that spatially and temporally concurrent haptic and S1 DES are able be independently perceived, and that the stimulus onset asynchrony in a temporal order judgment task recapitulates our previously published delays seen between haptic touch and DES stimulation in our response timing tasks. These results have implications for future neuroprosthetics, in which optimized stimulation waveforms would likely improve the perception and performance to DES of sensory cortex, and where the human brain will be tasked with performing natural processing as well as receiving non-natural, exogenous electrical stimulation to potentially spatiotemporally overlapping areas.

6.2 Experimental Design and Analysis Methods

We provided haptic stimulation through digital and analog touch probes to the same cutaneous region where sensation was perceived during DES of S1 hand cortex, as described in the general methods. We performed these experiments in three subjects. The first two subjects' data were acquired with custom digital touch probes as previously described and validated [45, 61]. The third subject's data were acquired using a different custom analog touch probe. See Appendix Figure D.1 for validation of this probe. The timing between the

two probes is comparable, with perhaps a smaller delay for the analog probe due to no need for digital triggering.

For the response timing experiments and waveform modifications, we performed experiments similar to those previously conducted [45] with additional modifications on the waveform amplitude. Similar to those experiments, we determined sensory thresholds for each subject for 200 ms trains of constant amplitude. After determining the sensory threshold, rather than using trains of constant amplitude, we added two initial high "priming" pulses on the waveform (Figure 6.1) to better mimic S1 response profiles to object contact. We refer in the rest of this work to "priming" conditions as waveforms with two pulses at a higher amplitude initially, followed by a train of pulses at a lower amplitude (In all of experiments, we use 200 ms trains, which meant that the following trains consisted of 38 pulses). We also used waveforms of only two pulses. The subjects were blindfolded, and in separate blocks were asked to respond as quickly as possible either to DES of S1, which resulted in a sensory percept on the hand, or haptic touch which was applied to the same area.

When possible, we performed intensity matching between the haptic touch and DES, in order to assess the reaction times differences between two stimuli of equal perceived strength. We touched the subjects' hands with our touch probes, and altered the stimulation amplitude for 200 ms DES trains until they verbally reported that both stimulus modalities felt of similar intensity.

For the temporal order judgment experiments, we first determined the delay in the response time between DES and natural haptic touch using the data from the 200 ms constant amplitude waveform part of the experiment using a similar experimental protocol as in Caldwell et al. 2019 [45]. We then presented haptic stimuli and DES stimuli (200 Hz, 500 ms trains), with a distribution of lags (stimulus onset asynchrony, SOA) between the two stimuli types. Lags were centered around this particular latency with the subject still blindfolded, which resulted in DES being applied in close temporal proximity to natural haptic touch

with varying time lags (Figure 6.2).

Our first subject was asked after each trial which stimulus was perceived first, and also responded via button press to stimulus onset to measure response times. The first subject was also given a third option ("same"), for conditions where they were unable to say which came first. This is called a "ternary-response task" [277], but due to potential subject variability in assessing the threshold for "same", we altered the procedure to be a TOJ task [263]. The second and third subjects were asked to respond via button press, say which stimulus came first, and give a rating (1-5) on how confident they were in which came first. We then analyzed the response times on each trial based off of the first stimulus presented (either haptic or DES). We acknowledge that the addition of a response time component changes the task from a classic TOJ task, but unlike other dual tasks where the second task required decision making and planning [112], we believe our response time task requires minimal additional cognitive processing that would substantially alter the results of the TOJ reports.

We delivered bipolar, biphasic stimulation. All stimulation trains were at 200 Hz, with 200 μs pulse widths. Pulses with 2 pulses were therefore approximately 5 ms in duration.

6.2.1 Subject Demographics

Table 6.1 details the experiments performed with the three subjects undergoing invasive clinical monitoring for seizure foci localization, as well as where they localized the percepts induced by DES. Figure 6.3 illustrates the individual subject cortical reconstructions and stimulation electrode locations within the ECoG electrodes.

6.2.2 Data Analysis

We tested for normality among the data groups with more than 7 data points using the Anderson-Darling test. Our data had a mix of normally and non-normally distributed groups,

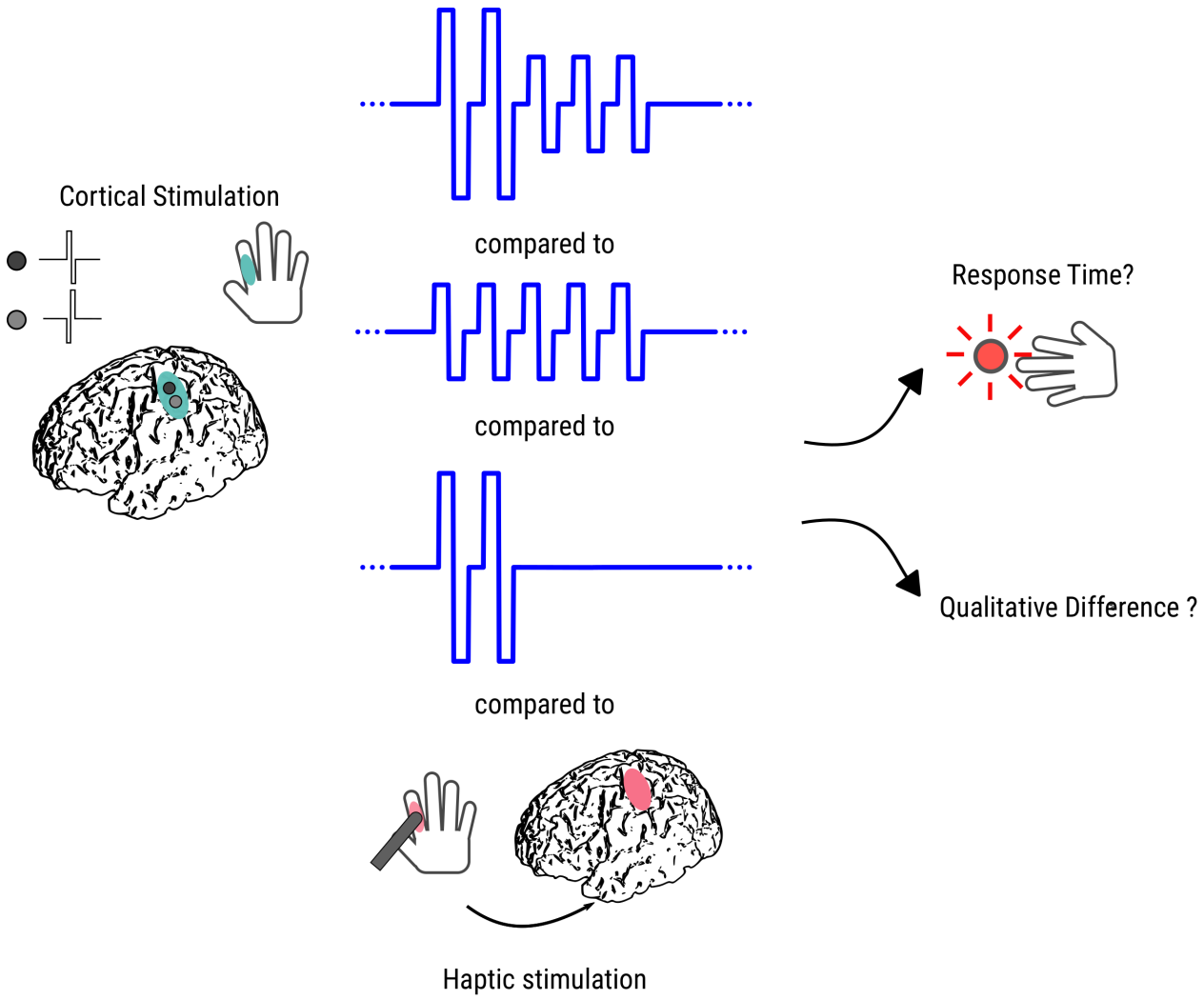

Figure 6.1: Experimental overview of modifications to waveforms to test response times. Waveforms with amplitude variation between the first two pulses and the remainder of the train were compared to waveforms with constant amplitude, with both perceptual reports and response times as output metrics. There are groups of neurons in primary somatosensory cortex which respond primarily to contact onset and offset, while others tonically fire during object contact maintenance. We therefore sought to stimulate with a waveform that contained initially high amplitude pulses and subsequently lower amplitude pulses to better mimic this behavior.

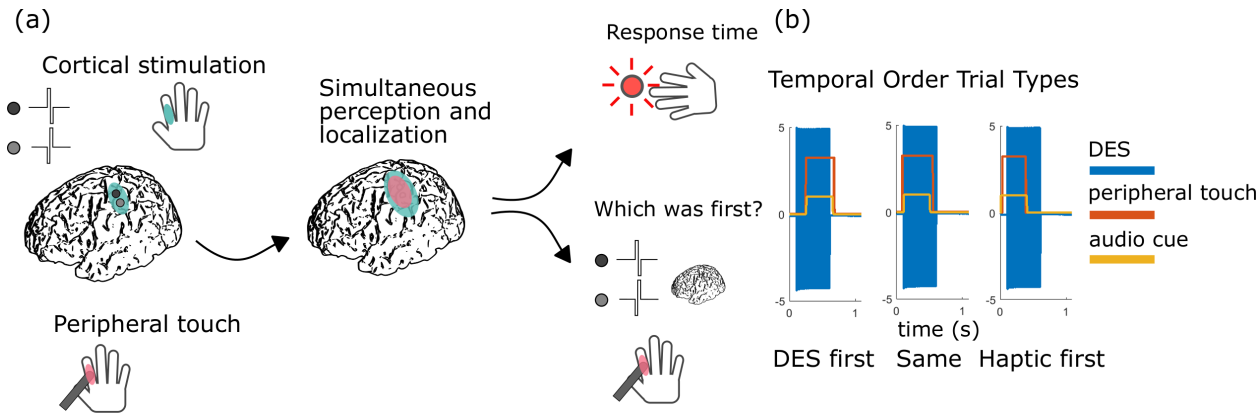

Figure 6.2: Overview of concurrent haptic stimulation and DES. (a) DES and peripheral haptic touch were applied to elicit percepts at the same spatial location on a subject's hand during a TOJ task. Subjects were asked to respond as quickly as possible, as well as to verbally say which stimulus came first. (b) The three different conditions were DES physically starting before peripheral touch, at approximately the same time, and haptic touch delivered before DES.

Subject	Gender	Age	Experiments	TOJ Stimulation Current	Coverage and DES percept localization	Handedness	Seizure Etiology
1	Male	28	Response Timing Ternary Response	1.5 mA	Right grid Middle three digits, palmar and dorsal aspects	Right	left medial temporal lobe epilepsy without hippocampal sclerosis (MRI negative) with seizures arising from the medial aspect of the left inferior temporal pole and hippocampus proper
2	Female	31	Response Timing Temporal Order Judgment	1.25 mA	Right grid Palmar aspect of digit 2	Right	right mesial temporal lobe epilepsy
3	Female	33	Response Timing Temporal Order Judgment	2 mA	Right grid Middle 3rd of 2nd digit	Right	right mesial temporal lobe epilepsy MRI negative

Table 6.1: Modified waveform and temporal order judgment subject demographics. This table shows the demographics for all the patients in this study, including experiments completed, stimulation currents used, and the localization of subjects' percepts, electrode locations, and seizure etiologies.

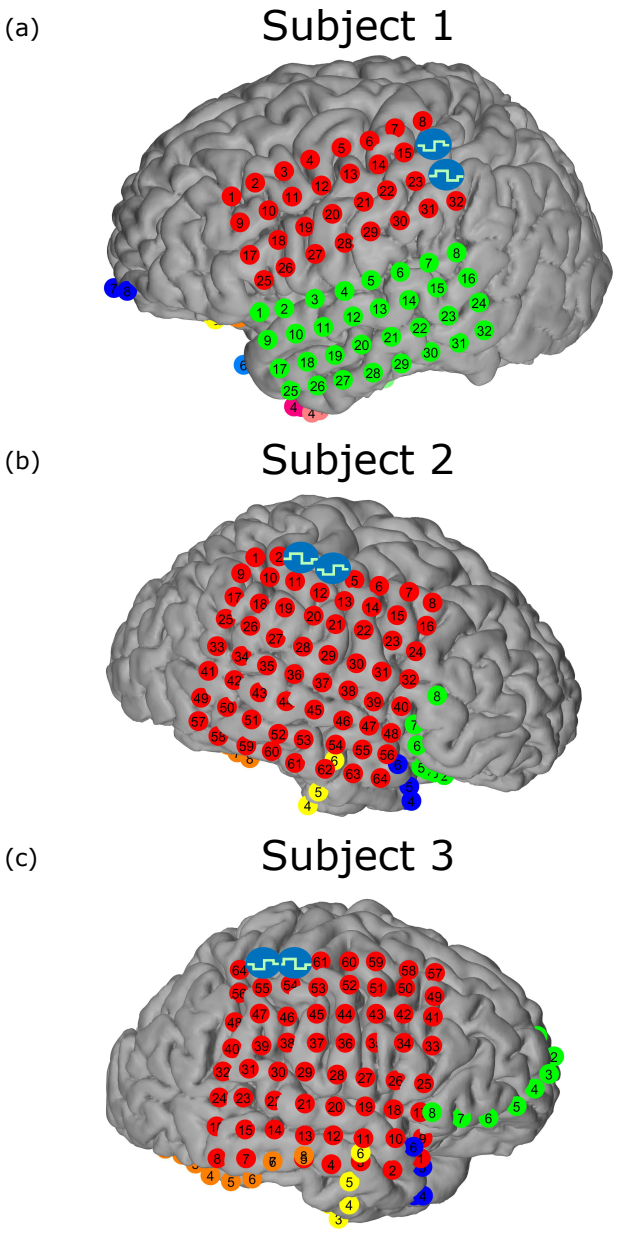

Figure 6.3: Stimulation electrode locations for the modified waveform and concurrent stimulation tasks. We used bipolar, biphasic stimulation between two adjacent contacts in a clinical ECoG array.

leading us to use non-parametric tests such as Kruskal-Wallis tests for statistical significance testing. We excluded any groups with fewer than 5 data points from the Kruskal-Wallis and subsequent post-hoc testing.

Custom code was written in MATLAB, Python, and R for analysis and visualization.

6.2.3 Modified Waveforms

Due to the presence of non-normally distributed groups, we proceeded with non-parametric testing for all subjects, using the non-parametric Wilcoxon Rank Sum and Kruskal-Wallis tests (with Dunn-Sidák corrections for post-hoc comparisons for mean ranks [73, 257] to assess differences between conditions with an alpha significance level of 0.05.) In order to interpret the Kruskal-Wallis test, we tested for equal variance between groups with at least 5 data points using the Brown-Forsythe test [40]. Due to the presence of unequal variances between groups in the second and third subjects ($p = 3.05e\text{-}8$ and $p = 6.79e\text{-}8$, respectively), significant post-hoc testing reveals stochastic dominance of one group over another, rather than a difference directly in medians.

Due to not seeing significant differences between the same conditions across blocks in our prior work, we combined any overlapping conditions between blocks for statistical analysis.

6.2.4 Temporal Order Judgment

To analyze the response timing differences between groups in the first subject (DES first, same, and haptic touch first), we used a Kruskal-Wallis test and Dunn-Sidák correction. For subjects two and three, we used a Wilcoxon Rank Sum test, as there were only two groups (DES and haptic touch first).

We performed psychometric curve fits to the TOJ data using cumulative Gaussian functions [297] as our model for the psychometric function, and estimated the parameters for the best fit cumulative Gaussian function for our observed data. We focused on the point of

subjective simultaneity (PSS) value, representing the point where the proportion of stimuli being judged as coming first is 50% for either stimulus. In our fits of the cumulative Gaussian functions, this is labeled as "threshold".

We used 1.5 mA, 500 ms, 200 Hz trains for Subject #1, 1.25 mA, 500 ms, 200 Hz trains for Subject #2, and 2 mA, 500 ms, 200 Hz trains for Subject #3.

6.3 Results

6.3.1 Waveform Modification

Table 6.2 contains the summary statistics of response times during the modified waveform tasks for all 3 subjects.

In the first subject, there was a trend towards faster response times with the 3 mA priming, 1.5 mA following compared with the 1.5 mA constant amplitude train (median response times of 414 ms for the priming condition vs 473 ms for the 1.5 constant stimulus train condition combined across two blocks), however, this is not significant as assessed through a Wilcoxon Rank sum test ($p = 0.167$) (Figure 6.4).

In a second subject, we used two blocks. In the first block we tested haptic stimulation, various constant 200 ms train amplitudes (1.25 mA, 3 mA, which were both suprathreshold, and 0.8 mA, which was sub threshold in a 200 ms train), as well as 3 mA priming, 1.25 or 0.8 mA trains following. In the second block, we tested 3 mA, 1.25 following, and 2 pulses at 3 mA (Figure 6.5). The subject reported during stimulation parameter screening that only two pulses at 3 mA felt more natural than the previously tested constant amplitude trains suggesting that using a small number of short pulses may have an effect on how natural a stimulus feels. The subject was not able to report feeling a change in the stimulation duration between the two pulses at 3 mA and longer trains at lower stimulation amplitudes from the stimulation parameter screening sessions.

In parallel with a well-established psychophysical principle [306], stronger stimuli resulted

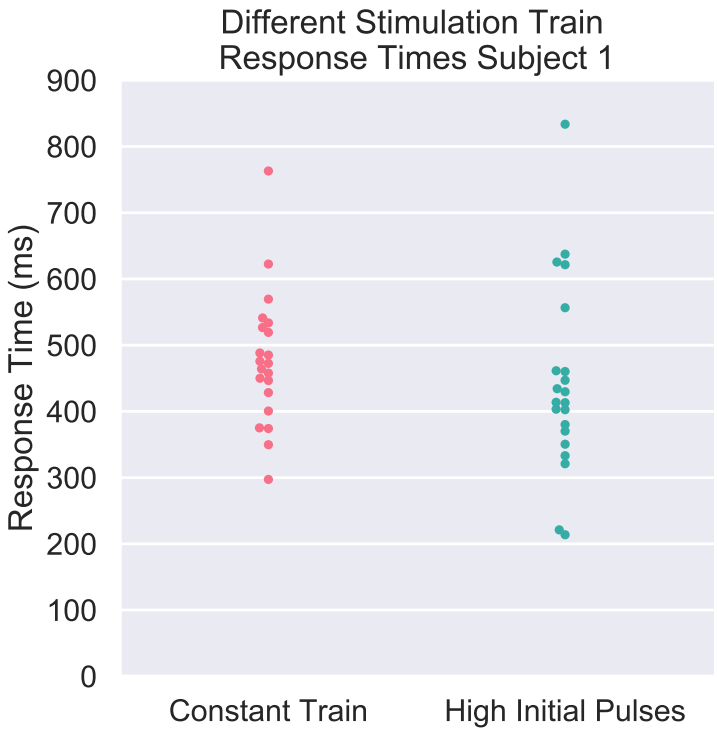

Figure 6.4: Modified waveform response timing results - first subject. The DES train with 3mA priming, 1.5 mA following has a trend towards faster response times than the 1.5 mA constant train (p=0.167, Wilcoxon Rank Sum test)

in faster response times. The 200 ms, 3 mA train was reported to feel very intense, whereas the 2 high pulse trains with priming pulses at 3 mA were not reported as so. Anecdotally, this subject also reported the 2 pulses at 3 mA as more "natural" than the longer, constant train stimuli.

There was a significant difference in response times between all groups (Kruskal-Wallis, p-value = 3.71e-10). We then performed post-hoc testing with the Dunn test. The constant train at 3 mA, which was perceived as nearly too intense, was not significantly different from the 3 mA priming, 1.25 mA following condition (p=0.1), but was significantly different from the 1.25 mA constant train condition (p=7.52e-3) (Figure 6.5). This points to the fact that two initial high pulses may aid with perception without creating an overly strong stimulus.

There was no significant difference between the 3 mA constant train and the haptic condition (p=0.051), suggesting that strong enough DES stimuli can approach natural haptic response times. However, we note that the subject would not have been comfortable with the sensation induced by the 200 ms, 3mA stimulus in a natural setting due to its intensity.

The two primed pulses resulted in significantly slower response times than the two primed pulses followed by a 1.25 mA train (p = 3.07e-3), suggesting that the primed pulses on their own do not increase performance as much as a train with continued suprathreshold charge delivery.

In a third subject, we completed two blocks of trials. In the first block we tested haptic stimulation, constant 200 ms train amplitudes (1.8 mA - matching the purported touch intensity, 1.47 mA - threshold stimulation, and 1.6 mA - charge balanced stimulation for the 1.8 mA priming condition), 2 pulses at 5.2 mA, and 5.4 mA priming, 1.8 or 1.47 mA following trains. In the second block we tested haptic stimulation, constant 200 ms train amplitudes (2.0 mA - matching the purported touch intensity, 1.6 mA - threshold stimulation, and 1.79 mA - charged balanced stimulation for the 6 mA priming, 1.6 mA following condition), as well as 6 mA priming, 1.6 or 2 mA following trains, and 2 pulses at 3.75 mA (Figure 6.6).

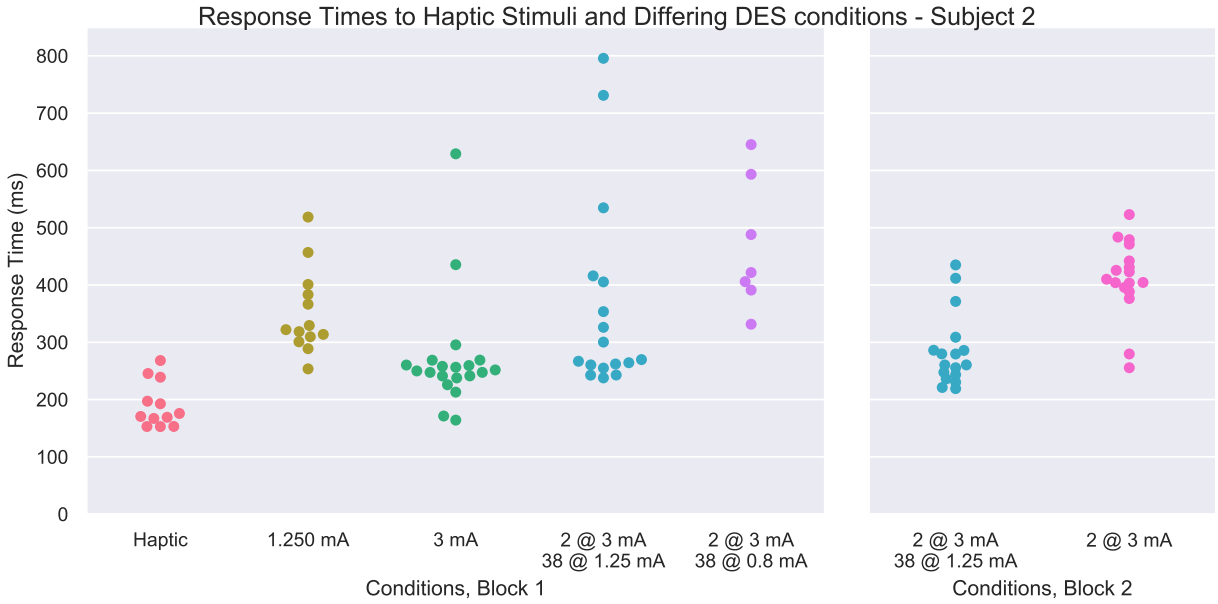

Figure 6.5: Modified waveform response timing results - second subject. The haptic feedback condition has a lower median response time than all other conditions. The 3 mA 200 ms train, which was perceived as very intense and stronger than the haptic touch, was not significantly different in response times than the haptic touch. The 3 mA priming, 1.25 mA following waveform was not perceived nearly as intensely as the 3 mA constant amplitude condition, but did not have significantly different response times, suggesting that primed pulses can increase performance in response DES without creating too intense of sensations.

Both the 1.8 mA constant amplitude condition in the first block and 1.6 mA constant amplitude condition in the second block only had one trial with responses within our response time bounds. This suggests that these amplitudes were not consistently suprathreshold for this subject.

There was a significant difference in response times between groups (Kruskal-Wallis, p-value = 9.99e-13). Haptic stimulation was significantly different from all other groups other than the 5.4 mA primed stimulus (p=0.21), and had the lowest median response times. Specifically, there was a significant difference between the 2.0 mA matched intensity condition and haptic stimulation (p=2.33e-8), reinforcing that the delays we see to DES are not simply due to the haptic touch being perceived as more intense.

Interestingly, the two pulses at 5.4 mA resulted in the fastest reaction times among all blocks, suggesting that some habituation had occurred between the first and second blocks, as the 6 mA primed pulses did not result in faster reaction times (Table 6.2).

The three train conditions with 5.4 mA priming were not significantly different from one another, suggesting that the most important factor in these conditions was the initial two higher amplitude stimulation pulses.

Four of the six conditions in the second block were not significantly different from one another. The 2 mA matched intensity, two conditions with 6 mA priming, and 2 pulses at 3.75 mA were not significantly different from one another. One potential reason for this is the high variability observed in the data (Figure 6.6).

6.3.2 Temporal Order Judgment

Only in trials where haptic touch trailed DES by over 200 ms did the first subject reliably perceive DES as being delivered first. From haptic touch trailing DES by 200 ms to approximately both arriving concurrently, there was ambiguity in the subject's perception of which stimulus arrived first (Figure 6.7, left).

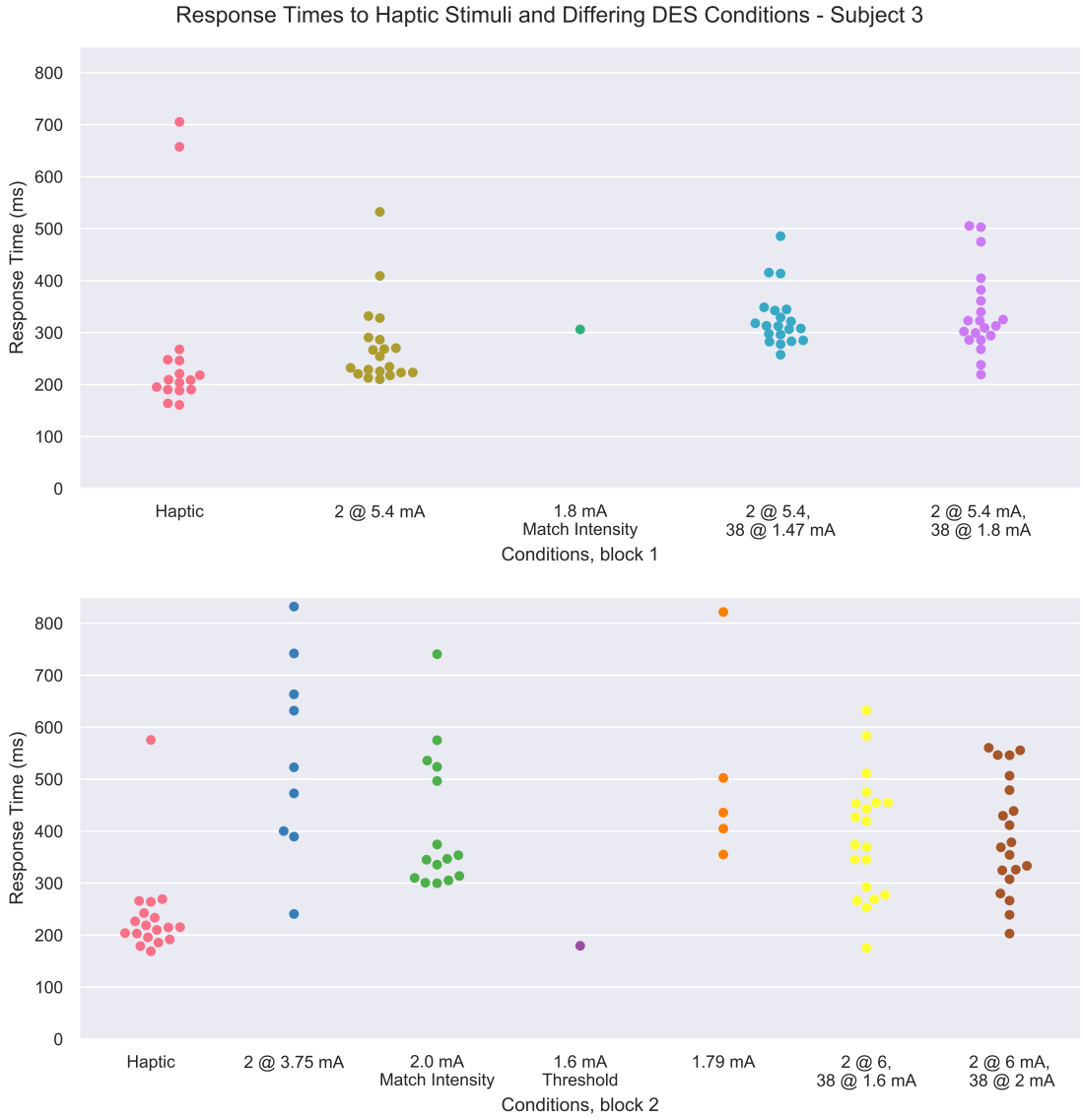

Figure 6.6: Modified waveform response timing results - third subject. The haptic feedback condition has a lower median response time than all other conditions. The 2 pulses at 5.4 mA resulted in the fastest reaction times among the conditions, suggesting that during the second block perceptual habituation may have occurred, resulting in the 6 mA primed waveforms not being faster. In the second block, the 2 mA condition was matched to the intensity of the haptic touch, and was significantly more slowly responded to. Only one trial for the 1.8 mA and 1.6 mA train conditions were responded to within the response timing bounds, suggesting that these amplitude values were not consistently perceived by the subjects.

Subject	Experimental Condition	Minimum (ms)	25% quartile (ms)	Median (ms)	75% quartile (ms)	Maximum (ms)	Num. trials
1	Constant Train	297	428	473	527	763	21
	2 Priming Pulses & Train	214	370	414	461	834	21
2	1.25 mA	254	310	322	383	519	13/20
	2 @ 3 mA	256	396	410	442	523	17/20
	2 @ 3 mA	219	249	268	347	796	34/40
	38 @ 1.25 mA						
	2 @ 3 mA	331	398	422	541	645	7/20
	38 @ 0.8 mA						
	3 mA	164	240	251	262	629	20/20
	Touch	153	164	173	208	268	12/20
3	1.47 mA	N/A	N/A	N/A	N/A	N/A	0/20
	Threshold						
	1.6 mA	N/A	179	N/A	N/A	N/A	1/20
	Threshold						
	1.79 mA	355	405	436	502	822	5/20
	Charge Balanced						
	1.8 mA	N/A	N/A	306	N/A	N/A	1/20
	Match Intensity						
	2 @ 3.75 mA	241	400	523	663	832	9/20
	2 @ 5.4 mA	210	223	244	287	532	20/20
	2 @ 5.4 mA	219	292	318	366	505	20/20
	38 @ 1.8 mA						
	2 @ 5.4 mA	257	293	313	343	485	20/20
	38 @ 1.47 mA						
	2 @ 6 mA	175	289	397	455	633	20/20
	38 @ 1.6 mA						
	2 @ 6 mA	203	320	374	486	560	20/20
	38 @ 2 mA						
	2 mA	300	319	364	565	939	18/20
	Match Intensity						
	Touch	161	193	212	245	705	34/40

Table 6.2: Response times for each subject and each condition with modified waveforms. Final column reports the number of trials responded to by each subject across both blocks for each of the trial types given our response time limits of 150-1000 ms, and appropriate signal detection. Response times outside of this range were considered outliers based on expected human performance.

As previously seen in Chapter 5, responses to DES (when perceived first) were slower than trials when haptic was perceived first (Figure 6.8, right). There was a significant difference between the haptic touch perceived first and DES perceived first reaction times (p=0.04). There was no significant difference between "same arrival time" and DES first or haptic touch first conditions. Due to the limited number of trials within each of these blocks, and large variability, these statistics are not as robust as the ones in the modified waveform task.

The subject described perception of both sensations as distinct in all conditions, indicating that perception of both stimuli independently was not masked by DES.

The second and third subjects similarly demonstrated a requirement of DES leading haptic touch to result in being reliably perceived first. For the second subject, the PSS, where either type of stimulus was equally judged to be occurring first, was -109 ms. For the third subject, the PSS was -121 ms (Figure 6.8). These values are to be taken as approximates, as the majority of points sampled lied within bins where the subject always guessed one stimulus or another.

The median response times for the second subject during the TOJ experiment were 418 ms for DES perceived first trials (n = 53) and 223 ms for haptic touch perceived first trials(n=26), with statistical significance between the two distributions (Wilcoxon Rank Sum test: p = 2.6e-8). The median response times for the third subject were 367 ms for DES perceived first trials (n=52) and 282 ms for haptic touch perceived first trials (n = 30), with a significant difference (Wilcoxon Rank Sum test: p = 3.2e-5). The median reaction time difference was 195 ms for subject two, and 85 ms for subject three.

Our data for each subject show there is a range of latencies for which overlapping spatial and temporal DES and natural stimuli are perceived as arriving simultaneously, but independently. Importantly, no subject reported any modification of the percepts when applied concurrently, suggesting that DES interferes minimally (if at all) with the bottom-up perception of normal tactile sensation.

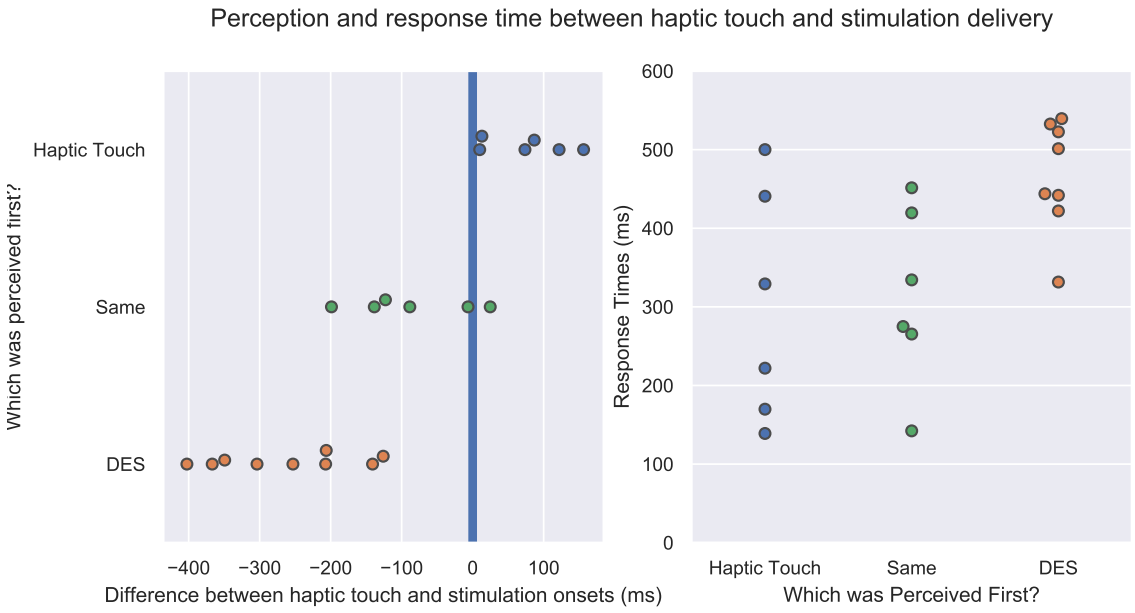

Figure 6.7: Results of ternary response task for the first subject. With DES delivered before haptic stimulation with a range of time deliveries from -400 ms to -200 ms, all trials were distinctly perceived as DES arriving first. Between -200 ms and 25 ms, with 25 ms representing DES onset 25 ms after haptic touch onset, the subject reported the stimuli arriving at approximately the same time. With DES onset between 75 ms to 150 ms after haptic touch, the subject always reported perceiving haptic touch first (Left panel). The right panel shows a distribution of response times, where following a Kruskal-Wallis test and Dunn's test for multiple comparisons, the haptic touch condition stochastically dominates the DES condition, consistent with our previous results that haptic touch results in faster response times than DES (right panel).

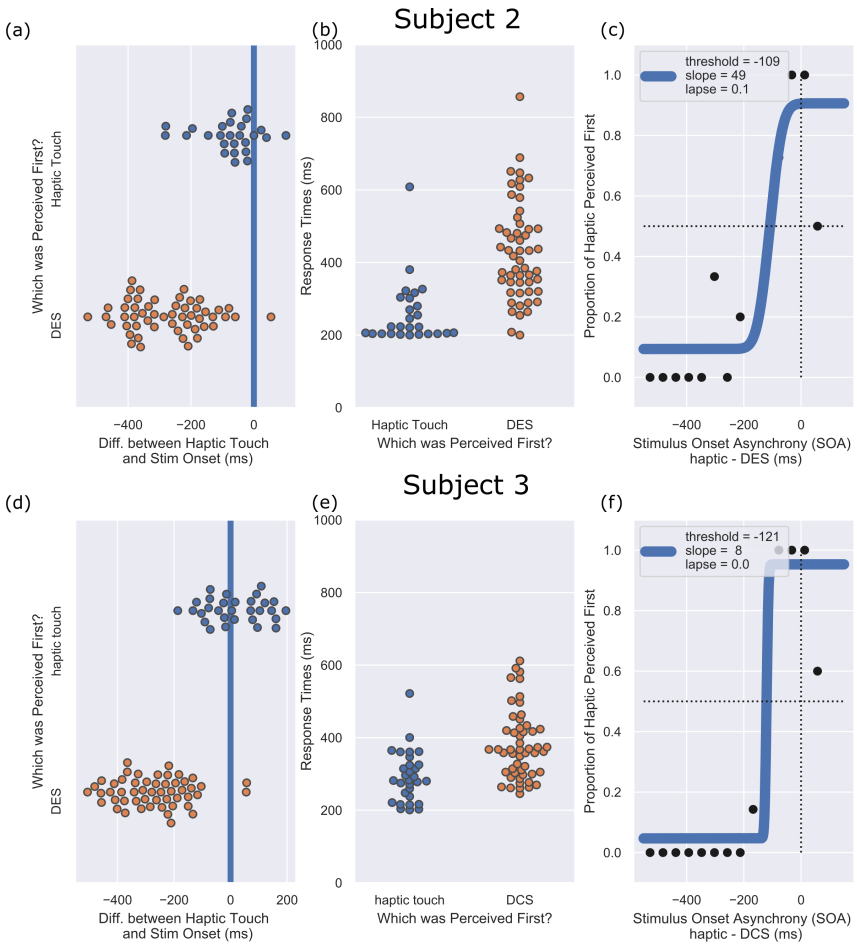

Figure 6.8: Results of the temporal order judgment task for the second and third subjects. We performed the formal TOJ task in two individuals. (a and d) For the second subject (a), and the third subject (d), there were clear regions where the stimuli were almost entirely perceived as either DES or haptic touch arriving first. (b and e) These plots shows a distribution of response times, where following a Wilcoxon Rank Sum test, the haptic touch condition stochastically dominates the DES condition, consistent with our previous results that haptic touch results in faster response times than DES. (c and f) After fitting a psychometric function (cumulative Gaussian function) to the binned frequencies of which stimulus was perceived first, we calculated a point of subjective simultaneity (PSS) of 109 ms for subject two (c) and 121 ms for subject three (f), which is the point where stimuli arriving would be judged to be either stimulus equally. This recapitulates the response time difference seen between the two stimulus types, where DES requires longer for the subject to respond.

6.4 Discussion

We have demonstrated that modifications of constant amplitude train waveforms are able to significantly affect human performance in a response timing task. For some subjects (ubject two), two individual pulses felt more natural than trains of stimuli, which suggests that initial charge delivery is critical for both performance and the quality of the percepts. From our prior work [45], we reported no differences between the naturalness of the percepts for 100, 200, 400, and 800 ms stimulation trains, reinforcing that the early initial periods are most critical. This would be supported by the observations in populations of S1 neurons that respond most intensely to object contact and offset [22].

Our observations are consistent with classic psychophysics literature [306], where stronger stimuli are responded to more quickly. However, as prior work has noted, the relationship between the difference in reaction times and the PSS can be highly variable [48]. Our TOJ data reinforces the idea that DES takes longer to process than natural haptic touch. One key insight from our results is that rather than relying on a motor response, which could be subject to inhibitory effects of stimulation, we looked at reported perception. This further supports the idea that DES does not induce a window of local cortical jamming, where no additional processing can occur [166], suggesting that the delayed response times to DES as compared to haptic touch arise from some other phenomenon.

There are a few limitations of our studies. One is the relatively limited number of trials for each of the stimulation conditions in the modified waveform task (20). This reduces our confidence about observed differences in response times and variability. Another is the imperfect timing of touch application from our digital and analog touch probes, which we acknowledge from the non-zero delays seen in our validation. These do not instantaneously register object contact, but as we have shown also do not significantly alter our results, as we observed the same trends with both analog and digital probes, and the TOJ results support a meaningful delay in perception. Due to the distribution of possible delays in touch probe

application (Figures C.1, D.1), there is some error in the precise timing of touch application. Future efforts will therefore need to more finely sample the regions near the PSS in order to accurately determine its relative value. However, these results support the interpretation of an increased processing burden for perceptual awareness of the the un-natural S1 DES relative to haptic touch.

Prior work with peripheral sensory stimulation combined with visual stimuli support the notion that the brain uses a window of temporal integration to provide multisensory synchronized sensations, on the order of 111 ms [56]. This has important implications for stimulation in cortical neuroprosthetics. Specifically, even if there is a lag in perception for DES relative to natural haptic touch, if it is within performance bounds that result in synchronous perception with another modality such as a visual stimulus, it is conceivable that the user may not perceive a substantial delay in the device output.

Our observation that DES does not inhibit natural sensory processing for percepts arriving from the same spatial location with close temporal proximity is complemented by prior observations that the brain can perform overt motor movements and task the same region with BCI control [18]. This suggests that brain regions can receive concurrent artificial and natural feedback, and process both independently, as well as perform a BCI task and normal motor functions. For a future neuroprosthetic device, these results imply that the brain could be tasked with both interpreting artificial input as well as performing its normal functions. More generally, this reinforces the immense capacity of the brain to adapt to the task at hand.

Other work in auditory cortex has suggested that low level electrical stimulation does not simply serve as a substitute for cortical activity; rather, it is integrated within naturally occurring neural activity and modulates responses, similar to what attention would do [282]. This points to the complexities of neural stimulation, and reinforces our observation here that DES does not purely substitute for or disrupt the normal processing circuitry.

Two keys points regarding future sensory neuroprosthetic devices are what happens to the cortical representation of hand sensory area following amputation or spinal cord damage, and how existing residual sensory function impacts the perception of stimulation. Although it is classically thought that following amputation areas, other preserved cortical areas take over the territory of the missing limb. This has been demonstrated in humans without a limb or hand, where activation of the preserved hand activates cortical areas previously responsible for the missing appendage [172]. However, decades after arm amputation in humans, a representation of the missing hand's fingers remains in primary somatosensory cortex as assessed through fMRI [135]. Similarly, in paraplegics, the hand sensory representation was not found to expand into adjacent cortical activities [276]. Intracortical microstimulation through penetrating arrays in a human has elicited similar percepts in both spared and deafferented regions in an individual with residual sensation in part of their hand, indicating that existing sensory input does not have an effect on the perception of stimulation [90], while in a human with arm paralysis and chronic impairment of somatosensory function, an microECoG stimulation provided meaningful sensory feedback [119]. Taken together, this points to a surprisingly robust representation of hand sensory function in cortex following injury, and the similarity in perception for both spared and deafferented regions supports the applicability of our results to cortical regions in individuals with stroke and paralysis. This in total illuminates the capacity to provide sensory feedback to individuals that may benefit from sensory restoration either through electrodes on the cortical surface or implanted within the brain.

Two approaches for sensory neuroprosthetics that need not be separate are biomimetic stimulation and adaptation [23]. Temporal biomimetic approaches mimicking SA-1 nerve fiber activity have been used for peripheral nerve interfaces to help users distinguish different textures [208]. Different stimulation patterns beyond constant trains have transformed peripheral stimulation percepts through nerve cuff electrodes into more natural feeling ones

such as vibration, moving touch, consistent pressure, and tapping [270]. Our work fits into this from a cortical stimulation avenue, and opens the doors for exploring different waveforms in cortical stimulation. As microECoG arrays with smaller electrodes and tighter spacing become more common to provide sensory feedback [149], these could be used to more finely pattern spatial percepts, which has already been demonstrated robustly in primates with ICMS [268].

The concept of adaptation exploits the ability of individuals to learn to use a novel stimulus, which has been demonstrated in rodents who used stimulation in S1 to learn to respond to invisible infrared light [273], as well as primates using an ICMS signal to guide a motor task, which was also able to be integrated with vision [65]. The plasticity of sensory cortices is well documented, where following neurological damage, adjacent regions undergo remapping to process sensory signals from the lost regions [39]. Sensory signals can also result in plasticity changes, as extensive cutaneous stimulation to a focal peripheral region can enhance the size of cortical receptive fields and reorganize somatosensory cortex [67]. An additional example of this in humans is the reorganization of the cortical representation of fingers in Braille readers [67]. Given the complexity of sensory function, it is unlikely that even more finely patterned stimulation with microECoG arrays will be able to emulate natural patterns of neural activation in response to peripheral touch. Despite this, by getting as close as possible to a biomimetic approach, and concurrently relying upon the brain's plasticity and demonstrated abilities to adapt to novel signals, we could improve the performance of DES of sensory cortex.

In summary, by combining biomimetic approaches with user adaptation, more efficacious stimulation can be engineered for sensory neuroprosthetic devices.

6.5 Conclusions

In three subjects, we have demonstrated that modifications of constant amplitude train waveforms are able to significantly affect human performance in a response timing task, and can alter the strength and quality of the percepts.

Furthermore, we have shown that concurrent DES and natural haptic stimuli to the same spatial location with close temporal proximity can be perceived independently, and that the stimulus onset asynchrony between the two modalities recapitulates differences in response times seen between DES and natural haptic touch.

These results have implications for the engineering of stimulation waveforms in sensory neuroprosthetic devices to ensure the closest to natural performance. Additionally, we observe that DES does not inhibit natural sensory processing for percepts arriving from the same spatial location with close proximity. This suggests that brain regions can receive concurrent artificial and natural feedback, and process both independently. For a future neuroprosthetic device, these results imply that the brain could be tasked with both interpreting artificial input as well as performing its normal functions.

6.6 Code Availability

Full MATLAB, Python, and R code is available at:

https://github.com/davidjuliancaldwell/StimulationResponseTimingPython

https://github.com/davidjuliancaldwell/ResponseTimingAnalysis

6.7 Related Publications and Presentations

Caldwell DJ, Cronin JA, Wu J, Weaver K, Ko AL, Rao RPN, Ojemann JG, "Spatiotemporally overlapping haptic and direct cortical stimulation in humans results in simultaneous perception with a range of delays predicted by the response time delay to cortical stimulation", Society for Neuroscience – Annual Meeting, San Diego, CA, November 2018

Caldwell DJ, Cronin JA, Tsai JJ, Rao RPN, Ko AL, Weaver K, Ojemann JG, "Direct cortical stimulation with non-uniform amplitudes modify behavioral response times and neural responses relative to constant stimuli", 2018 Neurofutures Meeting, Seattle, WA, July 2018

Caldwell DJ, "Behavioral and neural differences between haptic stimulation and direct cortical stimulation in humans: implications for neuroprosthetics", 7th International BCI Meeting, Workshop: Perception of Sensation Restored through Neural Interfaces, Asilomar, CA, May 2018

Chapter 7

DOSE DEPENDENT ENHANCEMENT OF CORTICALLY EVOKED POTENTIALS DURING BETA-OSCILLATION PHASE TRIGGERED DIRECT CORTICAL STIMULATION OF HUMAN CORTEX

Neuromodulation through direct electrical stimulation of the cerebral cortex may enhance neuroplasticity after stroke or trauma, potentially improving outcomes. Mechanistic theories of plasticity suggest that it may be critical to pair stimulation with endogenous neural activity. In order to better characterize the potential role of direct electrical stimulation for neurorehabilitation in humans, we studied the beta-oscillation (12-20 Hz) triggered ECoG stimulation through characterization of cortically evoked potentials (CEPs). In 10 human subjects, 7 of whom completed the experimental paradigm, we recorded beta oscillations, and in real-time delivered electrical stimuli during various phases of heightened beta oscillations at a site which elicited CEPs. Using a linear mixed model, we discern a statistically significant increase in CEP size immediately following conditioning, with larger increases for greater numbers of conditioning stimuli. In one subject, we compared beta-triggered oscillation with a control stimulation condition that was independent of underlying brain oscillations. We found electrodes where CEPs were larger during beta-band dependent stimulation when compared with the control. Heightened beta-oscillations alone did not enhance CEP magnitudes. When considering all electrodes across the cortex, we observe a trend towards increased CEP amplitudes at surface depolarizing phases relative to hyperpolarizing phases, with a significant effect at the greatest number of conditioning stimuli. In 3 subjects, the greatest percent increase in CEP magnitude was in the trigger channel. This study

demonstrates that activity-dependent cortical stimulation can increase the CEP amplitude, a surrogate marker of connectivity suggesting a role in neurological rehabilitation, relative to open-loop stimulation, although much remains unknown about optimum stimulation parameters and the relationship with functional outcomes in humans.

7.1 Introduction

7.1.1 "Closed-Loop" Stimulation Control

Beyond non-invasive and peripheral stimulation modalities, it is possible for brain DES to enhance outcomes. However, it is a challenge to operationally determine when the brain is actively engaged in a task, in real-time. Exploiting what is known about the importance of timing of stimuli for both synaptic potentiation and depression is an important place to start [85]. As discussed in the introduction, activity dependent stimulation may offer advantages relative to open-loop stimulation protocols for inducing cortical plasticity.

To investigate if these principles of activity-dependent modulation extend to the multicellular neural systems level, system-level markers of activity are needed. The beta band of cortical oscillations correlates with periodic firing of neuronal ensembles [198,199], suggesting the temporal summation of the activity of many neurons [210]. Additionally, beta waves are also associated with attention (Murthy and Fetz 1996a) and closely associated with a more common form of neuroplasticity — learning [118]. Beta rhythms are conserved across species, and are suggested to emerge from the tightly synchronized integration of excitatory synaptic drive which targets pyramidal neurons, primarily the proximal and distal dendrites [255].

Likewise, instead of single-cell markers of plasticity, we need alternative measures to quantify connectivity at the multicellular scale. One such electrophysiological measure is the cortico-cortical evoked potential (CCEP): when the brain is stimulated in one location with an electrical pulse, an evoked potential appears at a connected area of cortex [175,176]. Evoked potentials have been used to establish the effects of stimulation paradigms on neural

activity and connectivity in non-human primates [250], and as such we similarly seek to use the modulation of CCEPs as a metric for the efficacy of the induction of short term plasticity. An additional recent study has looked at the phenomenon of Volume-Conducted Potentials (VCPs) through high resolution ECoG recordings in humans [256] to study propagation of a single source of neural signals near stimulation electrodes. We acknowledge potential contributions from neurons directly under the stimulating electrode pair to adjacent local field potentials, and therefore rather than focusing on absolute magnitudes which are of unclear importance, we emphasize changes in evoked potential due to our conditioning paradigm.

Rather than specifically describe our recorded signals as cortico-cortical evoked potentials (CCEPs), we instead will refer to them simply as cortically evoked potentials, or CEPs [314], to avoid confusion with literature in reference to distant responses (on the order of centimeters) seen with higher levels of stimulation at connected sites.

Combining beta-band activity as a physiological marker of neural activity with the CEP as a surrogate measure of neural system connectivity and plasticity, we implemented a paradigm to record signals from the brain and provide stimulation in humans only during optimal periods of brain activity.

7.2 Materials and Methods

7.2.1 Recording and Stimulation

We recorded raw neural data at 12207 Hz to resolve short-latency signal components and for artifact suppression. We employed a constant-current stimulation mode, which delivered voltage to meet a given current requirement. Our pulse duration was approximately 1.23 ms for each phase of our biphasic, bipolar rectangular pulse stimulation.

7.2.2 Electrode Selection and Identification of CEPs

We identified primary motor cortex (M1) for stimulation and adjacent electrodes for recording. We identified M1 for stimulation and adjacent electrodes for recording. In most subjects we used multiple concurrent methods to determine the approximate anatomical location M1 electrodes: 1) on neuroimaging and subsequent cortical reconstructions, then 2) we located the focus of high-gamma response to overt and imagined hand movement (compared to rest) that corresponded to the approximate surface anatomical location of the hand motor cortex [158, 187], and 3) verified the functional location by evoking movements with stimulation. If clinically indicated, subjects previously underwent clinical stimulation mapping for the purposes or surgical planning. The results of the clinical mapping, when available, helped guide the selection of research stimulation amplitudes and aided identification of functional areas. We chose hand-motor area as the preferred target location in this study partially because of prior stimulation in this area in the EVEREST study and related studies [106, 122, 159, 221]. Additionally, the theoretical window for activity dependent plasticity is potentially longer in motor areas compared with sensory areas, as M1 neurons activated through median nerve stimulation fire for several milliseconds, where M1 activity that causes a ballistic hand movement lasts for up to 250 ms [62, 75]. Two adjacent electrodes were used for stimulation (bipolar configuration).

To evoke a CEP, we stimulated with individual pulses and increased the amplitude until we observed an evoked response in neighboring electrodes. We identified CEPs in recording channels by comparing all channels and selecting those with evoked potentials superimposed on the stimulation artifact. CEPs were qualitatively large amplitude, long duration, often biphasic responses present in a subset of channels in close proximity to the stimulation channels. As stimulation amplitudes were increased, CEP amplitudes would appear and increase in size in a nonlinear relationship with the stimulation artifact, and were subject to amplitude saturation.

Recording electrodes that demonstrated robust CEPs in response to stimulation were candidates for beta recording electrodes. We then selected the electrode with the largest evoked response and filtered for the beta band (biquad, cascaded high-pass and low-pass Butterworth filters between 12 and 20 Hz, with 12 dB roll off per Octave) component of the time-series neural signal. If the initially selected electrode did not have a beta component (location dependent), we selected the electrode with the next largest CEP. We identified the maximum amplitude of the CEP by titrating up the stimulation amplitude until reaching maximum CEP amplitude.

7.2.3 Stimulation Delivery and Recording Paradigm

Once stimulation and recording electrodes were identified, we recorded the baseline root-mean-square (RMS) of the filtered beta band from the beta recording electrode, and then empirically selected the RMS value of the filtered beta signal that differentiated between beta bursts and baseline beta activity. Then, we digitally processed the band passed beta signal, and delay-triggered a single stimulus after the zero crossing of the wave (0°, 90°, 180°, 270°, relative to a sine wave, or randomly, modified to match the experimental protocol) as long as the RMS value of the filtered signal exceeded that of baseline (Figure 7.1). Between beta bursts, we delivered test pulses every 500 ms to evoke a CEP. We recorded the pattern of stimuli to be later delivered in open loop fashion in the control condition described below.

7.2.4 Control Conditions (Stimulation Playback)

After a brief rest period, we delivered stimuli in an open-loop fashion to the subject, independent of the underlying beta activity or phase, with the exact timing specified by the timing file generated from the closed-loop experiment (Figure 7.1). For analysis, we considered conditioning stimuli in the playback condition to be stimuli marked as conditioning stimuli in the closed loop experiment, and probe stimuli in the playback condition to be

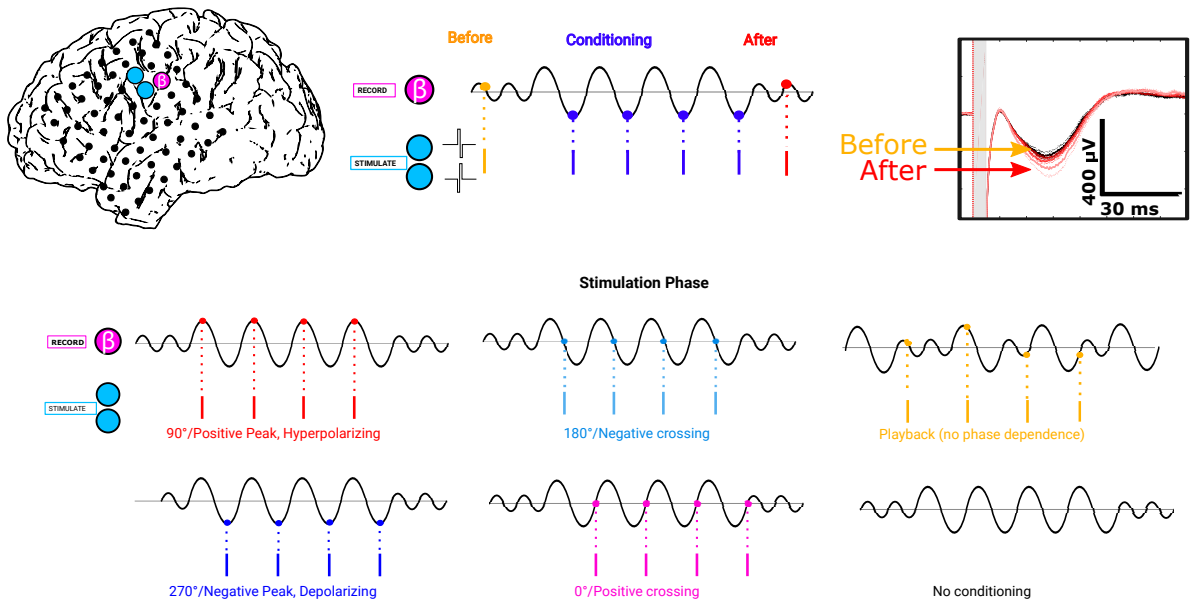

Figure 7.1: Experimental Paradigm and Example Electrode Locations: Bipolar, biphasic pulses were applied to the electrodes in blue. Conditioning pulses are illustrated to fall on a given part of the beta burst. Baseline pulses are test pulses which were more than 2 seconds away from the end of a beta burst. Probe pulses are test pulses which are less than 500 ms following a stimulation train. The targeted phase of delivery was determined a priori, and evaluated post hoc.

probe stimuli in the closed-loop experiment. We similarly tested a null condition, where we delivered probe stimuli before and after a beta burst, but delivered no conditioning stimuli within the beta burst.

7.2.5 Effect of Real-time Filtering on Stimulation Delivery

In the proprietary TDT software, the beta recording channel was bandpassed between 12-20 Hz using a digital, real-time biquad, cascaded high-pass and low-pass Butterworth filter between 12 and 20 Hz, with 12 dB roll off per Octave. A period of 20 ms was removed after each stimulus to avoid ringing through the real time band pass filter. This was determined by observing the filter response to a beta oscillatory signal with stimulation, and estimating the time for recovery to baseline. A zero crossing on either the rising or falling phase was used to trigger a stimulus a fixed number of samples later. For estimated delivery on the peak or trough of the beta signal, stimuli were delivered 16 ms later, corresponding to a quarter cycle for a 16 Hz oscillatory signal, which corresponds with the center frequency of the filter. Testing of the software with an oscilloscope phase lag dependent on the input frequency for the beta filtered signal relative to the center frequency due to the IIR filter in the frequency regimes of interest (12-20 Hz). We characterized the phase distortion due to the beta filtering as a function of frequency, by feeding in a sine wave of a fixed frequency in 1 Hz steps from 12-20 Hz (Supplemental Information, Figure E.1). Furthermore, we used a function generator with a fixed frequency output from 12-20 Hz, in 1 Hz steps, to both an oscilloscope and our recording system. We used this to trigger a stimulus in real time, which we then registered sequentially on the TDT. We compared the phase of delivery of the stimulus on the oscilloscope, and observed the non-linear phase difference we would expect from an IIR butterworth filter (Supplemental Information, Figure. E.1)

We acknowledge the difficulties of real time filtering and non-linear phase delays due to IIR filters implemented in software, but oscilloscope testing and post-hoc confirmation

supports the utility of our software design. We input signals from a function generator of sinusoidal, triangular, and square waveforms of varying amplitudes and frequencies to observe the real time effects of filtering (Supplemental Information, Figure E.2). We also visualized minimal signal interruption due to the blanking of the artifact (Supplemental Information, Figure E.2). We observe accurate tracking of the envelope of the magnitude of the beta oscillatory signal.

7.2.6 Safety

Seizures are a known risk of cortical stimulation. To minimize the chance of provoking a seizure in subjects with known epilepsy, we did not attempt to stimulate near any location that demonstrated interictal-spiking activity during the patient's clinical care. We also decreased or aborted stimulation if any epileptiform changes occurred on the clinical monitor during the course of research. We took precautions in each subject to avoid stimulation near the suspected (or confirmed) epileptic focus, as these areas may be particularly excitable at baseline [79, 169]. The EVEREST trial importantly demonstrated the safety of cortical stimulation in humans. When designing our stimulation protocol, we sought to ensure patient safety by remaining within the stimulation parameters for clinical studies. Additionally, we designed the custom simulation scripts with safety mechanisms to prevent unintended stimulation, and operating procedures to ensure safe delivery of stimulation according to experimental protocols. We halted the stimulation if there were signs of brain irritability (spiking activity), because of the increased risk of seizure.

7.2.7 Post-hoc Analysis

7.2.8 Classification of CEPs

We used custom MATLAB (MathWorks, Natick, Massachusetts, U.S.A.) and R (The R Foundation, USA) scripts for all data analysis. By convention, we classified pulses within

a 500 ms window following stimulation to be probe pulses, and pulses more than 2 seconds after a burst of stimulation to be baseline pulses (Figure 7.1). We compared the peak-to-peak amplitudes of CEPs associated with probe pulses to CEP amplitudes associated with baseline pulses. We subtracted the average neural response in each channel from 50 ms to 5 ms before the time of stimulation. We segregated responses based off of 1-2, 3-4, or greater than 5 conditioning pulses delivered in a train. We performed no filtering upon the entire signal, as filtering smears the stimulus artifact in time and can obscure early potentials. Instead, to reduce common noise and increase the signal-noise ratio, we re-referenced all of the signals against the median of the non-noise channels which did not demonstrate EPs. This was considered on a channel and subject basis where artifacts ended and CEPs began (Figure 7.2). We subsequently proceeded with our CEP peak analysis.

7.2.9 CEP Location Analysis

We analyzed all channels within our subjects, and excluded any from further analysis that were contaminated by amplifier recovery issues or were excessively noisy.

7.2.10 CEP Identification and Conventions

We focused on the peak-to-peak amplitude of the CEP in a 4 ms (or later, if obscured by stimulus artifact) to 60 ms (assuming no additional stimulation during this time) window following stimulation (free from the subsequent stimulation artifact) to represent early, excitatory connections, representing the strength of structural and functional connectivity between regions [134], which builds upon prior work that considered different latency responses (N1, P1, N2) [81, 132]. We did this because the functional significance of different evoked potential components is incompletely understood, nor how they relate to cortical output. For all analyses involving peak-to-peak magnitudes, we thresholded our mean peak-to-peak magnitudes at 150 μV, and only considered channels with magnitudes above this threshold.

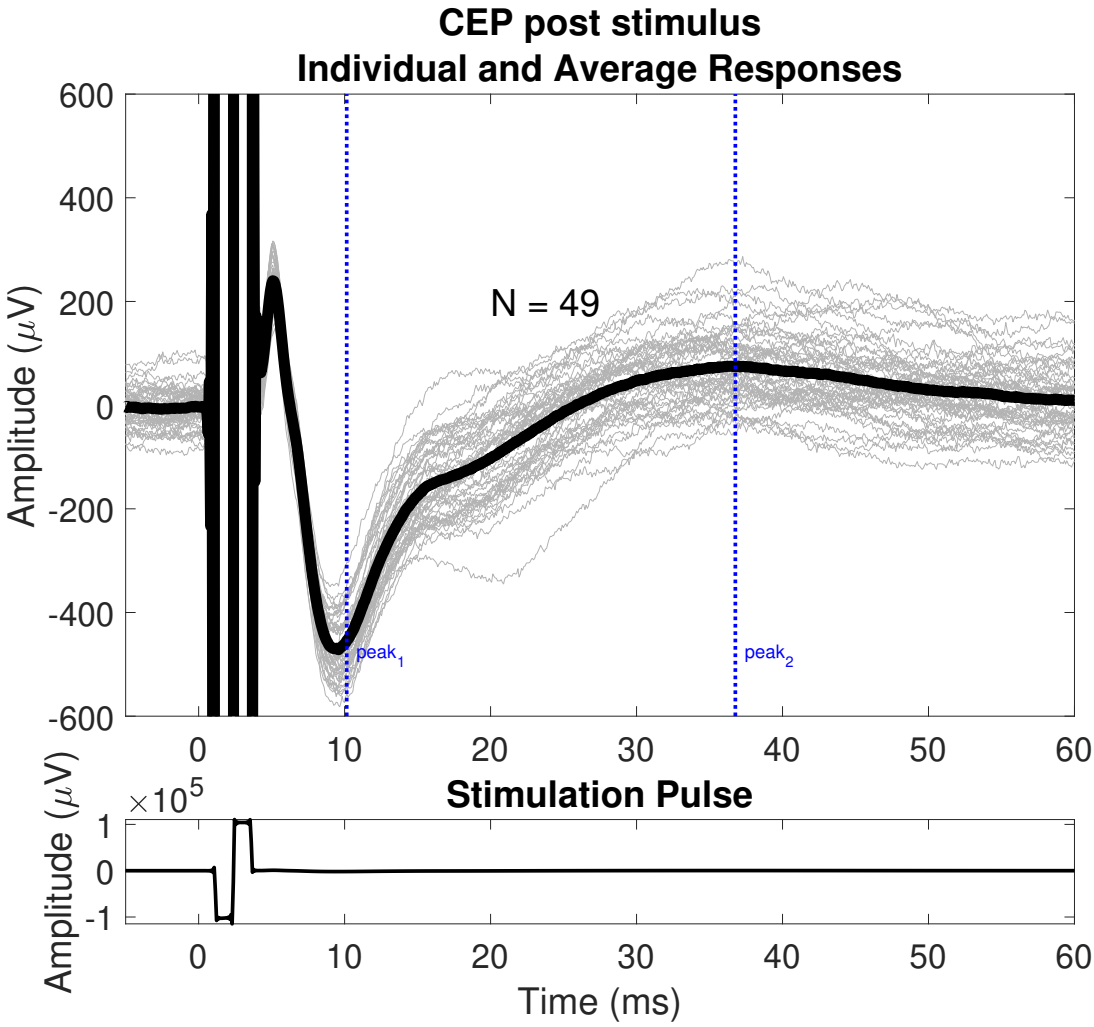

Figure 7.2: Characteristic cortically evoked potentials and stimulation pulse. The top plot shows individual (N=49) CEPs after re-referencing for the trigger channel in subject 7, along with an average waveform. The bottom plot shows for these pulses what the average stimulation pulse looks like as recorded. This demonstrates the relative scale of the stimulation pulse on a recording electrode to the evoked response observed. Of note is that the evoked response is on the order of 100-1000 times smaller than stimulation pulse. In order to account for potential amplifier recovery and artifacts from the stimulation pulses, the initial period of recording following the stimulation pulse were excluded from analysis owing to stimulation artifact. The colored lines indicate individual trials, where the dark black line indicates the average response. The magnitude of an evoked potential for this channel was considered to be the peak-to-peak voltage in the 4 (or later) - 60 ms window following stimulation.

Any single trial with a peak-to-peak magnitude less than 25 μV, or greater than 1500 μV was also discarded, as these tended to be artifacts. We performed Savitsky-Golay smoothing only within our time window of interest prior to extracting the peak-to-peak amplitudes in order to obtain a more reliable estimate of the peak-to-peak amplitude

7.2.11 Post-processing Analysis of Phase Delivery

For analyzing the phase of delivery of the conditioning stimuli, we fit the pre stimulus signal from 50 ms before the stimulus until the time of stimulus with a sine wave using nonlinear least squares fitting via Levenberg-Marquardt method [174], with a moving average smoothing filter of 51 samples (4 ms window) to minimize the amount of high frequency noise fit [314]. The parameters of the sine wave fit ranged with a frequency from 12-20 Hz, with an offset in the model to account for discrepancies from baseline, and the R^2 value was calculated over all conditioning pulses to assess phase delivery variability. Any fits with a R^2 below 0.7 were excluded from further analysis. Additionally, any fits that fell exactly on the boundaries of the frequency edges (< 12.01 or > 19.99 Hz), were also excluded from further analysis, as these often coincided with poor fits. We selected a 12-20 Hz fitting window, as this was the range over which our real time filter operated. Different frequency ranges would falsely estimate the trigger signals. The distribution of frequencies of the fit curves, the individual fitlines, and the phase at stimulus delivery were compiled for each subject and each channel

7.2.12 Statistical Analysis across Subjects

In order to consider the effects of subject variability, stimulation intensity, the number of stimuli delivered during conditioning trains, and the phase of stimulation, we constructed a linear mixed model. This allowed us to disentangle the effects of variables we explicitly tested (the binned phase of delivery, whether or not a channel was a trigger channel, and

how many conditioning stimuli we delivered) relative to ones that (particular channels nested within subjects). We implemented a linear mixed model in R, with the absolute difference from baseline as the dependent variable, and using the number of stimuli delivered during the conditioning trains, the binned phase ($0-180°$, or $180-360°$), whether or not a channel was a trigger channel for fixed effects, with random nested effects of channels within subject. The model also included interactions between the number of stimuli delivered as well as the binned phase, as well as the number of stimuli delivered during the conditioning train and the individual subject, to account for subject variability and potential effect on each of these fixed effects. Analysis of the residuals and cumulative distribution functions (supplementary Figure E.13, Figure E.14) indicated that these analyses were appropriate for most of the data. Of note is the tremendous variability that can be seen in individual trial CEP responses. Despite this, we report a high conditional R^2 which suggests that the combination of our random and fixed effects explains a large fraction of our observed responses.

7.2.13 Statistical Analysis with Subjects

For the seventh subject with the control stimulation condition, we fit a linear model with absolute magnitude as the independent variable, the number of stimuli in the conditioning train, the closed-loop or control status of the experiment, and an interaction effect between the conditioning effect and the number of conditioning stimuli.

7.3 Results

We carried out the experiments as described in the methods and illustrated in Figure 7.1. Ten subjects participated in the study, and seven completed the experiment protocol. We excluded one of these subjects (subject # 5) from further analyses due to overlap between stimulation artifact and the neural signal, and an inability to calculate a meaningful peak-to-peak voltage. Table 7.1 illustrates the various currents used for each of the subjects (See

Subject	Current (mA)	Voltage (V) (approx)	Phases set to be delivered	Age	Gender	Grid side and location
1	2	5.2	180°	35	F	Left temporal
2	3	5	0, 180°	19	M	Right frontal over central sulcus
3	3	4.2	180°	47	F	Right frontal
4	0.75	3.4	270°	37	F	Left frontal/temporal
5	0.75	2.4	90, 270°	38	F	Left temporal
6	1.75	3.5	90, 270°random	33	M	Lateral temporoparietal
7	1.75	4.9	90, 270°,null,playback	43	M	Left frontal/temporal

Table 7.1: Beta stimulation subject demographics. Demographics table showing the currents used for stimulation, phases tested, age, gender, grid location, and approximate location of epilepsy focus. Voltage applied was measured as a recorded representative voltage from the circuit monitoring the TDT stimulation in real-time.

supplemental information table E.1, supplementary Figure E.3 for the subjects not included in the analysis).

The stimulation currents ranged from 0.75 to 3.5 mA with voltages ranging from 2.4 volts to 5.2 volts, with some intra-subject variability due to constant-current stimulation settings. Individual subjects including demographics are shown in table 7.1. Of note, these currents were empirically selected for each subject during the CEP mapping and thresholding phases. The number of conditioning stimuli and test stimuli for each subject and test condition are highlighted in table 7.2. Grid locations are shown visually overlaid on the cortical reconstructions of the subjects (Figure 7.3).

7.3.1 Description of CEPs Observed

Figure 7.2 demonstrates characteristic CEPs from the study. We observed CEPs in locations primarily near the recording site, and restricted our analyses to the beta-recording channel and neighboring electrodes that demonstrated discernible CEPs (see Figure 7.4 for a depiction of the average CEPs across the brain for subject #7). We acknowledge the potential for the contributions of volume conducted potentials (VCPs) [81, 132, 256], and

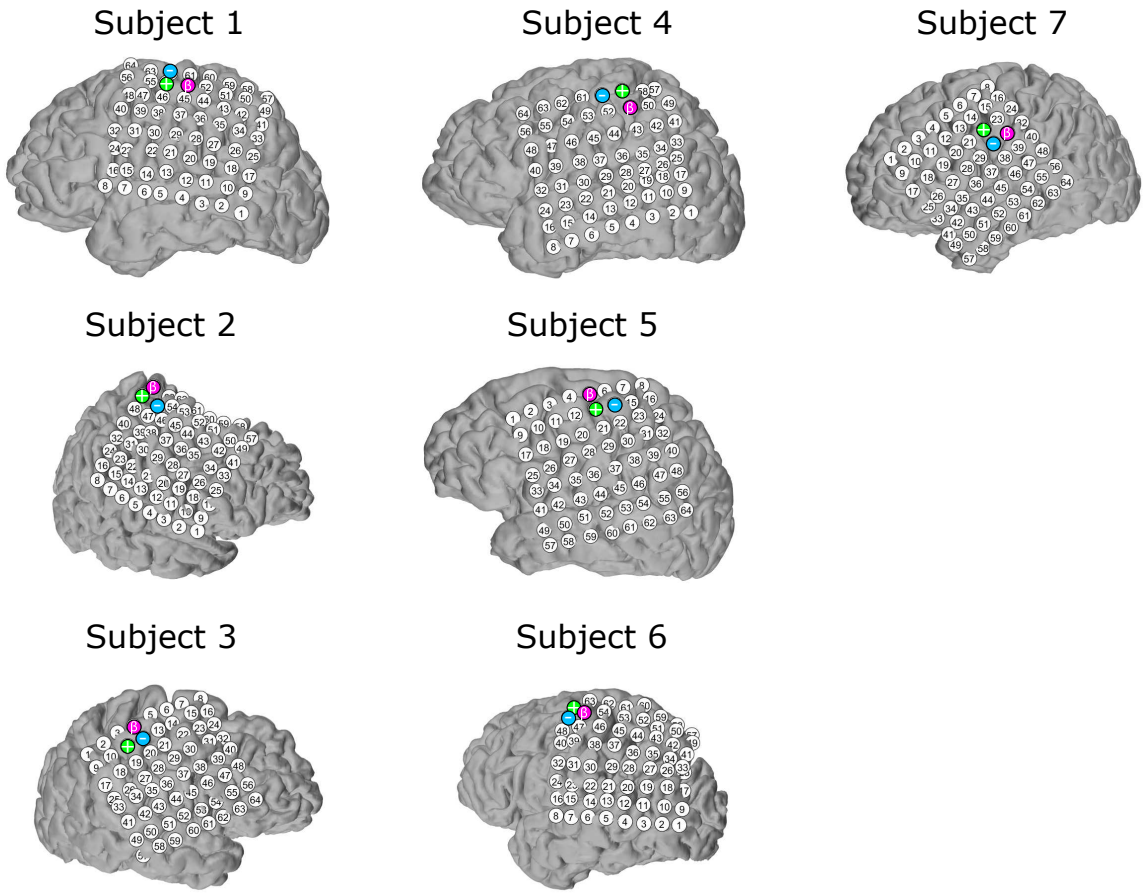

Figure 7.3: Subject cortical reconstructions. Cortical reconstructions of the seven subjects included in analysis (see appendix for subjects not analyzed further). The trigger channel is highlighted (β), and was the one selected for monitoring and triggering. The cathodic first (-) and anodic first (+) channels are also highlighted for each subject, and indicate the channels used both for conditioning and test pulses.

Subject	conditioning stimuli by targeted phase	# pulses after 1-2 stims	# pulses after 3-4 stims	# pulses after 5 or more stims	# baseline pulses
1	180° : 1451	882	176	58	78
2	0° : 1618	701	190	212	120
	180° : 2813	840	206	58	
3	180° : 6759	1341	593	695	98
4	270° : 4702	753	366	450	396
5	90° : 1618	414	86	414	25
	270° : 1278	171	65	90	
6	90° : 2473	119	79	201	45
	270° : 3247	84	154	168	
	Random: 2648	112	73	176	
5	90° : 916	167	108	55	49
	270° : 794	183	127	47	

Table 7.2: Number of Conditioning and Test Stimuli for Each Subject. The number of conditioning stimuli, along with the number of baseline and test pulses for each of the binned conditions (1-2, 3-4, 5 or greater conditioning stimuli) for all subjects which were supposed to correspond with the targeted phase. The set of baseline pulses for each subject served as the reference baseline for all conditions.

have included supplementary figures (Supplementary Figure E.4–E.9)) illustrating the individual average baseline waveform for all subjects at all channels across the grid to highlight temporal waveform differences between different channels, suggesting that we are analyzing additional waveform components beyond a solitary source beneath the stimulation channels. Additionally, we emphasize here that we analyze changes in CEPs as our output metric of interest, which are independent of volume conduction effects. Following our stimulation pulse, we observed characteristic and robustly reproducible CEPs (Figure 7.2), often with well defined peaks in the 4-60 ms range. We did not observe distant CEPs in our analysis. We believe this to be due to a combination of the low currents that we used for stimulation, as well as the fact that we often delivered stimuli within 50-80 ms of one another, potentially obscuring any delayed responses on the order of hundreds of milliseconds.

7.3.2 Dose Dependence

The major factor we observe is a dose dependence of the number of conditioning stimuli delivered during a beta burst (Figure 7.5). We binned all subjects together, and all test stimuli independent of the phase of conditioning stimulation during the beta burst, and included all channels where we saw EPs. As the number of conditioning stimuli delivered during a beta burst An ANOVA on the linear mixed model reveals a statistically significant effect of the number of conditioning stimuli (Table).

As the number of conditioning stimuli delivered during a beta burst increased, the absolute difference from the baseline CEPs increased. An ANOVA on the linear mixed model reveals a statistically significant effect of the number of conditioning stimuli (p=8.808e-6, Supplementary Table 7.3(a)). The individual estimates in CEP magnitude from baseline and p-values from the linear mixed model were 8.68 μV for [1,2] stimuli (p=0.176), an additional 4.32 μV for [3,4] stimuli (p = 0.01), and 10.25 μV for 5 or greater stimuli (p $<$ 0.001). Whether or not the channel was a trigger channel did not have a statistically significant

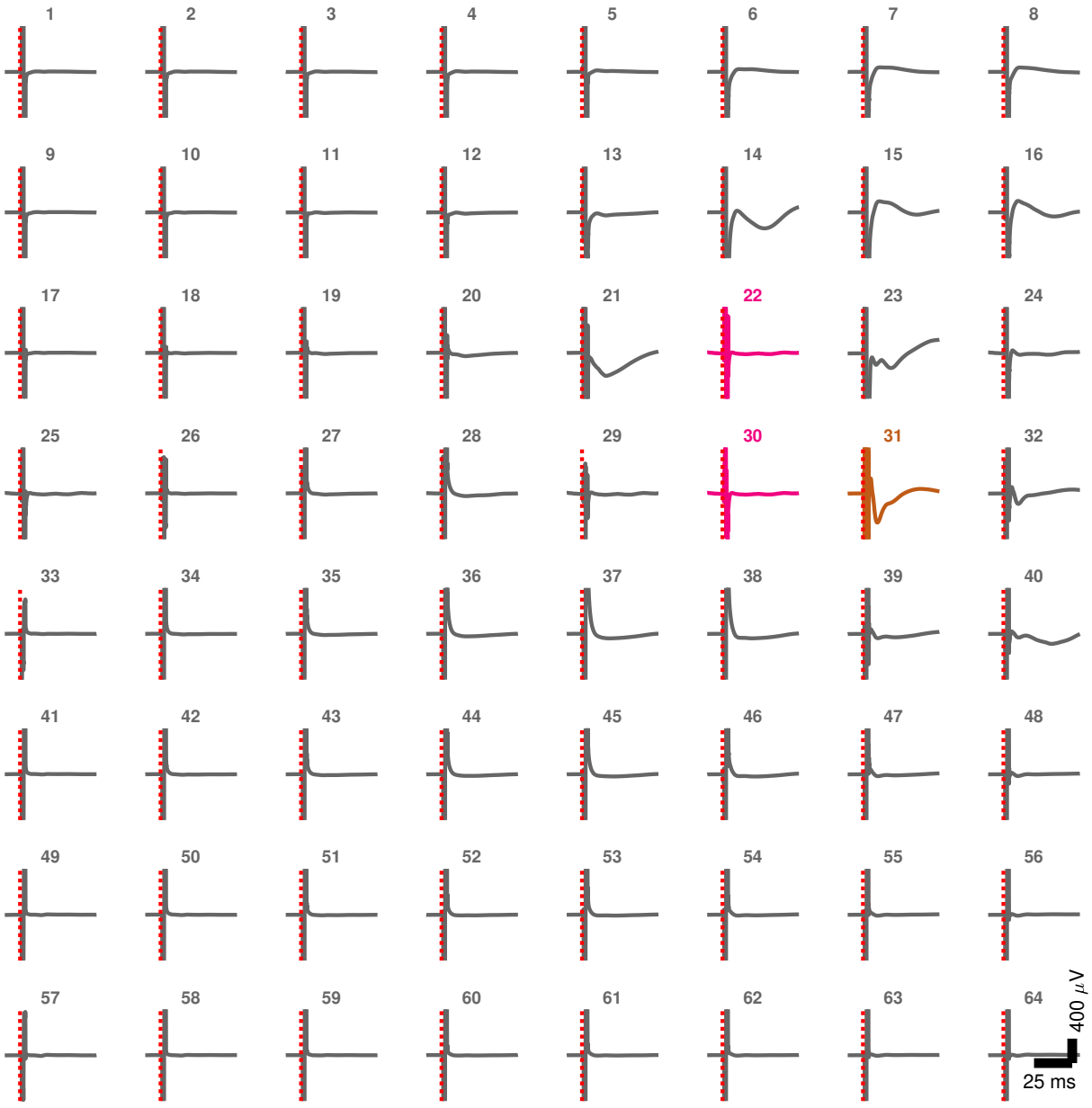

Figure 7.4: Map of CEPs across cortex for subject 7. Pink channels indicate the stimulation channels, while gold indicates the trigger channel. Note the complex and variable morphologies across the cortex, with primarily local responses. The scale bar in the lower right applies to all subplots within the image. We are unable to simultaneously record and stimulate from the stimulation channels, so any signal visualized there should be disregarded.

impact on the results (ANOVA, p = 0.172)

After examining the influence of the number of conditioning stimuli on the observed CEP magnitude, we then considered the effect of phase of stimulation on the degree of CEP change.

7.3.3 Accuracy of Phase Delivery

As described in the methods, the calculation of the phase of delivery was a critical issue for subsequent data analyses. For all of the non-stimulation channels, we performed the estimation of frequency and phase as described in the methods section, for all of our channels. We highlight individual trigger channels from the closed loop protocol for the first subject (Figure 7.6), the seventh subject (Figure 7.7, Figure 7.8), as well as the open-loop playback control for the seventh subject (Figure 7.9, Figure 7.10). The individual and average fitlines, distribution of phases at the time of stimulus delivery, frequency of the curve fits, and R^2 values are shown. For the phase distributions, we calculate the circular mean, standard deviation, and vector length [24] to ascertain the reliability of stimulus delivery for all channels across all subjects. We consider the mean vector length to be a marker of phase-stimulation consistency.

We additionally fit sinusoids to waveforms that had the time of the stimulus artifact and early response interpolated out and were subsequently filtered an acausal 4th order butterworth between 12-20 Hz. For the subjects shown below, the results corresponded well, but the difficulty determining the data interpolation length and the effects of remaining early CEPs or artifacts on the filtered data convinced us to proceed with fitting the raw data for more accurate estimations of phase. (Data not shown).

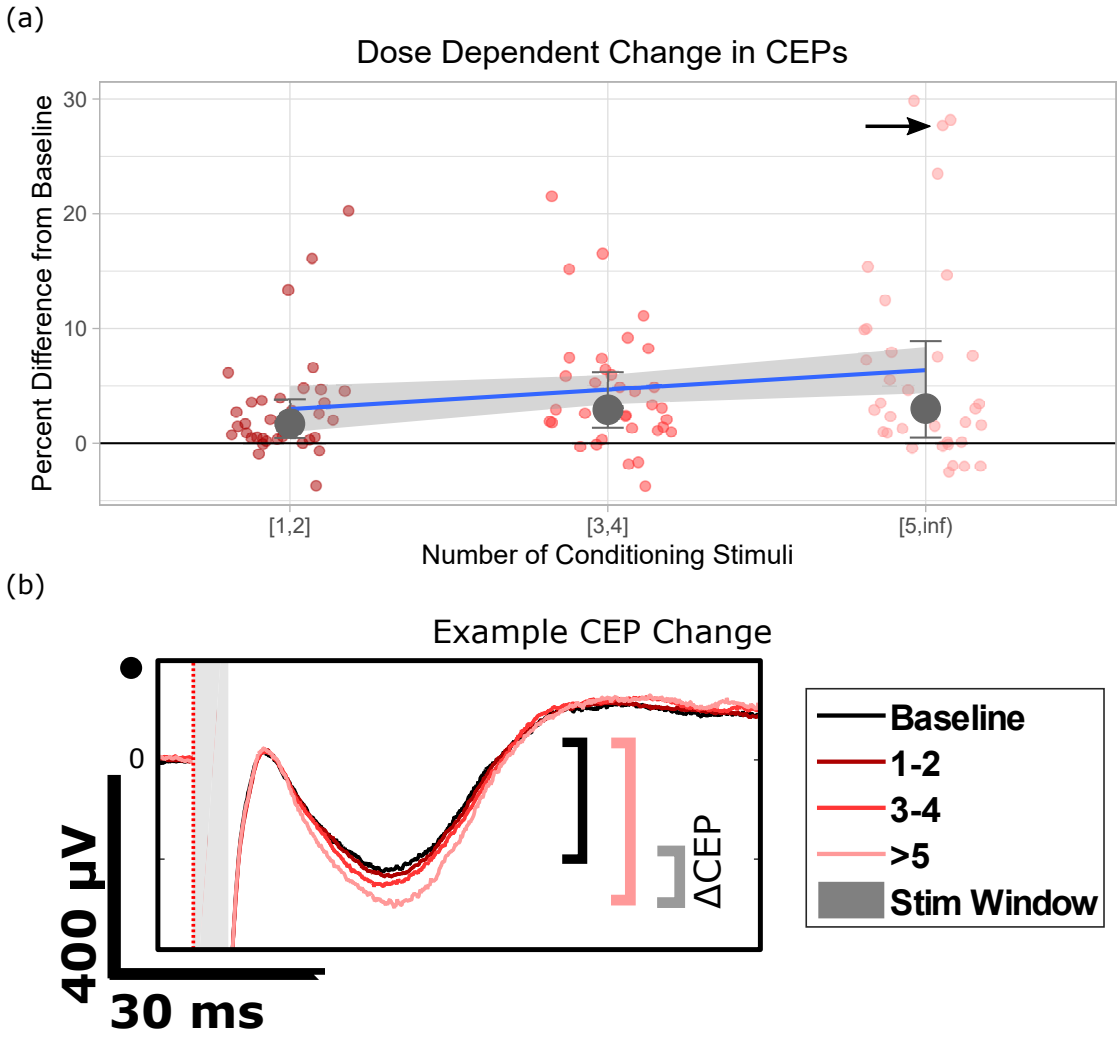

Figure 7.5: Dose dependent change in CEP magnitude. (a) The dominant effect that we observe is a dose dependent change in CEP magnitude, with an increasing percent change from baseline as the number of conditioning stimuli increased. We here plot all subjects, with all test stimuli binned together regardless of the phase of stimulation, for all channels that demonstrated CEPs. Each individual data point represents the average percent difference from baseline for a single channel from a subject. The median value for each binned number of conditioning stimuli, as well as the 25% and 75% quartiles are also plotted. The best fit linear line and 95% confidence intervals are also plotted. (b) Shown here are the mean CEPs in channel 14 from subject 7, illustrated by the black arrow in panel (a), where as the number of conditioning stimuli in a beta-oscillation cycle increase, the resultant test CEP magnitude immediately after increases as well relative to baseline.

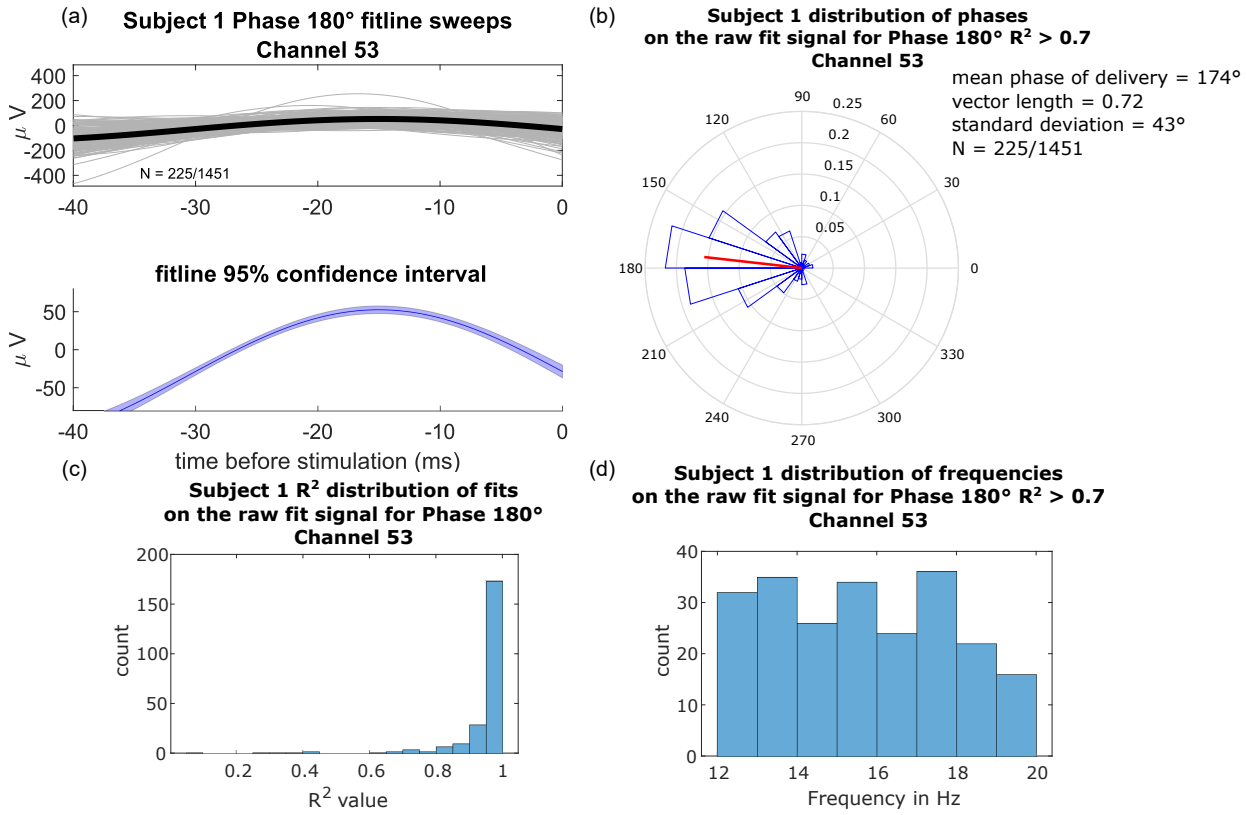

Figure 7.6: Fitlines, phase, goodness of fit, and frequency distributions for the phase estimations for the trigger channel for subject 1 for 180° target phase. (a) Individual and average (225) fitlines for all conditioning trials for the target 180° condition from 40 ms before to the time of stimulation that had an R^2 greater than 0.7, and were between 12.01 and 19.99 Hz. (b) Distribution of phases at the time of stimulus delivery for the fitlines in panel (a). The vector represents the circular mean direction of the distribution, and is our estimate of the average phase of delivery. (c) Distribution of the R^2 values for all of the conditioning stimuli. (d) Distribution of the frequencies of the sine waves from the fitlines of panel (a)

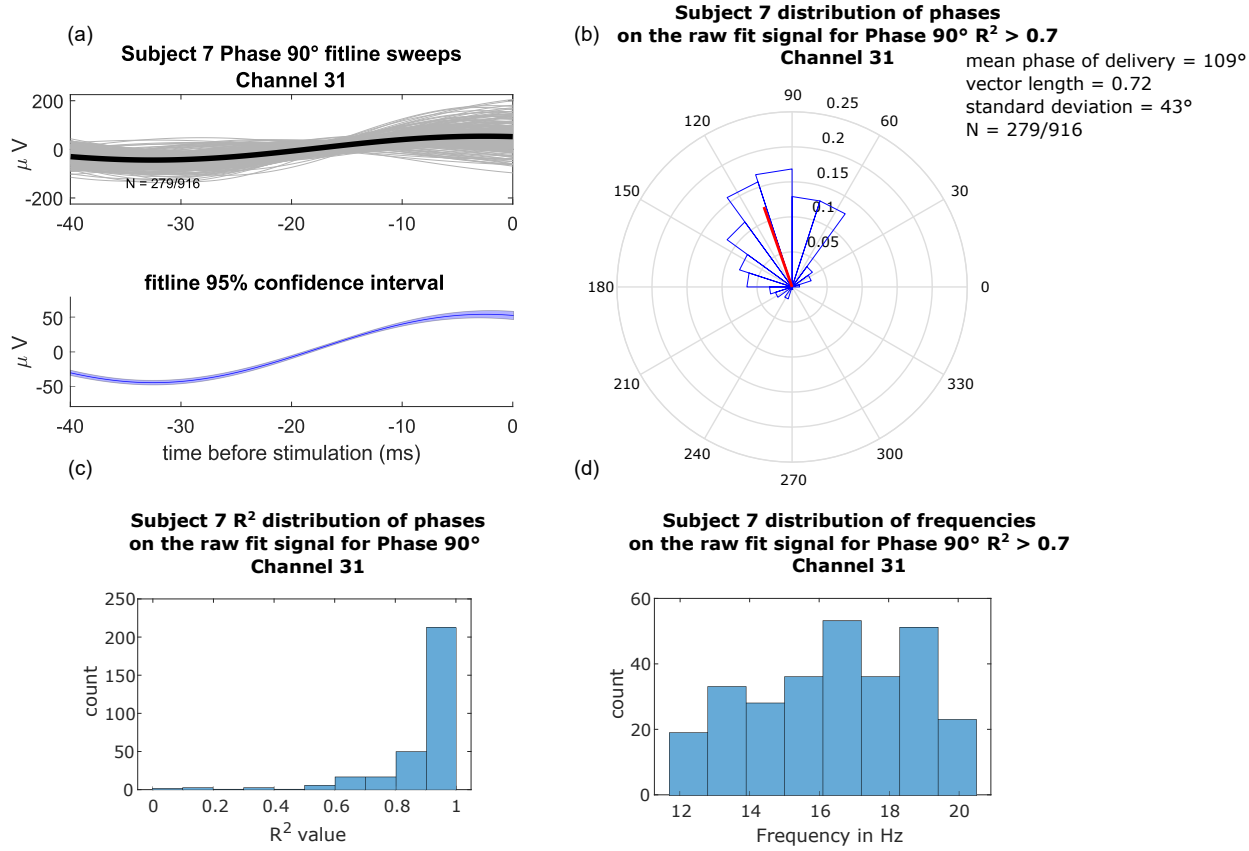

Figure 7.7: Fitlines, phase, goodness of fit, and frequency distributions for the phase estimations for the trigger channel for subject 7 for 90° target phase. (a) Individual and average (279) fitlines for all conditioning trials for the target 90° condition from 40 ms before to the time of stimulation that had an R^2 greater than 0.7, and were between 12.01 and 19.99 Hz. (b) Distribution of phases at the time of stimulus delivery for the fitlines in panel (a). The vector represents the circular mean direction of the distribution, and is our estimate of the average phase of delivery. (c) Distribution of the R^2 values for all of the conditioning stimuli. (d) Distribution of the frequencies of the sine waves from the fitlines of panel (a)

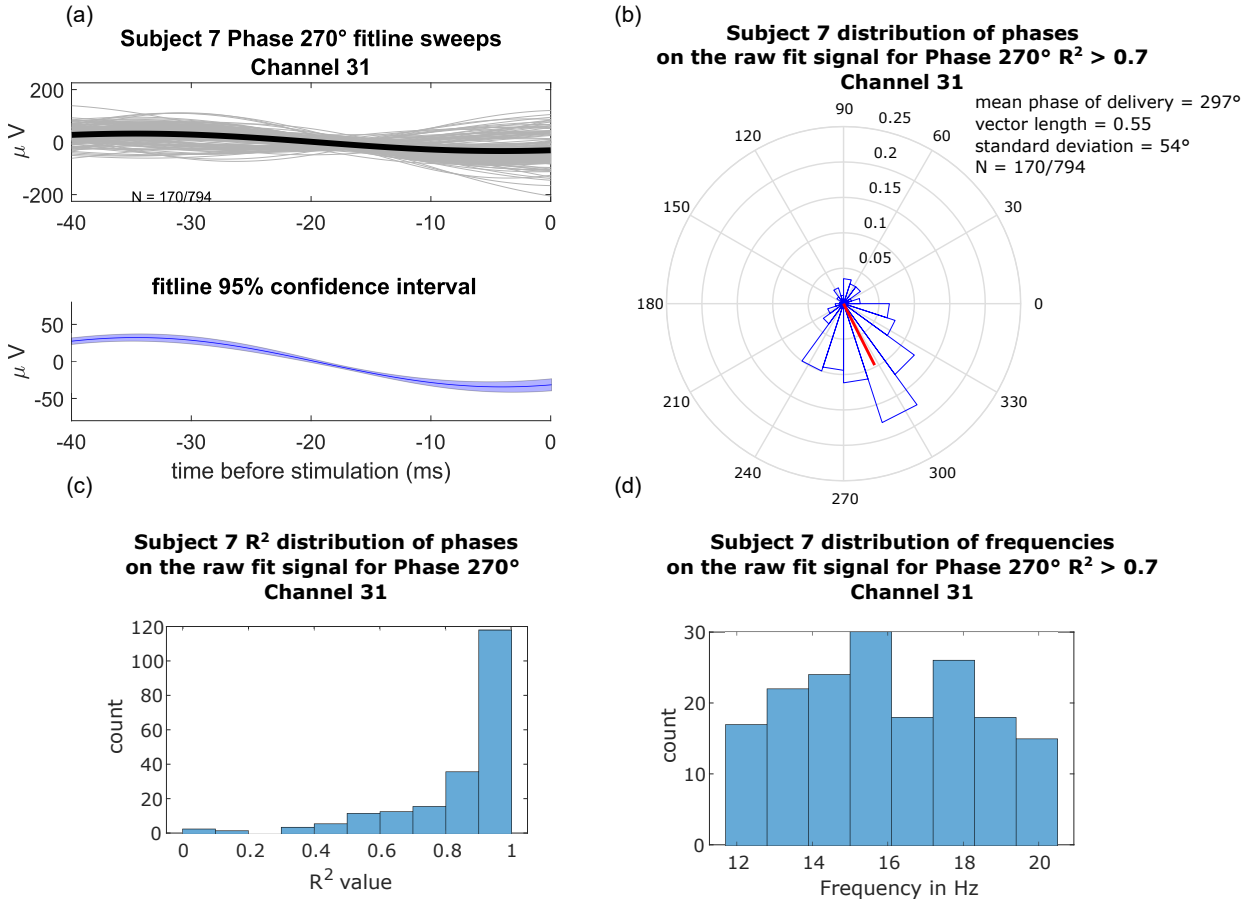

Figure 7.8: Fitlines, phase, goodness of fit, and frequency distributions for the phase estimations for the trigger channel for subject 7 for 270° target phase. (a) Individual and average (170) fitlines for all conditioning trials for the target 270° condition from 40 ms before to the time of stimulation that had an R^2 greater than 0.7, and were between 12.01 and 19.99 Hz. (b) Distribution of phases at the time of stimulus delivery for the fitlines in a). The vector represents the circular mean direction of the distribution, and is our estimate of the average phase of delivery. (c) Distribution of the R^2 values for all of the conditioning stimuli. (d) Distribution of the frequencies of the sine waves from the fitlines of panel (a)

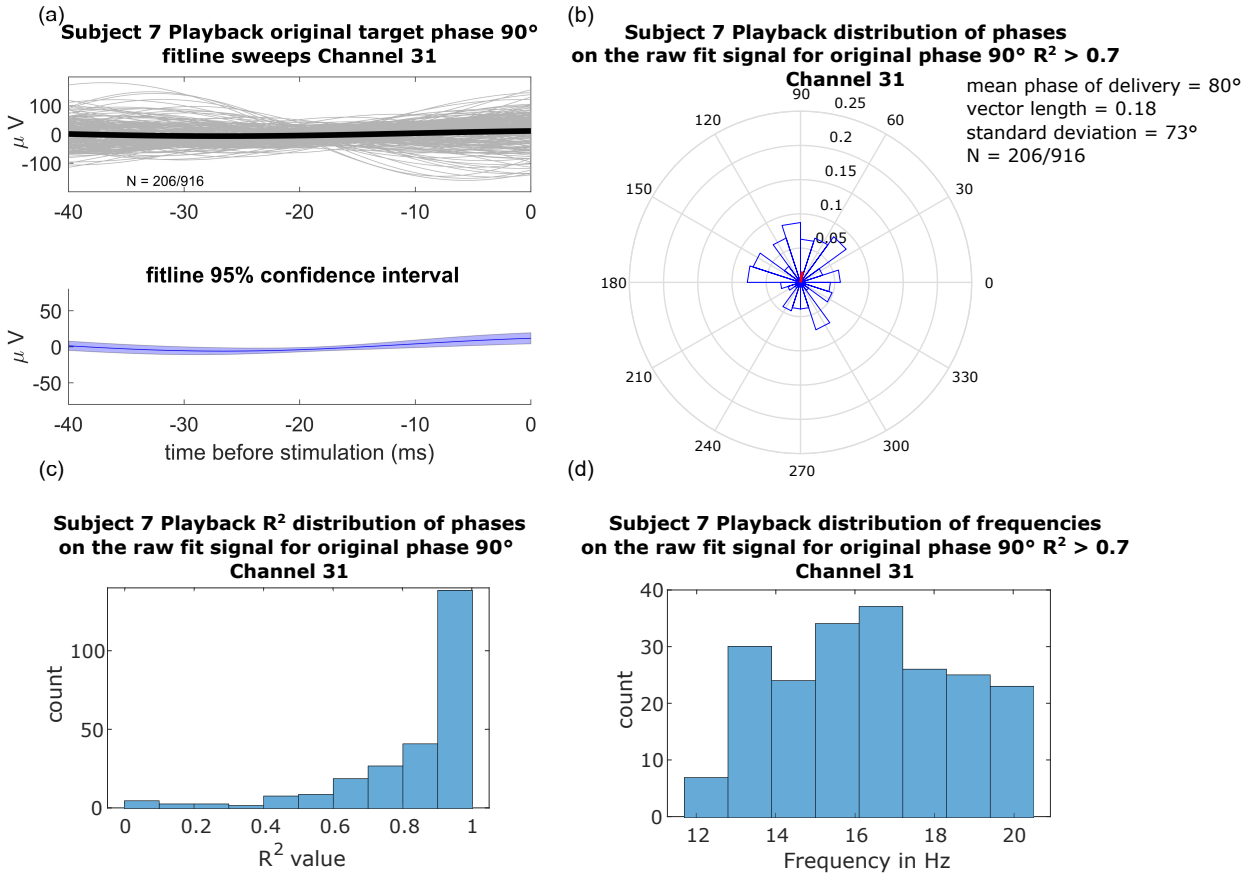

Figure 7.9: Fitlines, phase, goodness of fit, and frequency distributions for the phase estimations for the trigger channel for subject 7 for the playback control condition, for phases at 90° in closed-loop condition. (a) Individual and average (225) fitlines for all conditioning trials for the target 180° condition from 40 ms before to the time of stimulation that had an R^2 greater than 0.7, and were between 12.01 and 19.99 Hz. (b) Distribution of phases at the time of stimulus delivery for the fitlines in panel (a). The vector represents the circular mean direction of the distribution, and is our estimate of the average phase of delivery. (c) Distribution of the R^2 values for all of the conditioning stimuli. (d) Distribution of the frequencies of the sine waves from the fitlines of panel (a)

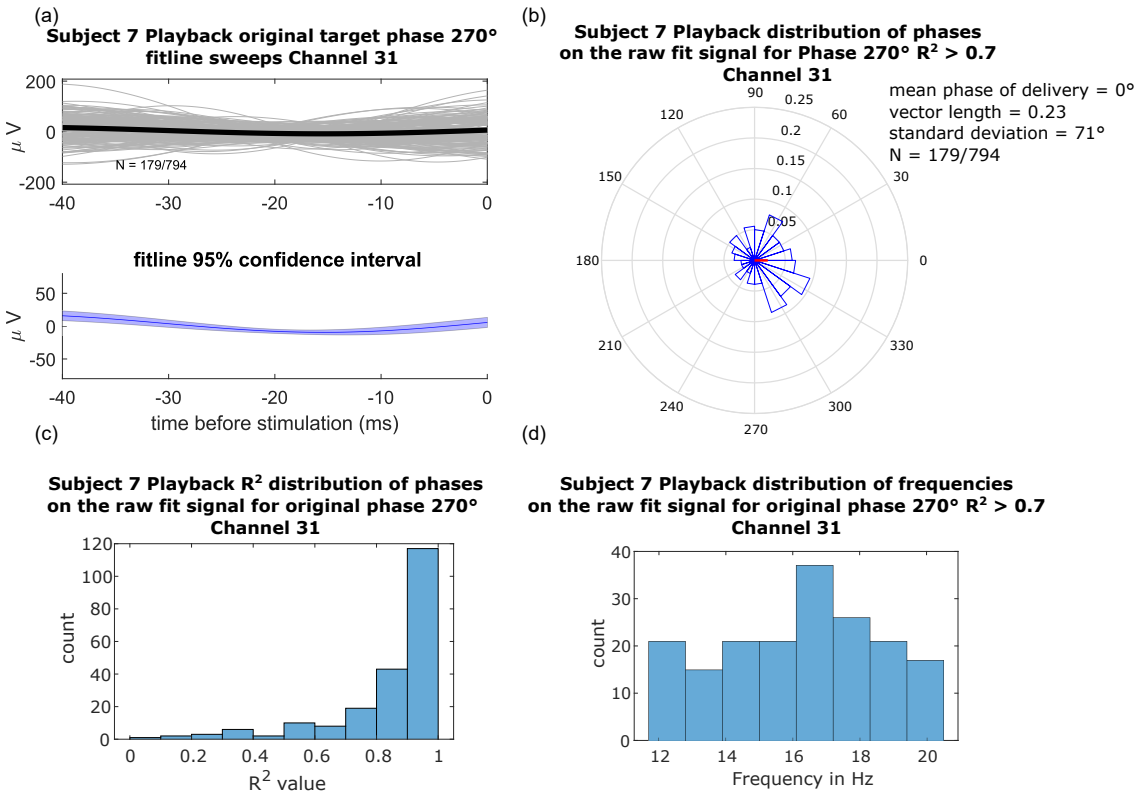

Figure 7.10: Fitlines, phase, goodness of fit, and frequency distributions for the phase estimations for the trigger channel for subject 7 for the playback control condition, for phases at 270° in closed-loop condition. (a) Individual and average (225) fitlines for all conditioning trials for the target 180° condition from 40 ms before to the time of stimulation that had an R^2 greater than 0.7, and were between 12.01 and 19.99 Hz. B) Distribution of phases at the time of stimulus delivery for the fitlines in panel (a). The vector represents the circular mean direction of the distribution, and is our estimate of the average phase of delivery. (c) Distribution of the R^2 values for all of the conditioning stimuli. (d) Distribution of the frequencies of the sine waves from the fitlines of panel (a).

7.3.4 Phases Across Cortex

For each channel in the electrode array that has reliable neural recordings, we use the length of the circular mean vector as described in the methods as a metric for goodness of fit. A small value indicates a more random distribution of phases. Figure 7.11 illustrates for the first subject the distribution of phases across cortex (indicated by color), while the size of the circle indicates the consistency of phase delivery. Of note is that the trigger channel demonstrates the greatest consistency of phase delivery, and is within 6° of the target frequency on average.

To further look at the accuracy of phase delivery within a beta burst in our real-time system, we analyzed random subsets of beta bursts and visualized the consistency of phase delivery (Figure E.10). To visualize post-hoc the real time performance of our beta filtering, blanking, and peak detection, we visualized a random subsection of our output (Figure E.11). In general, the real time filter was able to stimulate near the desired phase.

7.3.5 Beta Burst Lengths

To characterize the number of stimuli delivered during each calculated beta burst, we constructed histograms for each subject and each stimulation type (Figure E.12). This was also critical to ascertain the amount of retriggering off of prior stimuli during the conditioning phases. Most stimuli trains fell under 10 stimuli per beta burst. Physiologic studies in primates have shown beta oscillations during normal behavior to be less than 10 cycles [314], indicating that the majority of our beta oscillations and stimuli were physiologically based, rather than due to retriggering.

7.3.6 Aggregate Analysis: Dose Dependence and Binned Phase

We next looked at the spatial selectivity and phase selectivity. After calculating the phase of each channel, we binned channels with conditioning phases between 0-180 into one bin, and between 180-360 degrees into another. With this as a categorical variable, we performed

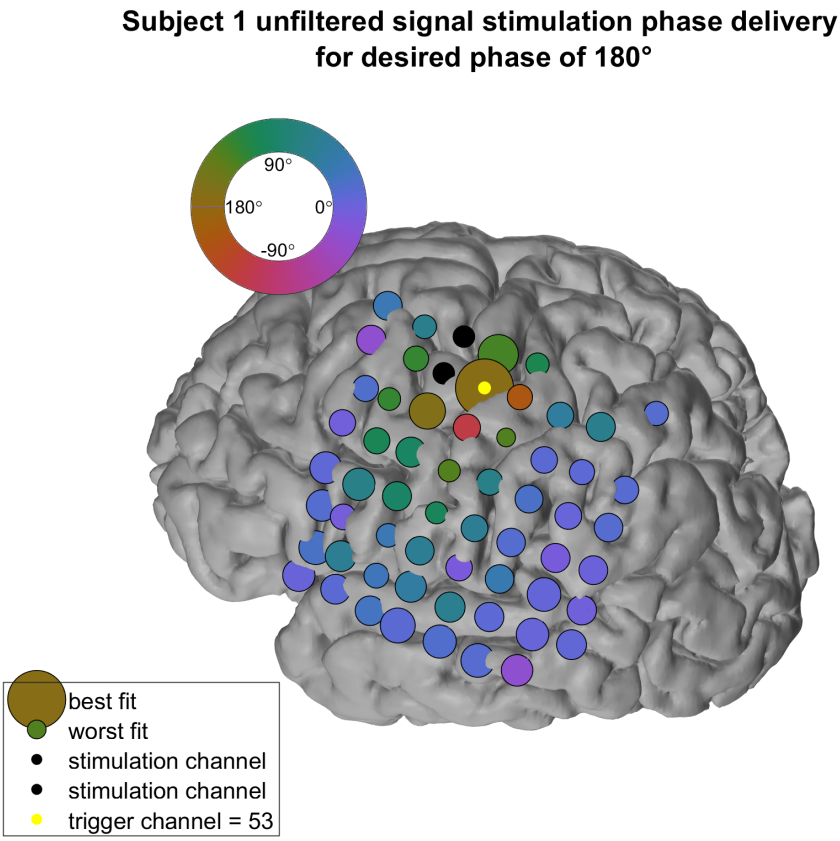

Figure 7.11: Phase of delivery across the cortex for subject 1. The size of each circle represents the circular mean vector length of the phase distribution, while colors indicate the circular mean phase of delivery. The triggering channel indicates the channel from which the filtered beta oscillations were used to trigger conditioning stimuli (black electrodes). Of note is that the trigger channel had the most consistent phase of delivery, which was at 174°, relative to the desired phase of 180°. Adjacent channels may have a phase similar to the triggering channel, which undergoes a shift in phase and less consistent delivery at electrodes further from the triggering electrode.

a linear mixed model analysis to ascertain the effect of the number of conditioning stimuli, the current delivered, the binned phase of stimulation as well as the subject ID. When we look across subjects (Figure 7.12), we saw variability both in the size of the baseline and conditioned CEPs, as well as the degree of dose dependence. Individual trends for subjects can be seen in figure 7.13, where some subjects display clear increases in CEPs (subjects 2,7), while others show little change across electrodes (subjects 1, 6).

Testing our hypothesis of the stimulating in a putatively more excitable neuronal state (depolarizing phase of beta-oscillations), we observe a trend towards increased CEP modulation on the depolarizing stimulus, and a statistically significant phase dependence at the greatest number of conditioning pulses (Table 7.3)). An ANOVA on the linear mixed model reveals no significant phase effect on its own (p=0.076), but there does exist a statistically significant interaction effect between phase and the number of conditioning stimuli (p = 0.043). There is no interaction effect between the number of stimuli and whether or not a channel was a trigger channel (p=0.53, (Table 7.3)). Post-hoc testing with estimated marginal means and tukey-correction revealed a significant interaction effect for the number of conditioning stimuli and phase of delivery for the 5 or greater conditioning stimuli delivered (estimate = 7.033 μV, p = 0.0062)

The increase in EP magnitude from baseline is evident in Figure 7.14, as well as the interaction effect between whether or not the stimuli were delivered on average in the hyperpolarizing or depolarizing phase of stimulation. The major effect is the dose dependence.

7.3.7 Randomized Stimulation, Beta-oscillatory Activity Alone, and Playback Controls

We tested the effect of a beta burst on the pre- and post-CEP amplitudes in the absence of any stimulation during the burst, as well as a control playback condition as described in the methods (stimulation pattern previously recorded, delivered asynchronously with beta activity). The null test pulses in most channels following a beta burst had a CEP magnitude

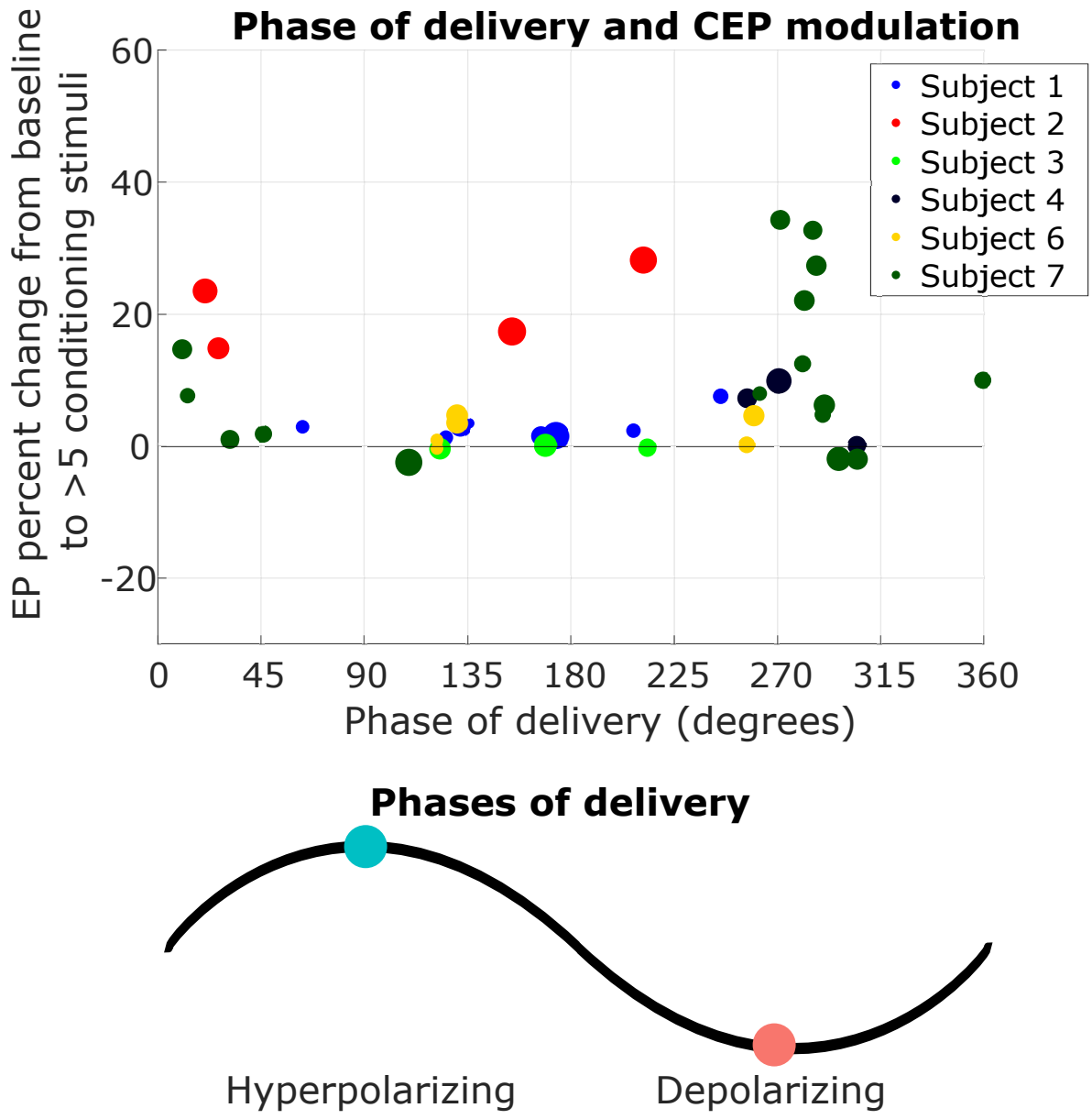

Figure 7.12: Compiled subject effect of percent change in CEP magnitudes across subjects at all channels with CEPs as a function of mean phase angle of conditioning at that electrode. The condition of 5 or greater stimuli in a conditioning train is compared to the baseline. The size of the circle indicates the mean circular vector length for the delivered phase. Larger circles indicate a more consistent phase of delivery.

Predictor	Sum Square Error	Mean Square Error	Numerator DF	Denominator DF	F Value	Pr(>F)
# conditioning stimuli (NCS)	143522	71761	2	31788	11.644	8.808e-6
Phase of stim (PS)	19440	19440	1	2761	3.154	0.076
Trigger channel (TC)	12355	12355	1	19	2.005	0.173
$NCS : TC$ inter.	7812	3906	2	31202	0.634	0.531
$NCS : PS$ inter.	38824	19412	2	31238	3.145	0.0429

Scaled Residuals				
Min	First Quartile	Median	Third Quartile	Max
-7.1911	-0.538	-0.0281	0.5112	14.2860

Predictor	Estimates	Confidence Interval	p-value
Intercept	8.68	-2.13 – 19.50	0.176
$[3, 4]$ conditioning stimuli	4.32	1.05 – 7.58	0.010
$[5, inf)$ conditioning stimuli	10.25	6.68 – 13.83	<0.001
90° phase class	-0.77	-4.70 – 3.15	0.700
Non-trigger channel	7.34	-2.32 – 17.00	0.152
$[3, 4]$:trigger channel interaction	1.05	-3.96 – 6.06	0.681
$[5, inf)$:trigger channel	-2.40	-7.82 – 3.01	0.385
$[3, 4] : 90°$ phase	-1.02	-5.38 – 3.34	0.646
$[5, inf) : 90°$ phase	-6.26	-11.17 – -1.35	0.012

σ^2	6162.86
τ_{00} channel:subject	92.50
τ_{00} subject	133.96
ICC channel:subject	0.01
ICC subject	0.02
Observations	31889
$Marginal R^2$ / $Conditional\ R^2$	0.003/0.039

Table 7.3: Output from linear mixed model. ANOVA on the linear mixed model. Distribution of residuals following fitting. Post-hoc comparisons of factors and interaction effects. Welch's method is used to obtain estimates of the p values for the given pairwise comparison of fixed effects following the original ANOVA. Analysis of random effects following fitting.

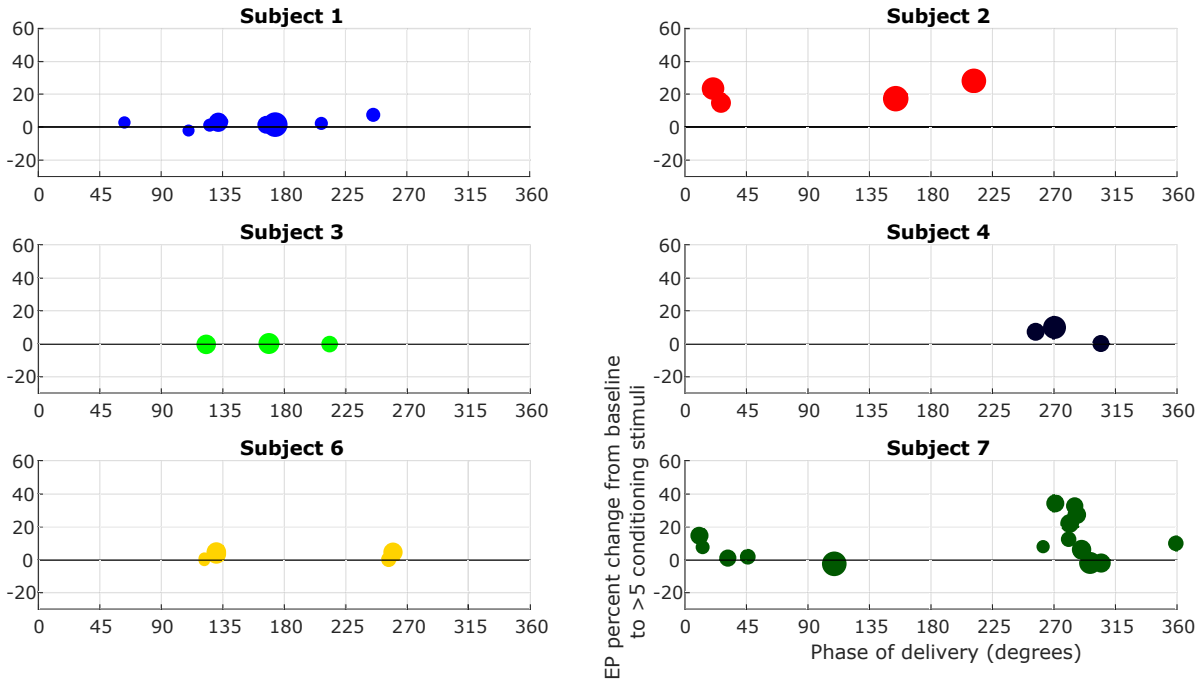

Figure 7.13: Individual plot of percent change in CEP magnitudes across subjects at all channels with CEPs as a function of mean phase angle of conditioning at that electrode. Plot of percent change in CEP magnitudes across subjects for all electrodes with CEPs that met our criteria mentioned in the methods. The condition of 5 or greater stimuli in a conditioning train is compared to the baseline. The size of the circle indicates the mean circular vector length for the delivered phase. Larger circles indicate a more consistent phase of delivery.

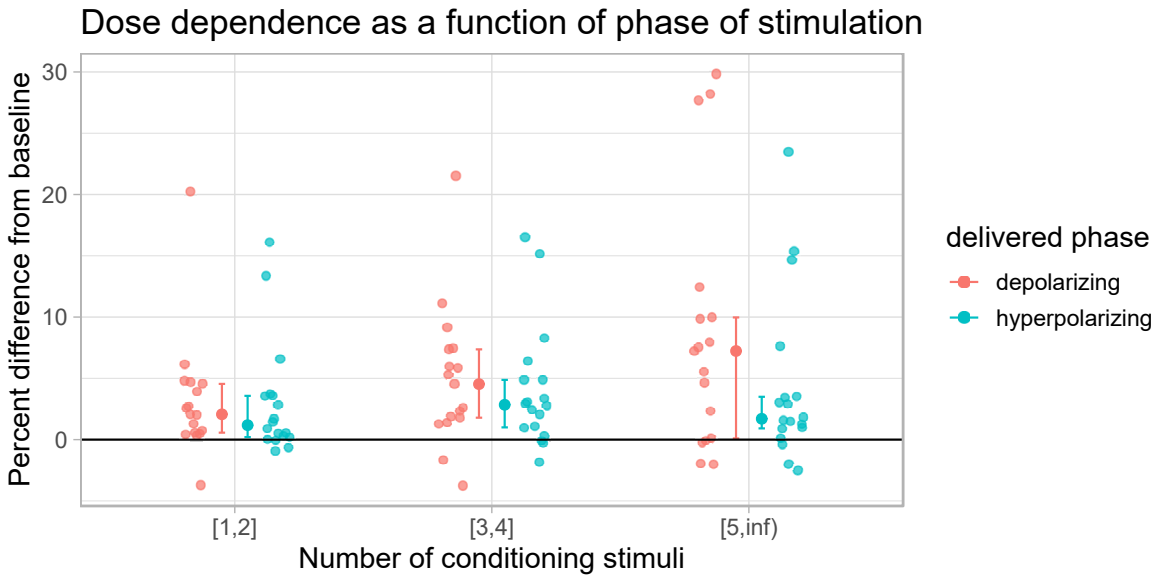

Figure 7.14: Dose dependent conditioning effect between phase groupings. For all subjects and channels with robust evoked potentials, the circular mean phase angle was used to bin the data into either hyperpolarizing (0-180°) or depolarizing (180-360°) groupings. The percent difference from baseline was then calculated for each stimulation condition. The trend towards increasing number of conditioning stimuli increasing the magnitude in EP is highly significant ($p<0.001$), while there is a significant effect at greater than 5 conditioning stimuli for the depolarizing phase (270°) relative to the hyperpolarizing phase (90°). Individual points represent a single channel, with subjects 1 through 4 and 6 through 7 represented. The median, 25%, and 75% quartiles are also visualized.

that was not significantly different than baseline (for an example channel from subject 7, see table 7.4).

We next sought to quantify the effect of activity dependent stimulation compared to our control, playback condition. As an example, in a channel adjacent to the beta-recording channel in Subject 7 (Figure 7.15), we saw significantly lower CEP magnitudes for the conditioning trains with 5 or more pulses (estimate = -106.34 μV, p-value < 0.001, estimated marginal means with tukey-correction, Table 7.4) across conditions for the playback control condition relative to the beta-triggered stimulation paradigm, with no difference in baseline levels (estimate = -23 μV, p-value = 0.345, Table 7.4). This increase in CEP magnitude during the beta-triggered case suggests a greater increase in short term plasticity. Of note, however, is that there does appear to be a weaker, although still present effect for short term plasticity induction via rhythmic delivery of stimuli.

In subject 6, we tested hyperpolarizing stimulation, depolarizing stimulation, and a randomized phase condition where the phase for any given stimulation train was randomly picked. In this subject, we did not observe any robust differences between groups (Figure 7.16). The lack of large scale effects in this subject (5% change in CEP magnitude) may explain the similarity between groups.

Specificity for the trigger channel. Although our linear mixed model did not reveal a clear role for the trigger channel always eliciting the greatest change, in a number of subjects (2,3,4, and 6), the greatest degree of change was seen in the trigger channel (Figure 7.17, supplemental figures)

7.4 Discussion

: In this study we investigated the effects of beta-triggered cortical stimulation on a physiological marker of neural connectivity, the CEP, and found a dose-dependent increase in the amplitude of the CEP, related to the number of stimuli delivered in a beta burst. This result

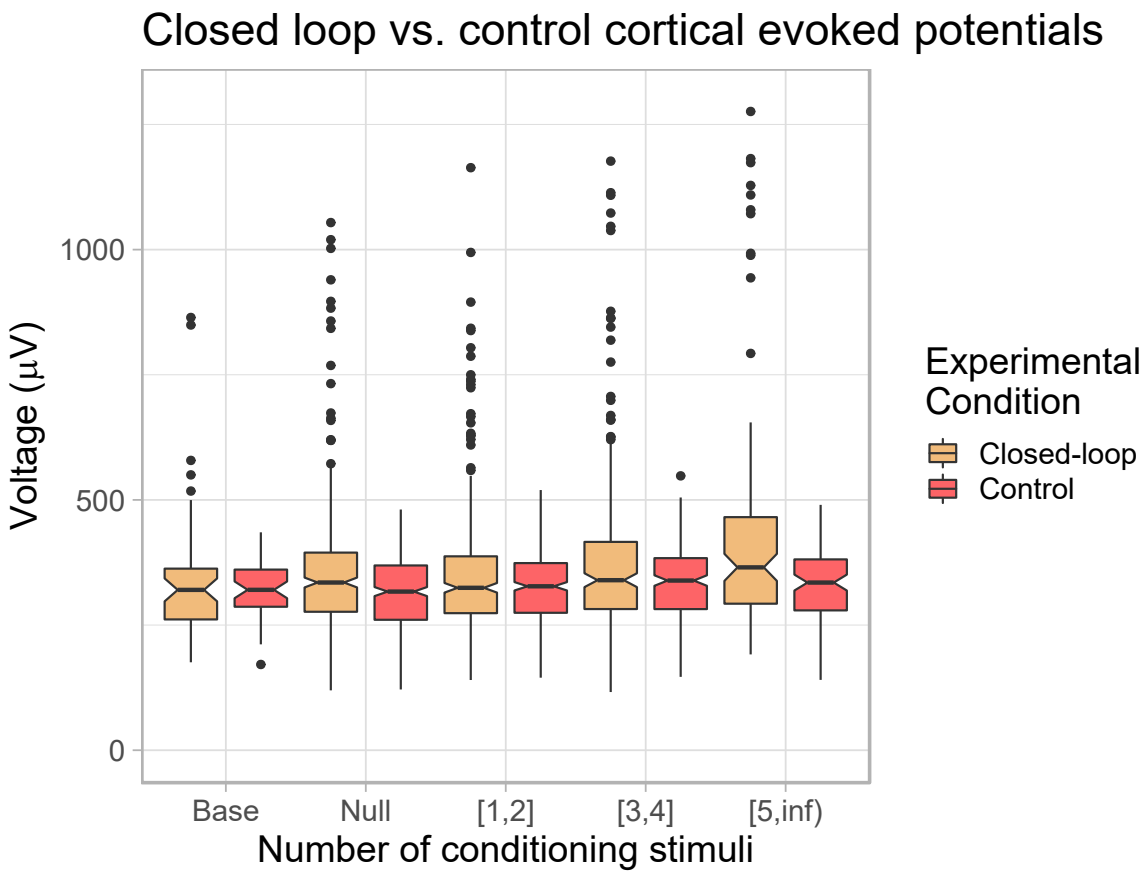

Figure 7.15: Beta-triggered playback vs. control condition for Subject 7, Channel 14. Additional figure illustrating the differences in the activity dependent and playback condition for an additional channel adjacent to the beta recording channel. None of the playback conditions differed significantly from one another (while all beta-triggered stimulation conditions other than the baseline and 1-2 conditioning pulse experiment were significantly different than the playback condition. Box plots indicate the median, 25% and 75% interquartile range (IQR), while notches illustrate (1.58 * IQR / sqrt (n)) for each condition.

Predictor	DF	Sum Square Error	Mean Square Error	F Value	Pr(>F)
# conditioning stimuli (NCS)	4	71761	154397	10.628	1.573e-8
Open vs. closed loop (OLCL)	1	19440	971275	66.858	4.892e-16
OLCL:NCS inter.	4	12355	70964	4.885	6.378e-4

Scaled Residuals				
Min	First Quartile	Median	Third Quartile	Max
-267.89	-69.14	-10.30	46.91	843.54

Predictor	Estimates	Confidence Interval	p-value
Intercept	345.69	311.92 – 379.46	<0.001
Null case	7.10	-28.90 – 43.09	0.699
$[1, 2]$ conditioning stimuli	2.54	-33.5 – 38.59	0.890
$[3, 4]$ conditioning stimuli	38.42	1.30 – 75.54	0.042
$[5, inf)$ conditioning stimuli	95.74	54.66 – 136.83	<0.001
Playback control	-23.00	-70.75 – 24.75	0.345
Null:playback interaction	-13.30	-64.20 – 37.60	0.608
$[1, 2]$:playback interaction	-2.59	-53.57 – 48.40	0.921
$[3, 4]$:playback interaction	-28.68	-81.17 – 23.8	0.284
$[5, inf)$:playback interaction	-83.32	-141.42 – - 25.22	0.005

Observations	2192
$Marginal R^2$ / $Conditional\ R^2$	0.056/0.054

Table 7.4: Linear model results for closed-loop vs open-loop stimulation in Subject 7. ANOVA on the linear model for the closed loop vs. open-loop stimulation. b) Residuals for linear fit model. Post hoc comparisons of interaction effects, with the number of stimuli, as well as the interaction between the number of conditioning stimuli and the closed loop playback being significant for the linear model used.

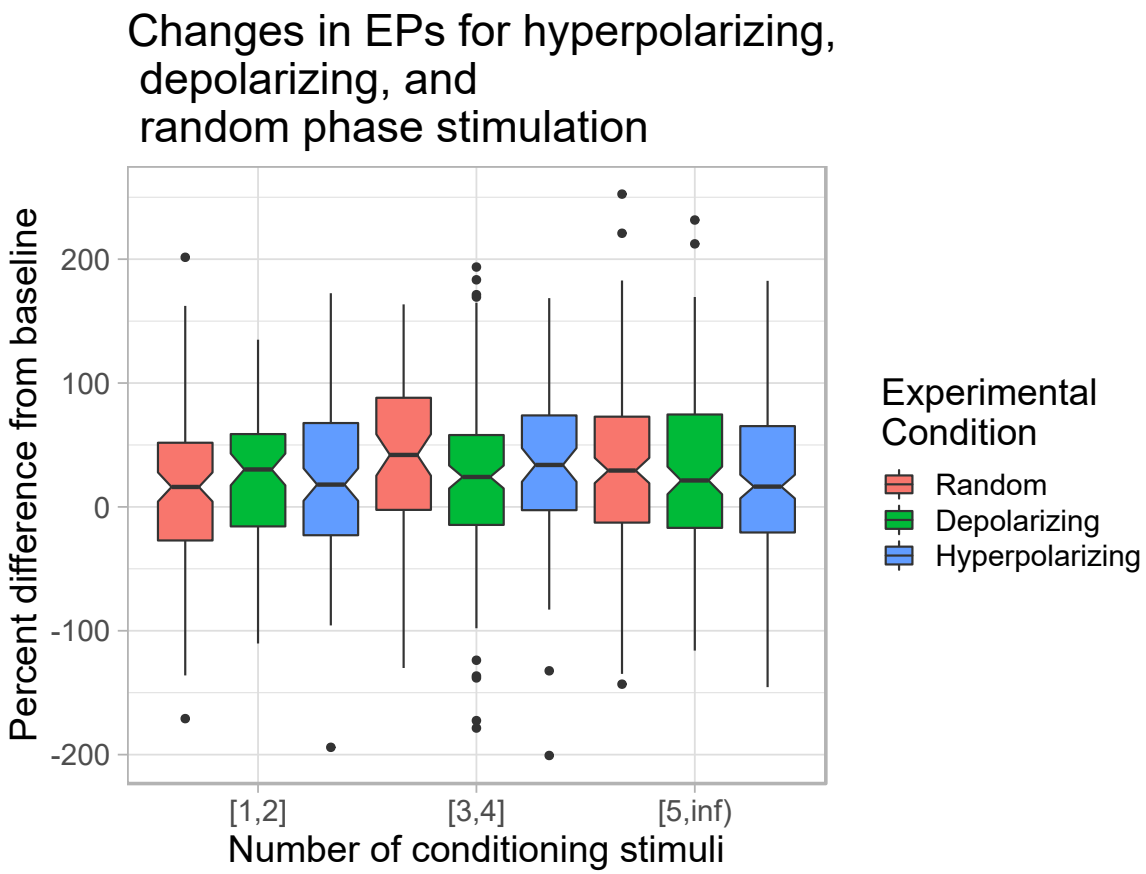

Figure 7.16: Dose dependent conditioning effect for subject 6. Test pulses belonging to each either a targeted hyperpolarizing, depolarizing, or random (but constant within a train) phase are compared for subject 6 as a function of the number of conditioning stimuli. For this subject, there did not seem to be a clear effect of phase. Box plots indicate the median, 25% and 75% interquartile range (IQR), while notches illustrate (1.58 * IQR / sqrt (n)) for each condition.

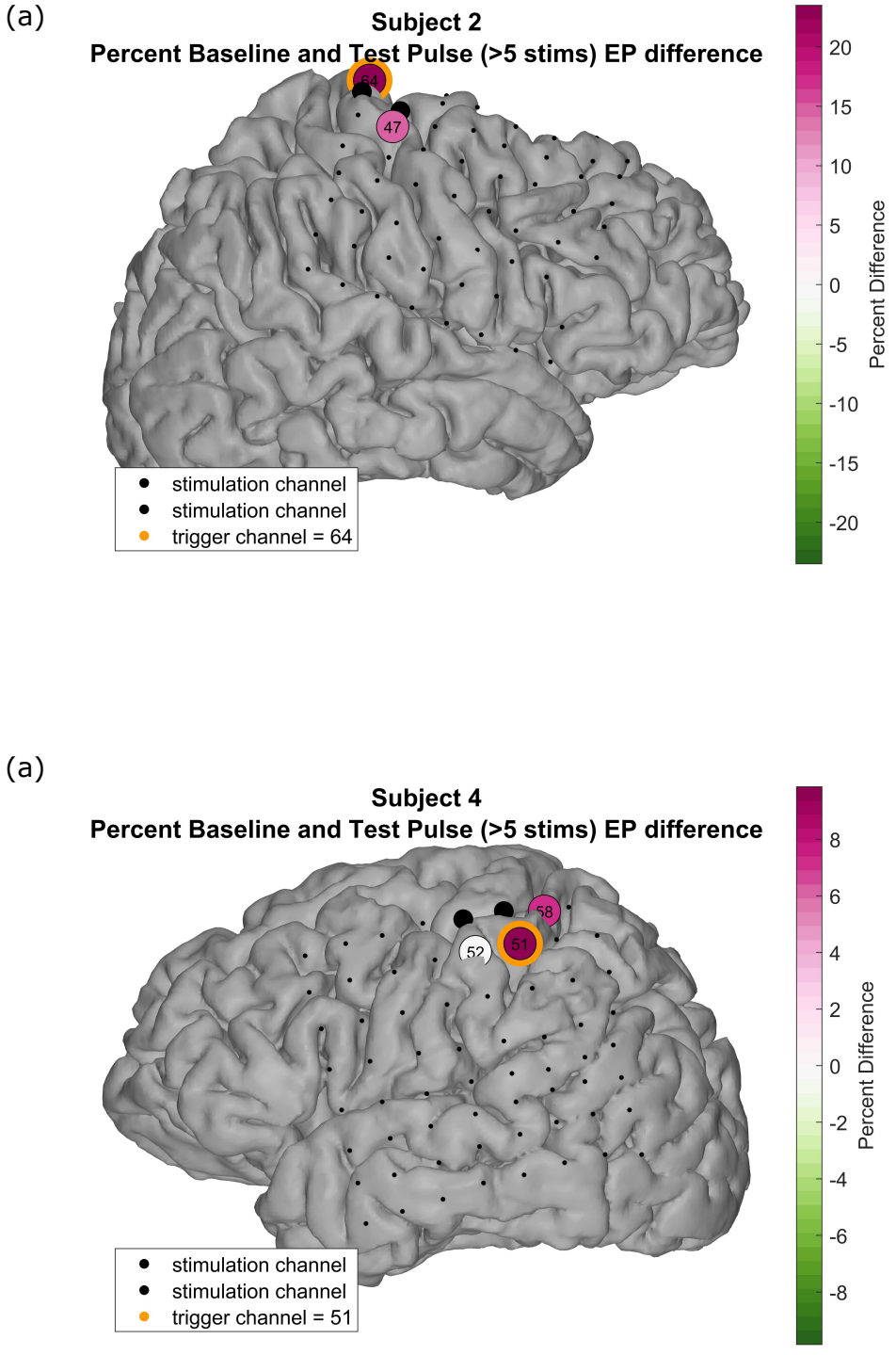

Figure 7.17: Percent change across cortex. Visualized are two subjects (2, 4) for whom the degree of change was greatest in the triggering channel.

was consistent across subjects, however the absolute magnitude of the CEPs varied between subjects. Overall, we found that the measured CEPs were polymorphic across subjects and across channels within subjects, which posed a challenge to standardized measurement. Despite this, we observed high within-subject and within-channel repeatability. The duration of effect was transient and lasted less than two seconds. In one patient, the degree of CEP modulation was decreased in the control playback conditions suggesting that the effect was dependent upon synchronization with endogenous neural activity. Beta-bursts alone did not result in enhanced CEP magnitude. These physiological findings in humans are consistent with prior animal studies that link cortical stimulation with motor activity and/or associated neural activity [27, 66, 85, 96, 125, 168]. Also, these findings are consistent with a possible mechanism to explain prior clinical studies that showed improved neurological outcomes when linking non-invasive stimulation with motor activity [142, 195].

We observed a trend towards increased CEP magnitudes in the depolarizing phase of stimulation, similar to prior primate work [314]. However, our results were less consistent than seen in the prior literature. Possible reasons for this will be discussed below. We additionally see a more network wide increase in CEP magnitude, rather than any particular dependence on whether or not a channel was a trigger channel.

Additionally, we observed CEPs that were similar in character to those described in prior human studies. We observed a clear early response representative of the A1/N1 previously described [133, 175, 176]. Due to our stimulation protocol, and stimulation amplitude level which resulted only in local CEPs, we did not robustly observe the A2/N2 response, which is often seen 100-300 ms post stimulation [133].

Overall, we found that the measured CEPs were polymorphic across subjects and across channels within subjects, which posed a challenge to standardized measurement. However we observed high within-subject and within-channel repeatability.

7.4.1 Subject Variability and Dose Response

We observed a clear dose dependent effect across subjects through our linear mixed model analysis. On an individual subject basis, we see a variability both in the size of the baseline and conditioned CEPs, as well as the degree of dose dependence. A likely explanation for this is the placement of the electrodes, which differed from subject to subject and was determined for clinical reasons. Subject 7 did not demonstrate a clear increase in CEP magnitude at the beta-recording electrode, while demonstrating clear CEP enhancement at channels adjacent to the beta-recording channel, while subjects 2, 4, and 6 showed the greatest percent increase effect at the trigger channel relative to other channels with their electrode grids (Figure 7.17)). This suggests a complex relationship between our conditioning paradigm and every subject.

Differences in baseline excitability were clear, as despite our varying stimulation levels, the size of response did not always map to the stimulation current used. For example, subject 4 had the smallest magnitude of CEPs, with a current delivery level of 0.75 mA, while subject 5 also had a current delivery of 0.75 mA, but with magnitudes after conditioning comparable to other subjects with higher stimulation currents.

Additional potential modulating factors include the cognitive state of the subject during the experiment, medication status, and the level of stimulation used. As patients were being treated for epilepsy, and were on a variety of painkillers and anti-epileptic drugs, there could be baseline differences in cortical excitability. Beyond these factors, a subject's inherent characteristics and baseline excitability could determine the influence of a conditioning paradigm, similar to the wide variety of responses seen in individuals to pharmaceuticals. This highlights the potential individual subject characteristics that may need to be considered for closed loop therapy applications, where one treatment strategy may not be appropriate or optimal for all individuals.

7.4.2 Network Wide Changes

The changes seen in channels outside of the triggering channel speaks to the complex effects of stimulation on the brain. There is an intersection of phase, stimulation level, subject variability, number of conditioning stimuli, and other unknown factors which contribute to the responses we see here. In total, (Figures 7.5, 7.14, 7.12, and 7.13), we see an overall enhancement of CEP magnitude across cortex, speaking to potentiation of connection strength, but the changes that would be seen over longer time periods remain unknown.

7.4.3 Limitations of Findings

While this study demonstrates physiological effects of cortical stimulation in humans, we were somewhat limited by subject availability and testing time in our capacity to explore the parameter space of cortical stimulation. We were able to conduct the study protocol only once per subject, limiting our capacity to test and compare multiple stimulation and beta recording sites. We were also not able to test a broad range of stimulation pulse parameters (amplitude, width, shape, and variations of charge balance, or variations on stimulation frequencies) that likely have an effect. These are limitations to the generalizability of the findings and suggest that the technique could be further optimized in future studies. Additional animal studies could allow for greater testing time within subjects and could speed the optimization process.

We also acknowledge that this study demonstrates the ability to modulate a short-term physiological marker of neural connectivity (the CEP), and that it was beyond the scope of this study to test humans with neurological impairments for cumulative changes in functional outcomes. Similarly, it has not yet been definitively demonstrated in the literature that changes in the CEP correlate with changes in neurological outcomes or function. However, in the context of prior human cortical stimulation studies [42, 106, 122, 142, 159, 195, 221], the changes in CEPs that we observed could be a physiological marker of the neuroplastic

changes involved in neurological recovery. Given the invasiveness of ECoG based neural stimulation and recording, linking CEPs with functional outcomes would likely require a long-term neural implant, and therefore may require further testing in animal models. To test the effects on functional outcomes in humans, a fully implanted system would likely be required for chronic stimulation.

7.4.4 Phase Delivery Accuracy

We acknowledge the limitations of this method of phase delivery, but the difficulties of real time filtering and concurrent stimulation necessitated an approximate method to determine beta-oscillations in real time with concurrent stimulation. Trials with long duration artifacts or large CEP magnitudes from can affect the estimation of phase on the next conditioning stimulus.

7.4.5 Comparisons with Existing Literature

A reason underlying the diversity of responses seen could be due to the size and placement of the clinical grid electrodes. The electrode grids in human subjects are currently of a larger area than those used recently in primate studies for cycle triggered stimulation (4.15 mm^2 exposed vs. 0.06 mm^2 exposed area [233, 314]). Additionally, our grids are placed subdurally, while those in prior primate studies were often epidural electrodes. The large volume of neurons targeted may result in a large enough subpopulation being stimulated on their appropriate phase of oscillation, regardless of the overall phase measured at the beta recording electrode, to invoke short term synaptic plasticity and CEP enhancement.

Additionally, the 1.23 ms pulse width used (chosen to be similar to clinical mapping), is longer than that used in a recent primate study which employed beta-oscillation driven stimulation [314]. We believe it is possible that these longer pulses result in a different response to stimulation, which catches a large enough population cells in an excitable state

to result in enhanced short term connectivity.

Additionally, work in humans with TMS has shown that repetitive TMS (rTMS) of motor cortical regions at a high fixed frequency ($\geq$ 5 Hz) increases motor evoked potential (MEP, a marker of cortical excitability) size, which is considered as a marker of cortical excitability [89]. 10 Hz stimulation in humans through implanted electrcorticography electrodes has been demonstrated to elicit both potentiation and depression lasting at least 10 minutes, depending on the location of stimulation and existing connectivity patterns [134]. Additionally, CCEPs from single-pulse electrical stimulation at distant cortical sites was modulated by the power, but not phase of local alpha and beta oscillations [278]. These results show the diversity of responses found in humans, depending on the scale of stimulation, the anatomical targets, and the network wide interactions.

We did not observe any distant CEPs with our stimulation and conditioning protocol, and reiterate that at our stimulation levels we are not exploring the same phenomena as other studies [132, 176, 177] which looked at larger networks and distant CCEPs. Our observance of only local effects may have been due to our lower current levels used (750-3500 μA), or location of stimulation. The fact that we used pulses of 1.23 ms in duration, relative to the 200-300 μs used by other groups, suggests that one of the most important features for activating neurons is the amplitude of the stimulation current. We additionally have observed smaller CEPs at the same site for the same current density with a smaller amplitude but larger pulse width (unpublished).

Although electrodes were selected that did not seem to be a part of the epileptic networks in patients, and data were screened for epileptiform artifacts, it is still possible that altered brain connectivity patterns resulting from epilepsy could have results that differ from those that would be seen in non-epileptic brains. Change in control of hand or speech are the second type risk to the subject. In theory, the stimulation could change how the brain controls their hand or speech. We think the change will be similar to what is seen with

simple practice or exercise [49, 214].

7.4.6 Consideration for Volume Conduction of Stimulation Pulse

In addition to the expected time delay of 2 – 4 ms for activation of neurons following a pulse as noted above, based on previous experimental [7,78,166,238]; and theoretical studies [144,202] we expect little direct effect of cortical surface stimulation at distances greater than 5-10mm.

7.4.7 Heterogeneity of Responses

Further examples of the heterogeneity of CEP responses seen in different subjects is found in recent work with a paired-pulse stimulation for spike-timing dependent plasticity in primate sensorimotor cortex [250]. The outcome measure in these experiments was CEP magnitude. The authors observed that only 2/15 sites tested in somatosensory cortex demonstrated an increase in CEP magnitude based off of the paired-pulse conditioning paradigm. This suggests that optimal enhancement of connectivity is influenced by a myriad of factors, many of which we currently do not understand. Furthermore, heterogeneity of responses were also observed in non-invasive studies of humans where in 200 subjects analyzed from data pooled across 3 laboratories , researchers did not see significant effect of TMS paired associative stimulation, but saw significant differences between studies [147].

7.4.8 Anti Hebbian STDP

Part of these heterogeneous responses may be due to the existence of both Hebbian (presynaptic stimulation leads postsynaptic spike) STDP, and anti Hebbian STDP (postsynaptic stimulation leads presynaptic spike) [85, 155]. Our widespread electrical stimulation most likely activates a mixed population of inhibitory and excitatory synapses, due to the indiscriminate nature of stimulation activating axons passing through the region of cortical tissue [133].

7.4.9 Note on Safety

Our use of 2.3 mm exposed diameter electrodes, for a surface area of 4.15 mm^2 (classifying our electrodes as "macro" electrodes), a maximum delivery current of 3500 μA, and 1.23 ms pulse widths, yielded a per phase charge density of 100 μC/cm2, above a maximum charge density limit for chronic stimulation of 30 μC/cm2 noted in a recent review of human stimulation studies [59], although the majority of stimulation was below that level. Stimulation levels were well within those used routinely for clinical studies, which can reach into the 10-20 mA range. Further refinement of stimulation parameters, locations, and materials may allow for safe, lower charge densities in an optimized therapeutic application.

7.4.10 Seizure Potential

We have run stimulation studies on dozens of individuals, with one seizure to date. This subject's typical seizure activity was in the mesial temporal region, however the post-stimulation seizure began after the cessation of a short conditioning stimulation session (aborted because of post-stimulation spiking activity) and was observed to start as a left temporal complex partial seizure, then it generalized. The timing related to stimulation and differing seismology suggests that the seizure was possibly related to research stimulation.

While any seizure activity connected with stimulation experiments is to be avoided, it should be noted that these research subjects are implanted for clinical epilepsy monitoring because of intractable seizures. It is a known risk that epileptic patients may experience a seizure in relation to clinical stimulation mapping, and may not preclude rehabilitative applications at low levels of stimulation in otherwise healthy individuals.

7.4.11 Future Directions and Considerations

Rather than definitely determining the effects of phase and the conditioning dose, we instead suggest that our results warrant further, in-depth exploration of activity-dependent stimu-

lation for rehabilitation purposes. We demonstrate here that connectivities can be modified on short time scales in-vivo with humans, but future work should more robustly quantify the duration of the effects and the extent to which these results couple to functional recovery. Questions remain regarding what the optimal closed loop paradigm in humans would be.

7.4.12 Conclusions

In 7 human subjects, we in real time delivered electrical stimulation during various phases of heightened beta oscillations recorded electrode at a site which elicited CEPs. Using a linear mixed model, we establish a statistically significant dose dependent increase in CEP size relative to baseline CEPs immediately following conditioning, with effects that last less than two seconds. In one subject, we compared beta-triggered oscillation with a control stimulation condition that was independent of underlying brain oscillations and found electrodes with enhanced CEPs during beta-band dependent stimulation relative to the control. Heightened beta-oscillations alone did not enhance CEP magnitudes. When considering all electrodes across the cortex, we observe a trend towards increased CEP amplitudes at surface depolarizing phases relative to hyperpolarizing phases, with a significant effect at the greatest number of conditioning stimuli. In 3 subjects, the greatest percent increase in CEP magnitude was in the trigger channel from which beta-oscillations were recorded in real time. This study demonstrates that activity-dependent cortical stimulation can induce neural plasticity, suggesting a role in neurological rehabilitation, although future research into the optimum stimulation parameters and the relationship with functional outcomes in humans is required.

7.5 Related Publications and Presentations

Caldwell DJ*, Olson JD*, Wander JD, Zanos S, Sarma D, Su D, Cronin JA, Collins K, Wu J, Johnson L, Buckley R, Richardson A, Weaver KE, Ko AL, Fetz E, Rao, RPN, Ojemann

JG, “Dose Dependent Enhancement of Cortically Evoked Potentials During Beta-Oscillation Phase Triggered Direct Cortical Stimulation of Human Cortex”, in preparation, *These authors contributed equally

Caldwell DJ, Olson JD, Wander JD, Zanos S, Sarma D, Su D, Cronin J, Collins K, Wu J, Johnson L, Weaver K, Casimo K, Fetz E, Rao RPN, Ojemann JG, “Exploration of the phase and dose dependence of cortico-cortical evoked potentials during beta-oscillation triggered direct electrical stimulation in humans”, Society for Neuroscience - Annual Meeting, San Diego, CA, November 2016

Caldwell DJ, Olson JD, Wander JD, Zanos S, Sarma D, Su D, Cronin J, Collins K, Wu J, Johnson L, Weaver K, Fetz E, Rao RPN, Ojemann JG, “Enhancement of Cortico-Cortical Evoked Potentials by Beta-Oscillation Triggered Direct Electrical Stimulation in Humans”, NANS-NIC Meeting, Baltimore, MD, June 2016

Caldwell DJ, Olson JD, Wander JD, Zanos S, Sarma D, Su D, Cronin J, Collins K, Johnson L, Weaver K, Fetz E, Rao RPN, Ojemann JG, “Effect of distance on the magnitude and timing of Cortico-Cortical Evoked Potentials in oscillation triggered direct electrical stimulation in humans”, Neurofutures Meeting, Seattle, WA, June 2016

Chapter 8

INTRACORTICAL PAIRED PULSE CONDITIONING PARADIGMS FOR IN-VIVO PLASTICITY INDUCTION IN HUMANS

Appropriately timed stimulation protocols can induce plasticity changes in cortex and potentially facilitate a positive influence on functional rehabilitation outcomes. However, the optimal parameters for inducing measurable changes in cortical excitability are currently unknown. Here we implement paired pulse conditioning paradigms intraoperatively in patients receiving DBS implants through acutely implanted ECoG electrodes to induce changes in cortical plasticity. The key parameters tested are the use of paired site cortical stimulation relative to single site stimulation, and time lags including 25 ms and 200 ms between conditioning trains. Our output metrics for measuring excitability are cortically evoked potentials (EPs, or CEPs). We perform these conditioning experiments in patients with Essential Tremor, Dystonia, and Parkinson's disease, and under varying states of anesthesia. We observe conditioning paradigms with 200 ms delays resulting in greater degrees of change than 25 ms conditions, and with paired stimulation between sites being more effective than single site stimulation. We similarly note no significant differences between disease conditions, supporting the extensibility of these results beyond being limited to studies in a particular disease process. We note minimal impact within a subject on cortical excitability during different levels of combined propofol/dexmedetomidine anesthesia, suggesting that intraoperative EP paradigms reveal meaningful connectivity patterns that could translate to neuroprosthetics in awake individuals. Additionally, longer conditioning sessions result in greater potentiation of EP magnitude relative to shorter sessions. These results likely

reflect the complexities of cortical network dynamics both locally and across distributedd nodes and the impact of stimulation at the scale of macroscale ECoG. Taken together, the current results with respect to the extant literature are likely a consequence of an increase in extent of depolarized cortex by macroscale direct electrical stimulation, yielding compound and multiplexed effects.

8.1 Introduction

8.1.1 Clinical Need

Contemporary neuromodulation affords the ability to help restore brain function, which could shape the recovery process [75] and enhance patient recovery. In the field of neuromodulation, DES using stimulation through implanted electrodes in the brain, is an appealing technique. Despite these advancements, optimal stimulation parameters for driving and shaping neural plasticity in an efficacious, translational capacity have yet to be established.

8.1.2 Plasticity and Timing

A potential protocol to induce plasticity between regions is paired pulse stimulation, where stimulation between two sites with existing connectivity is performed with a fixed temporal delay between two sites. This technique has been shown in rodent models with paired stimulation changes to drive behavioral changes, suggestive of strengthened functional connections in sensorimotor cortex [232]. Recently, this work has been extended into a primate model [250], where paired stimulation between a surface electrode and a deeper penetrating electrode at two different sites was shown to elicit STDP in 2 out of the 15 sites tested in sensorimotor cortex as assessed through the measurement of evoked potentials (EPs), also known as cortically evoked potentials (EPs) [314]. A key advantage of this method is the simplicity of hardware programming that would be required for implementation, as the only requirements are the delivery of stimuli to two sites with a consistent, known delay.

Simple repeated stimulation can either inhibit or potentiate neuronal excitability. For instance, repetitive stimulation through implanted electrodes in animal models at a fixed high frequency can potentiate neuronal excitability [30, 74, 259]. Transcranial magnetic stimulation (TMS), a non-invasive neuromodulation technique, is another way to modulate neural activity. Repetitive TMS (rTMS) of motor cortical regions at a high fixed frequency ($\geq$ 5 Hz) increases motor evoked potential sizes (MEP, a marker of cortical excitability) and reduces cortical inhibition, while low stimulation rTMS (0.1 - 1 Hz) reduces MEP sizes [89]. 10 Hz stimulation in humans through iEEG (intracranial electroencephalography) has been demonstrated to elicit both potentiation and depression lasting at least 10 minutes, depending on the location of stimulation and existing connectivity patterns [134]. This points to the necessity of studying more nuanced stimulation protocols to optimally shape neural plasticity. The question remains to the degree of overlap between protocols to induce plasticity on a single cell, network wide, or brain wide level.

8.1.3 Objective

Here we seek to translate studies from NHPs to humans, and explore the scaling of the principles of STDP to larger network-wide regions. Specifically, we explore the length of conditioning required for plasticity induction in human cortex, what the effects of anesthesia may be for intraoperative screening of evoked potentials, and what may be the most effective time lag when performing a paired pulse paradigm. To do this, we perform EP stimulation and measurement protocols through acutely placed ECoG strips over sensorimotor cortex in patients undergoing DBS lead implantation surgery for the treatment of Parkinson's disease, Dystonia, and Essential Tremor.

8.2 Methods

8.2.1 Human Subjects

The particular target for each subject tested are outlined in table 8.1. Subjects with GPi or STN targets were Parkinson's disease patients, who remained anesthetized for the duration of the surgery, while subjects with VIM targets were Essential Tremor patients (except for subject 1, a dystonia patient), who were frequently woken up during the course of surgery. Depending on the diagnosis, different combinations of anesthetics were used (Table 8.1). We excluded 6 subjects (not shown in table 8.1) from analysis either due to no EPs being visualized during the screening procedure (5 subjects), or differences in the geometric arrangement of the stimulation channels from the rest of the subjects (1 subject).

8.2.2 Recording and Stimulation

We recorded raw neural data at 12207 Hz to resolve short-latency signal components and for artifact suppression. We employed a constant-current stimulation mode, which delivered voltage to meet a given current requirement. Our pulse duration ranged from 200 μs to 1000 μs for each phase of our biphasic, bipolar rectangular pulse stimulation.

8.2.3 Screening

In a subset of patients, we located the central sulcus, and corresponding sensory and motor regions using phase reversals of somatosensory evoked potentials (SSEP) [52, 305]. We then tested bipolar stimulation pairs in sensory, motor, and premotor cortex to elicit EPs in adjacent contacts (Figure 8.1). We additionally switched the polarity of the stimulation pair to ensure that any visualized presumed EP was not simply an artifact of DES. A similar shape of EP in both polarities of stimulation confirmed neural, rather than artifactual, origin, as we would expect stimulation artifacts tohave a polarity-dependent shape. A channel pair

Subject	Age	Gender	Disease	DBS Target	Anesthesia
1	69	M	PD	Right DBS - VIM	2x dose Propofol
					Remifentanil
					Rocuronium
2	53	M	PD	Bilateral DBS - STN	Propofol (2000 mg / 200 mL)
				Left Recording	Remifentanil (2000 mcg / 40 mL)
3	64	M	Dystonia	Bilateral DBS - GPi	Remifentanil (1000 mcg / 20 mL)
				Left Recording	Propofol
4	59	M	PD	Bilateral DBS - GPi	2x dose Propofol 300 mL
				Left Recording	Remifentanil 4 mg
5	72	F	PD	Bilateral DBS - STN	Propofol, 500 mg /50 mL, 50 mL
				Left Recording	Fentanyl - 100 ucg/2 mL
					Dexmedetomidine - titrated, 100 mL
6	81	F	PD	Left DBS - STN	Dexmedetomidine
7	43	M	PD	Left DBS - STN	Propofol 1000 mg/100 mL, 100 mL
					Propofol 2000 mg/200 mL, 200 mL
					Dexmotodomidine - 50 mg, titrated
					Vecuronium - 20 mg
					Rocuronium - 50 mg/5 mL, 5mL
8	71	M	ET	Left DBS - VIM	400 mcg, 100 mL Dexmedetomidine
					Propofol
9	69	M	PD	Bilateral DBS - STN	Propofol
				Left Recording	Remifentanil
					Rocuronium
10	72	M	PD	Bilateral DBS - STN	2x Propofol 2000 mg/200 mL, 200 mL
				Left Recording	Remifentanil 2 mg
11	79	F	PD	Bilateral DBS - GPi	Started on gas, transitioned to Propofol
				Left Recording	Rocuronium
					Succinylcholine
12	60	M	PD	Bilateral DBS - GPi	Propofol 2500 mg/250 mL, 250 mL
				Left Recording	Remifentanil 1000 mcg/20 mL, 20 mL
13	43	M	ET	Bilateral DBS - VIM	Propofol (1500 mg / 150 mL)
				Left Recording	Dexmedetomidine (200 mcg/ 50 mL) ?
14	51	M	ET	Right DBS - VIM	Propofol - 1500 mg/150ml, 150 mL
					Dexmedetomidine - 400 mcg

Table 8.1: Paired pulse subject demographics. Demographics table for the subjects included for analysis. PD - Parkinson's Disease. ET - Essential Tremor. GPi - globus pallidus internus. STN - subthalamic nucleus. VIM - ventral intermediate nucleus of thalamus. Parkinson's disease and dystonia patients remained anesthetized for the duration of the surgery, while Essential Tremor patients were woken up during the course of surgery. Subject 14 underwent EP measurement testing during various states of anesthesia sedation.

was then identified (site A) that reliably elicited EPs in a different electrode (site B). Site A was then defined as the seed location for driving plasticity.

8.2.4 Conditioning and Testing

Once EPs were localized, a paired paired pulse conditioning paradigm, inspired by Seeman et al. 2017 [250] was initiated. We applied 3 pulses at 330 Hz in 2 Hz intervals to both site A and site B, with site A leading site B stimulation by 25 or 200 ms (Figure 8.2(a)). We call this **A/B** conditioning. An additional control conditioning paradigm was presented, consisting of paired pulse stimulation at the same site, which we call **A/A**. We chose the conditioning amplitude to be 80% of the maximum EP testing value, and used the same pulse widths for conditioning and testing. The specific conditioning experiments we were able to acquire for each patient ran, as well as the conditioning and testing parameters are in Table 8.2. Conditioning time ran between 5 and 25 minutes and was solely dictated by the constraints of the operating room on a patient by patient basis. With respect to the stimulation parameters, (-) represents cathodic first stimulation (negative current first), while (+) represents anodic first stimulation (positive current first) for the biphasic, bipolar stimulation pairs.

Before and after every conditioning session, we used single ramping stimulation pulses at 4 stimulation currents, with a 2 Hz stimulation frequency (Figure 8.2(b)). Subject 1 had 1 minute of testing, hence there were 30 stimulation pulses at each current tested. The remainder of the subjects had 2 minute testing periods, yielding 60 stimulation pulses at each tested current, unless a given recording session had to be cut short by operating room constraints. Subject 3 only had 3 consistently used amplitudes across different testing periods, so we focused on those 3 amplitudes for subsequent analysis.

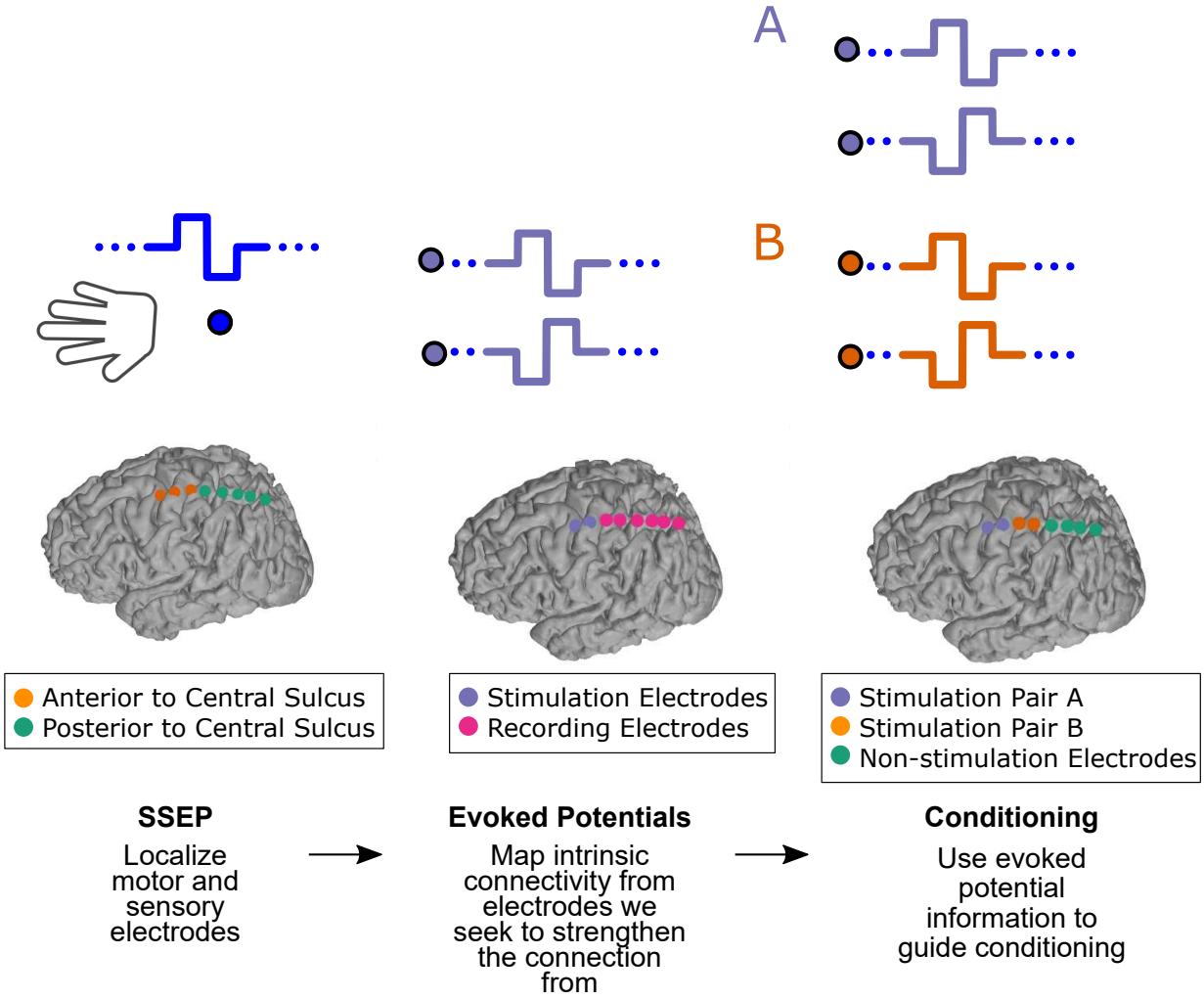

Figure 8.1: Paired pulse screening and conditioning protocol. The first step for a subset of patients in the paradigm is localization of sensory cortex via phase reversal through SSEP testing. The next is assessing baseline cortical excitability through EP screening, and subsequent EP testing at four different stimulation current amplitude levels at electrode pairs which elicit reliable and robust EPs. After establishing a baseline EP level, we perform conditioning between either the same site (site A), or between two sites (A and B), where site B is where we observed EPs from stimulation at A during our screening protocol.

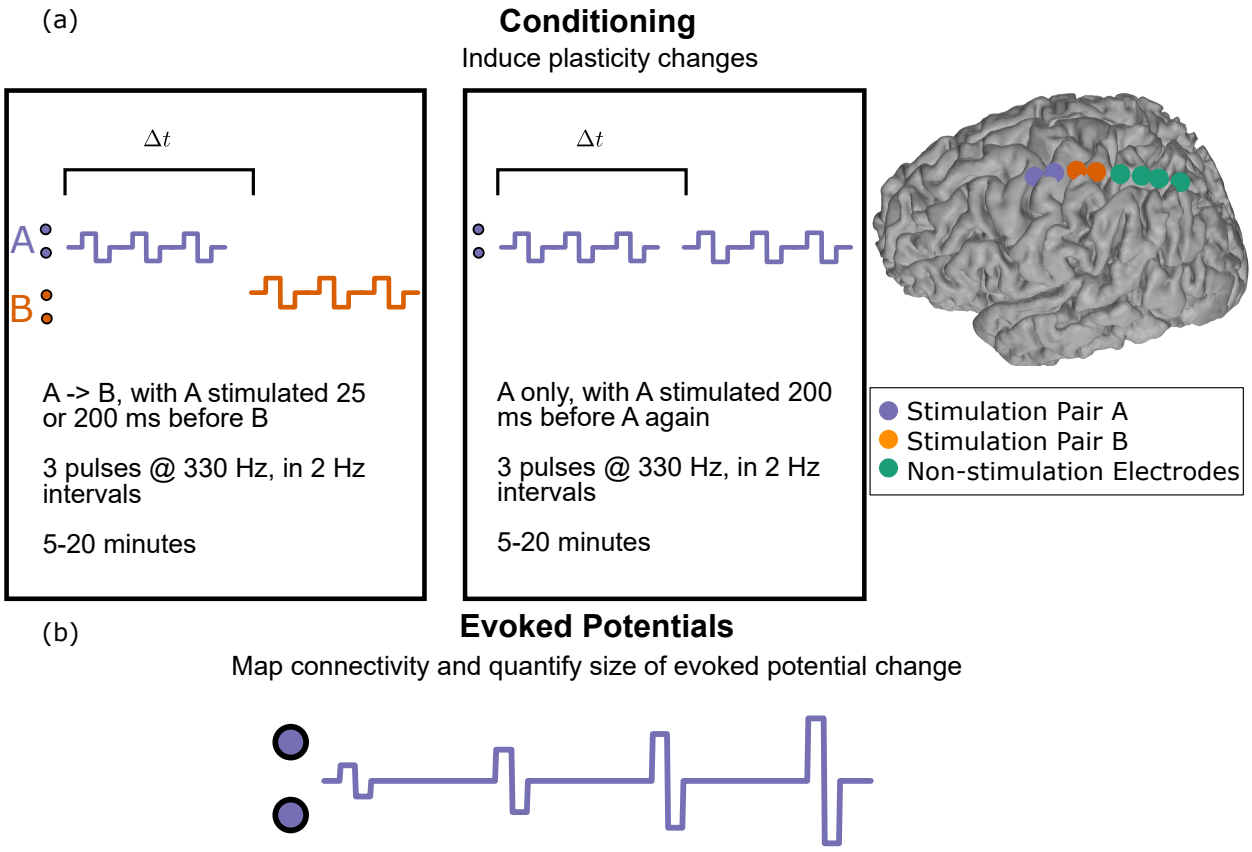

Figure 8.2: Different paired pulse conditioning protocols (a) and subsequent measurement (b). We tested various lags between stimulation at the two sites. With these lags, we tested two different conditioning protocols (a). The first was paired bipolar stimulation between two sites (represented as A/B stimulation). The second was stimulation within the same site with a latency between the bipolar pulses. Following conditioning, we measured the sizes of the EPs with ramping single pulse 2 Hz stimulation (b)

.

Subject	Experiments	Conditioning Params.	EP Test Params.	Electrode Pairs	SSEP
1	25 ms A/B, 10 min	2.4 mA, 0.2 ms	0.5,1,2,3 mA, 0.2 ms	A: 7-/8+ B: 6-/5+	6/5
2	25 ms A/B, 20 min	2.4 mA, 0.2 ms	0.5,1,2,3 mA, 0.2 ms	A: 7-/8+ B: 6-/5+	5/4
3	25 ms A/B, 15 min	2.8 mA, 0.2 ms	1,2.5,3.5 mA, 0.2 ms	A: 5-/6+ B: 4-/3+	6/5
4	25 ms A/B, 10 min 200 ms A/B, 10 min	4.8 mA, 0.2 ms	3.5,5,5,5.6 mA, 0.2 ms	A: 7-/8+ B: 6-/5+	6/5
5	200 ms A/B, 10 min 25 ms A/B, 10 min 25 ms A/A, 10 min	2.4 mA, 0.2 ms	1.5,2,2.5,3 mA, 0.2 ms	A: 7-/8+ B: 6-/5+	N/A
6	25 ms A/B, 15 min 200 ms A/B, 15 min 25 ms A/B, 15 min	3.6 mA, 0.5 ms	3,3.5,4,4.5 mA, 0.5 ms	A: 5-/6+ B: 3-/4+	4/5
7	200 ms A/B, 15 min	3.6 mA, 0.2 ms	3,3.5,4,4.5 mA, 0.2 ms	A: 6-/7+ B: 4-/5+	N/A
8	200 ms A/B, 10 min 200 ms A/A, 10 min	2.4 mA, 0.2 ms	1.5,2,2.5,3 mA, 0.2 ms	A: 7-/8+ B: 5-/6+	4/5
9	200 ms A/A, 15 min 200 ms A/B, 15 min 25 ms A/B, 15 min 25 ms A/A, 15 min	3.2 mA, 0.2 ms	2.5,3,3.5,4 mA, 0.2 ms	A: 7-/8+ B: 6-/5+	N/A
10	200 ms A/B, 15 min 200 ms A/A, 15 min	6.8 mA, 0.2 ms	5.5,6.5,7.5,8.5 mA, 0.2 ms	A: 6-/7+ B: 5-/4+	N/A
11	200 ms A/B	6.8 mA, 0.2 ms	5.5,6.5,7.5,8.5 mA, 0.2 ms	A: 6-/5+ B: 4-/3+	N/A
12	200 ms A/B, 15 min	6.4 mA, 0.2 ms	5,6,7,8 mA, 0.2 ms	A: 6-/7+ B: 5-/4+	N/A
13	200 ms A/B, 5 min 200 ms A/B, 15 min 200 ms A/A, 15 min	6.4 mA, 0.5 ms	5.5,6.5,7.5,8.5 mA, 0.5 ms	A: 6-/7+ B: 5-/4+	N/A
14	awake vs. asleep	N/A	2,3,3.5,4 mA, 0.2 ms	Pair 1: 7-/8+ Pair 2: 6-/5+	N/A

Table 8.2: Stimulation experiments by patient. The "ms" value under "Experiments" shows the delay between the two stimulation trains, while "min" shows the conditioning duration in minutes. For conditioning and EP test parameters, the "mA" value represents the peak current, while the "ms" value represents the pulse width of a single phase of the biphasic pulses. Under "Electrode Pairs", site A is the site stimulated first, with site B following. (-) is for cathodic first stimulation, and (+) for anodic first stimulation. The pair under "SSEP" indicates the electrode pair between which the phase reversal characteristic of the central sulcus was seen. Higher electrode numbers are anterior to lower electrode numbers

8.2.5 Data Analysis

We quantified the peak-to-peak amplitude of the EP in a per subject specified window (epoch) following stimulation (free from the subsequent stimulation artifact) to isolate early, excitatory connections, representing the strength of structural and functional connectivity between regions [134], building upon prior work that considered different latency responses (N1, P1, N2) [81,132]. We focused on peak-to-peak values because the functional significance of the different EP components is incompletely understood, and we do not currently understand how they relate to functional output from a specific cortical region. We performed Savitsky-Golay smoothing [245] only within our time window of interest prior to extracting the peak-to-peak amplitudes in order to obtain a more reliable estimate of the peak-to-peak amplitude. We discarded any peak-to-peak values with magnitudes below 25 μV or above 1500 μV. As these experiments were intraoperative, a subset of trials were contaminated by artifacts from concurrent electrocautery. We screened the measurement data for artifacts in each recording due to electrocautery or electrode movement, and removed any epochs where noise precluded accurate calculation of peak-to-peak voltages.

8.2.6 Model Fitting

In order to assess the effect of various conditioning lengths, level of sedation, and conditioning protocols, we built linear and linear mixed models in R [223] using the lmerTest package [146]. The use of linear mixed models allowed us to disentangle the effects of variables we explicitly tested (the conditioning experiment used) relative to inter-subject variability. In order to compare across subjects with different stimulation amplitudes, we modeled the stimulation level as an ordered fixed variable, $(1 < 2 < 3 < 4)$, rather than an absolute numeric value or categorical variable. Therefore, in our model fits, there exist a linear, quadratic, and cubic term for the fixed effects estimates. We calculated the estimated marginal means to calculate post hoc differences between groups. We visualized the residual distributions and quantile-

quantile fits to assess model validity (Appendix). We used the R emmeans package [154] to calculate the estimated marginal means.

8.2.7 Duration of Conditioning

In order to consider the effect of the duration of conditioning, we built a linear model for one subject where we had the capacity to test 200 ms A/B conditioning for both 5 and 15 minutes, and considered peak-to-peak voltage as our output, the measurement stimulation level used as an ordered fixed variable (with the lowest stimulation current used for measurements as 1, and the highest stimulation current used as 4, with $1 < 2 < 3 < 4$), and how long stimulation was performed for (5 vs. 15 minutes).

8.2.8 Anesthesia Level

In order to consider the effect of propofol and dexmedetomidine induced anesthesia sedation on EP magnitude we built a linear mixed model for one subject who was woken up during the course of surgery. We considered peak-to-peak voltage as our output, the particular EP measurement level as an ordered fixed variable (with the lowest stimulation current used for measurements as 1, and the highest stimulation current used as 4, with $1 < 2 < 3 < 4$), and whether the patient was lightly (awake) or heavily (asleep) anesthetized, as relayed by the neurosurgeon and anesthesia clinical team, and observations of patient activity. Our random effects were modeled by the particular channel measured, as there were two bipolar pairs which evoked EPs.

8.2.9 Across Subjects

In order to look across subjects and evaluate global trends, we built linear mixed models with the peak-to-peak voltage as our output, the particular EP measurement level as an ordered variable (with the lowest stimulation current used for measurements as 1, and the

highest stimulation current used as 4, with $1 < 2 < 3 < 4$), whether or not the measurement channel was in site **B**, whether or not the patient had Parkinson's disease, or Essential Tremor/dystonia, and the particular experimental condition tested. Our random effects were modeled as individual subject variation.

8.3 Results

8.3.1 Screening

To illustrate our intraoperative screening protocol, we highlight the EPs resulting from the switching of polarity on two stimulation channels later used for conditioning for Subject 13. (Figure 8.3). The peak-to-peak amplitude and order of peak and trough immediately following the stimulation artifact remains similar between the two polarities on channel 5, highlighting the neural origin of the measured signal. We performed this polarity switching protocol for all subjects. In general, we observed the greatest density of EPs in electrodes surrounding the central sulcus (as confirmed by SSEP mapping and intraoperative CT imaging), suggesting the electrodes primarily stimulated were in premotor, motor, and sensory cortices.

8.3.2 Measurements

We used the peak-to-peak voltage distribution across each individual trial as the dependent variable to assess the effect of conditioning, anesthesia level (while under dexmedetomidine and propofol), or length of conditioning. The temporal position of the peak-to-peak voltage analyzed depended on each individual subject's EP waveform, as these can be highly complex, non-uniform morphologies between individuals, as shown by the variety of responses seen in the literature [132, 134, 176, 177]. As an example, we highlight the average EP following 8.5 mA stimulation for a baseline and three different conditioning sessions from subject 11 (Figure 8.4)

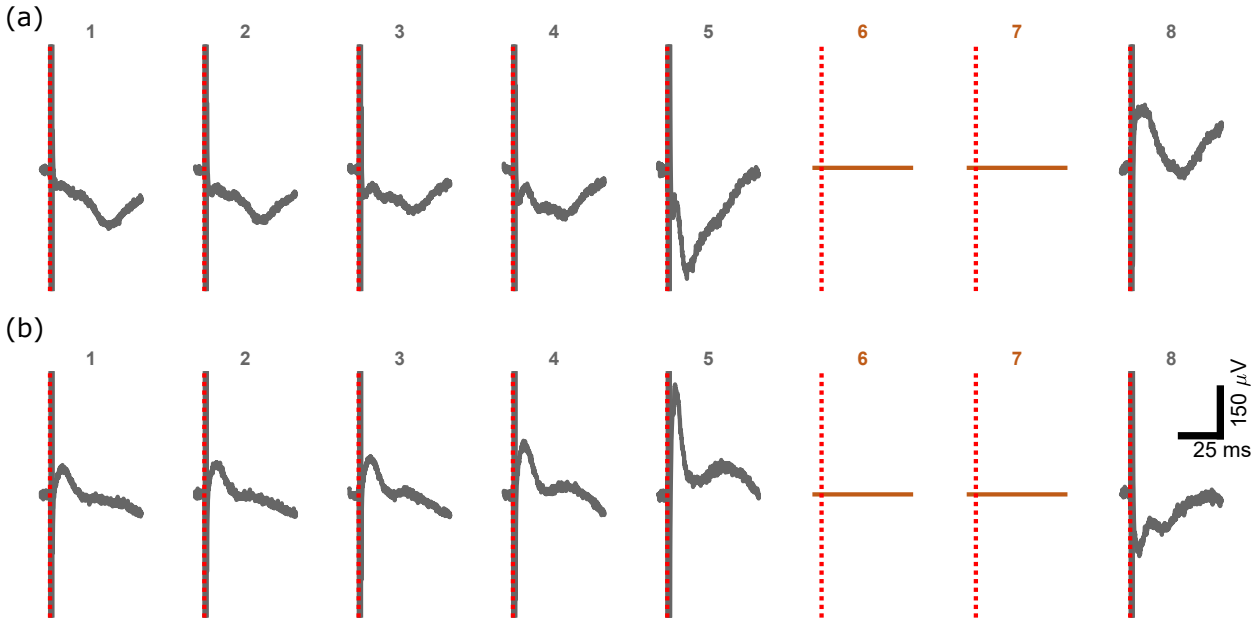

Figure 8.3: Paired pulse screening protocol results. (a,b) Average short latency components following EP screening with 8.5 mA pulse amplitudes and 500 μs pulse widths at channels 6/7 on the strip for Subject 13. (a) Represents the average of 14 stimulation pulses with one polarity of stimulation (b) Represents the average of 9 stimulation pulses for the opposite polarity of stimulation. We used this protocol to confirm the neural origin of EPs, as we sought out channels where the peaks and troughs followed a consistent pattern with different stimulation polarities. Channels where we observed an exponential-like decay that flipped sign with a different stimulation polarity were considered to be artifacts.

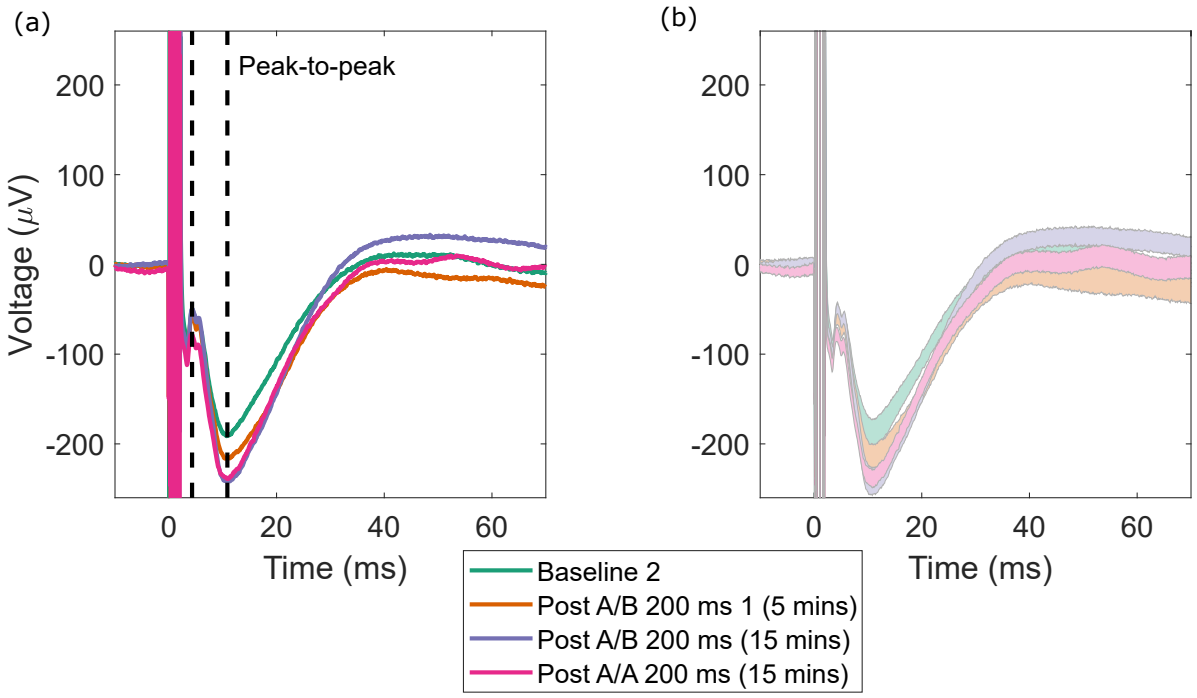

Figure 8.4: Example peak-to-peak voltages on measurement waveforms. (a) shows the mean waveform during an example baseline session (second baseline), 200 ms A/B conditioning for 5 minutes, for 15 minutes, and the A/A conditioning for 15 minutes. (b) shows the 95% confidence intervals around the mean for each of the conditions (60 trials within each condition). This example from one subject reveals a significantly different baseline from the other conditions based on our linear mixed model.

8.3.3 Effect of Different Conditioning Paradigms

We fit our linear mixed model on data from 13 subjects. See appendix table F.1 for the model fit details.

The major effect of comparing different conditoning paradigms was that the 200 ms A/B condition resulted in the largest peak-to-peak voltages relative to the other conditioning paradigms and baseline EP measurements. Statistically, there was a significant difference between experimental conditions ($p < 0.001$, ANOVA on the linear mixed model). Upon post-hoc testing, EPs following 25 ms A/B conditioning demonstrated a significant decrease relative to baseline EPs (estimate = -21.18 μV, $p < 0.001$), while those following 200 ms A/B conditioning showed a significant increase relative to baseline EPs (estimate = 15.33 μV, $p < 0.001$), EPs following 25 ms A/B conditioning (estimate = 36.51 μV, $p < 0.001$), and EPs following 200 ms A/A conditioning (estimate = 11.59 μV, $p = 0.046$). For EPs following 200 ms A/A conditioning, there was no increase from baseline EPs (estimate = -3.75 μV, p = 0.78).

Site B channel pairs (defined by the existence of a pre-condition EP after site A stimulation) elicited significantly greater EPs than those that were outside of site B (estimate = 199.78 μV , $p < 0.001$).

There was no significant effect of disease for our model (p = 0.797), suggesting that our results are not particular to the disease process or diagnosis.

The was an increase in peak-to-peak amplitude with an increase in stimulation current (p < 2.2e-16 ANOVA on the linear mixed model Table F.1), with the linear trend dominating (estimate = 101.10 μV, $p < 0.001$), as well as a significant quadratic term (estimate = -8.37 μV, $p < 0.001$).

Figure 8.5 highlights across all subjects, for each individual channel and stimulation level, the average absolute difference peak-to-peak voltage value in μV following EP measurements (Figure 8.5, as well as appendix Table F.1). For estimating the difference from baseline,

in general, each experimental conditioning testing block was compared to its immediately proceeding baseline testing block. We emphasize the change in peak-to-peak magnitudes in this plot, rather than the magnitudes themselves, as we are comparing across subjects with large variations in EP magnitudes.

Individual absolute difference voltages on every trial, for all channels with analyzed EPs within each subject, are shown in appendix Figure F.1. Of note is that there is jitter in these plots which accentuates the spread in the y-direction of measured values. There exists heterogeneity in both the direction and magnitude of effect for different conditioning paradigms between subjects.

See appendix Figure F.2, and Figure F.3 for the quantile-quantile and the residuals plots following our model fit. We emphasize that our goal here was not to build a predictive model of precise conditioning effects for any given subject, but rather we highlight trends that are worth exploring further in long term testing scenarios. We assume a linear model captures the main effects of our data, and we do not believe in the field there exists sufficient knowledge for an error distribution model beyond the normal distribution for linear regression.

8.3.4 Length of Conditioning

In one subject (Subject 13), we explicitly tested five vs. fifteen minutes of conditioning at two sites with a 200 ms latency (Figure 8.6, appendix Table F.2). We highlight here the peak-to-peak magnitudes, rather than changes in magnitudes, as we are only considering a single channel within one subject.

We found that 15 minutes of conditioning resulted in a larger increase in peak-to-peak EP magnitude than did 5 minutes of conditioning. Statistically, there was a significant difference between the baseline, five and fifteen minutes of conditioning ($p < 2.2e\text{-}16$) as assessed through an ANOVA on the linear mixed model. All of the contrasts between baseline, five, and fifteen minute conditioning sessions were significant ($p < 0.001$), with fifteen minutes

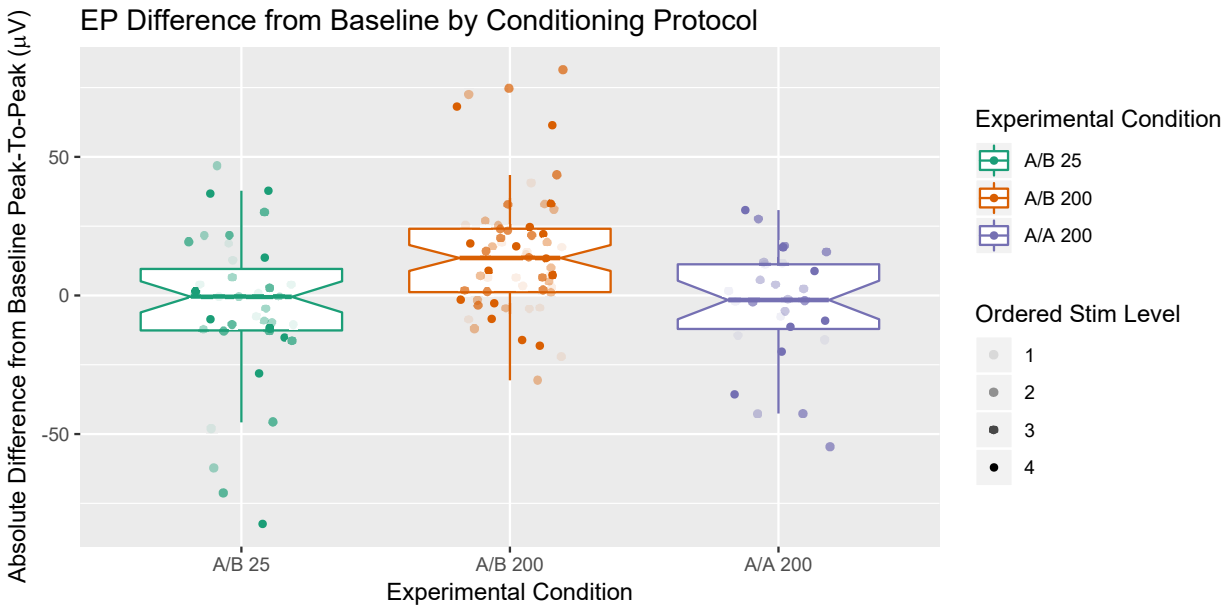

Figure 8.5: Difference in EP peak-to-peak magnitudes from baseline for paired pulse conditioning protocols. For the different conditioning paradigms tested across our 13 subjects, we plotted the average EP magnitude difference from an average baseline EP for each channel analyzed for each stimulation current used during our EP measurement protocol (4 increasing stimulation levels all but one subject) from each subject. We observed a significantly higher peak-to-peak EP magnitude following A/B stimulation with a 200 ms latency, relative to either the baseline, A/B 25 ms, or a 200 ms latency within the same site (A/A 200 ms). The transparency in the plotted points represents what stimulation measurement level was used for that set of EPs (4 for the majority of subjects). We did not observe any systematic influence of which stimulation level was used for the measurement and the difference from baseline.

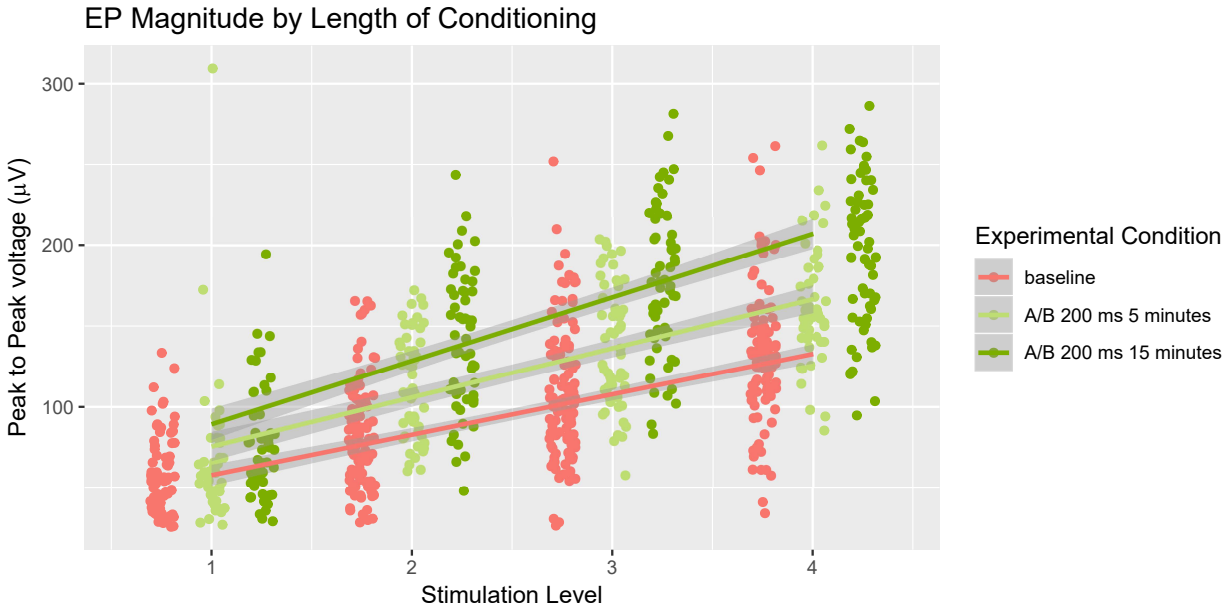

Figure 8.6: Effect of different lengths of conditioning. We tested the effect of the length of conditioning under the same conditioning paradigm (200 ms A/B), with five vs. fifteen minute conditioning times, and observed a statistically significant increase in peak-to-peak voltages under the 15 minute conditioning paradigm relative to both the baseline and 5 minute conditioning period. The linear fit line is for each experimental condition, and the shaded area indicates the 95% confidence interval.

having the greatest effect (estimate = 53.94 μV, p $<$ 0.001), and five minutes a lesser effect (estimate = 26.37 μV, p $<$ 0.001).

There was an increase in peak-to-peak amplitude with an increase in stimulation current (p $<$ 2.2e-16 = ANOVA on the linear mixed model Table F.2), with the linear trend dominating (estimate = 68.86 μV, p $<$ 0.001), as well as a significant quadratic term (estimate = -10.47 μV, p $<$ 0.001).

8.3.5 Awake vs. Asleep

In one Essential Tremor patient (Subject 14) brought in and out of propofol/dexmedetomidine anesthesia during evoked potential measurement, we quantified the peak-to-peak voltages without conditioning across measurement sessions in both anesthetized (3 measurement sessions for 2 channels) and awake states (2 measurement sessions for 2 channels).

There was no significant difference between the anesthetized and awake states ($p = 0.253$).

The lack of a significant difference between the anesthetized and awake states suggests that the EPs elicited during deeper anesthesia are relatable to the EPs elicited during more awake states within a given patient, under anesthetics such as propofol and dexmedetomidine (Figure 8.7). We highlight here the peak-to-peak magnitudes, rather than changes in magnitudes, as we are only considering two channels within one subject, rather than comparisons across subjects with large differences in EP magnitudes.

There was an increase in peak-to-peak amplitude with an increase in stimulation current ($p < 2.2e-16$ ANOVA on the linear mixed model, appendix Table F.2), with the linear trend dominating (estimate = 178.31 μV, p < 0.001), as well as a significant quadratic term (estimate = -19.05 μV, $p < 0.001$).

8.4 Discussion

8.4.1 STDP, Plasticity, and Anatomy

In contrast to previous primate literature studies with paired-pulse stimulation between a surface and intracortical electrode [250], we observed greater potentiation at longer delays between stimulation sites, suggesting that the mechanisms responsible are less dependent on spike-timing dependent plasticity and rather on larger network-scale phenomena due to the scale of our stimulation electrodes and larger areas of cortex targeted (clinical ECoG electrodes in our study). Other studies exploring plasticity induction in animal models frequently used single neuron activity or spiking when driving stimulation to induce plasticity

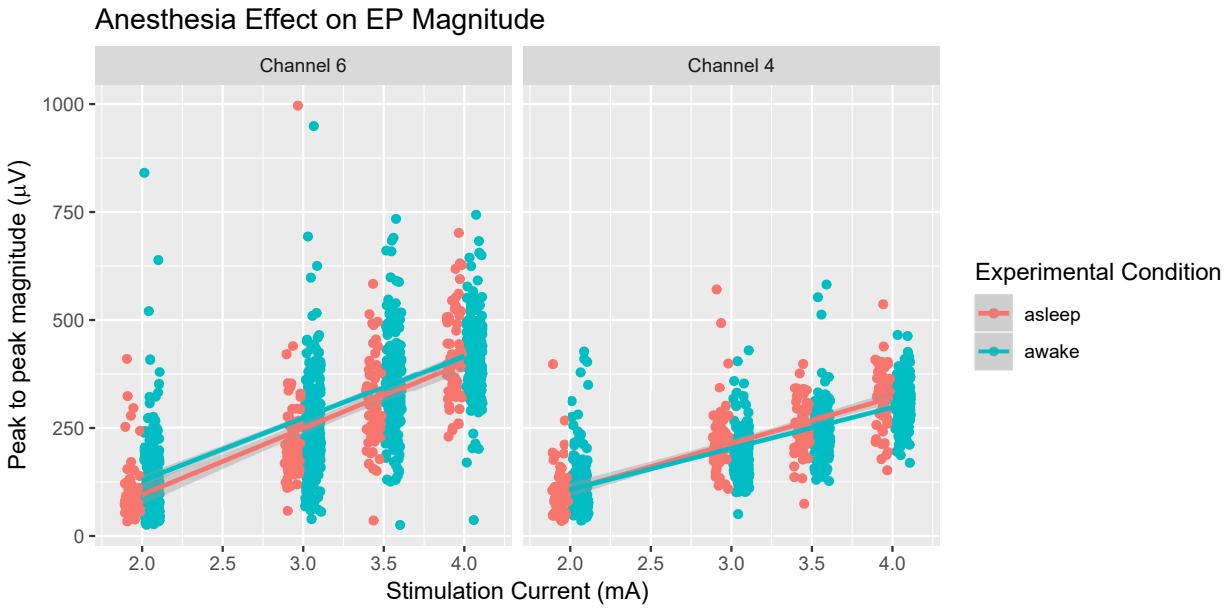

Figure 8.7: Effect of levels of sedation on EP magnitude within one subject. We tested two separate stimulation pairs in this subject, and observed two distinct EPs. Stimulation at channel pair 7/8 resulted in an EP at channel 6, while stimulation at 5/6 resulted in an EP at channel 4. We binned together all of the more sedated states in this subject relative to the awake testing states, and measured no significant difference between the two states. This suggests that the EPs elicited under light anesthesia may be predictive of the EPs that would be observed in an awake patient.

[125, 231]. Jackson et al. observed a clear dependence on the time window between spiking and stimulation for effective motor output mapping changes in line with classic STDP [125]. In the context of these studies, we believe our results reinforce that we are recording and stimulating from networks of neurons.

Cortical plasticity is a complex phenomena. There exist both Hebbian (presynaptic stimulation leads postsynaptic spike) STDP, and anti Hebbian STDP (postsynaptic stimulation leads presynaptic spike) [85, 155]. Our DES most likely activates a mixed population of inhibitory and excitatory neurons, due to the indiscriminate nature of stimulation activating axons passing through the region of cortical tissue [133]. This supports findings of both potentiation and depression with DES.

Brain activity is coordinated by a balance of excitatory and inhibitory neurons. Pyramidal cells tend to make connections with other pyramidal cells [136], and motor cortex neurons in NHPs have been seen to have collateral extents of 3 mm [98]. Excitatory layer V neurons can have long range axonal projections (up to 1000 μm in rodent somatosensory cortex), which transmit information across several cortical columns [86]. Inhibitory neurons tend to densely inhibit local neighborhoods, beyond which their influence falls off rapidly [87, 88]. For example, in rat frontal and somatosensory cortex, somatostatin- and parvalbumin- positive neurons reached a connection probability of 0 after 500 μm [87, 88]. On the scale of our macroECoG contacts, where the minimum spacing is 1 cm, we are likely stimulating and recording from separate populations of neurons, where the dominant connections between regions are likely to be excitatory. One additional factor is that the lateral connections of neurons are thought to be relatively unexcitable, as they are frequently unmyelinated [271]. Similarly, electrical stimulation is thought to activate the most excitable neurons in a population, which are often the ones with the largest diameter axons [271]. Therefore, excitatory pyramidal neurons around the central sulcus where we primarily stimulated could therefore be preferentially activated. Since we are dealing with networks of neurons across a multi-

centimeter length scale, it is not surprising that the principles of STDP or local inhibition may not have as specific an impact.

One potential method of synchronization and communication across different brain networks is cortical oscillations. Theta waves (4-8 Hz) are thought to modulate and coordinate distant connections [315]. Our 200 ms stimulation paradigm is between 4 and 5 Hz, suggesting that theta wave synchronization between regions could be a possible mechanism of synchronization and plasticity enhancement. The idea of theta-like stimulation being useful is supported by the prevalence of "theta-burst" stimulation in TMS studies to potentiate excitability [123], as well as other rTMS studies [89].

The decrease in EP magnitude with the A/B 25 ms condition suggests that on the network level too rapid of pulses could cause local inhibition. However, this stimulation frequency is above the 0.1-1 Hz stimulation suggested by Fitzgerald et al. from rTMS that causes a decrease in cortical excitability, reinforcing recent findings by Keller et al. [134] that speak to the complex nature of stimulation through intracranial electrodes.

In contrast to previous intracranial EP modulation studies [134], we note potentiation and depression of EPs with stimulation in motor, premotor, and sensory cortices with the 200 ms delay condition, rather than the depression seen by Keller et al. when stimulating in motor cortex at 10 Hz. This difference in EP modulation at the same anatomic site through clinical ECoG electrodes suggests that the phenomena surrounding plasticity induction through intracranial electrodes is complex and multifactorial.

A key component of brain function, particularly with motor and sensory regions, is the subcortical networks in the brain. Preliminary data (unpublished) suggests that stimulation of subcortical regions can modulate the EPs on the surface.

8.4.2 Variability

As noted in the results section, there exists heterogeneity in both the direction and magnitude of EP modulation for the different conditioning paradigms between subjects (Figure F.1). Subjects 7 and 13 demonstrate large effects for the 200 ms A/B conditioning paradigm, while subject 12 shows less of an effect. Subject 1 demonstrated a potentiation effect with 25 ms A/B conditioning, which is different from the overall trend observed across subjects. These results points to the variability between subjects, potentially due to the complex effects of DES or the inherent variability between human subjects which has been observed previously with rTMS in humans [221].

8.4.3 Size of Evoked Potential

The size of the EP increasing with the level of electrical stimulation has been noted before both in NHPs [250] and humans [64]. This is the dominant factor in our model fit for all models that we fit. In all of our models, we note statistically significant linear and quadratic predictors, which suggests that our EPs, on average, begin to plateau at higher stimulation levels.

8.4.4 Level of Sedation

Anesthesia is known to alter cortical excitability as a function both of the particular anesthetic used, as well as the dosage [15]. However, prior work which focused on motor evoked potentials (MEP) demonstrated MEP elicitation under both a xylazinezoletil combination and urethane anesthesia [267], highlighting that proper anesthesia selection can preserve cortical excitability. In humans propofol and dexmedtomidine are thought to be anesthetic agents that have minimal impact on cortical excitability, compared to other inhaled halogenated compounds [170]. Specifically, dexmedetomidine has been shown to have minimal impact on motor and somatosensory evoked potentials in adolescents [274], and the

use of propofol does not prohibit useful intraoperative MEP measurements during spinal surgery [127]. Our results showing no significant difference between various levels of propofol and dexmedetomidine anesthesia induction suggest that EPs elicited during anesthesia would be transferable to those in an awake state, and that intraoperative EP screening during neuromodulation device placement under appropriate anesthetics could be informative for ensuring effective outwardly driven connectivity from the stimulation site (Figure 8.7, appendix Table F.3). Similarly, the fact that we are able observe EPs in both Essential Tremor patients, who are woken up during surgery, and Parkinson's patients, who remain sedated for the entirety of the operation, speaks to the generalizability of our studies.

8.4.5 Conditioning Length

Our results on the length of conditioning, with longer conditioning demonstrating a greater effect than shorter conditioning (Figure 8.6, appendix Table F.2), suggest that changes in plasticity could be enhanced with longer sessions. The optimal duration and frequency remains unknown, but future studies with implanted intracranial devices could further explore this. This is a critical point for translation to individuals with stroke where prior work in six individuals with stroke treated with epidural cortical stimulation found motor improvements with less than four hours of stimulation a day, while longer durations resulted in increases in spasticity [307].

8.4.6 Effect of Disease

Parkinson's disease, Essential Tremor, and dystonia are known to be diseases that affect the thalamocortical loop and motor function. For instance, Parkinson's disease is known to affect motor cortical excitability by inhibiting corticortical inhibition [234]. Essential Tremor patients however, are thought to have normal motor cortex excitability [236], as well as cerebellothalamocortical excitability [219]. DBS stimulation of VIM is thought to

excite motor neurons directly, as assessed through greater MEP amplitudes at high TMS stimulation levels [191]. This points to the complexities of looking into connectivity and excitability with motor and sensory regions in these individuals. It is therefore important to extend these studies into individuals with neurotypical motor pathways. However, the fact that we are able to see effects in patients with both diseases, with no significant effect of the disease process on our statistical results, speaks to the generalizability of the phenomena that we are studying.

8.5 Conclusions

For the first time in humans, we measured intraoperative EPs, which are a marker of cortical excitability and connectivity, before and after a conditioning paradigm to induce plasticity during DBS surgery. We observed the greatest density of intraoperatively measured responses in premotor, motor, and sensory cortices, and we were able to modulate these EPs with paired-pulse conditioning protocols. In contrast to previous primate literature, there was greater potentiation at longer delays between stimulation sites, suggesting that the mechanisms responsible are less dependent on spike-timing dependent plasticity and rather on larger network scale phenomena due to the scale of our stimulation electrodes and larger areas of cortex targeted. There were not significant differences between different disease processes, suggesting that these are generalizable results not confined to one of these motor disorders, and that this protocol may help individuals suffering from diseases such as stroke and paralysis. We measured a greater effect of conditioning with longer conditioning protocols, suggesting there exists a total stimulation dosage effect. EP magnitudes during various levels of propofol and dexmedetomidine anesthesia do not significantly change, suggesting that intraoperative screening for EPs could be illustrative of connectivity during awake states. Therefore, intraoperative EP screening in individuals undergoing stimulator placement for a neuromodulation device may be a viable approach for mapping out cortical connections for

plasticity induction. In sum, these studies further our understanding of plasticity induction in humans, and pave the way for future exploration of how to enhance cortical connections in a rehabilitation context following neurological damage from diseases such as stroke.

8.6 Related Publications and Presentations

Caldwell DJ, Cronin JA, Paschall C, Brown A, Martinez V, Weaver KE, Perlmutter SI, Rao RPN, Ojemann JG, Ko AL, "Intracortical Paired Pulse Conditioning Paradigms for In-Vivo Plasticity Induction in Human", in preparation

Chapter 9

CONCLUSIONS

9.0.1 Review of Work

Direct electrical stimulation (DES) within a neural engineering context has the potential to restore sensation and enhance connectivity through in-dwelling intracranial electroencephalograpy (iEEG, also known as electroencephalography, or ECoG)) electrodes. This offers promise for ameliorating the sensory and motor deficits caused by damage to the nervous system due to stroke, spinal cord injury, and limb loss accounts. However, further clinical translation of DES requires that we understand how it spreads through cortex, how we can interpret of the underlying cortical dynamics in response to stimulation, the behavioral effects induced by it in regions such as sensory cortex, and how it can be employed in neuromodulation to induce neuronal plasticity. These elements are essential to properly engineer closed-loop functional neuroprosthetics for sensory restoration and neuromodulation for plasticity enhancement.

This work addresses a number of aspects of engineering DES of the human brain for neuroprosthetic applications. The focus of this research was stimulation of sensorimotor cortex, but the principles may apply to other brain regions for auditory or visual neuroprosthetics.

We first explored the physics of DES. Rather than focus on computationally intensive finite-element models, we used analytic models with different geometric assumptions to model the flow of current in the brain. We demonstrated that simple analytic models fit the experimentally measured and verified data well, and that the assumptions of flat or spherical geometry in these models impact the interpretation of the resistivity of the brains' con-

stituents. Similarly, for the first time in humans, we validated three different classic material characterization techniques (2, 3, and 4-point measurements) with clinical electrodes in a saline phantom to test their applicability to human measurements. We found that 2-point measurements through our electrodes do not accurately measure the underlying resistivity, while the 3 and 4-point measurements do. These results provide bounds on the apparent resistivity of the human brain as measured through clinical electrodes, data that further models should be validated against, and insight into the appropriate ways to measure the resistivity of cortical tissue.

Understanding the flow of current is one piece of engineering DES. Another is how to extract neural activity from neural recordings in the response to current flow from concurrent stimulation and recording. Prior work has explored this issue extensively for combinations of microelectrodes, concurrent EEG and DBS, and ECoG electrodes, in both non-human and human models. However, the availability of real human data against which these algorithms have been validated is sparse, as much of the existing work in the field uses synthetic data sets for validation. Additionally, many algorithms are demonstrated on a single channel basis. We therefore sought to develop and release code to process both DBS and ECoG stimulation human data, verified with expected biologic results from multiple subjects performing different motor and sensory tasks, that was optimized to perform well across an entire array of electrodes at once. This work helps establish a benchmark of in-vivo human neural data from multiple subjects, along with the implementation of different algorithms for others in the field to compare their own results against.

Two engineered applications of DES we then studied were stimulation of sensory cortex to restore sensation and stimulation of motor and motor adjacent cortical areas to induce plasticity.

Our sensory stimulation work revealed a significant delay in response times to DES relative to natural haptic touch [45]. We did not observe any learning over a two block window,

suggesting that the delay was not simply due to the electrical stimulus being novel. This delay, which varies by subject, is crucial to account for in future sensory neuroprosthetics, as if sensory feedback is processed too late to be integrated into ongoing decision making and motor planning, neuroprosthetic performance could suffer.

Based on these results, we then explored the behavioral effects of modified waveforms that better mimic the underlying activity in sensory cortex in response to touch, as well as what happens when natural touch and DES are applied in temporally and spatially overlapping windows. We discovered that modifications to constant train waveforms with initially high priming pulses were able to modify perception and response times, and that initial charge delivery within the first 10 ms may be a key part of encoding sensory information into the brain through DES and ECoG arrays. We additionally observed that spatially and temporally overlapping DES and haptic touch are able to be perceived independently, and that the point of subjective simultaneity (PSS), which is the point where either stimulus type has a 50% chance of being judged arriving first, recapitulates the delays observed for response times to DES. This importantly suggests for future neuroprosthetics that the brain regions can perform natural processing concurrently with receiving artificial feedback, and illustrates the tremendous flexibility of cortical circuitry.

To explore the induction of plasticity in cortex, we carried out a beta-oscillation triggered stimulation paradigm in epilepsy patients, and a paired-pulse stimulation paradigm in subjects with movement disorders undergoing DBS stimulator placement. These were protocols that were previously tested in NHP models, and we sought to extend these into humans in the next step towards clinical application in the treatment of individuals with stroke and paralysis.

Our beta-oscillation triggered paradigm induced short term plasticity (less than 2 seconds) as measured through CEPs by delivering stimulation during spontaneous beta-oscillations, that demonstrated a significant dose dependent conditioning effect, and an interaction effect

which led to the depolarizing phase of stimulation being more effective than the hyperpolarizing phase with greater numbers of conditioning pulses. We similarly saw an increase in evoked potentials during closed loop stimulation relative to open loop stimulation. These results build off of the prior NHP work, and provide a path forward for testing this protocol in humans with motor deficits to test for rehabilitative improvements.

Our paired-pulse stimulation paradigm demonstrated the optimal lag to induce plasticity as assessed through CEPs was longer than that predicted by the principles of spike timing dependent plasticity, or what had been found on a smaller spatial scale in NHPs. We found that paired site stimulation was more effective than stimulation within the same site, suggesting that paired-pulse stimulation protocols may be more effective for plasticity induction between sites than single site stimulation strengthening connections between regions a centimeter apart. Furthermore, we did not observe any significant impact of an individual's disease (Essential Tremor, Parkinson's, or Dystonia) on our results, indicating that these results should be generalizable to a larger population. Longer conditioning sessions resulted in greater potentiation of EPs, indicating that further studies into the optimal dose and duration protocol are necessary. In one patient woken up during surgery, we did not observe any significant impact of the depth of anesthesia under propofol and dexmedetomidine, suggesting that CEP screening to identify sites for plasticity induction could be be performed intraoperatively.

We have here both addressed a number of the fundamental engineering barriers to successful DES translation in humans, and paved the way for future explorations to more effectively provide sensory feedback and induce plasticity. The exploration of these barriers has revealed connections between the the various directions pursued. The analytic modeling work leads into the idea of targeted stimulation, where maximizing current delivery to a particular region of interest could more effectively accomplish the goals of sensory and plasticity inducing neuroprosthetics. Similarly, better algorithms to process the neural data in response to

stimulation allows us to tie together both behavior and the resultant neural signals from our engineered stimulation. The study of both sensory and motor cortex is intricately linked, due both to the extensive anatomical and functional connections between the two, and the idea that in a functional BCI neuroprosthetic with feedback the two systems work hand-in-hand. The principles of enhancing plasticity play a role in both parts of the cortex, as damage due to stroke can occur in both regions. Additionally, the enhancing of connectivity in sensory cortex could perhaps enhance the performance of sensory neuroprosthetics, and help a user more quickly learn to use stimulation as input.

9.0.2 Limitations of Current Studies

We acknowledge that there exist limitations with our results given our patient population. We worked with individuals who were receiving treatment for intractable epilepsy, or undergoing DBS stimulator placement for movements disorders such as Essential Tremor, Parkinson's disease, and Dystonia. Epilepsy, as a disease which causes seizures across cortical networks and disrupts their normal patterns of activity, could potentially influence both the behavior and neural signals recorded. However, for the epilepsy patients, we purposefully did not focus on stimulation of regions near the putative epilepsy focus, and we therefore believe these results to be generalizable to a healthy population. Further studies would need to be carried out in individuals without epilepsy for confirmation, but the use of S1 stimulation to successfully provide sensory feedback in tetraplegic individuals with ICMS [17, 90], and an individual with chronic somatosensory deficits with ECoG stimulation [119], supports the extensibility of DES for sensory neuroprosthetics.

Clinical ECoG electrodes are not the optimal electrodes for either sensory restoration or plasticity induction. Prior work has shown that single digit sensory discrimination can be achieved with smaller ECoG electrodes in humans [149]. ICMS in humans [90] appears to create even smaller percept areas than seen with microECoG arrays. Furthermore, although

not the focus of this work, the percepts created by clinical ECoG electrodes have never been described by our participants as natural, while ICMS in humans appears to result in more natural percepts [17, 90]. The results of the response timing, concurrent haptic and DES, and modified waveform experiments would need to be further explored in smaller ECoG arrays and penetrating arrays. However, even if technologies other than those implemented here are used for sensory neuroprosthetics, we believe our work establishes foundations for comparisons with existing clinical technologies and illustrates principles which need to be considered for effective sensory neuroprosthetic development.

Similarly, the electrodes are placed purely for the epilepsy patients' clinical needs, and our ECoG strip electrode placement during DBS surgery is limited by the burrhole placement for the DBS electrode. For the sensory stimulation work, this means that are electrodes are placed over Brodmann area 1 primarily, rather than directly in area 3b where the majority of thalamic projections relaying touch contact synapse [3]. Different percepts, or different behavioral results may be obtained with either penetrating electrodes, or ECoG electrodes placed more closely to area 3b.

For our DBS patients, Parkinson's disease, Essential Tremor, and dystonia are diseases that affect the thalamocortical loop and motor function. For instance, Parkinson's disease affects motor cortical excitability by inhibiting corticortical inhibition [234]. In contrast, Essential Tremor patients are thought to have normal motor cortex excitability [236], as well as cerebellothalamocortical excitability [219]. There are therefore complex disease process effects in the regions that we stimulated, and this points to the importance of extending these studies into healthy individuals. However, the fact that we are able to see effects in patients with both disease, with no significant effect of the disease process on our statistical results, speaks to the generalizability of the phenomena that we are studying.

The extent to which modulation of our observed CEPs correlates with rehabilitative recovery is an open question, and cannot be addressed within the confines of our patient

population. This is multifaceted, as we are limited in the duration of stimulation with our patients (at most a few hours for a single day), and our patients are not representative of the disorders which we seek to treat with neuroprosthetics (for example, limb loss, stroke, and paralysis). To our knowledge, there have not been extensive studies in directly correlating implanted electrode measured EP changes and functional recovery, which are needed to validate the use of EPs as a marker for plasticity induction. Short-latency paired stimulation protocols in rats have demonstrated a relation between inferred neural functional connectivity and an altered perceptual threshold [231], while activity dependent stimulation in rats to route information around damaged primary motor cortex demonstrated both increases in functional connectivity as assessed through changes in spiking and improved functional recovery [103]. This suggests that modulations of neural activity measured via electrophysiology do have meaningful functional consequences. In humans, an associative EEG based BCI with peripheral nerve stimulation resulted in both enhanced MEPs and functional improvements, suggesting a link between markers of cortical excitability and recovery [195].

Our methods for marking touch onset in the sensory experiments are inherently noisy, due to the mechanical deflection required for touch registration which can vary from trial to trial, experimenter variability, and may be perceived at different times depending on the individual and the location of touch. Our characterization of our devices leads us to believe that the results we measure are orders of magnitude greater than the error in our measurements, but we nevertheless acknowledge this source of variability in our experiments.

For both our analytic models to understand the spread of current in the cortex, and our data driven signal processing approaches, there are a number of methodological and technical constraints.

When considering the use of analytic models, there is an unavoidable element of uncertainty in localizing the electrodes. This is because we use preoperative MRI to reconstruct the cortical cortex, and postoperative CT to localize the electrodes. The merging of the

two modalities is a compromise between the physical constraints imposed by the electrode arrays and the geometry of the cortex. Brain shift following surgery can be significant, and our stimulation sessions are often seven days following implantation, during which further changes can occur. This is therefore not an issue that could be solved be simply taking a postoperative MRI in addition to the preoperative MRI. As we use the electrode positions in our models, and calculate the appropriate spherical geometries from the cortical surfaces, the errors propagate into our models. We do not believe this to be a critical flaw, as we use the CT electrode coordinates, which maintain the physical spacing of the electrodes better than the reconstructed electrodes. Our inability precisely localize the electrodes reduces the insight we can gain into the precise composition of cortical layers beneath the electrodes. The amount of CSF, which can shunt significant amounts of current in a thick enough layer [202], is very difficult to determine on a per-electrode and array-wide basis. This is a greater issue for finite-element models, which rely upon the precise reconstructed geometry beneath the electrodes, but we acknowledge these limitations as well. Although we validated our 2,3, and 4-point measurements in saline, we acknowledge that clinical ECoG electrodes are not ideal for making resistivity measurements. The 2.3 mm diameter electrodes do not allow for focal measurements to the degree penetrating arrays would, and the clinical cables are not shielded to eliminate all possible cross-talk contributions [203] and capacitive coupling.

Due to the time-varying, complex electrochemical interface between the stimulation electrodes and the tissue interface [181], as well as spatial recording electrode dependent differences, precisely characterizing all of the electrical artifacts and differentiating them from neural data across an array is a challenge. Similarly, predicting what the expected neural response to a train of stimuli should be is a difficult task, as there exist time-varying responses to individual stimuli, responses to the train as a whole, and ongoing background neural activity. Characterization in saline is insufficient to accurately measure what precisely will occur in the brain, and stimulating at low levels in-vivo to measure the artifact without resultant

stimulation elicited neural activity would not completely capture the nature of the artifact at a higher stimulation level, and this approach still does not discount the background neural activity. Therefore, both model based approaches and data driven approaches are bound to imperfectly recover the underlying neural activity. We do not claim to perfectly extract neural activity with our methods, and as demonstrated, incomplete signal extraction can occur. Rather, we highlight an approach that works well as tested on multiple datasets, and recovers what we believe to be meaningful neural activity as validated against expected ground truth neural activity during discrete tasks.

9.0.3 Future Directions and New Technologies

Our work in analytic models to understand the spread of current in cortex could be extended in the future to explore additional geometries (prolate spheroidal models, for instance [287]), as well as multilayer models to isolate the effects of different cortical layers [249]. Finite-element models (FEM), despite their computational complexity, offer advantages in modeling the voltages and currents at sulci, gyri, and in the different constituents such as CSF, white, and gray matter [252]. FEM based models also offer the ability to incorporate optimization based approaches to better target particular regions of the brain [104]. Making measurements of stimulation voltages on amplifiers that have a large linear dynamic range and do not saturate, as done here, along with a baseline comparison in an easily computable analytic model, will allow for comparisons with these more computationally intensive FEM models. Incorporating biologically realistic neuron models into stimulation modeling [144, 252], with patient specific anatomy as explored with DBS electrodes [55], will allow for new opportunities in individually tailored neuromodulation and neuroprosthetic targeting. Concurrent measuring of the evoked responses or behavioral data in a closed loop fashion, with an optimization routine to best target a desired cortical region or network, would increase the efficacy of sensory neuroprosthetics and plasticity induction.

The DBS field is replete with examples of new modeling techniques to optimize stimulation of deep cortical targets. These advances could carry over more generally to DES in ECoG-BCIs. Patient specific models of the volume of tissue activated (VTA) enable better understanding of the effects of stimulation at various locations in a given individual [44]. With the advent of electrodes with many contacts and different geometries, an open question is how to best target the region of interest. Recent algorithmic advances combine electrodes with different contact geometries, including cylindrical and directional leads, and patient specific models, including tissue anisotropy, to best target the sub-thalamic nucleus (STN) [13]. A multi-objective particle swarm optimization technique to select a combination of stimulation electrodes was found to be more effective than a single monopolar electrode in targeting the desired efferents from the STN [217]. As ECoG electrodes become smaller and more numerous, algorithmic techniques such as the ones described above and more advanced ones based on artificial neural networks [229] would enable precisely targeted DES with the right combination of electrodes.

Modern methods in simulation and machine learning will drive further advances in the analysis of concurrent recording and stimulation, Beyond the data driven approaches outlined in this work, a combination of model-based [275, 288]. and data driven approaches would help construct a more principled set of templates to separate neural activity from electrical artifacts. Deep learning, which has found great success in text translation, image recognition, and audio settings, is finding applications in signal processing [312] and ECoG processing [291]. If enough training data were available, perhaps enabled by institutions pooling together their data, these methods could aid the artifact processing community. A complementary, valuable approach would be front-end, hardware based artifact cancellation, which is currently being explored for ICMS in humans [296] and in DBS platforms [116]. Integration with multichannel ECoG arrays would mitigate the artifact on the front-end signal acquisition side. However, front end artifact processing does not obviate the need for

back-end approaches, as residual artifacts exist even with front-end approaches [316]. We think therefore optimal results will be achieved in the future using a combination of front-end and back-end approaches in ECoG arrays.

We have primarily focused on the behavioral responses to sensory stimulation in this work. We have developed tools to enable the analysis of the neural data resulting from these experiments, but the interpretation of these results is compromised by the limited number of subjects and lack of overlapping cortical regions. Adequate spatial sampling of different cortical regions involved in decision making and downstream sensory processing consistently across subjects would enable a nuanced look into the different perceptual. Electrodes in secondary somatosensory cortex, frontal regions, and hippocampal areas would all provide further context into how individuals process these signals beyond simple recognition, and reveal the neural substrate for decision making and learning these artificial percepts. As depth electrodes become more common for the monitoring of epilepsy, we will be able to gain insight into many of these regions.

Putative regions, as assessed through fMRI, that would be important for better understanding the temporal order judgment (TOJ) results would include left ventral, bilateral dorsal premotor cortex, and left posterior parietal cortex for areas of activation specific to a temporal order judgment task. These areas are known to be part of the motor and perception temporal prediction network [190]. Furthermore, the bilateral premotor cortices, the bilateral middle frontal gyri, the bilateral inferior parietal cortices and supramarginal gyri, and the bilateral posterior part of the superior and middle temporal gyri all were shown to be preferentially activated in a TOJ task compared to a numerosity task, as assessed by fMRI [269]. As more subjects are implanted with greater numbers of electrodes across different cortical regions, we may be able to gain insight into these processing mechanisms previously observed primarily through fMRI.

We only studied the responses to human applied mechanical touch sensations. The dif-

ferent neural representations of texture in NHPs has been demonstrated to be rich and high dimensional, reflecting the complex percepts that exist for different textures [162], and we think that similar studies in humans would provide additional insight into how humans process different textures, and enable self-reports of the experience to see how finely humans can distinguish these textures. Regarding neural input, different stimulation waveform parameters in peripheral nerve stimulation have been able to modulate the textures which uses feel [208, 270]. Focusing on exploring how different textures could be encoded through DES in humans would open up additional axes of manipulation for sensory neuroprosthetics, and is part of the concept of biomimetic stimulation.

Touch application devices that better allowed for consistent force application, as well as different sensations such as vibration, would enable complementary insight into the precise timing of behavioral and neural responses, and may allow for analysis methods such as phase amplitude coupling to study relationships between different frequency bands. One such device could be a device that delivers a puff of air upon triggering, although the additional auditory stimulus would be an additional confounder. Vibratory devices pressed up against the skin would enable precise triggering, but there would always be a baseline level of contact, and potential signal interference. Actuator based devices would enable controlled contact, but these can be noisy, and it would be complex to ensure that the stimulus could be delivered to the same spatial spot where the focal sensations were elicited.

Biomimetic stimulation and adaptation are two complementary approaches for future sensory neuroprosthetics [23]. As discussed above, natural textures can be encoded via appropriate stimulation. It remains to be seen if clinical ECoG electrodes are capable of the same degree of percept modulation, but the principles are worth further exploration. The development and implementation of ECoG arrays with smaller electrodes and tighter spacing, which have already been used to delivery more finely patterned percepts [149], provides support for the utility of studying these with smaller ECoG arrays. Smaller percepts, for

tasks such as object manipulation, would be progress towards more biomimetic stimulation.

Adaptation utilizes an individual's ability to learn to use a novel stimulus. This has been demonstrated in rodents who used stimulation in S1 to learn to respond to invisible infrared light [273], and in primates using feedback delivered by ICMS to guide a motor task [65]. On a biological level of adaptation, sensory cortex exhibits plasticity where following neurological damage, regions adjacent to the damaged region undergo remapping to process sensory signals from the lost regions [39]. Afferent sensory signals themselves can result in plasticity changes [67], and a well known example is humans is the reorganization of the cortical representation of fingers in Braille readers [67]. More concretely studying plasticity, perhaps as measured through evoked potentials in sensory cortex, concurrently with the learning of the use of a sensory neuroprosthetic, would provide insight into the mechanisms and most efficacious ways to implement stimulation for sensory restoration.

As mentioned above, ECoG arrays with tighter electrode spacing are under development. Advances in materials science and electronics are enabling the creation of robust intracranial arrays with thousands of electrode contacts, with closer spacing than is currently used clinically. Current ECoG arrays based on silicone and platinum have been extended to microECoG arrays [54]. Further reductions in electrode diameter and increases in array density are enabled by micromanufacturing techniques, and in particular, microelectricomechanical systems (MEMS) technologies. Platinum electrodes and polyimide foil substrates similarly have been patterned using micromachining, allowing for electrode contact diameters of 1 mm with electrode spacings between 2 and 3 mm [241]. Through these MEMS technologies, electrode arrays with tighter spacings and smaller diameters can be constructed and placed across large regions of cortex and within sulci (Fukushima et al. 2014). Fukushima et al. created an array with 0.8 mm diameter electrodes and 1.8 mm spacing [95].

MicroECoG arrays have recently been used to resolve finer features of cortical activity, particularly in the broadband gamma range, for measurement of phonetic features in single

electrodes [182]. Arrays with electrode diameters of 0.87 mm and spacings of 1.68 mm have resolved cortical activity patterns with response peaks less than the standard clinical spacing of 1 cm apart, pointing to the advantages seen with smaller electrode arrays [292].Novel, thin film MEMS arrays are being implanted in humans [197], illustrating the translation of these materials and manufacturing techniques to humans. The ability to place more electrodes within a given area could allow for finer patterning of stimulation.

Advances in materials science are enabling electrodes and arrays made of other materials, such as glassy carbon [102, 131]. Glassy carbon electrodes have higher charge injection capacities (CIC, which is the amount of charge that can be injected before irreversible chemical reactions take place) than traditional platinum electrodes, and require less stimulation current to activate neurons [131]

Combinations of ECoG and penetrating electrode arrays are also being constructed for recording and stimulating both surface and deeper structures simultaneously [102, 139, 211]. Currently being used in animal models, such arrays will open the door to a better understanding of network-wide and across cortex effects of stimulation.

For the plasticity induction protocols, as mentioned in the limitations section, the degree of overlap between potentiation of CEPs and positive rehabilitation needs to be determined. These questions cannot be adequately addressed in our patient population, and the testing of these protocols should be translated into humans with sensory and motor deficits over a longer term period. Questions of the optimal duration of stimulation are yet to be addressed, as prior work in six individuals with stroke treated epidural cortical stimulation found that less than four hours of stimulation a day resulted in motor improvements, while longer durations resulted in increases in spasticity [307]. This makes clear the need for further research into how long cortical conditioning sessions should be. As activity dependent stimulation demonstrates clear advantages over open-loop stimulation, the amount of time for maximal recovery may depend on exactly when stimulation is delivered, rather than simply the total

duration for which it is delivered.

An interesting extension enabled by working with individuals implanted with DBS electrodes is the effect of DBS stimulation on motor cortical excitability and potentials. Stimulating VIM in patients with Essential Tremor has been shown to increase MEP magnitude [191], and future research could explore the effect of thalamocortical neuromodulation on plasticity induction.

Recent advances in hardware have allowed both real time artifact cancellation and wireless communication with 128 channels of local field potential recording in NHPs [317]. Other implantable devices with microelectrode arrays in NHP model have included wireless charging and data transfer capabilities [35], which are critical for an out-of-hospital device. The development of wireless technologies, as well as real time simultaneous stimulation and recording techniques, opens the door to explorations of the neural basis of naturalistic behavior and long-term effects of closed-loop stimulation. Recent work in non-human primates has demonstrated both wireless recording and stimulation of motor regions over a 6 month time period, with no observed neurological or behavioral consequences [235]. This points to the future translatability of wireless long-term ECoG implants with both recording and stimulation. Such implants would be useful for both sensory and motor neuroprosthetics.

9.1 Related Publications and Presentations

Caldwell DJ, Ojemann JG, Rao RPN, "Direct Electrical Stimulation in Electrocorticographic Brain-Computer Interfaces: Enabling Technologies for Input to Cortex", Frontiers in Neuroscience, Neuroprosthetics, In revision, 2019.

BIBLIOGRAPHY

[1] Semiconductor Measurement Technology: Spreading Resistance Symposim. In James R Ehrstein, editor, *NBS Special Publication 400-10*, 1974.

[2] Seminconductor Measurement Technology: Spreading Resistance Analysis for Silicon Layers with Nonuniform Resistivity. In David H Dickey and James R Ehrstein, editors, *NBS Special Publication 400-48*. Elsevier, 1979.

[3] Rochelle Ackerley and Anne Kavounoudias. The role of tactile afference in shaping motor behaviour and implications for prosthetic innovation. *Neuropsychologia*, 79:192–205, 2015.

[4] DeAnna L Adkins, Jeffery Boychuk, Michael S Remple, and Jeffrey A Kleim. Motor training induces experience-specific patterns of plasticity across motor cortex and spinal cord. *Journal of applied physiology (Bethesda, Md. : 1985)*, 101(6):1776–1782, nov 2006.

[5] DeAnna L. Adkins, J. Edward Hsu, and Theresa A. Jones. Motor cortical stimulation promotes synaptic plasticity and behavioral improvements following sensorimotor cortex lesions. *Experimental Neurology*, 212(1):14–28, jul 2008.

[6] DeAnna L Adkins-Muir and Theresa a Jones. Cortical electrical stimulation combined with rehabilitative training: enhanced functional recovery and dendritic plasticity following focal cortical ischemia in rats. *Neurological research*, 25(8):780–788, 2003.

[7] E. D. Adrian. The spread of activity in the cerebral cortex. *The Journal of Physiology*, 88(2):127–161, nov 1936.

[8] Saeed Aghabozorgi, Ali Seyed Shirkhorshidi, and Teh Ying Wah. Time-series clustering - A decade review. *Information Systems*, 53:16–38, 2015.

[9] Tarik Al-ani, Fanny Cazettes, Stéphane Palfi, and Jean Pascal Lefaucheur. Automatic removal of high-amplitude stimulus artefact from neuronal signal recorded in the subthalamic nucleus. *Journal of Neuroscience Methods*, 198(1):135–146, 2011.

[10] Sankaraleengam Alagapan, Hae Won Shin, Flavio Fröhlich, and Hau-tieng Wu. Diffusion geometry approach to efficiently remove electrical stimulation artifacts in intracranial electroencephalography. *Journal of Neural Engineering*, 2018.

[11] David P. Allen, Elizabeth L. Stegemöller, Cindy Zadikoff, Joshua M. Rosenow, and Colum D. MacKinnon. Suppression of deep brain stimulation artifacts from the electroencephalogram by frequency-domain Hampel filtering. *Clinical Neurophysiology*, 121(8):1227–1232, 2010.

[12] A Alonso, M De Curtis, and R Llinast. Postsynaptic Hebbian and non-Hebbian long-term potentiation of synaptic efficacy in the entorhinal cortex in slices and in the isolated adult guinea pig brain (synaptic plasticity/intracellular recording/N-methyl-n-aspartate/ionic channels). *Neurobiology*, 87(December):9280–9284, 1990.

[13] Daria Nesterovich Anderson, Braxton Osting, Johannes Vorwerk, Alan D. Dorval, and Christopher R. Butson. Optimized programming algorithm for cylindrical and directional deep brain stimulation electrodes. *Journal of Neural Engineering*, 15(2), 2018.

[14] Kim D Anderson. Targeting Recovery: Priorities of the Spinal Cord-Injured Population. *Journal of Neurotrauma*, 21(10):1371–1383, oct 2004.

[15] A. ANGEL and DENISE A GRATTON. THE EFFECT OF ANAESTHETIC AGENTS ON CEREBRAL CORTICAL RESPONSES IN THE RAT. *British Journal of Pharmacology*, 76(4):541–549, aug 1982.

[16] Charles Arber and Meng Li. Cortical interneurons from human pluripotent stem cells: prospects for neurological and psychiatric disease. *Frontiers in Cellular Neuroscience*, 7(March):1–11, 2013.

[17] Michelle Armenta Salas, Luke Bashford, Spencer Kellis, Matiar Jafari, HyeongChan Jo, Daniel Kramer, Kathleen Shanfield, Kelsie Pejsa, Brian Lee, Charles Y Liu, and Richard A Andersen. Proprioceptive and cutaneous sensations in humans elicited by intracortical microstimulation. *eLife*, 7:1–11, 2018.

[18] L. Bashford, J. Wu, D. Sarma, K. Collins, R. P.N. Rao, J. G. Ojemann, and C. Mehring. Concurrent control of a brain-computer interface and natural overt movements. *Journal of Neural Engineering*, 15(6), 2018.

[19] Stephen B. Baumann, David R. Wozny, Shawn K. Kelly, and Frank M. Meno. The electrical conductivity of human cerebrospinal fluid at body temperature. *IEEE Transactions on Biomedical Engineering*, 44(3):220–223, 1997.

[20] Bruce P. Bean. The action potential in mammalian central neurons. *Nature Reviews Neuroscience*, 8(6):451–465, 2007.

[21] M R Behrend, a K Ahuja, and J D Weiland. Dynamic Curent Density of the Disk Electrode Double-Layer. *IEEE T Bio-Med Eng*, 55(3):1056–1062, 2008.

[22] Sliman J Bensmaia. Biological and bionic hands : natural neural coding and artificial perception. *Philosophical Transactions Royal Society, B*, 370(figure 1):20140209, 2015.

[23] Sliman J Bensmaia and Lee E Miller. Restoring sensorimotor function through intracortical interfaces: progress and looming challenges. *Nature reviews. Neuroscience*, 15(5):313–25, 2014.

[24] Philipp Berens, Kenneth Baclawski, Philipp Berens, and Kenneth Baclawski. CircStat: A MATLAB Toolbox for Circular Statistics. *Journal of Statistical Software*, 30(April):1–3, 2009.

[25] Mitchel S. Berger, Joseph Kincaid, George A. Ojemann, and Ettore Lettich. Brain Mapping Techniques to Maximize Resection, Safety, and Seizure Control in Children with Brain Tumors. *Neurosurgery*, 25(5):786–792, nov 1989.

[26] Mitchel S. Berger and George A. Ojemann. Intraoperative Brain Mapping Techniques in Neuro-Oncology. *Stereotactic and Functional Neurosurgery*, 58(1-4):153–161, 1992.

[27] G Q Bi and M M Poo. Synaptic modifications in cultured hippocampal neurons: dependence on spike timing, synaptic strength, and postsynaptic cell type. *The Journal of neuroscience : the official journal of the Society for Neuroscience*, 18(24):10464–10472, 1998.

[28] Elaine Biddiss, Dorcas Beaton, and Tom Chau. Consumer design priorities for upper limb prosthetics. *Disability and Rehabilitation: Assistive Technology*, 2(6):346–357, jan 2007.

[29] Tim Blakely, Kai J Miller, Stavros P Zanos, Rajesh P N Rao, and Jeffrey G Ojemann. Robust, long-term control of an electrocorticographic brain-computer interface with fixed parameters. *Neurosurgical Focus*, 27(1):E13, jul 2009.

[30] T. V. P. Bliss and T. Lomo. Long-lasting poteniation of synpatic transmission in the dentate area of the anaesthetized rabbit following stimulation fo the perforant path. *J Physiol.*, 232:331–356, 1973.

[31] Nadia Bolognini, Cristina Russo, and Dylan J. Edwards. The sensory side of post-stroke motor rehabilitation. *Restorative Neurology and Neuroscience*, 34(4):571–586, aug 2016.

[32] P. Boon, K. Vonck, T. Vandekerckhove, M. D'have, L. Nieuwenhuis, G. Michielsen, H. Vanbelleghem, I. Goethals, J. Caemaert, L. Calliauw, and J. De Reuck. Vagus nerve stimulation for medically refractory epilepsy; efficacy and cost-benefit analysis. *Acta Neurochirurgica*, 141(5):447–453, 1999.

[33] Svenja Borchers, Marc Himmelbach, Nikos Logothetis, and Hans-Otto Karnath. Direct electrical stimulation of human cortex — the gold standard for mapping brain functions? *Nature reviews. Neuroscience*, 13(1):63–70, nov 2012.

[34] M. R. Borich, S. M. Brodie, W. A. Gray, S. Ionta, and L. A. Boyd. Understanding the role of the primary somatosensory cortex: Opportunities for rehabilitation. *Neuropsychologia*, 79:246–255, 2015.

[35] David A Borton, Ming Yin, Juan Aceros, and Arto Nurmikko. An implantable wireless neural interface for recording cortical circuit dynamics in moving primates. *Journal of Neural Engineering*, 10(2):026010, apr 2013.

[36] Kristofer E Bouchard, Nima Mesgarani, Keith Johnson, and Edward F Chang. Functional organization of human sensorimotor cortex for speech articulation. *Nature*, 495(7441):327–32, 2013.

[37] J. Brill and J. R. Huguenard. Robust Short-Latency Perisomatic Inhibition onto Neocortical Pyramidal Cells Detected by Laser-Scanning Photostimulation. *Journal of Neuroscience*, 29(23):7413–7423, 2009.

[38] Jeff M. Bronstein, Michele Tagliati, Ron L. Alterman, Andres M. Lozano, Jens Volkmann, Alessandro Stefani, Fay B. Horak, Michael S. Okun, Kelly D. Foote, Paul Krack, Rajesh Pahwa, Jaimie M. Henderson, Marwan I. Hariz, Roy A. Bakay, Ali Rezai, William J. Marks, Elena Moro, Jerrold L. Vitek, Frances M. Weaver, Robert E. Gross, and Mahlon R. DeLong. Deep Brain Stimulation for Parkinson Disease. *Archives of Neurology*, 68(2):165–171, feb 2011.

[39] C. E. Brown, K. Aminoltejari, H. Erb, I. R. Winship, and T. H. Murphy. In Vivo Voltage-Sensitive Dye Imaging in Adult Mice Reveals That Somatosensory Maps Lost to Stroke Are Replaced over Weeks by New Structural and Functional Circuits with Prolonged Modes of Activation within Both the Peri-Infarct Zone and Distant Sites. *Journal of Neuroscience*, 29(6):1719–1734, 2009.

[40] Morton B. Brown and Alan B. Forsythe. Robust Tests for the Equality of Variances. *Journal of the American Statistical Association*, 69(346):364–367, jun 1974.

[41] Andreas Bruns. Fourier-, Hilbert- and wavelet-based signal analysis: are they really different approaches? *Journal of neuroscience methods*, 137(2):321–32, aug 2004.

[42] Cathrin Buetefisch, Roman Heger, Wilfried Schicks, Rudiger Seitz, and Johannes Netz. Hebbian-type stimulation during robot-assisted training in patients with stroke. *Neurorehabilitation and neural repair*, 25(7):645–55, 2011.

[43] Sergejus Butovas and Cornelius Schwarz. Spatiotemporal effects of microstimulation in rat neocortex: a parametric study using multielectrode recordings. *Journal of neurophysiology*, 90(5):3024–39, 2003.

[44] Christopher R. Butson, Scott E. Cooper, Jaimie M. Henderson, and Cameron C. McIntyre. Patient-specific analysis of the volume of tissue activated during deep brain stimulation. *NeuroImage*, 34(2):661–670, 2007.

[45] David J. Caldwell, Jeneva A. Cronin, Jing Wu, Kurt E. Weaver, Andrew L. Ko, Rajesh P. N. Rao, and Jeffrey G. Ojemann. Direct stimulation of somatosensory cortex results in slower reaction times compared to peripheral touch in humans. *Scientific Reports*, 9(1):3292, 2019.

[46] Thierri Callier, Aneesha K Suresh, and Sliman J Bensmaia. Neural Coding of Contact Events in Somatosensory Cortex. *Cerebral Cortex*, pages 1–15, 2018.

[47] Ricardo J G B Campello, Davoud Moulavi, and Joerg Sander. Density-Based Clustering Based on Hierarchical Density Estimates. In Jian Pei, Vincent S Tseng, Longbing Cao, Hiroshi Motoda, and Guandong Xu, editors, *Advances in Knowledge Discovery and Data Mining*, pages 160–172, Berlin, Heidelberg, 2013. Springer Berlin Heidelberg.

[48] Pedro Cardoso-Leite, Andrei Gorea, and Pascal Mamassian. Temporal order judgment and simple reaction times: Evidence for a common processing system. *Journal of Vision*, 7(6):11, apr 2007.

[49] Christophe Carel, Isabelle Loubinoux, Kader Boulanouar, Claude Manelfe, Olivier Rascol, Pierre Celsis, and François Chollet. Neural Substrate for the Effects of Passive Training on Sensorimotor Cortical Representation: A Study with Functional Magnetic Resonance Imaging in Healthy Subjects. *Journal of Cerebral Blood Flow & Metabolism*, 20(3):478–484, mar 2000.

[50] Andres Carvallo, Julien Modolo, Pascal Benquet, Stanislas Lagarde, Fabrice Bartolomei, and Fabrice Wendling. Biophysical modeling for brain tissue conductivity estimation using sEEG electrodes. *IEEE Transactions on Biomedical Engineering*, PP:1, 2018.

[51] CDC. Stroke Facts, 2015.

[52] C Cedzich, M Taniguchi, S Schafer, and J Schramm. Somatosensory evoked potential phase reversal and direct motor cortex stimulation during surgery in and around the central region. *Neurosurgery*, 38(5):962–970, 1996.

[53] Edward F. Chang. Towards large-scale, human-based, mesoscopic neurotechnologies. *Neuron*, 86(1):68–78, 2015.

[54] Zenas C Chao, Yasuo Nagasaka, and Naotaka Fujii. Long-term asynchronous decoding of arm motion using electrocorticographic signals in monkey. *Frontiers in Neuroengineering*, 3(March), 2010.

[55] Ashutosh Chaturvedi, Christopher R. Butson, Scott F. Lempka, Scott E. Cooper, and Cameron C. McIntyre. Patient-specific models of deep brain stimulation: Influence of field model complexity on neural activation predictions. *Brain Stimulation*, 3(2):65–77, 2010.

[56] Breanne P. Christie, Emily Lauren Graczyk, Hamid Charkhkar, Dustin J Tyler, and Ronald J Triolo. Visuotactile synchrony of stimulation-induced sensation and natural somatosensation. *Journal of Neural Engineering*, pages 11–14, apr 2019.

[57] Christopher & Dana Reeve Foundation. Stats about paralysis, 2013.

[58] Robert J. Coffey. Deep brain stimulation devices: A brief technical history and review. *Artificial Organs*, 33(3):208–220, 2009.

[59] Stuart F Cogan, Kip A Ludwig, Cristin G Welle, and Pavel Takmakov. Tissue damage thresholds during therapeutic electrical stimulation. *Journal of neural engineering*, 13(2):021001, jan 2016.

[60] Jennifer L Collinger, Michael L Boninger, Tim M Bruns, Kenneth Curley, Wei Wang, and Douglas J Weber. Functional priorities, assistive technology, and brain-computer interfaces after spinal cord injury. *Journal of rehabilitation research and development*, 50(2):145–60, 2013.

[61] Kelly L Collins, Arvid Guterstam, Jeneva Cronin, Jared D Olson, H Henrik Ehrsson, and Jeffrey G Ojemann. Ownership of an artificial limb induced by electrical brain stimulation. *Proceedings of the National Academy of Sciences*, 114(1):166–171, jan 2017.

[62] D J Crammond and J F Kalaska. Prior information in motor and premotor cortex: activity during the delay period and effect on pre-movement activity. *Journal of neurophysiology*, 84(2):986–1005, 2000.

[63] Jeneva A. Cronin, Jing Wu, Kelly L. Collins, Devapratim Sarma, Rajesh P. N. Rao, Jeffrey G. Ojemann, and Jared D. Olson. Task-Specific Somatosensory Feedback via Cortical Stimulation in Humans. *IEEE Transactions on Haptics*, 1412(c), 2016.

[64] Lawrence J Crowther, Peter Brunner, Christoph Kapeller, Christoph Guger, Kyousuke Kamada, Marjorie E Bunch, Bridget K Frawley, Timothy M Lynch, Anthony L Ritaccio, and Gerwin Schalk. A quantitative method for evaluating cortical responses to electrical stimulation. *Journal of neuroscience methods*, 311(July 2018):67–75, 2018.

[65] Maria C Dadarlat, Joseph E O'Doherty, and Philip N Sabes. A learning-based approach to artificial sensory feedback leads to optimal integration. *Nature Neuroscience*, 18(1):138–144, jan 2015.

[66] Yang Dan and Mu Ming Poo. Spike timing-dependent plasticity of neural circuits. *Neuron*, 44(1):23–30, 2004.

[67] C Darian-Smith. Plasticity of somatosensory function during learning, disease and injury. 2008.

[68] Alireza Dastan. Gaussian and mean curvatures calculation on a triangulated 3d surface, 2017.

[69] Karl Deisseroth. Optogenetics. *Nature Methods*, 8(1):26–29, jan 2011.

[70] Benoit P. Delhaye, Katie H. Long, and Sliman J. Bensmaia. Neural Basis of Touch and Proprioception in Primate Cortex. *Comprehensive Physiology*, 8(October):1575–1602, 2018.

[71] Benoit P. Delhaye, Hannes P. Saal, and Sliman J. Bensmaia. Key considerations in designing a somatosensory neuroprosthesis. *Journal of Physiology Paris*, pages 1–7, 2016.

[72] Eliana Della Flora, Caryn L. Perera, Alun L. Cameron, and Guy J. Maddern. Deep brain stimulation for essential tremor: A systematic review. *Movement Disorders*, 25(11):1550–1559, 2010.

[73] Alexis Dinno and H Joseph Newton. Nonparametric Pairwise Multiple Comparisons in Independent Groups Using Dunn ' s Test. *Stata Journal*, pages 292–300, 2015.

[74] Robert McKellar Douglas. Long lasting synaptic potentiation in the rat dentate gyrus following brief high frequency stimulation. *Brain Research*, 126(2):361–365, 1977.

[75] M. A. Edwardson, T. H. Lucas, J. R. Carey, and E. E. Fetz. New modalities of brain stimulation for stroke rehabilitation. *Experimental Brain Research*, 224(3):335–358, feb 2013.

[76] James R Ehrstein. Two-Probe (Spreading Resistance) Measurements for Evaluation of Semiconductor Materials and Devices. In Jay N Zemel, editor, *Nondestructive Evaluation of Semiconductor Materials and Devices*, volume 3, pages 1–66. Springer US, Boston, MA, 1979.

[77] Thomas Elbert, Annette Sterr, Herta Flor, Brigitte Rockstroh, Stefan Knecht, Christo Pantev, Christian Wienbruch, and Edward Taub. Input-increase and input-decrease types of cortical reorganization after upper extremity amputation in humans. *Experimental Brain Research*, 117(1):161–164, 1997.

[78] G A El'kina and V D Trush. Effect of level of spatial synchronization of cortical potentials on spread of evoked responses to cortical electrical stimulation. *Neuroscience and behavioral physiology*, 12(4):301, 1982.

[79] Rei Enatsu, Zhe Piao, Timothy O'Connor, Karl Horning, John Mosher, Richard Burgess, William Bingaman, and Dileep Nair. Cortical excitability varies upon ictal onset patterns in neocortical epilepsy: A cortico-cortical evoked potential study. *Clinical Neurophysiology*, 123(2):252–260, 2012.

[80] Dario J. Englot and Edward F. Chang. Rates and predictors of seizure freedom in resective epilepsy surgery: an update. *Neurosurgical Review*, 37(3):389–405, jul 2014.

[81] László Entz, Emília Tóth, Corey J. Keller, Stephan Bickel, David M. Groppe, Dániel Fabó, Lajos R. Kozák, Loránd Eross, István Ulbert, and Ashesh D. Mehta. Evoked effective connectivity of the human neocortex. *Human Brain Mapping*, 00(March), 2014.

[82] Yaara Erez, Hadass Tischler, Anan Moran, and Izhar Bar-Gad. Generalized framework for stimulus artifact removal. *Journal of Neuroscience Methods*, 191(1):45–59, 2010.

[83] Emad N. Eskandar, Alice Flaherty, G. Rees Cosgrove, Leslie A. Shinobu, and Fred G. Barker. Surgery for Parkinson disease in the United States, 1996 to 2000: practice patterns, short-term outcomes, and hospital charges in a nationwide sample. *Journal of Neurosurgery*, 99(5):863–871, 2009.

[84] Martin Ester, Hans-Peter Kriegel, Jörg Sander, and Xiaowei Xu. A Density-based Algorithm for Discovering Clusters a Density-based Algorithm for Discovering Clusters in Large Spatial Databases with Noise. In *Proceedings of the Second International Conference on Knowledge Discovery and Data Mining*, volume 70 of *KDD'96*, pages 156–7. Elsevier, mar 1996.

[85] Daniel E. Feldman. The Spike-Timing Dependence of Plasticity. *Neuron*, 75(4):556–571, 2012.

[86] Dirk Feldmeyer and Bert Sakmann. Synaptic efficacy and reliability of excitatory connections between the principal neurones of the input (layer 4) and output layer (layer 5) of the neocortex. *The Journal of Physiology*, 525(1):31–39, may 2000.

[87] Elodie Fino, Adam M. Packer, and Rafael Yuste. The logic of inhibitory connectivity in the neocortex. *Neuroscientist*, 19(3):228–237, 2013.

[88] Elodie Fino and Rafael Yuste. Dense inhibitory connectivity in neocortex. *Neuron*, 69(6):1188–1203, 2011.

[89] Paul B. Fitzgerald, Sarah Fountain, and Zafiris J. Daskalakis. A comprehensive review of the effects of rTMS on motor cortical excitability and inhibition. *Clinical Neurophysiology*, 117(12):2584–2596, 2006.

[90] Sharlene N Flesher, Jennifer L Collinger, Stephen T Foldes, Jeffrey M Weiss, John E Downey, Elizabeth C Tyler-Kabara, Sliman J Bensmaia, Andrew B Schwartz, Michael L Boninger, and Robert A Gaunt. Intracortical microstimulation of human somatosensory cortex. pages 1–11, 2016.

[91] Robert D Flint, Joshua M Rosenow, Matthew C Tate, Marc W Slutzky, Abu Hamdeh S et Al, Acharya S et Al, Aflalo T et Al, Agashe H A L, Contreras-Vidal J, Aggarwal V et Al, Bansal A K et Al, Bansal A K et Al, Barrese J C et Al, Bleichner M G et Al, Bundy D T et Al, Carmena J M et Al, Chao Z C et Al, Chapin J K et Al, Chen C et Al, Chestek C A et Al, Crone N E et Al, Dunn O J, Erman T et Al, Fagg A H et Al, Fifer M S et Al, Flint R D et Al, Flint R D et Al, Flint R D et Al, Flint R D et Al, Flint R D et Al, Gharabaghi A et Al, Gilja V et Al, Hermes D et Al, Hochberg L R et Al, Hotson G et Al, Hwang E J A, Andersen R, Ingram J N et Al, Kennedy P R A, Bakay R, Korinek A M et Al, Kubanek J et Al, Ledochowitsch P et Al, Liang N L, Bougrain, Marathe A R M, Taylor D, Mehring C et Al, Mehring C et Al, Morrell M J, Nakanishi Y et Al, Olson J D et Al, Perel S et Al, Perge J A et Al, Pfurtscheller G et Al, Pistohl T et Al, Pistohl T et Al, Pohlmeyer E A et Al, Ramon C et Al, Rickert J et Al, Rouse A G et Al, Santello M et Al, Schalk G et Al, Schieber M H, Serruya M D et Al, Shimoda K et Al, Shin D et Al, Simeral J D et Al, Slutzky M W et Al, Slutzky M W et Al, So K et Al, Soekadar S R et Al, Stark E M, Abeles, Stavisky S D et Al, Taylor D M et Al, Viventi J et Al, Wang D et Al, Wang P T et Al, Williams J J et Al, Wissel T et Al, Wodlinger B et Al, Xie T et Al, Yanagisawa T et Al, and Zhuang J et Al. Continuous decoding of human grasp kinematics using epidural and subdural signals. *Journal of Neural Engineering*, 14(1):016005, feb 2017.

[92] Wilson F.N and Bayley R.H. The electric field of an eccentric dipole in a homogeneous spherical conducting medium. *Circulation*, 1(1):84–92, 1950.

[93] Peter T. Fox, Shalini Narayana, Nitin Tandon, Hugo Sandoval, Sarabeth P. Fox, Peter Kochunov, and Jack L. Lancaster. Column-Based Model of Electric Field Excitation of Cerebral Cortex. *Human Brain Mapping*, 22(1):1–14, 2004.

[94] Ernest Frank. Electric Potential Produced by Two Point Current Sources in a Homogenous Conducting Sphere. *Journal of Applied Physics*, 102(1927), 1952.

[95] Makoto Fukushima, Richard C. Saunders, Matthew Mullarkey, Alexandra M. Doyle, Mortimer Mishkin, and Naotaka Fujii. An electrocorticographic electrode array for simultaneous recording from medial, lateral, and intrasulcal surface of the cortex in macaque monkeys. *Journal of Neuroscience Methods*, 233:155–165, aug 2014.

[96] Karunesh Ganguly and Mu ming Poo. Activity-dependent neural plasticity from bench to bedside. *Neuron*, 80(3):729–741, 2013.

[97] S Geyer, a Schleicher, and K Zilles. Areas 3a, 3b, and 1 of human primary somatosensory cortex. *NeuroImage*, 10(1):63–83, 1999.

[98] B Y S Ghosh and R Porter. Morphology of Pyramidal Neurones in Monkey Motor. *Journal of Physiology*, 400:593–615, 1988.

[99] Phillip M. Gilley, Anu Sharma, Michael Dorman, Charles C. Finley, Arunachalam S. Panch, and Kathryn Martin. Minimization of cochlear implant stimulus artifact in cortical auditory evoked potentials. *Clinical Neurophysiology*, 117(8):1772–1782, 2006.

[100] Carlo Giussani, Frank Emmanuel Roux, Jeffrey Ojemann, Erik Pietro Sganzerla, David Pirillo, and Costanza Papagno. Is preoperative functional magnetic resonance imaging reliable for language areas mapping in brain tumor surgery? Review of language functional magnetic resonance imaging and direct cortical stimulation correlation studies. *Neurosurgery*, 66(1):113–120, 2010.

[101] Jason M. Godlove, Erin O. Whaite, and Aaron P. Batista. Comparing temporal aspects of visual, tactile, and microstimulation feedback for motor control. *Journal of Neural Engineering*, 11(4):046025, aug 2014.

[102] Noah Goshi, Elisa Castagnola, Maria Vomero, Calogero Gueli, Claudia Cea, Elena Zucchini, David Bjanes, Emma Maggiolini, Chet Moritz, Sam Kassegne, Davide Ricci, and Luciano Fadiga. Glassy carbon MEMS for novel origami-styled 3D integrated intracortical and epicortical neural probes. *Journal of Micromechanics and Microengineering*, 28(6):065009, jun 2018.

[103] David J. Guggenmos, Meysam Azin, Scott Barbay, Jonathan D. Mahnken, Caleb Dunham, Pedram Mohseni, and Randolph J. Nudo. Restoration of function after brain damage using a neural prosthesis. *Proceedings of the National Academy of Sciences*, 110(52):21177–21182, dec 2013.

[104] Seyhmus Guler, Moritz Dannhauer, Biel Roig-Solvas, Alexis Gkogkidis, Rob Macleod, Tonio Ball, Jeffrey G. Ojemann, and Dana H. Brooks. Computationally optimized ECoG stimulation with local safety constraints. *NeuroImage*, 173(July 2017):35–48, 2018.

[105] Casey H Halpern, Uzma Samadani, Brian Litt, Jurg L Jaggi, and Gordon H Baltuch. Deep Brain Stimulation for Epilepsy. 5(January):59–67, 2008.

[106] Richard L Harvey and Carolee J Winstein. Design for the everest randomized trial of cortical stimulation and rehabilitation for arm function following stroke. *Neurorehabilitation and neural repair*, 23:32–44, 2009.

[107] Group. Harvey RL. Winstein CJ. Everest Trial. Design for the everest randomized trial of cortical. *Neurorehabilitation & Neural Repair*, 23(1):32–44, 2009.

[108] Takao Hashimoto, Christopher M. Elder, and Jerrold L. Vitek. A template subtraction method for stimulus artifact removal in high-frequency deep brain stimulation. *Journal of Neuroscience Methods*, 113(2):181–186, 2002.

[109] D. O. Hebb. *The Organization of Behavior; A Neuropsychological Theory*. oct 1949.

[110] Leon F Heffer and James B Fallon. A novel stimulus artifact removal technique for high-rate electrical stimulation. *Journal of neuroscience methods*, 170(2):277–84, may 2008.

[111] L. Heller and D. B. van Hulsteyn. Brain stimulation using electromagnetic sources: theoretical aspects. *Biophysical Journal*, 63(1):129–138, 1992.

[112] Elisabeth Hendrich, Tilo Strobach, Martin Buss, Hermann J. Müller, and Torsten Schubert. Temporal-order judgment of visual and auditory stimuli: modulations in situations with and without stimulus discrimination. *Frontiers in Integrative Neuroscience*, 6(August):1–9, 2012.

[113] Dora Hermes, Kai J. Miller, Herke Jan Noordmans, Mariska J. Vansteensel, and Nick F. Ramsey. Automated electrocorticographic electrode localization on individually rendered brain surfaces. *Journal of Neuroscience Methods*, 185(2):293–298, 2010.

[114] Dora Hermes, Mai Nguyen, and Jonathan Winawer. *Neuronal synchrony and the relation between the blood-oxygen-level dependent response and the local field potential*, volume 15. 2017.

[115] Jim D Herring, Gregor Thut, Ole Jensen, and Til O Bergmann. Attention Modulates TMS-Locked Alpha Oscillations in the Visual Cortex. *Journal of Neuroscience*, 35(43):14435–14447, oct 2015.

[116] Jeffrey Herron, Scott Stanslaski, Tom Chouinard, Rob Corey, Timothy Denison, and Heather Orser. Bi-directional brain interfacing instrumentation. *I2MTC 2018 - 2018 IEEE International Instrumentation and Measurement Technology Conference: Discovering New Horizons in Instrumentation and Measurement, Proceedings*, pages 1–6, 2018.

[117] Jeffrey Herron, Margaret Thompson, Tim Brown, Howard Chizeck, Jeffrey Ojemann, and Andrew Ko. Cortical brain computer interface for closed-loop deep brain stimulation. *IEEE Transactions on Neural Systems and Rehabilitation Engineering*, 25(11):1–1, 2017.

[118] Okihide Hikosaka, Kae Nakamura, Katsuyuki Sakai, and Hiroyuki Nakahara. Central mechanisms of motor skill learning. *Current Opinion in Neurobiology*, 12(2):217–222, 2002.

[119] Shivayogi V. Hiremath, Elizabeth C. Tyler-Kabara, Jesse J. Wheeler, Daniel W. Moran, Robert A. Gaunt, Jennifer L. Collinger, Stephen T. Foldes, Douglas J. Weber, Weidong Chen, Michael L. Boninger, and Wei Wang. Human perception of electrical stimulation on the surface of somatosensory cortex. *PLOS ONE*, 12(5):e0176020, may 2017.

[120] Mark H. Histed, Vincent Bonin, and R. Clay Reid. Direct Activation of Sparse, Distributed Populations of Cortical Neurons by Electrical Microstimulation. *Neuron*, 63(4):508–522, aug 2009.

[121] Guy Hotson, David P McMullen, Matthew S Fifer, Matthew S Johannes, Kapil D Katyal, Matthew P Para, Robert Armiger, William S Anderson, Nitish V Thakor, Brock A Wester, and Nathan E Crone. Individual finger control of a modular prosthetic limb using high-density electrocorticography in a human subject. *Journal of Neural Engineering*, 13(2):026017, 2016.

[122] Mark Huang, Richard L. Harvey, Mary Ellen Stoykov, Sean Ruland, Martin Weinand, David Lowry, and Robert Levy. Cortical Stimulation for Upper Limb Recovery Following Ischemic Stroke: A Small Phase II Pilot Study of a Fully Implanted Stimulator. *Topics in Stroke Rehabilitation*, 15(2):160–172, 2008.

[123] Ying Zu Huang, Mark J. Edwards, Elisabeth Rounis, Kailash P. Bhatia, and John C. Rothwell. Theta burst stimulation of the human motor cortex. *Neuron*, 45(2):201–206, 2005.

[124] Andy Hung, Ira B. Goldberg, and Jack W. Judy. Stimulation Electrode Materials and Electrochemical Testing Methods. In *Implantable Neural Prostheses 2 Techniques and Engineering Approaches*, pages 191–216. 2009.

[125] Andrew Jackson, Jaideep Mavoori, and Eberhard E Fetz. Long-term motor cortex plasticity induced by an electronic neural implant. *Nature*, 444(7115):56–60, nov 2006.

[126] Robert Jech, Evžen Růžička, Dušan Urgošík, Tereza Serranová, Markéta Volfová, Olga Nováková, Jan Roth, Petr Dušek, and Petr Mečíř. Deep brain stimulation of the subthalamic nucleus affects resting EEG and visual evoked potentials in Parkinson's disease. *Clinical Neurophysiology*, 117(5):1017–1028, 2006.

[127] David Jellinek, Doreen Jewkes, and Lindsay Symon. Noninvasive intraoperative monitoring of motor evoked potentials under propofol anesthesia: effects of spinal surgery on the amplitude and latency of motor evoked potentials. *Neurosurgery*, 29(4):551–557, 1991.

[128] Roland S. Johansson. Sensory Control of Dexterous Manipulation in Humans. In *Hand and Brain*, number September, pages 381–414. Elsevier, 1996.

[129] L A Johnson, J D Wander, D Sarma, D K Su, E E Fetz, and J G Ojemann. Direct electrical stimulation of the somatosensory cortex in humans using electrocorticography electrodes: a qualitative and quantitative report. *Journal of neural engineering*, 10(3):036021, jun 2013.

[130] Eric R Kandel, James H Schwartz, Thomas M Jessell, Steven Siegelbaum, and A J Hudspeth. *Principles of neural science*, volume 5. McGraw-Hill, 2013.

[131] Sam Kassegne, Maria Vomero, Roberto Gavuglio, Mieko Hirabayashi, Emre Özyilmaz, Sebastien Nguyen, Jesus Rodriguez, Eda Özyilmaz, Pieter van Niekerk, and Ajit Khosla. Electrical impedance, electrochemistry, mechanical stiffness, and hardness tunability in glassy carbon MEMS μECoG electrodes. 2015.

[132] Corey J Keller, Christopher J Honey, Laszlo Entz, Stephan Bickel, David M Groppe, Emilia Toth, Istvan Ulbert, Fred a Lado, and Ashesh D Mehta. Corticocortical evoked potentials reveal projectors and integrators in human brain networks. *The Journal of neuroscience : the official journal of the Society for Neuroscience*, 34(27):9152–63, jul 2014.

[133] Corey J Keller, Christopher J Honey, Pierre Mégevand, Laszlo Entz, Istvan Ulbert, and Ashesh D Mehta. Mapping human brain networks with cortico-cortical evoked potentials. *Philosophical transactions of the Royal Society of London. Series B, Biological sciences*, 369(1653), oct 2014.

[134] Corey J. Keller, Yuhao Huang, Jose L. Herrero, Maria Fini, Victor Du, Fred A. Lado, Christopher J. Honey, and Ashesh D. Mehta. Induction and quantification of excitability changes in human cortical networks. *The Journal of Neuroscience*, 38(23):1088–17, 2018.

[135] Sanne Kikkert, James Kolasinski, Saad Jbabdi, Irene Tracey, Christian F. Beckmann, Heidi Johansen Berg, and Tamar R. Makin. Revealing the neural fingerprints of a missing hand. *eLife*, 5(AUGUST):1–19, 2016.

[136] Z F Kisvarday, K A C Martin, T F Freund, D Whitteridge, and P Somogyi. Synaptic targets of HRP-filled layer III pyramidal cells in the cat striate cortex. pages 541–552, 1986.

[137] Christian Klaes, Ying Shi, Spencer Kellis, Juri Minxha, Boris Revechkis, and Richard A. Andersen. A cognitive neuroprosthetic that uses cortical stimulation for somatosensory feedback. *Journal of Neural Engineering*, 11(5):056024, oct 2014.

[138] Eran Klein and Jeffrey Ojemann. Informed consent in implantable BCI research: Identification of research risks and recommendations for development of best practices. *Journal of Neural Engineering*, 13(4):0–23, 2016.

[139] Jessica E. Kleinbart, Amy L. Orsborn, John S. Choi, Charles Wang, Shaoyu Qiao, Jonathan Viventi, and Bijan Pesaran. A Modular Implant System for Multimodal Recording and Manipulation of the Primate Brain. *2018 40th Annual International Conference of the IEEE Engineering in Medicine and Biology Society (EMBC)*, pages 3362–3365, 2018.

[140] P. Christiaan Klink, Bruno Dagnino, Marie Alice Gariel-Mathis, and Pieter R. Roelfsema. Distinct Feedforward and Feedback Effects of Microstimulation in Visual Cortex Reveal Neural Mechanisms of Texture Segregation. *Neuron*, 95(1):209–220.e3, 2017.

[141] Laurent Koessler, Sophie Colnat-Coulbois, Thierry Cecchin, Janis Hofmanis, Jacek P. Dmochowski, Anthony M. Norcia, and Louis G. Maillard. In-vivo measurements of human brain tissue conductivity using focal electrical current injection through intracerebral multicontact electrodes. *Human Brain Mapping*, 986(April 2016):974–986, 2016.

[142] Dominic Kraus, Georgios Naros, Robert Bauer, Fatemeh Khademi, Maria Teresa Leão, Ulf Ziemann, and Alireza Gharabaghi. Brain State-Dependent Transcranial Magnetic Closed-Loop Stimulation Controlled by Sensorimotor Desynchronization Induces Robust Increase of Corticospinal Excitability. *Brain Stimulation*, 9(3):415–424, may 2016.

[143] Simon Kristiansson, Shiva P. Kagganti, Fredrik Ingvarson, and Kjell O. Jeppson. A comparison of the exact and an approximate solution for the resistance between two coplanar circular discs. *Solid-State Electronics*, 49(2):275–277, feb 2005.

[144] Pawel Kudela and William S. Anderson. Computational Modeling of Subdural Cortical Stimulation: A Quantitative Spatiotemporal Analysis of Action Potential Initiation in a High-Density Multicompartment Model. *Neuromodulation: Technology at the Neural Interface*, 18(7):552–565, oct 2015.

[145] Alexis M. Kuncel and Warren M. Grill. Selection of stimulus parameters for deep brain stimulation. *Clinical Neurophysiology*, 115(11):2431–2441, 2004.

[146] Alexandra Kuznetsova, Per B Brockhoff, and Rune H B Christensen. {lmerTest} Package: Tests in Linear Mixed Effects Models. *Journal of Statistical Software*, 82(13):1–26, 2017.

[147] Jacob Lahr, Sven Paßmann, Jonathan List, Werner Vach, Agnes Flöel, and Stefan Klöppel. Effects of Different Analysis Strategies on Paired Associative Stimulation. A Pooled Data Analysis from Three Research Labs. *PloS one*, 11(5):e0154880, 2016.

[148] J Latikka, T Kuurne, and H Eskola. Conductivity of living intracranial tissues. *Physics in medicine and biology*, 46(6):1611–1616, 2001.

[149] Brian Lee, Daniel Kramer, Michelle Armenta Salas, Spencer Kellis, David Brown, Tatyana Dobreva, Christian Klaes, Christi Heck, Charles Liu, and Richard A Andersen. Engineering Artificial Somatosensation Through Cortical Stimulation in Humans. *Frontiers in Systems Neuroscience*, 12(June):1–11, jun 2018.

[150] Brian Lee, Muhammad N. Zubair, Yvette D. Marquez, David M. Lee, Laura A. Kalayjian, Christianne N. Heck, and Charles Y. Liu. A Single-Center Experience with the NeuroPace RNS System: A Review of Techniques and Potential Problems. *World Neurosurgery*, 84(3):719–726, 2015.

[151] Bradley C Lega, Casey H Halpern, Jurg L Jaggi, and Gordon H Baltuch. Neurobiology of Disease Deep brain stimulation in the treatment of refractory epilepsy : Update on current data and future directions. *Neurobiology of Disease*, 38(3):354–360, 2010.

[152] P. P. Lele, D. C. Sinclair, and G. Weddell. The reaction time to touch. *The Journal of Physiology*, 123(1):187–203, jan 1954.

[153] Scott F. Lempka, Svjetlana Miocinovic, Matthew D. Johnson, Jerrold L. Vitek, and Cameron C. McIntyre. In vivo impedance spectroscopy of deep brain stimulation electrodes. *Journal of Neural Engineering*, 6(4), 2009.

[154] Russell Lenth. *emmeans: Estimated Marginal Means, aka Least-Squares Means*, 2018.

[155] J. J. Letzkus, B. M. Kampa, and G. J. Stuart. Learning Rules for Spike Timing-Dependent Plasticity Depend on Dendritic Synapse Location. *Journal of Neuroscience*, 26(41):10420–10429, 2006.

[156] Eric C Leuthardt, Kai J Miller, Gerwin Schalk, Rajesh P N Rao, and Jeffrey G Ojemann. Electrocorticography-Based Brain Computer Interface — The Seattle Experience. 14(2):194–198, 2006.

[157] Eric C. Leuthardt, Gerwin Schalk, Daniel Moran, and Jeffrey G. Ojemann. The emerging world of motor neuroprosthetics: A neurosurgical perspective. *Neurosurgery*, 59(1):1–13, 2006.

[158] Eric C Leuthardt, Gerwin Schalk, Jonathan R Wolpaw, Jeffrey G Ojemann, and Daniel W Moran. A brain-computer interface using electrocorticographic signals in humans. *Journal of neural engineering*, 1(2):63–71, jun 2004.

[159] Robert Levy, Sean Ruland, Martin Weinand, David Lowry, Rima Dafer, and Roy Bakay. Cortical stimulation for the rehabilitation of patients with hemiparetic stroke: a multicenter feasibility study of safety and efficacy. *Journal of Neurosurgery*, 108(4):707–714, 2008.

[160] Robert M. Levy, Richard L. Harvey, Brett M. Kissela, Carolee J. Winstein, Helmi L. Lutsep, Todd B. Parrish, Steven C. Cramer, and Lalit Venkatesan. Epidural Electrical Stimulation for Stroke Rehabilitation: Results of the Prospective, Multicenter, Randomized, Single-Blinded Everest Trial. *Neurorehabilitation and neural repair*, 30(2):107–19, feb 2016.

[161] B Libet, W W Alberts, E W Wright, L D Delattre, G Levin, and B Feinstein. Production of threshold levels of conscious sensation by electrical stimulation of human somatosensory cortex. *Journal of neurophysiology*, 27:546–78, jul 1964.

[162] Justin D. Lieber and Sliman J. Bensmaia. High-dimensional representation of texture in somatosensory cortex of primates. *Proceedings of the National Academy of Sciences*, 116(8):201818501, 2019.

[163] Guillaume Lio, Stéphane Thobois, Bénédicte Ballanger, Brian Lau, and Philippe Boulinguez. Removing deep brain stimulation artifacts from the electroencephalogram: Issues, recommendations and an open-source toolbox. *Clinical Neurophysiology*, 129(10):2170–2185, 2018.

[164] Simon Little, Alex Pogosyan, Spencer Neal, Baltazar Zavala, Ludvic Zrinzo, Marwan Hariz, Thomas Foltynie, Patricia Limousin, Keyoumars Ashkan, James FitzGerald, Alexander L. Green, Tipu Z. Aziz, and Peter Brown. Adaptive deep brain stimulation in advanced Parkinson disease. *Annals of Neurology*, 74(3):449–457, sep 2013.

[165] Donald Lloyd-Jones, Robert J. Adams, Todd M. Brown, Mercedes Carnethon, Shifan Dai, Giovanni De Simone, T. Bruce Ferguson, Earl Ford, Karen Furie, Cathleen Gillespie, Alan Go, Kurt Greenlund, Nancy Haase, Susan Hailpern, P. Michael Ho, Virginia Howard, Brett Kissela, Steven Kittner, Daniel Lackland, Lynda Lisabeth, Ariane Marelli, Mary M. McDermott, James Meigs, Dariush Mozaffarian, Michael Mussolino, Graham Nichol, Véronique L. Roger, Wayne Rosamond, Ralph Sacco, Paul Sorlie, Randall Stafford, Thomas Thom, Sylvia Wasserthiel-Smoller, Nathan D. Wong, and Judith Wylie-Rosett. Heart Disease and Stroke Statistics–2010 Update: A Report From the American Heart Association. *Circulation*, 121(7):e46–e215, feb 2010.

[166] Nikos K Logothetis, Mark Augath, Yusuke Murayama, Alexander Rauch, Fahad Sultan, Jozien Goense, Axel Oeltermann, and Hellmut Merkle. The effects of electrical microstimulation on cortical signal propagation. *Nature neuroscience*, 13(10):1283–1291, 2010.

[167] Yiliang Lu, Pengjia Cao, Jingjing Sun, Jing Wang, Liming Li, Qiushi Ren, Yao Chen, and Xinyu Chai. Using independent component analysis to remove artifacts in visual cortex responses elicited by electrical stimulation of the optic nerve. *Journal of Neural Engineering*, 9(2), 2012.

[168] Timothy H. Lucas and Eberhard E. Fetz. Myo-Cortical Crossed Feedback Reorganizes Primate Motor Cortex Output. *Journal of Neuroscience*, 33(12):5261–5274, mar 2013.

[169] Iwasaki M., Enatsu R., Matsumoto R., Novak E., Thankappen B., Piao Z., O'Connor R T., Horning K., Bingaman W., and Nair D. Accentuated cortico-cortical evoked potentials in neocortical epilepsy in areas of ictal onset. *Epileptic Disorders*, 12(4):292–302, 2010.

[170] David B. MacDonald. Intraoperative Motor Evoked Potential Monitoring: Overview and Update. *Journal of Clinical Monitoring and Computing*, 20(5):347–377, oct 2006.

[171] Sergey N Makarov, Gregory M Noetscher, and Ara Nazarian. *Low-frequency electromagnetic modeling for electrical and biological systems using MATLAB*. John Wiley & Sons, 2015.

[172] Tamar R. Makin, Alona O. Cramer, Jan Scholz, Avital Hahamy, David Henderson Slater, Irene Tracey, and Heidi Johansen-Berg. Deprivation-related and use-dependent plasticity go hand in hand. *eLife*, 2(November2013):1–15, 2013.

[173] Henry Markram, Maria Toledo-Rodriguez, Yun Wang, Anirudh Gupta, Gilad Silberberg, and Caizhi Wu. Interneurons of the neocortical inhibitory system. *Nature reviews. Neuroscience*, 5(10):793–807, 2004.

[174] Donald W. Marquardt. An Algorithm for Least-Squares Estimation of Nonlinear Parameters, 1963.

[175] Riki Matsumoto, Dileep R. Nair, Akio Ikeda, Tomoyuki Fumuro, Eric Lapresto, Nobuhiro Mikuni, William Bingaman, Susumu Miyamoto, Hidenao Fukuyama, Ryosuke Takahashi, Imad Najm, Hiroshi Shibasaki, and Hans O. Lüders. Parieto-frontal network in humans studied by cortico-cortical evoked potential. *Human Brain Mapping*, 33(12):2856–2872, 2012.

[176] Riki Matsumoto, Dileep R. Nair, Eric LaPresto, William Bingaman, Hiroshi Shibasaki, and H. O. Luders. Functional connectivity in human cortical motor system: a cortico-cortical evoked potential study. *Brain*, 130(1):181–197, nov 2006.

[177] Riki Matsumoto, Dileep R Nair, Eric LaPresto, Imad Najm, William Bingaman, Hiroshi Shibasaki, and Hans O Lüders. Functional connectivity in the human language system: a cortico-cortical evoked potential study. *Brain : a journal of neurology*, 127(Pt 10):2316–30, oct 2004.

[178] D.B. McCreery, W.F. Agnew, T.G.H. Yuen, and L. Bullara. Charge density and charge per phase as cofactors in neural injury induced by electrical stimulation. *IEEE Transactions on Biomedical Engineering*, 37(10):996–1001, 1990.

[179] Cameron C. McIntyre and Warren M. Grill. Selective Microstimulation of Central Nervous System Neurons. *Annals of Biomedical Engineering*, 28(3):219–233, 2000.

[180] Gonzalo E Mena, Lauren E Grosberg, Sasidhar Madugula, Paweł Hottowy, Alan Litke, John Cunningham, E J Chichilnisky, and Liam Paninski. Electrical stimulus artifact cancellation and neural spike detection on large multi-electrode arrays. *PLOS Computational Biology*, 13(11):e1005842, nov 2017.

[181] Daniel R. Merrill, Marom Bikson, and John G.R. Jefferys. Electrical stimulation of excitable tissue: design of efficacious and safe protocols. *Journal of Neuroscience Methods*, 141(2):171–198, 2005.

[182] Nima Mesgarani, Connie Cheung, Keith Johnson, and Edward F Chang. Phonetic feature encoding in human superior temporal gyrus. *Science (New York, N.Y.)*, 343(6174):1006–10, 2014.

[183] Mark Meyer, Mathieu Desbrun, Peter Schröder, and Alan H. Barr. Discrete Differential-Geometry Operators for Triangulated 2-Manifolds. pages 35–57. 2003.

[184] I. Miccoli, F. Edler, H. Pfnür, and C. Tegenkamp. The 100th anniversary of the four-point probe technique: The role of probe geometries in isotropic and anisotropic systems. *Journal of Physics Condensed Matter*, 27(22), 2015.

[185] Stéphanie Miceli, Torbjørn V. Ness, Gaute T. Einevoll, and Dirk Schubert. Impedance Spectrum in Cortical Tissue: Implications for Propagation of LFP Signals on the Microscopic Level. *Eneuro*, 4(1):ENEURO.0291–16.2016, 2017.

[186] D. C. Millard, C. J. Whitmire, C. A. Gollnick, C. J. Rozell, and G. B. Stanley. Electrical and Optical Activation of Mesoscale Neural Circuits with Implications for Coding. *Journal of Neuroscience*, 35(47):15702–15715, 2015.

[187] Kai J Miller, Eric C Leuthardt, Gerwin Schalk, Rajesh P N Rao, Nicholas R Anderson, Daniel W Moran, John W Miller, and Jeffrey G Ojemann. Spectral changes in cortical surface potentials during motor movement. *The Journal of Neuroscience*, 27(9):2424–32, feb 2007.

[188] Kai J. Miller, Pradeep Shenoy, Marcel den Nijs, Larry B Sorensen, Rajesh P N Rao, and Jeffrey G Ojemann. Beyond the Gamma Band: The Role of High-Frequency Features in Movement Classification. *IEEE Transactions on Biomedical Engineering*, 55(5):1634–1637, may 2008.

[189] Lee E. Miller and Douglas J. Weber. Guest Editorial Brain Training: Cortical Plasticity and Afferent Feedback in Brain-Machine Interface Systems. *IEEE Transactions on Neural Systems and Rehabilitation Engineering*, 19(5):465–467, 2011.

[190] Makoto Miyazaki, Hiroshi Kadota, Kozue S. Matsuzaki, Shigeki Takeuchi, Hirofumi Sekiguchi, Takuo Aoyama, and Takanori Kochiyama. Dissociating the neural correlates of tactile temporal order and simultaneity judgements. *Scientific Reports*, 6(July 2015):1–10, 2016.

[191] G. F. Molnar, A. Sailer, C. A. Gunraj, D. I. Cunic, A. E. Lang, A. M. Lozano, E. Moro, and Robert Chen. Changes in cortical excitability with thalamic deep brain stimulation. *Neurology*, 64(11):1913–1919, 2005.

[192] Erwin B. Montgomery and John T. Gale. Mechanisms of action of deep brain stimulation (DBS). *Neuroscience & Biobehavioral Reviews*, 32(3):388–407, jan 2008.

[193] M. J. Morrell. Responsive cortical stimulation for the treatment of medically intractable partial epilepsy. *Neurology*, 77(13):1295–1304, sep 2011.

[194] B. E. Mouthaan, M. A. Van't Klooster, D. Keizer, G. J. Hebbink, F. S S Leijten, C. H. Ferrier, M. J A M Van Putten, M. Zijlmans, and G. J M Huiskamp. Single Pulse Electrical Stimulation to identify epileptogenic cortex: Clinical information obtained from early evoked responses. *Clinical Neurophysiology*, 127(2):1088–1098, 2016.

[195] Natalie Mrachacz-Kersting, Ning Jiang, Andrew James Thomas Stevenson, Imran Khan Niazi, Vladimir Kostic, Aleksandra Pavlovic, Sasa Radovanovic, Milica Djuric-Jovicic, Federica Agosta, Kim Dremstrup, and Dario Farina. Efficient neuroplasticity induction in chronic stroke patients by an associative brain-computer interface. *Journal of neurophysiology*, page jn.00918.2015, 2015.

[196] Rosel M. Mulkey and Robert C. Malenka. Mechanisms underlying induction of homosynaptic long-term depression in area CA1 of the hippocampus. *Neuron*, 9(5):967–975, 1992.

[197] Leah Muller, Sarah Felix, Kedar G Shah, Kye Lee, Satinderpall Pannu, and Edward F Chang. Thin-film, high-density micro-electrocorticographic decoding of a human cortical gyrus. In *2016 38th Annual International Conference of the IEEE Engineering in Medicine and Biology Society (EMBC)*, pages 1528–1531. IEEE, aug 2016.

[198] V N Murthy and E E Fetz. Oscillatory activity in sensorimotor cortex of awake monkeys: synchronization of local field potentials and relation to behavior. *Journal of Neurophysiology*, 76(6):3949–3967, 1996.

[199] V N Murthy and E E Fetz. Synchronization of neurons during local field potential oscillations in sensorimotor cortex of awake monkeys. *Journal of neurophysiology*, 76(6):3968–3982, 1996.

[200] Solveig Næss, Chaitanya Chintaluri, Torbjørn V. Ness, Anders M. Dale, Gaute T. Einevoll, and Daniel K. Wójcik. Corrected Four-Sphere Head Model for EEG Signals. *Frontiers in Human Neuroscience*, 11(October):1–7, 2017.

[201] J. H Nagel. "Biopotential Amplifiers.". In *The Biomedical Engineering Handbook: Second Edition*. 2000.

[202] Surendar S. Nathan, Saurabh R. Sinha, Barry Gordon, Ronald P. Lesser, and Nitish V. Thakor. Determination of current density distributions generated by electrical stimulation of the human cerebral cortex. *Electroencephalography and Clinical Neurophysiology*, 86(3):183–192, 1993.

[203] Matthew J. Nelson, Silvana Valtcheva, and Laurent Venance. Magnitude and behavior of cross-talk effects in multichannel electrophysiology experiments. *Journal of Neurophysiology*, 118(1):574–594, 2017.

[204] John Newman. Resistance for Flow of Current to a Disk. *Journal of The Electrochemical Society*, 113(5):501, 1966.

[205] Lionel G. Nowak and Jean Bullier. Axons, but not cell bodies, are activated by electrical stimulation in cortical gray matter. I. Evidence from chronaxie measurements. *Experimental Brain Research*, 118(4):477–488, 1998.

[206] R J Nudo, W M Jenkins, and M M Merzenich. Repetitive microstimulation alters the cortical representation of movements in adult rats. *Somatosensory & motor research*, 7(4):463–83, 1990.

[207] Paul L Nunez, Ramesh Srinivasan, and Others. *Electric fields of the brain: the neurophysics of EEG*. Oxford University Press, USA, 2006.

[208] Calogero Maria Oddo, Stanisa Raspopovic, Fiorenzo Artoni, Alberto Mazzoni, Giacomo Spigler, Francesco Petrini, Federica Giambattistelli, Fabrizio Vecchio, Francesca Miraglia, Loredana Zollo, Giovanni Di Pino, Domenico Camboni, Maria Chiara Carrozza, Eugenio Guglielmelli, Paolo Maria Rossini, Ugo Faraguna, and Silvestro Micera. Intraneural stimulation elicits discrimination of textural features by artificial fingertip in intact and amputee humans. *eLife*, 5:1–27, mar 2016.

[209] G Ojemann, J Ojemann, E Lettich, and M Berger. Cortical language localization in left, dominant hemisphere. An electrical stimulation mapping investigation in 117 patients. *Journal of neurosurgery*, 71(3):316–326, 1989.

[210] M. Okun, A. Naim, and I. Lampl. The Subthreshold Relation between Cortical Local Field Potential and Neuronal Firing Unveiled by Intracellular Recordings in Awake Rats. *Journal of Neuroscience*, 30(12):4440–4448, 2010.

[211] Amy L. Orsborn, Charles Wang, Ken Chiang, Michel M. Maharbiz, Jonathan Viventi, and Bijan Pesaran. Semi-chronic chamber system for simultaneous subdural electrocorticography, local field potentials, and spike recordings. *International IEEE/EMBS Conference on Neural Engineering, NER*, 2015-July:398–401, 2015.

[212] Daniel J. O'Shea and Krishna V. Shenoy. ERAASR: An algorithm for removing electrical stimulation artifacts from multielectrode array recordings. *bioRxiv*, pages 1–27, 2017.

[213] Stephen J. Page, Lynne V. Gauthier, and Susan White. Size doesn't matter: Cortical stroke lesion volume is not associated with upper extremity motor impairment and function in mild, chronic hemiparesis. *Archives of Physical Medicine and Rehabilitation*, 94(5):817–821, 2013.

[214] Stephen J Page, Jerzy P Szaflarski, James C Eliassen, Hai Pan, and Steven C Cramer. During Mental Practice in Stroke. pages 382–388, 2009.

[215] Paul W. Nicholson. Specific Impedance of Cerebral White Matter. *Experimental Neurology*, 13:386–401, 1965.

[216] Y.-C. Pei, P. V. Denchev, S. S. Hsiao, J. C. Craig, and S. J. Bensmaia. Convergence of Submodality-Specific Input Onto Neurons in Primary Somatosensory Cortex. *Journal of Neurophysiology*, 102(3):1843–1853, 2009.

[217] Edgar Peña, Simeng Zhang, Remi Patriat, Joshua E Aman, Jerrold L Vitek, Noam Harel, and Matthew D Johnson. Multi-objective particle swarm optimization for post-operative deep brain stimulation targeting of subthalamic nucleus pathways. *Journal of neural engineering*, (February 2016):0–39, 2018.

[218] Erlick AC Pereira, Alexander L Green, Dipankar Nandi, and Tipu Z Aziz. Deep brain stimulation: indications and evidence. *Expert Review of Medical Devices*, 4(5):591–603, sep 2007.

[219] Andrew D. Pinto, Anthony E. Lang, and Robert Chen. The cerebellothalamocortical pathway in essential tremor. *Neurology*, 60(12):1985–1987, 2003.

[220] Tobias Pistohl, Deepak Joshi, Gowrishankar Ganesh, Andrew Jackson, and Kianoush Nazarpour. Artificial Proprioceptive Feedback for Myoelectric Control. *IEEE Transactions on Neural Systems and Rehabilitation Engineering*, 23(3):498–507, may 2015.

[221] Ela B Plow, James R Carey, Randolph J Nudo, and Alvaro Pascual-Leone. Invasive cortical stimulation to promote recovery of function after stroke: a critical appraisal. *Stroke; a journal of cerebral circulation*, 40(5):1926–31, may 2009.

[222] N.N Polyaakov and V.L L Kon'kov. Spreading resistance of a flat circular contact. *Soviet Physics Journal*, 13(9):1203–1207, 1970.

[223] R Core Team. *R: A Language and Environment for Statistical Computing*. R Foundation for Statistical Computing, Vienna, Austria, 2013.

[224] N.F. Ramsey, M.P.V.D. Heuvel, K.H. Kho, and F.S.S. Leijten. Towards Human BCI Applications Based on Cognitive Brain Systems: An Investigation of Neural Signals Recorded From the Dorsolateral Prefrontal Cortex. *IEEE Transactions on Neural Systems and Rehabilitation Engineering*, 14(2):214–217, jun 2006.

[225] James B. Ranck. Which elements are excited in electrical stimulation of mammalian central nervous system: A review. *Brain Research*, 98(3):417–440, nov 1975.

[226] Jr. Ranck J. B. and S L Bement. The specific impedance of the dorsal columns of cat: an inisotropic medium. *Exp Neurol*, 11:451–463, 1965.

[227] Radu Ranta, Steven Le Cam, Louise Tyvaert, and Valérie Louis-Dorr. Assessing human brain impedance using simultaneous surface and intracerebral recordings. *Neuroscience*, 343:411–422, 2017.

[228] Rajesh P N Rao. *Brain-Computer Interfacing: An Introduction*. Cambridge University Press, New York, NY, USA, 2013.

[229] Rajesh PN Rao. Towards neural co-processors for the brain: combining decoding and encoding in brain–computer interfaces. *Current Opinion in Neurobiology*, 55(1):142–151, 2019.

[230] P G Ray, K J Meador, J R Smith, J W Wheless, M Sittenfeld, and G L Clifton. Physiology of perception: cortical stimulation and recording in humans. *Neurology*, 52(5):1044–1049, 1999.

[231] James M. Rebesco and Lee E. Miller. Altering function in cortical networks by short-latency, paired stimulation. In *2010 Annual International Conference of the IEEE Engineering in Medicine and Biology*, pages 1674–1677. IEEE, aug 2010.

[232] James M. Rebesco and Lee E. Miller. Enhanced detection threshold for in vivo cortical stimulation produced by Hebbian conditioning. *Journal of Neural Engineering*, 8(1), 2011.

[233] Irene Rembado, Stavros Zanos, and Eberhard E. Fetz. Cycle-Triggered Cortical Stimulation during Slow Wave Sleep Facilitates Learning a BMI Task: A Case Report in a Non-Human Primate. *Frontiers in Behavioral Neuroscience*, 11(April):1–13, 2017.

[234] M. C. Ridding, J. C. Rothwell, and R. Inzelberg. Changes in excitability of motor cortical circuitry in patients with parkinson's disease. *Annals of Neurology*, 37(2):181–188, 1995.

[235] Pantaleo Romanelli, Marco Piangerelli, David Ratel, Christophe Gaude, Thomas Costecalde, Cosimo Puttilli, Mauro Picciafuoco, Alim Benabid, and Napoleon Torres. A novel neural prosthesis providing long-term electrocorticography recording and cortical stimulation for epilepsy and brain-computer interface. *Journal of Neurosurgery*, pages 1–14, 2018.

[236] Stefano Romeo, Alfredo Berardelli, Francesca Pedace, Maurizio Inghilleri, Morena Giovannelli, and Mario Manfredi. Cortical excitability in patients with essential tremor. *Muscle and Nerve*, 21(10):1304–1308, 1998.

[237] R Romo, a Hernández, a Zainos, C D Brody, and L Lemus. Sensing without touching: psychophysical performance based on cortical microstimulation. *Neuron*, 26(1):273–278, 2000.

[238] J Rosenthal, H J Waller, and V E Amassian. An analysis of the activation of motor cortical neurons by surface stimulation. *Journal of Neurophysiology*, 30(4):844–858, jul 1967.

[239] Boris Rosin, Maya Slovik, Rea Mitelman, Michal Rivlin-Etzion, Suzanne N. Haber, Zvi Israel, Eilon Vaadia, and Hagai Bergman. Closed-loop deep brain stimulation is superior in ameliorating parkinsonism. *Neuron*, 72(2):370–384, 2011.

[240] Bradley J. Roth, Joshua M. Saypol, Mark Hallett, and Leonardo G. Cohen. A theoretical calculation of the electric field induced in the cortex during magnetic stimulation. *Electroencephalography and Clinical Neurophysiology/ Evoked Potentials*, 81(1):47–56, 1991.

[241] Birthe Rubehn, Conrado Bosman, Robert Oostenveld, Pascal Fries, and Thomas Stieglitz. A MEMS-based flexible multichannel ECoG-electrode array. *Journal of Neural Engineering*, 6(3), 2009.

[242] Elena Ryapolova-Webb, Pedram Afshar, Scott Stanslaski, Tim Denison, Coralie de Hemptinne, Krystof Bankiewicz, and Philip A Starr. Chronic cortical and electromyographic recordings from a fully implantable device: preclinical experience in a nonhuman primate. *Journal of Neural Engineering*, 11(1):016009, feb 2014.

[243] Hannes P. Saal and Sliman J. Bensmaia. Touch is a team effort: Interplay of submodalities in cutaneous sensibility. *Trends in Neurosciences*, 37(12):689–697, 2014.

[244] Jerome N Sanes and John P Donoghue. Plasticity and Primary Motor Cortex. *Annual Review of Neuroscience*, 23(1):393–415, mar 2000.

[245] Abraham Savitzky and M. J. E. Golay. Smoothing and Differentiation of Data by Simplified Least Squares Procedures. *Analytical Chemistry*, 36(8):1627–1639, jul 1964.

[246] Gerwin Schalk. A general framework for dynamic cortical function: the function-through-biased-oscillations (FBO) hypothesis. *Frontiers in Human Neuroscience*, 9(June):1–10, 2015.

[247] Matthew Schiefer, Daniel Tan, Steven M Sidek, and Dustin J Tyler. Sensory feedback by peripheral nerve stimulation improves task performance in individuals with upper limb loss using a myoelectric prosthesis. *J Neural Eng*, 13(1):016001, 2016.

[248] Lauren E. Schrock, Jonathan W. Mink, Douglas W. Woods, Mauro Porta, Dominico Servello, Veerle Visser-Vandewalle, Peter A. Silburn, Thomas Foltynie, Harrison C. Walker, Joohi Shahed-Jimenez, Rodolfo Savica, Bryan T. Klassen, Andre G. Machado, Kelly D. Foote, Jian Guo Zhang, Wei Hu, Linda Ackermans, Yasin Temel, Zoltan Mari, Barbara K. Changizi, Andres Lozano, M. Auyeung, Takanobu Kaido, Yves Agid, Marie L. Welter, Suketu M. Khandhar, Alon Y. Mogilner, Michael H. Pourfar, Benjamin L. Walter, Jorge L. Juncos, Robert E. Gross, Jens Kuhn, James F. Leckman, Joseph A. Neimat, and Michael S. Okun. Tourette syndrome deep brain stimulation: A review and updated recommendations. *Movement Disorders*, 30(4):448–471, 2015.

[249] P. a. Schumann and E. E. Gardner. Application of Multilayer Potential Distribution to Spreading Resistance Correction Factors. *Journal of The Electrochemical Society*, 116(1):87, 1969.

[250] Stephanie C. Seeman, Brian J. Mogen, Eberhard E. Fetz, and Steve I. Perlmutter. Paired Stimulation for Spike-Timing-Dependent Plasticity in Primate Sensorimotor Cortex. *The Journal of Neuroscience*, 37(7):1935–1949, 2017.

[251] Hyeon Seo, Donghyeon Kim, and Sung Chan Jun. Computational Study of Subdural Cortical Stimulation: Effects of Simulating Anisotropic Conductivity on Activation of Cortical Neurons. *PLOS ONE*, 10(6):e0128590, jun 2015.

[252] Hyeon Seo, Donghyeon Kim, and Sung Chan Jun. Effect of Anatomically Realistic Full-Head Model on Activation of Cortical Neurons in Subdural Cortical Stimulation-A Computational Study. *Scientific Reports*, 6(May):1–12, 2016.

[253] Hyeon Seo, Natalie Schaworonkow, Sung Chan Jun, and Jochen Triesch. A multi-scale computational model of the effects of TMS on motor cortex. *F1000Research*, 5(May):1945, feb 2017.

[254] R.V. Shannon. A model of safe levels for electrical stimulation. *IEEE Transactions on Biomedical Engineering*, 39(4):424–426, apr 1992.

[255] Maxwell A Sherman, Shane Lee, Robert Law, Saskia Haegens, Catherine A Thorn, Matti S Hämäläinen, Christopher I Moore, and Stephanie R Jones. Neural mechanisms of transient neocortical beta rhythms: Converging evidence from humans, computational modeling, monkeys, and mice. *Proceedings of the National Academy of Sciences*, 113(33):E4885–E4894, aug 2016.

[256] Seijiro Shimada, Naoto Kunii, Kensuke Kawai, Takeshi Matsuo, Yohei Ishishita, Kenji Ibayashi, and Nobuhito Saito. Impact of volume-conducted potential in interpretation of cortico-cortical evoked potential: Detailed analysis of high-resolution electrocorticography using two mathematical approaches. *Clinical neurophysiology : official journal of the International Federation of Clinical Neurophysiology*, 128(4):549–557, 2017.

[257] Zbyněk Šidák. Rectangular Confidence Regions for the Means of Multivariate Normal Distributions. *Journal of the American Statistical Association*, 62(318):626–633, jun 1967.

[258] S. Silva, P.J. Basser, and P.C. Miranda. Elucidating the mechanisms and loci of neuronal excitation by transcranial magnetic stimulation using a finite element model of a cortical sulcus. *Clinical Neurophysiology*, 119(10):2405–2413, oct 2008.

[259] K. K. Skrede and D. Malthe-Sørenssen. Increased resting and evoked release of transmitter following repetitive electrical tetanization in hippocampus: a biochemical correlate to long-lasting synaptic potentiation. *Brain Research*, 208(2):436–441, 1981.

[260] Magdalena W. Sliwinska, Sylvia Vitello, and Joseph T. Devlin. Transcranial Magnetic Stimulation for Investigating Causal Brain-behavioral Relationships and their Time Course. *Journal of Visualized Experiments*, (89):1–9, 2014.

[261] Clemens J. Sommer. Ischemic stroke: experimental models and reality. *Acta Neuropathologica*, 133(2):245–261, 2017.

[262] Jordan Sorokin. HDBSCAN, 2018.

[263] Charles Spence and Cesare Parise. Prior-entry: A review. *Consciousness and Cognition*, 19(1):364–379, 2010.

[264] A. J. Suminski, D. C. Tkach, A. H. Fagg, and N. G. Hatsopoulos. Incorporating Feedback from Multiple Sensory Modalities Enhances Brain-Machine Interface Control. *Journal of Neuroscience*, 30(50):16777–16787, dec 2010.

[265] Limin Sun and Hermann Hinrichs. Moving average template subtraction to remove stimulation artefacts in EEGs and LFPs recorded during deep brain stimulation. *Journal of Neuroscience Methods*, 266:126–136, 2016.

[266] Yinming Sun, Faranak Farzan, Luis Garcia Dominguez, Mera S. Barr, Peter Giacobbe, Andres M. Lozano, Willy Wong, and Zafiris J. Daskalakis. A novel method for removal of deep brain stimulation artifact from electroencephalography. *Journal of Neuroscience Methods*, 237:33–40, 2014.

[267] Matthew Sykes, Natalie A. Matheson, Philip W. Brownjohn, Alexander D. Tang, Jennifer Rodger, Jonathan B. H. Shemmell, and John N. J. Reynolds. Differences in Motor Evoked Potentials Induced in Rats by Transcranial Magnetic Stimulation under Two Separate Anesthetics: Implications for Plasticity Studies. *Frontiers in Neural Circuits*, 10(October):1–11, 2016.

[268] G. A. Tabot, J. F. Dammann, Joshua A Berg, Francesco V Tenore, J. L. Boback, R Jacob Vogelstein, and Sliman J Bensmaia. Restoring the sense of touch with a prosthetic hand through a brain interface. *Proceedings of the National Academy of Sciences*, 110(45):18279–18284, nov 2013.

[269] Toshimitsu Takahashi, Kenji Kansaku, Makoto Wada, Satoshi Shibuya, and Shigeru Kitazawa. Neural correlates of tactile temporal-order judgment in humans: An fMRI study. *Cerebral Cortex*, 23(8):1952–1964, 2013.

[270] D. W. Tan, M. a. Schiefer, M. W. Keith, J. R. Anderson, J. Tyler, and D. J. Tyler. A neural interface provides long-term stable natural touch perception. *Science Translational Medicine*, 6(257):257ra138–257ra138, oct 2014.

[271] E J Tehovnik, A S Tolias, F Sultan, W M Slocum, and N K Logothetis. Direct and indirect activation of cortical neurons by electrical microstimulation. *Journal of neurophysiology*, 96(2):512–21, 2006.

[272] Edward J Tehovnik and Warren M Slocum. Depth-dependent detection of microampere currents delivered to monkey V1. *The European journal of neuroscience*, 29(7):1477–89, apr 2009.

[273] Eric E. Thomson, Rafael Carra, and Miguel A L Nicolelis. Perceiving invisible light through a somatosensory cortical prosthesis. *Nature Communications*, 4:1–7, 2013.

[274] Joseph D. Tobias, Timothy J. Goble, Guy Bates, John T. Anderson, and Daniel G. Hoernschemeyer. Effects of dexmedetomidine on intraoperative motor and somatosensory evoked potential monitoring during spinal surgery in adolescents. *Paediatric Anaesthesia*, 18(11):1082–1088, 2008.

[275] Lena Trebaul, David Rudrauf, Anne Sophie Job, Mihai Dragos Mălîia, Irina Popa, Andrei Barborica, Lorella Minotti, Ioana Mîndruţă, Philippe Kahane, and Olivier David. Stimulation artifact correction method for estimation of early cortico-cortical evoked potentials. *Journal of Neuroscience Methods*, 264:94–102, 2016.

[276] Jessica A. Turner, Jae S. Lee, Steven L. Schandler, and Michael J. Cohen. An fMRI investigation of hand representation in paraplegic humans. *Neurorehabilitation and Neural Repair*, 17(1):37–47, 2003.

[277] Rolf Ulrich. Threshold models of temporal-order judgments evaluated by a ternary response task. *Perception & Psychophysics*, 42(3):224–239, 1987.

[278] Kiyohide Usami, Griffin W. Milsap, Anna Korzeniewska, Maxwell J. Collard, Yujing Wang, Ronald P. Lesser, William S. Anderson, and Nathan E. Crone. Cortical Responses to Input From Distant Areas are Modulated by Local Spontaneous Alpha/Beta Oscillations. *Cerebral cortex (New York, N.Y. : 1991)*, 29(2):777–787, 2019.

[279] R. G Van Nostrand and K.L. L Cook. Interpretation of resistivity data. *Geological Survey Professional Paper*, (499):310, 1966.

[280] Marion Vincent, Olivier Rossel, Mitsuhiro Hayashibe, Guillaume Herbet, Hugues Duffau, David Guiraud, and François Bonnetblanc. The difference between electrical microstimulation and direct electrical stimulation - Towards new opportunities for innovative functional brain mapping? *Reviews in the Neurosciences*, 27(3):231–258, 2016.

[281] H. S. Vitense, J. A. Jacko, and V. K. Emery. Multimodal feedback: An assessment of performance and mental workload. *Ergonomics*, 46(1-3):68–87, 2003.

[282] Mathias Benjamin Voigt, Prasandhya Astagiri Yusuf, and Andrej Kral. Intracortical microstimulation modulates cortical induced responses. *The Journal of Neuroscience*, 38(36):0928–18, 2018.

[283] Tobias Voigt, Ulrich Katscher, and Olaf Doessel. Quantitative conductivity and permittivity imaging of the human brain using electric properties tomography. *Magnetic Resonance in Medicine*, 66(2):456–466, 2011.

[284] Mihály Vöröslakos, Yuichi Takeuchi, Kitti Brinyiczki, Tamás Zombori, Azahara Oliva, Antonio Fernández-Ruiz, Gábor Kozák, Zsigmond Tamás Kincses, Béla Iványi, György Buzsáki, and Antal Berényi. Direct effects of transcranial electric stimulation on brain circuits in rats and humans. *Nature Communications*, 9(1), 2018.

[285] Daniel A. Wagenaar and Steve M. Potter. Real-time multi-channel stimulus artifact suppression by local curve fitting. *Journal of Neuroscience Methods*, 120(2):113–120, 2002.

[286] Tim Wagner, Jarrett Rushmore, Uri Eden, and Antoni Valero-Cabre. Biophysical foundations underlying TMS: Setting the stage for an effective use of neurostimulation in the cognitive neurosciences. *Cortex*, 45(9):1025–1034, 2009.

[287] James R. Wait. The potential of two current point sources in a homogeneous conducting prolate spheroid [2]. *Journal of Applied Physics*, 24(4):496–497, 1953.

[288] Harrison C. Walker, He Huang, Christopher L. Gonzalez, James E. Bryant, Jeffrey Killen, Gary R. Cutter, Robert C. Knowlton, Erwin B. Montgomery, Bart L. Guthrie, and Ray L. Watts. Short latency activation of cortex during clinically effective subthalamic deep brain stimulation for Parkinson's disease. *Movement Disorders*, 27(7):864–73, jun 2012.

[289] Jeremiah D Wander and Rajesh P N Rao. Brain-computer interfaces: a powerful tool for scientific inquiry. *Current opinion in neurobiology*, 25:70–5, apr 2014.

[290] Jeremiah D. Wander, Devapratim Sarma, Lise a. Johnson, Eberhard E. Fetz, Rajesh P. N. Rao, Jeffrey G. Ojemann, and Felix Darvas. Cortico-Cortical Interactions during Acquisition and Use of a Neuroprosthetic Skill. *PLOS Computational Biology*, 12(8):e1004931, aug 2016.

[291] Nancy Xin Ru Wang, Ali Farhadi, Rajesh Rao, and Bingni Brunton. AJILE Movement Prediction: Multimodal Deep Learning for Natural Human Neural Recordings and Video. 2018.

[292] Xi Wang, Alexis Gkogkidis, Olga Iljina, Lukas Fiederer, Chiristian Henle, Irina Mader, Jan Kaminsky, Thomas Stieglitz, Mortimer Gierthmuehlen, and Tonio Ball. Mapping the fine structure of cortical activity with different micro-ECoG electrode array geometries. *Journal of Neural Engineering*, 265(2-3):197–212, jun 2017.

[293] Zuha Warraich and Jeffrey A. Kleim. Neural plasticity: The biological substrate for neurorehabilitation. *PM and R*, 2(12 SUPPL):208–219, 2010.

[294] Douglas J. Weber, Rebecca Friesen, and Lee E. Miller. Interfacing the somatosensory system to restore touch and Proprioception: Essential considerations. *Journal of Motor Behavior*, 44(6):403–418, 2012.

[295] Xuefeng F Wei and Warren M Grill. Impedance characteristics of deep brain stimulation electrodes in vitro and in vivo. *Journal of Neural Engineering*, 6(4):046008, aug 2009.

[296] Jeffrey M Weiss, Sharlene N Flesher, Robert Franklin, Jennifer L Collinger, and Robert A Gaunt. Artifact-free recordings in human bidirectional brain–computer interfaces. *Journal of Neural Engineering*, 16(1):016002, feb 2019.

[297] Felix a Wichmann and N Jeremy Hill. The Psychometric function I : fitting , sampling , and goodness-of-fit. 2000.

[298] Alik S. Widge. Cross-Species Neuromodulation from High-Intensity Transcranial Electrical Stimulation. *Trends in Cognitive Sciences*, 22(5):372–374, 2018.

[299] Justin C. Williams, Joseph A. Hippensteel, John Dilgen, William Shain, and Daryl R. Kipke. Complex impedance spectroscopy for monitoring tissue responses to inserted neural implants. *Journal of Neural Engineering*, 4(4):410–423, 2007.

[300] J. Adam Wilson, Elizabeth A. Felton, P. Charles Garell, Gerwin Schalk, and Justin C. Williams. ECoG factors underlying multimodal control of a brain-computer interface. *IEEE Transactions on Neural Systems and Rehabilitation Engineering*, 14(2):246–250, 2006.

[301] F. P. Wirth and J. M. Van Buren. Referral of pain from dural stimulation in man. *Journal of Neurosurgery*, 34(5):630–642, may 1971.

[302] R.E. Sheriff W.M. Telford, L.P Geldart. *Applied Geophysics*. jan 1990.

[303] Steven L Wolf, Carolee J Winstein, J Philip Miller, and David Morris. Effect of Constraint-Induced Movement. *Journal of American Medical Association*, 296(17):2095–2104, 2006.

[304] Amorn Wongsarnpigoon and Warren M Grill. Computational modeling of epidural cortical stimulation. *J Neural Eng*, 5(4):443–454, dec 2008.

[305] Charles C. Wood, Dennis D. Spencer, Truett Allison, Gregory McCarthy, Peter D. Williamson, and William R. Goff. Localization of human sensorimotor cortex during surgery by cortical surface recording of somatosensory evoked potentials. *Journal of Neurosurgery*, 68(1):99–111, 1988.

[306] Robert S. Woodworth and Harold Schlosberg. *Experimental Psychology*. New York, Holt, 1954.

[307] Takamitsu Yamamoto, Yoichi Katayama, Mitsuru Watanabe, Kohichiro Sumi, Toshiki Obuchi, Kazutaka Kobayashi, Hideki Oshima, and Chikashi Fukaya. Changes in Motor Function Induced by Chronic Motor Cortex Stimulation in Post-Stroke Pain Patients. *Stereotactic and Functional Neurosurgery*, 89(6):381–389, 2011.

[308] Yuxiao Yang, Allison T. Connolly, and Maryam M. Shanechi. A control-theoretic system identification framework and a real-time closed-loop clinical simulation testbed for electrical brain stimulation. *Journal of neural engineering*, 15(6):066007, 2018.

[309] Azadeh Yazdan-Shahmorad, Daryl R. Kipke, and Mark J. Lehmkuhle. Polarity of cortical electrical stimulation differentially affects neuronal activity of deep and superficial layers of rat motor cortex. *Brain Stimulation*, 4(4):228–241, 2011.

[310] Azadeh Yazdan-Shahmorad, Daniel B Silversmith, Viktor Kharazia, and Philip N Sabes. Targeted cortical reorganization using optogenetics in non-human primates. *eLife*, 7:1–21, 2018.

[311] Ofer Yizhar, Lief E. Fenno, Thomas J. Davidson, Murtaza Mogri, and Karl Deisseroth. Optogenetics in Neural Systems. *Neuron*, 71(1):9–34, 2011.

[312] Dong Yu and Li Deng. Deep Learning and Its Applications to Signal and Information Processing [Exploratory DSP]. *IEEE Signal Processing Magazine*, 28(1):145–154, jan 2011.

[313] Abraham Zangen, Yiftach Roth, Bernhard Voller, and Mark Hallett. Transcranial magnetic stimulation of deep brain regions: Evidence for efficacy of the H-Coil. *Clinical Neurophysiology*, 116(4):775–779, 2005.

[314] Stavros Zanos, Irene Rembado, Daofen Chen, and Eberhard E. Fetz. Phase-Locked Stimulation during Cortical Beta Oscillations Produces Bidirectional Synaptic Plasticity in Awake Monkeys. *Current Biology*, pages 1–12, aug 2018.

[315] Honghui Zhang, Andrew J. Watrous, Ansh Patel, and Joshua Jacobs. Theta and Alpha Oscillations Are Traveling Waves in the Human Neocortex. *Neuron*, 98(6):1269–1281.e4, 2018.

[316] Andy Zhou, Benjamin C Johnson, and Rikky Muller. Toward true closed-loop neuromodulation: artifact-free recording during stimulation. *Current Opinion in Neurobiology*, 50:119–127, 2018.

[317] Andy Zhou, Samantha R Santacruz, Benjamin C Johnson, George Alexandrov, Ali Moin, Fred L Burghardt, Jan M Rabaey, Jose M Carmena, and Rikky Muller. A wireless and artefact-free 128-channel neuromodulation device for closed-loop stimulation and recording in non-human primates. *Nature Biomedical Engineering*, 2018.

Appendix A

MACROSCOPIC RESISTIVITY APPENDIX

Here are additional plots of the recorded waveforms for the rest of our subjects.

Subject #	# Channels Discarded	Specific Channels
1	3	[17, 18, 19]
2	9	[23, 27, 28, 29, 30, 32, 44, 52, 60]
3	1	[57]
4	4	[2, 3, 31, 57]
5	4	[1, 49, 58, 59]
6	10	[57–64]
7	5	[1, 9, 10, 35, 43]

Table A.1: Channels excluded by visual inspection for resistivity values calculated in Table A.2.

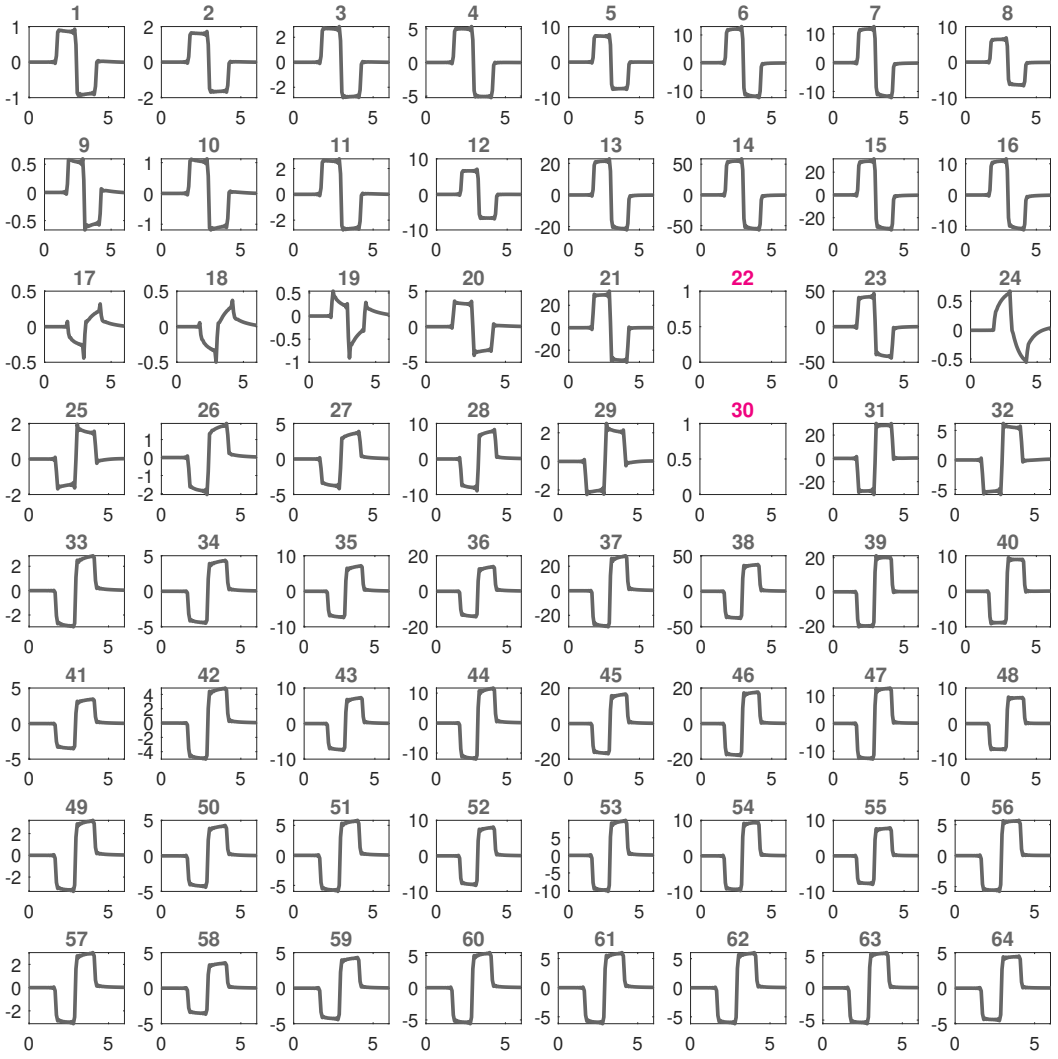

Figure A.1: Average recorded waveforms for subject 1. The x-axis units are in milliseconds, while the y-axis units are in millivolts. The stimulation channels are represented by the blank channels. The channels not included in supplementary analysis (17, 18, 19) are shown in Table A.1. Discarding these channels did not change the resistivity values appreciably, as shown in Table A.2.

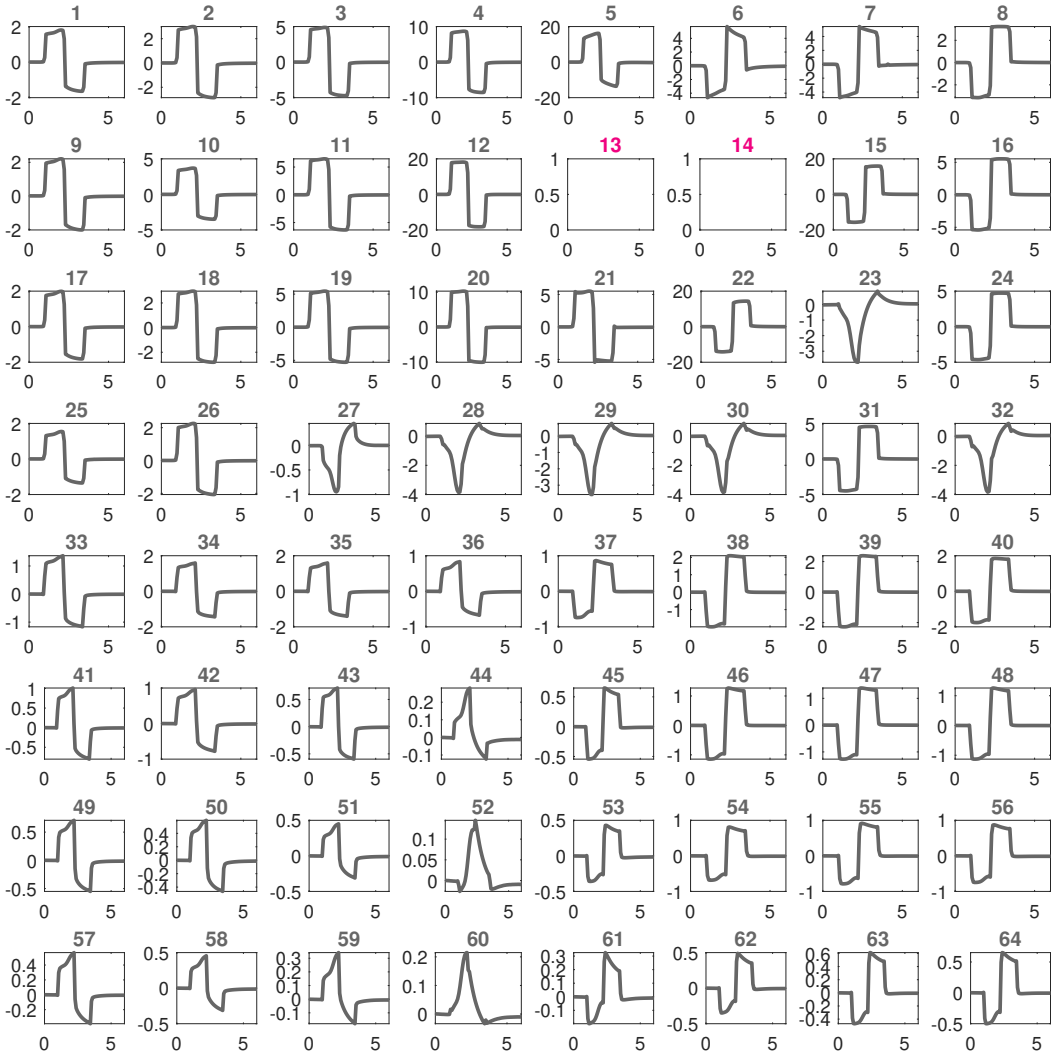

Figure A.2: Average recorded waveforms for subject 2. The x-axis units are in milliseconds, while the y-axis units are in millivolts. The stimulation channels are represented by the blank channels. The channels not included in supplementary analysis (23, 27, 28, 29, 30, 32, 44, 52, 60) are shown in Table A.1. Discarding these channels did not change the resistivity values appreciably, as shown in Table A.2.

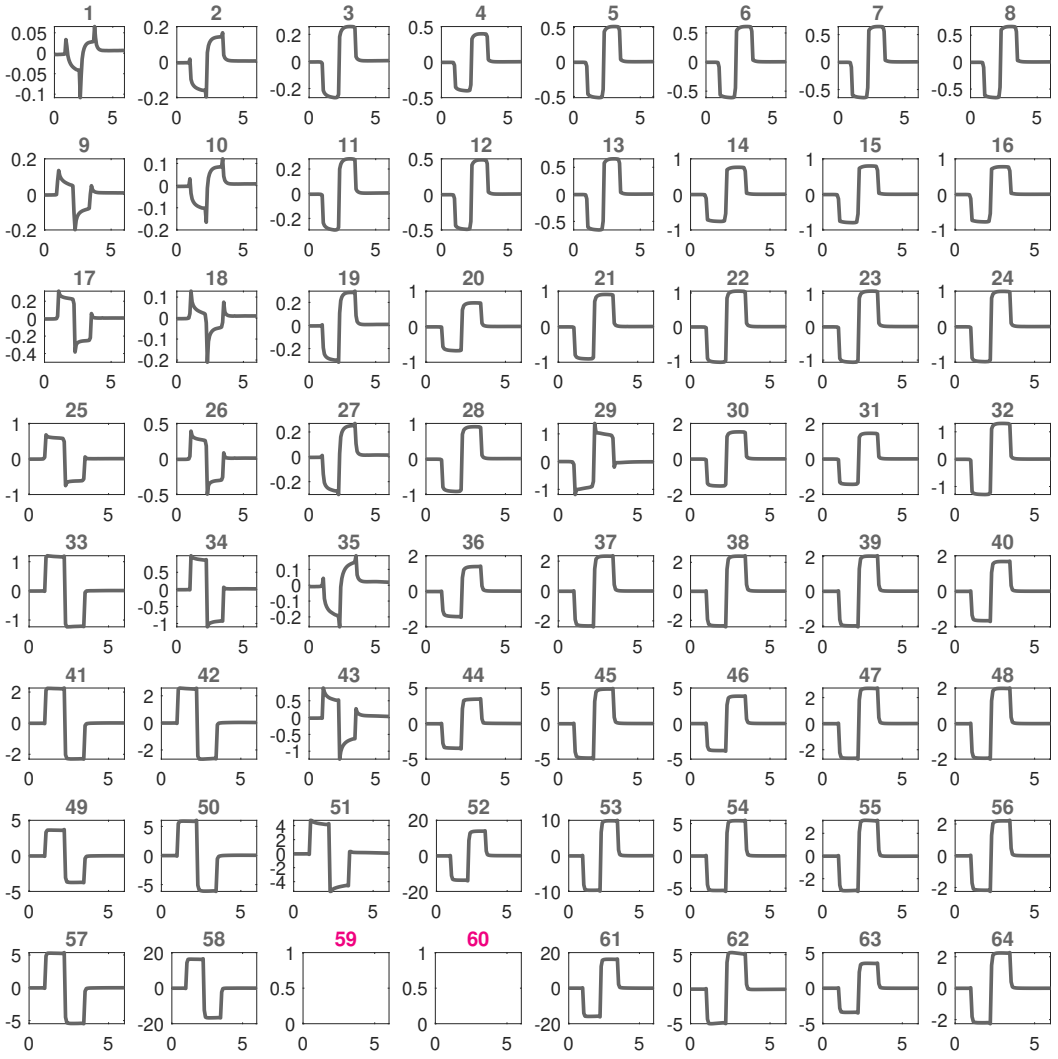

Figure A.3: Average recorded waveforms for subject 4. The x-axis units are in milliseconds, while the y-axis units are in millivolts. The stimulation channels are represented by the blank channels. The channels not included in supplementary analysis (2, 3, 31, 57) are shown in Table A.1. Discarding these channels did not change the resistivity values appreciably, as shown in Table A.2.

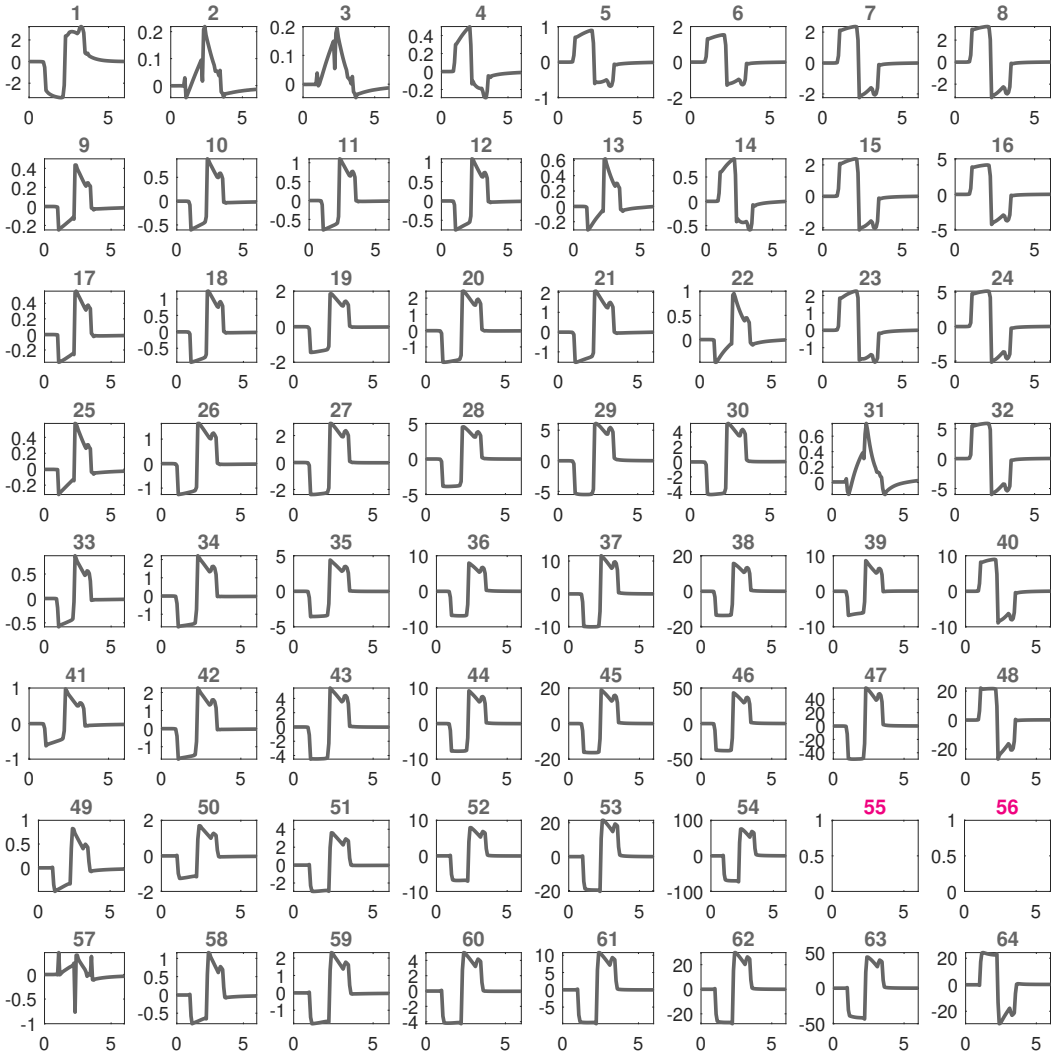

Figure A.4: Average recorded waveforms for subject 5. The x-axis units are in milliseconds, while the y-axis units are in millivolts. The stimulation channels are represented by the blank channels. The channels not included in supplementary analysis (1, 49 , 58, 59) are shown in Table A.1. Discarding these channels did not change the resistivity values appreciably, as shown in Table A.2.

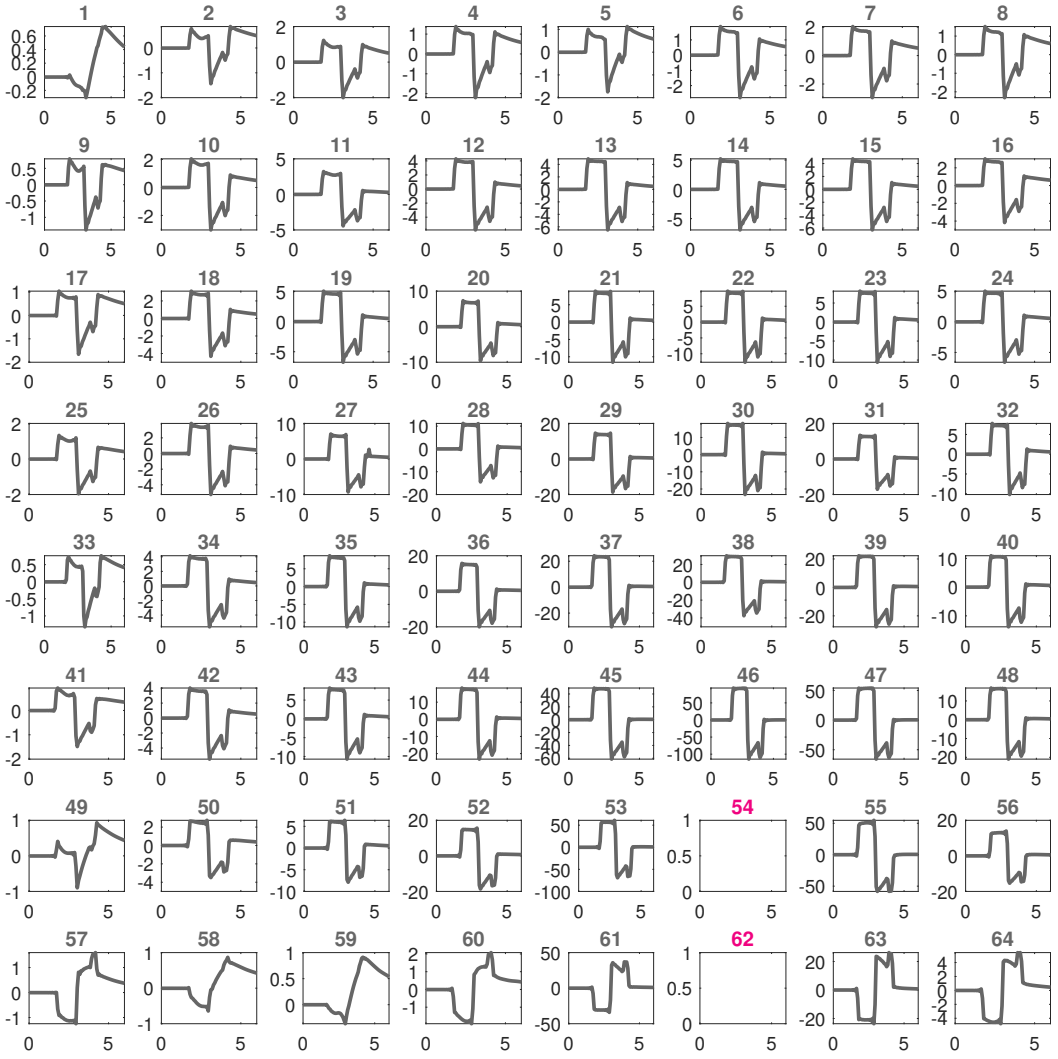

Figure A.5: Average recorded waveforms for subject 6. The x-axis units are in milliseconds, while the y-axis units are in millivolts. The stimulation channels are represented by the blank channels. The channels not included in supplementary analysis (57 – 64) are shown in Table A.1. Discarding these channels did not change the resistivity values appreciably, as shown in Table A.2.

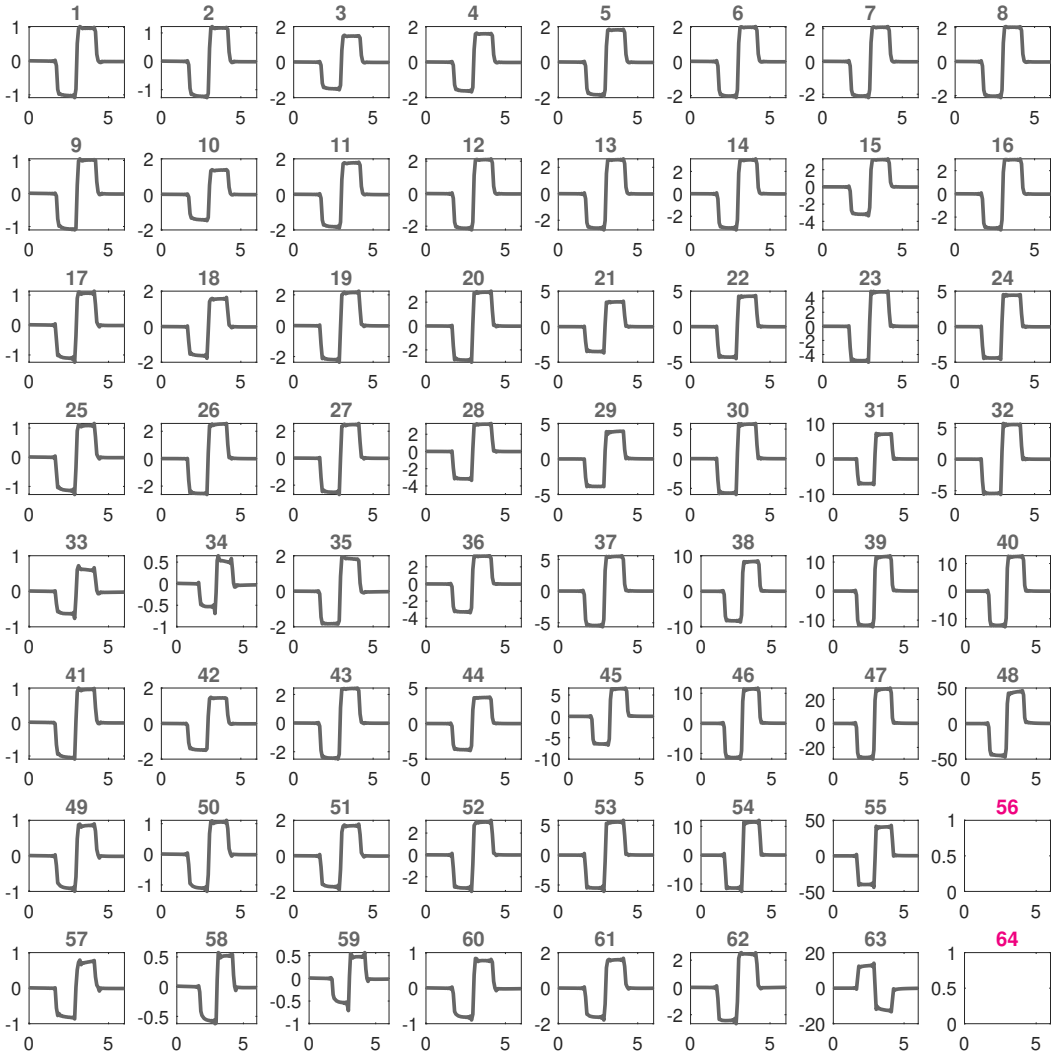

Figure A.6: Average recorded waveforms for subject 7. The x-axis units are in milliseconds, while the y-axis units are in millivolts. The stimulation channels are represented by the blank channels. The channels not included in supplementary analysis (1, 9, 10, 35, 43) are shown in Table A.1. Discarding these channels did not change the resistivity values appreciably, as shown in Table A.2.

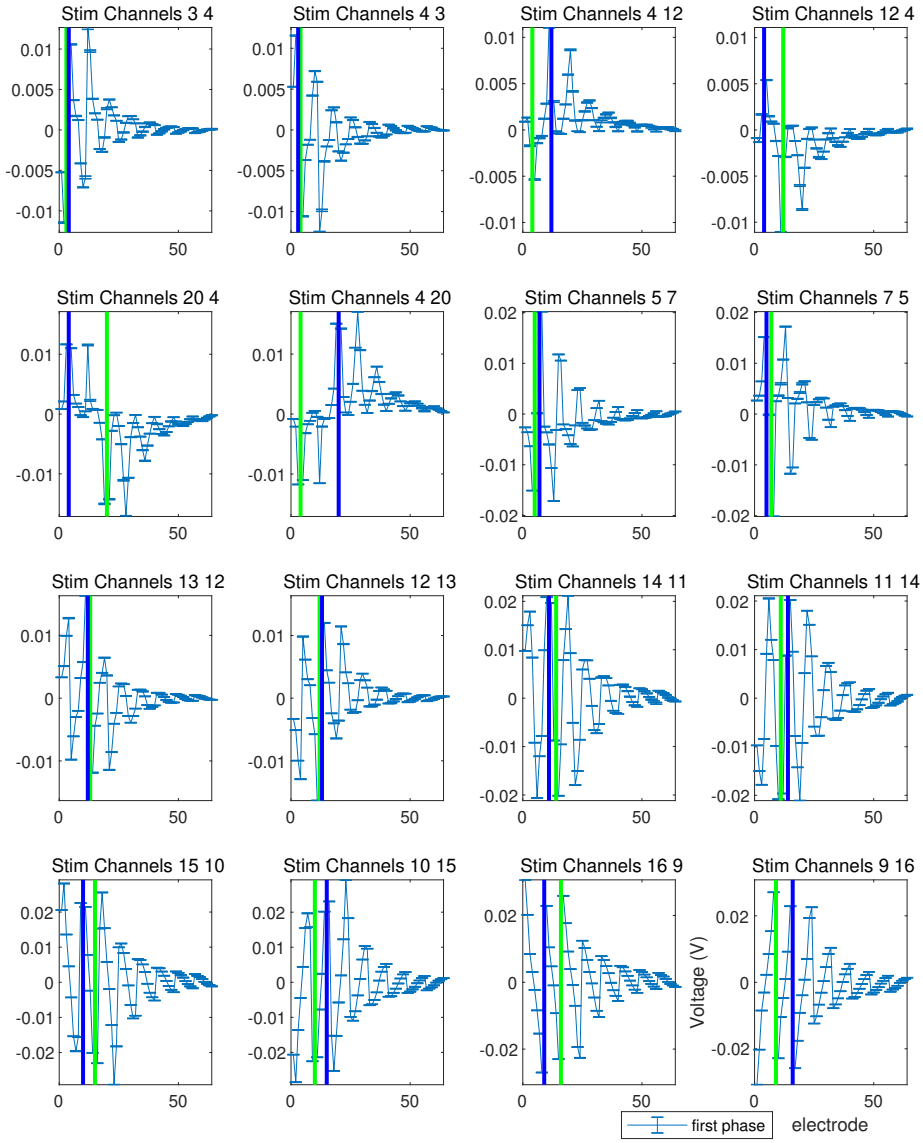

Figure A.7: The means and standard deviations of the data for the eighth subject. The means and standard deviations of the magnitudes of the stimulation artifacts for each stimulation pair and polaritiy for the eight subject following our signal extraction algorithm are plotted versus the electrode number. The mean is the mean voltage across all trials within the extracted region illustrated in Figure 3.11. The standard deviation is the standard deviation of the means of extracted regions from each individual trial. The blue and green lines indicate the stimulation electrodes. The stimulation artifact was not measured at the stimulation electrodes. Note the reproducibility of the measurements.

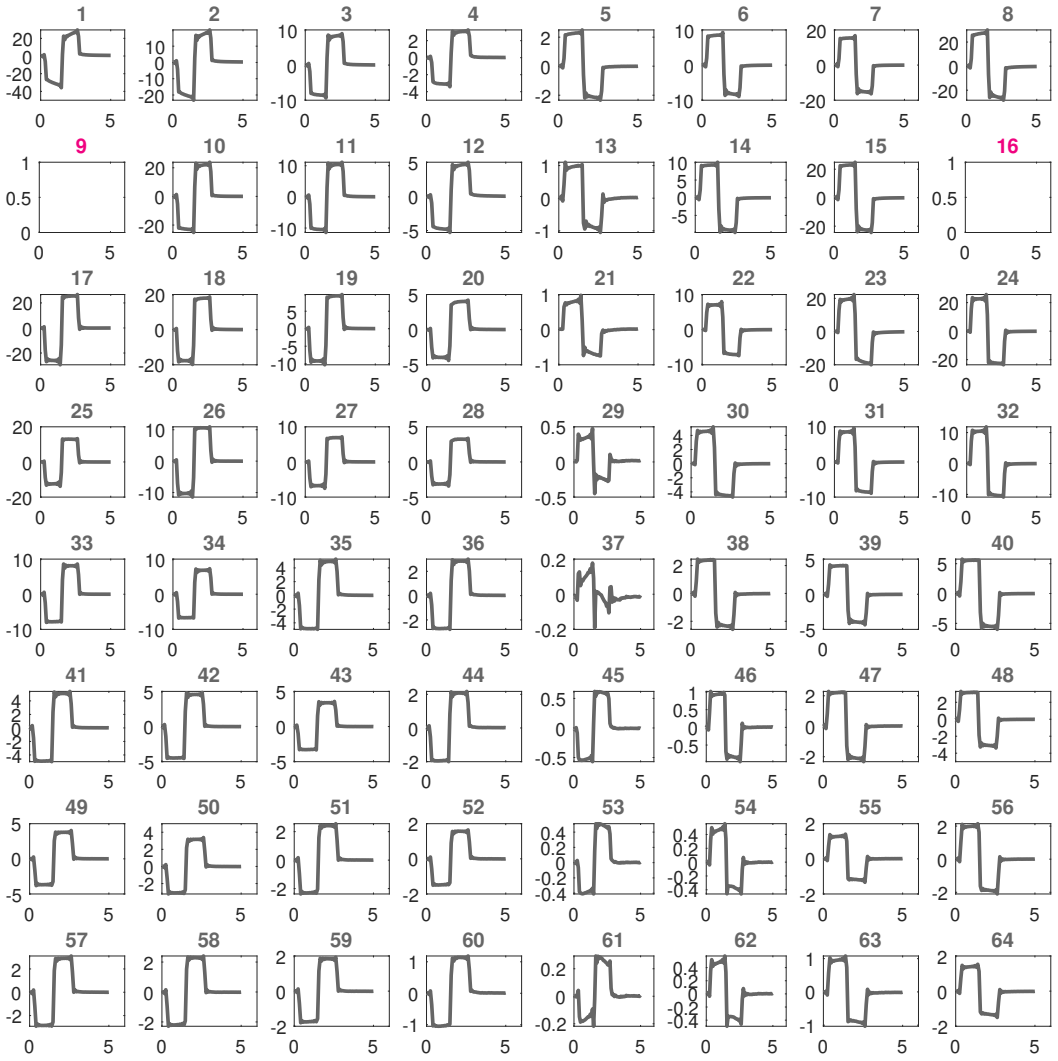

Figure A.8: Average recorded waveforms for subject 8. The x-axis units are in milliseconds, while the y-axis units are in millivolts. The stimulation channels are represented by the blank channels. We show an example of far apart electrode separation to highlight that the recorded signals are of high quality even when the stimulation pair is not adjacent, as it was for the first seven subjects.

Subject #	# Channels Discarded	Flat Three-Point	Spherical Three-Point	Flat Four-Point Mean	Flat Four-Point Median	Flat Four-Point Standard Deviation	Spherical Four-Point Mean	Spherical Four-Point Median	Spherical Four-Point Standard Deviation
1	3	3.27	3.01	3.54	3.45	1.27	3.12	2.99	1.17
2	9	2.74	2.32	3.42	3.44	1.34	2.62	2.57	1.08
3	1	2.97	2.62	3.41	3.25	0.96	2.74	2.71	0.70
4	4	2.76	2.42	3.17	3.08	1.05	2.45	2.31	0.92
5	4	2.67	2.48	3.07	3.13	1.28	2.64	2.64	1.16
6	10	4.55	4.07	5.35	5.38	1.84	4.57	4.65	1.77
7	5	2.44	2.52	3.19	2.79	1.79	2.61	2.25	1.68

Table A.2: Table showing the resistivities by subject after qualitatively removing bad channels

Appendix B

ARTIFACT REJECTION APPENDIX

B.1 Array-wide processed signals

To better illustrate the performance of our algorithm across all channels processed, we highlight two subjects, where we used one set of parameters for all of the channels. Parameter tuning for subsets of channels would result in better performance of the algorithm, but we seek to highlight that with one global set of parameters reasonable performance is achieved.

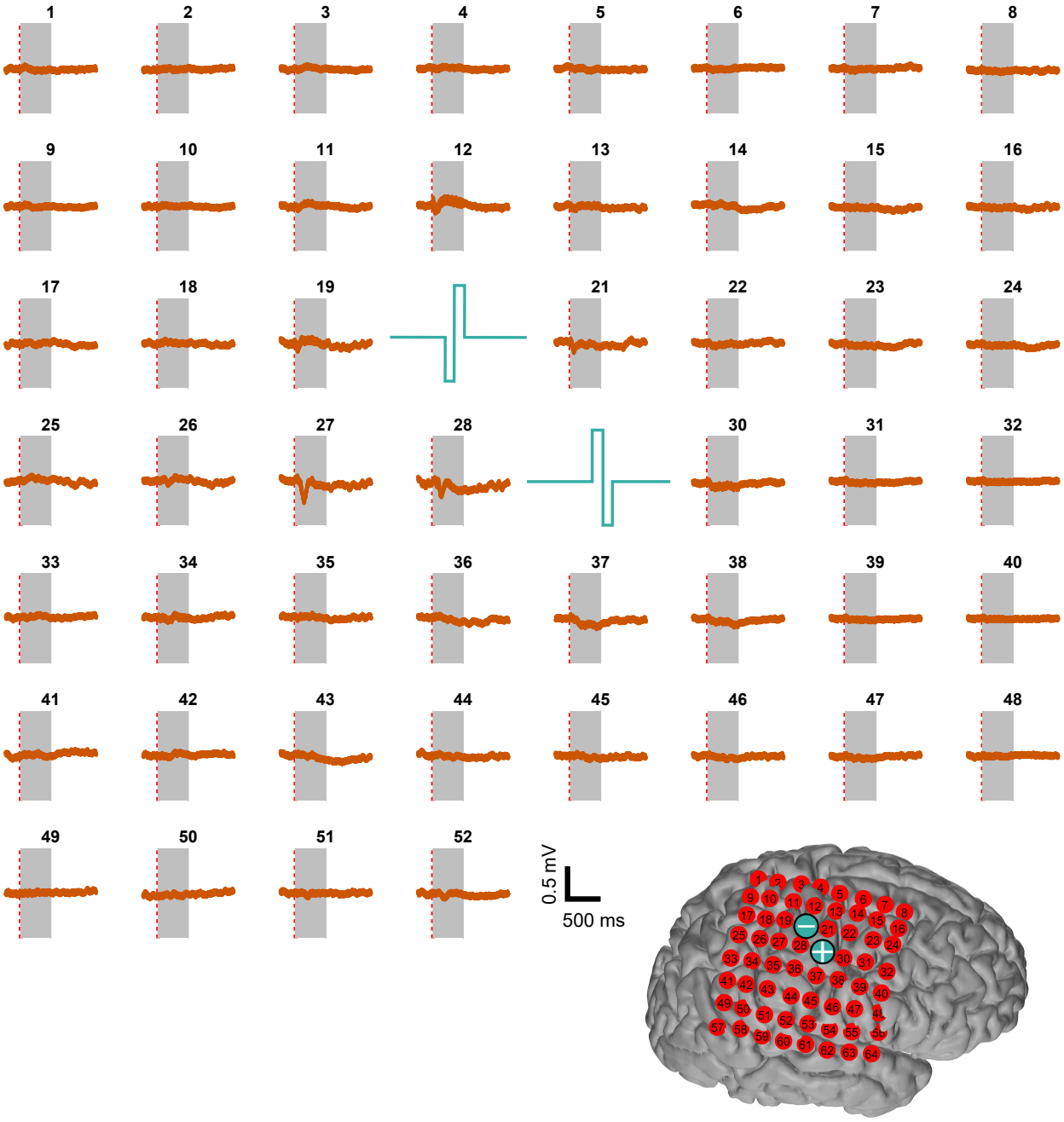

Figure B.1: Average time-series responses following processing across cortex. Gray window highlights stimulation time period, example data file 1. Blue bipolar waveforms indicate the stimulation channels. Cortical reconstruction for this subject, with the corresponding stimulation waveforms plotted over the stimulation electrodes.

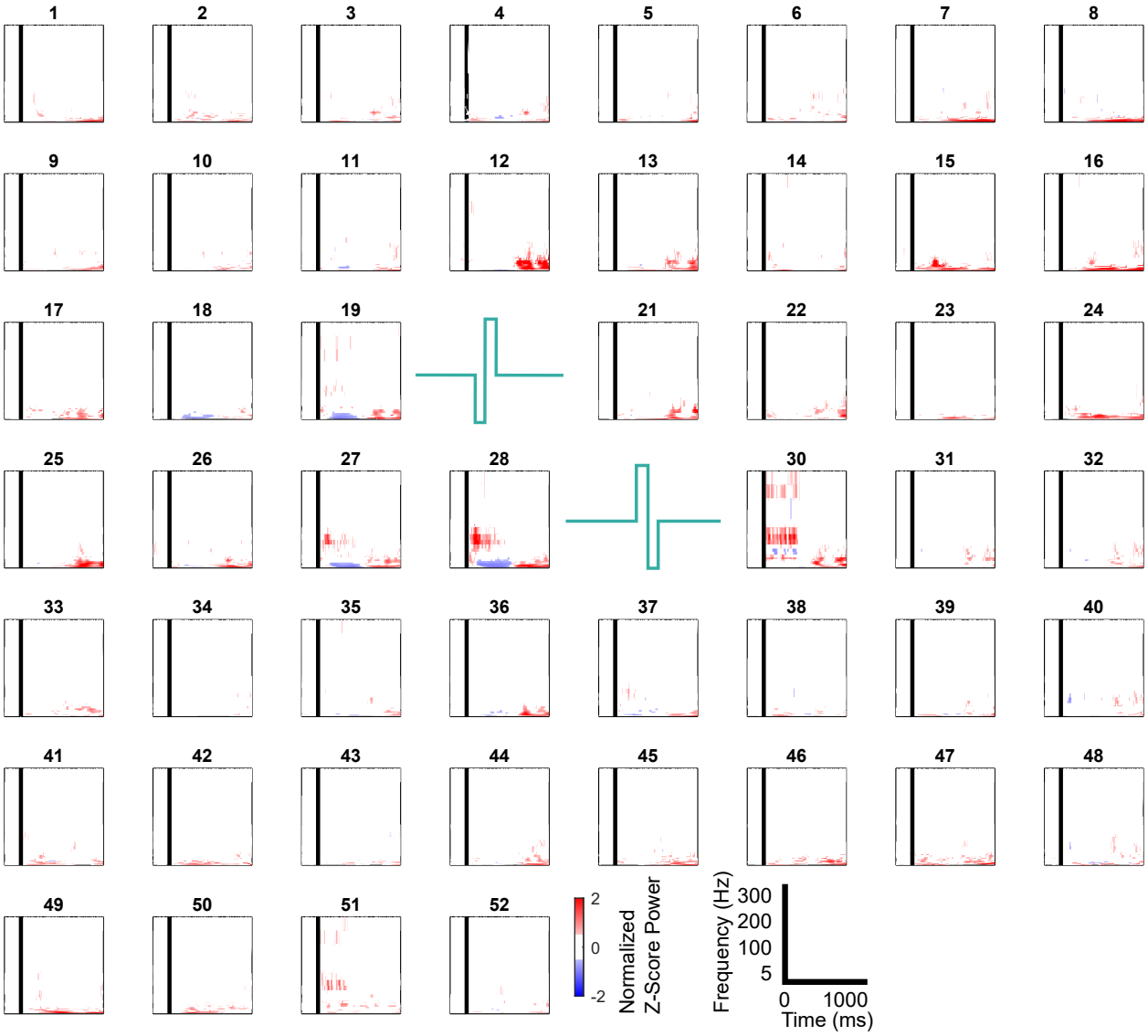

Figure B.2: Average time-frequency responses following processing across cortex for example data file 1. Black bar indicates the beginning of the stimulation window. Blue bipolar waveforms indicate the stimulation channels.

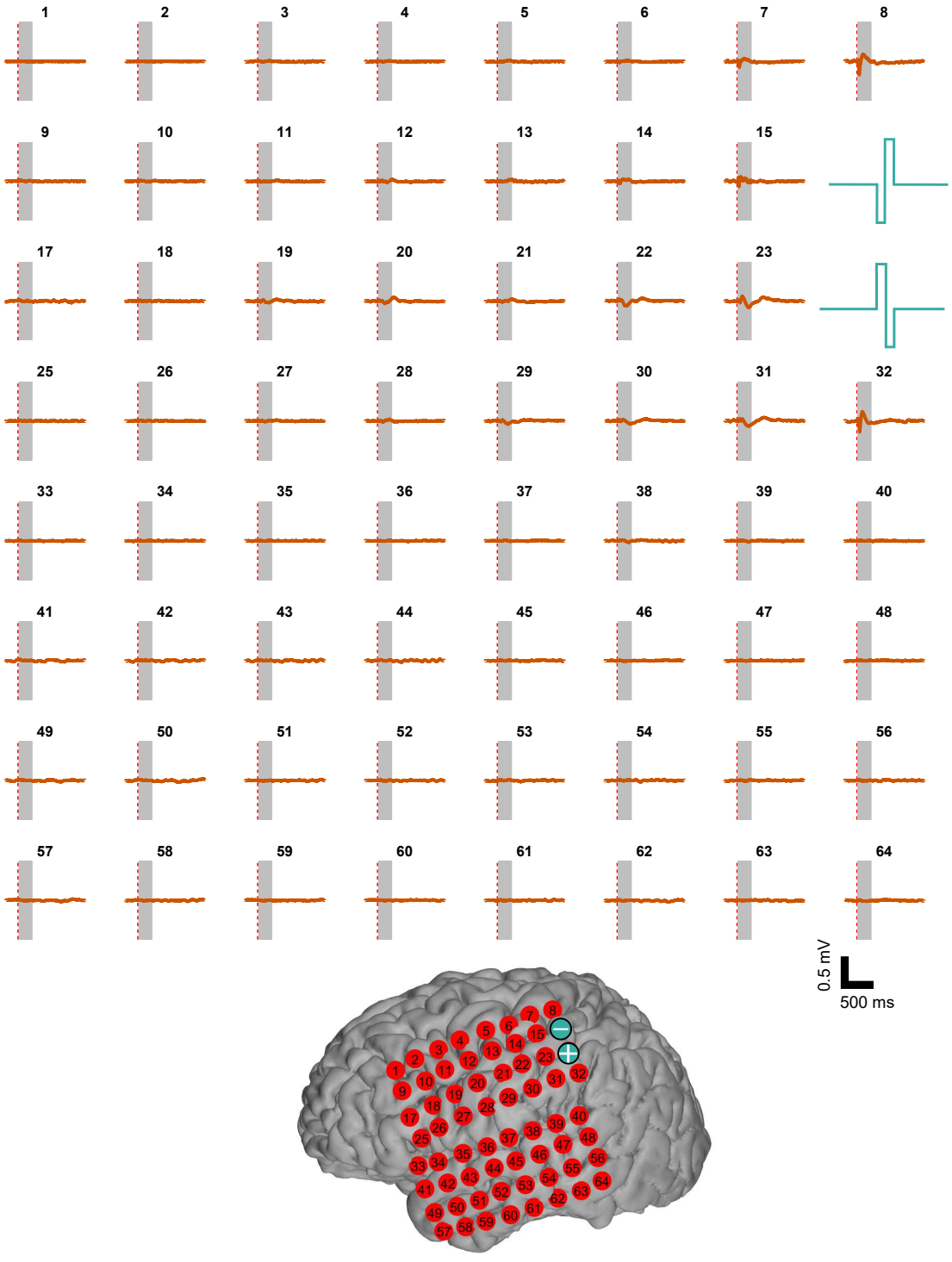

Figure B.3: Average time-series responses following processing across cortex. Gray window highlights stimulation time period, example data file 2. Blue bipolar waveforms indicate the stimulation channels. Cortical reconstruction for this subject, with the corresponding stimulation waveforms plotted over the stimulation electrodes.

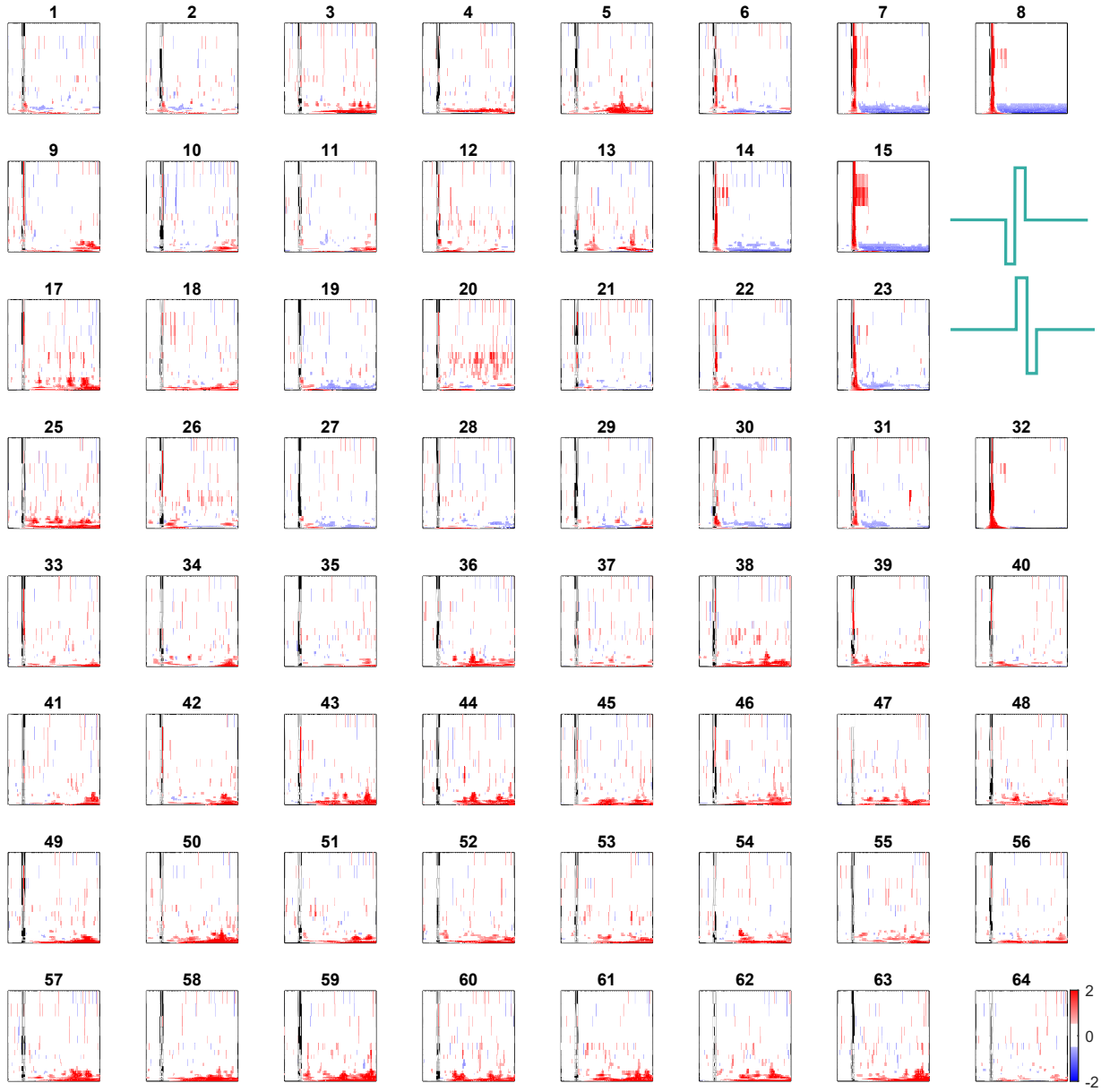

Figure B.4: Average time-frequency responses following processing across cortex for example data file 2. Black bar indicates the beginning of the stimulation window. Blue bipolar waveforms indicate the stimulation channels. The x,y, and colorbar scales are the same as for figure B.2

Appendix C

RESPONSE TIMING APPENDIX

C.0.1 Digital touch probe latency

In order to assess reaction times to natural haptic touch via mechanical means, we measured the latency between contact of the digital touch probe to the surface and the digitally registered contact. Previous literature [61] and corresponding work with our group demonstrated the digital touch probes to have an average onset latency of 1.04 ms $\pm$ 0.48 ms standard deviation. To account for experimenter variability and possible hardware sensitivity changes over time, we characterized the latency in onset of the digital touch probes by comparing the registered digital touch probe output relative to an electrical short circuit that triggered on digital touch probe contact with a surface with 294 touches (Figure C.1).

Each trial was registered on the Tucker Davis Technologies RZ5D analog inputs via the front panel, and the two triggered onsets were subtracted from one another to calculate an onset latency. We calculated a mean onset latency of 5.83 ms, a standard deviation of 3.26 ms, and a median onset latency of 5.24 ms (Figure C.2).

Based on these measurements, we acknowledge that our response timing results are minimally shifted towards a faster reaction time for natural, haptic touch by an average of approximately 6 ms. Adjusting the current findings for these delays (measured reaction times by the mean onset latency) does not significantly impact our results or interpretations. To specifically illustrate this, we recalculated the statistics after adjustments. These resulting p-values, shown in Table C.1, are nearly identical with respect to the originally estimated p-values and thus do not change our conclusions.

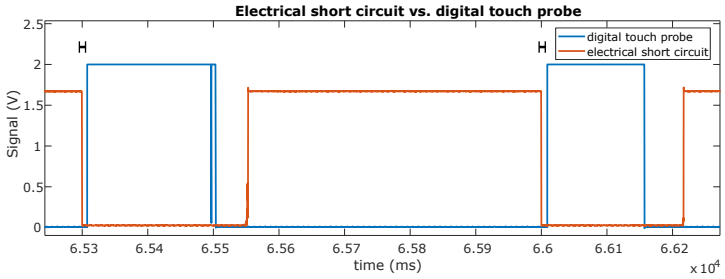

Figure C.1: Example electrical short circuit and digital touch probe signal traces. Time course of pull-up electrical short circuit relative to the digital touch probe onset. Each touch probe onset was compared to the electrical short circuit that preceded it, as indicated by the horizontal black bars, and these onset latencies were used to generate the distribution of latencies in Figure C.1.

Subject	Experimental Condition Digital Touch Probe vs.	p-value
1	200 ms	2.101e-15
2	100 ms	1.834e-7
	200 ms	2.900e-4
	400 ms	9.369e-6
	800 ms	9.046e-6
3	200 ms	0.033
	400 ms	7.019e-8
	800 ms	1.609e-10
4	200 ms	2.225e-3
	400 ms	1.125e-4
	800 ms	1.422e-4

Table C.1: Adjusted statistics for haptic touch compared to DES. Adjusted p-values, by adding on the latency for the digital touch probe to the haptic response times, and subsequently comparing them to the DES conditions.

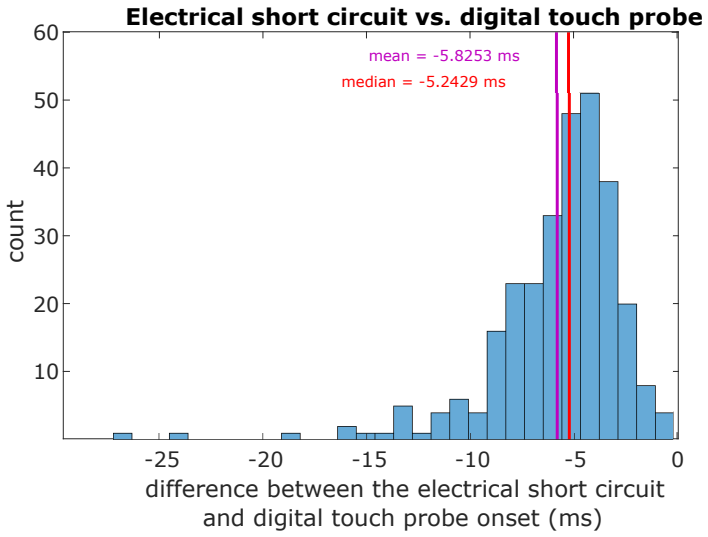

Figure C.2: Distribution of onset delays for digital touch probe. Distribution of latencies between an electrical short circuit and the registered application of contact onset using the digital touch probe. Not visualized or included in the calculations are 3 outliers at 63, 68, and 69 ms, due to light or inconsistent experimenter force application.

Appendix D

CONCURRENT STIMULATION AND WAVEFORM MODIFICATION APPENDIX

D.0.1 Analog touch probe latency

In order to assess response times to natural haptic touch via mechanical means, we measured the latency between contact of the analog touch probe to the surface and the digitally registered contact. Previous literature [61] and corresponding work with our group demonstrated the digital touch probes to have an average onset latency of 1.04 ms ± 0.48 ms standard deviation at construction, and a mean onset latency of 5.83 ms, a standard deviation of 3.26 ms, and a median onset latency of 5.24 ms after extensive use [45]. We built new analog touch probes, and characterized the latency in onset of the analog touch probes by comparing the registered digital touch probe output relative to an electrical short circuit that triggered on electrical touch probe contact with a surface.

Each trial was registered on the Tucker Davis Technologies RZ5D analog inputs via the front panel, and the two triggered onsets were subtracted from one another to calculate an onset latency. We discarded any trials where the analog sensor registered contact before the electrical short circuit, or where the difference was greater than 40 ms. We calculated a mean onset latency of 5.62 ms, a standard deviation of 4.92 ms, and a median onset latency of 3.99 ms (Figure D.1).

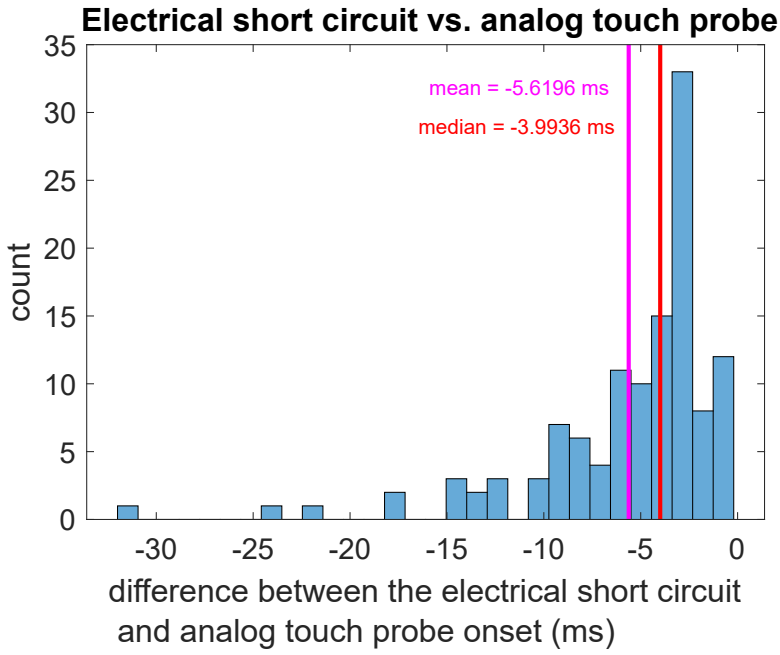

Figure D.1: Distribution of latencies between an electrical short circuit and the registered application of contact onset using the analog touch probe. Not visualized or included in the calculations are outliers with a difference less than 0 or greater than 40 ms.

Appendix E

BETA-OSCILLATION TRIGGERED STIMULATION APPENDIX

Subject	Current (mA)	Phases set to be delivered		Age	Gender	Grid side and location	Reason for failure
SS1	Unknown	Unknown		42	F	48 channel right frontal	No evoked potentials recorded
SS2	1.5	90°	270°	39	M	48 channel left tempo-ral/occipital	Seizure
SS3	2	90°	270°	25	M	64 channel right side grid	Possible abnormal anatomy due to schizencephaly

Table E.1: Beta stimulation supplemental subject demographics. Subjects (SS, supplementary subjects) for whom beta-oscillation triggered stimulation was attempted, but not successfully completed or carried out.

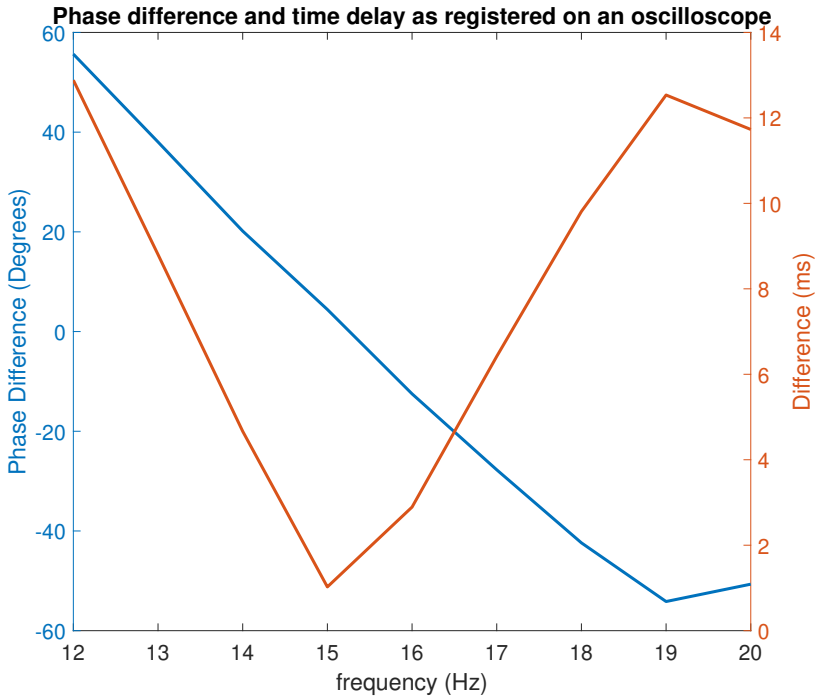

Figure E.1: Oscilloscope test of real time filter. A pure sinusoidal signal generated at frequencies between 12 and 20 Hz was fed into an oscilloscope, as well as our hardware and closed loop processing chain. We triggered stimulation on the TDT, and fed the stimulation into the oscilloscope. We subsequently calculated the phase difference, and delay in milliseconds, at each sinusoidal frequency, between the ideal and actual phase of stimulation. The IIR nature of our real time filter can be seen due to the non-linear changes in phase.

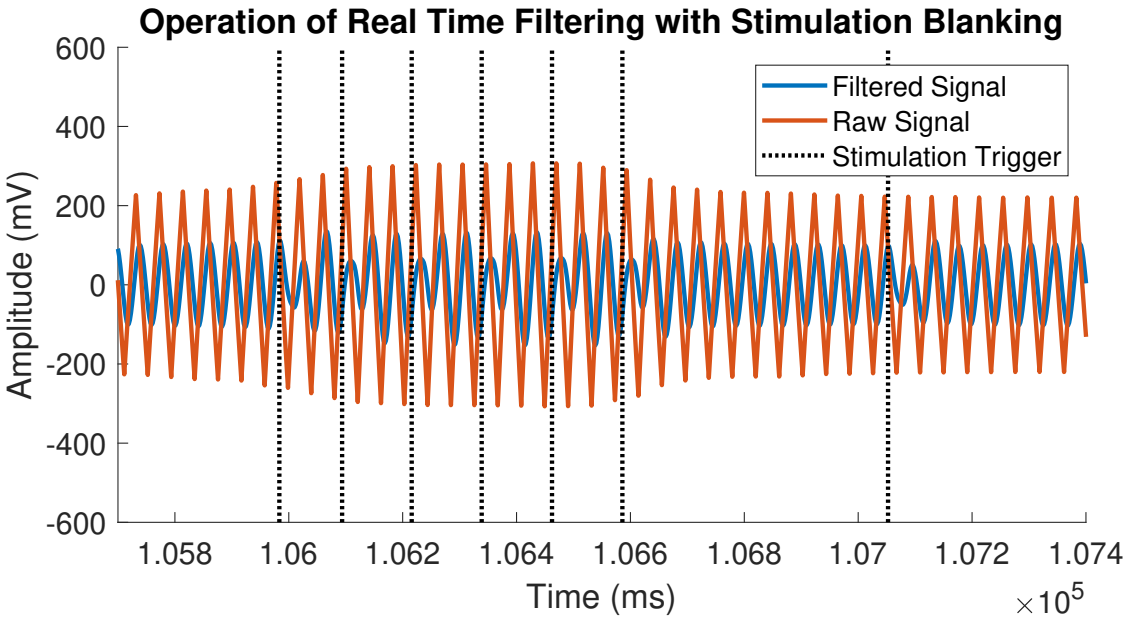

Figure E.2: Real time tracking of triangular waveform. Generated triangular waveform fed through TDT processing chain and band pass filtering. High amplitude signal around 9.7e4 ms represents a "null" trial condition where no stimuli are supposed to be delivered, while the higher amplitude signal beginning around 9.9e4 ms represents conditioning stimuli set to be delivered on the peak of the beta filtered signal. Black vertical lines indicate start of stimulation trigger, and subsequent blanking of the signal before bandpass filtering. Distortion immediately after black vertical line indicates effect of blanking the signal before bandpass filtering.

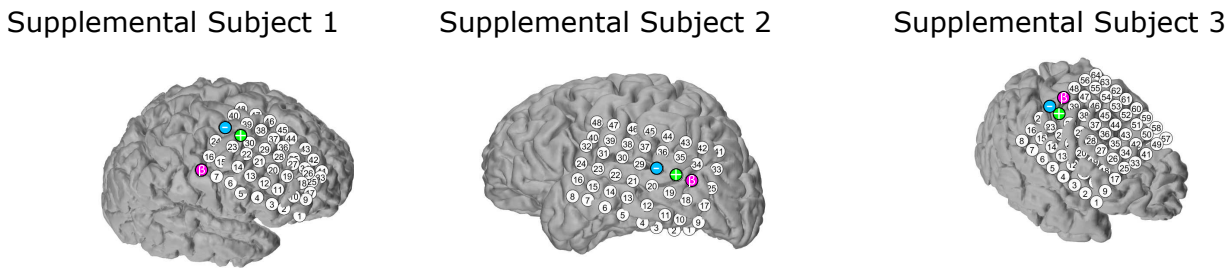

Figure E.3: Cortical reconstructions of the three subjects in supplementary table E.1 not included in analysis (did not complete study protocol

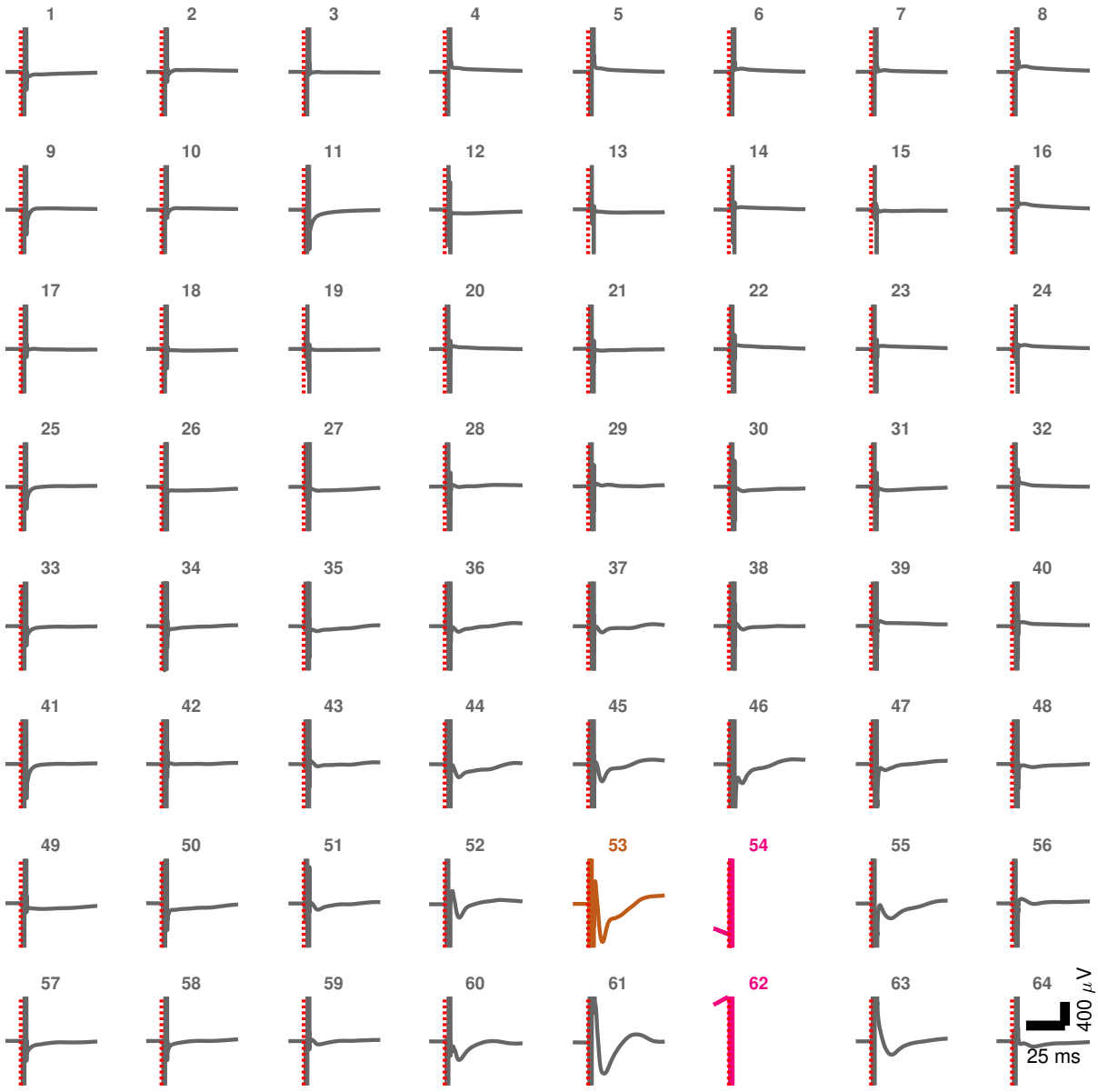

Figure E.4: Map of CEPs across cortex for subject 1. Pink channels indicate the stimulation channels, while gold indicates the trigger channel. Note the complex and variable morphologies across the cortex, with primarily local responses. The scale bar in the lower right applies to all subplots within the image. We are unable to simultaneously record and stimulate from the stimulation channels, so any signal visualized there should be disregarded.

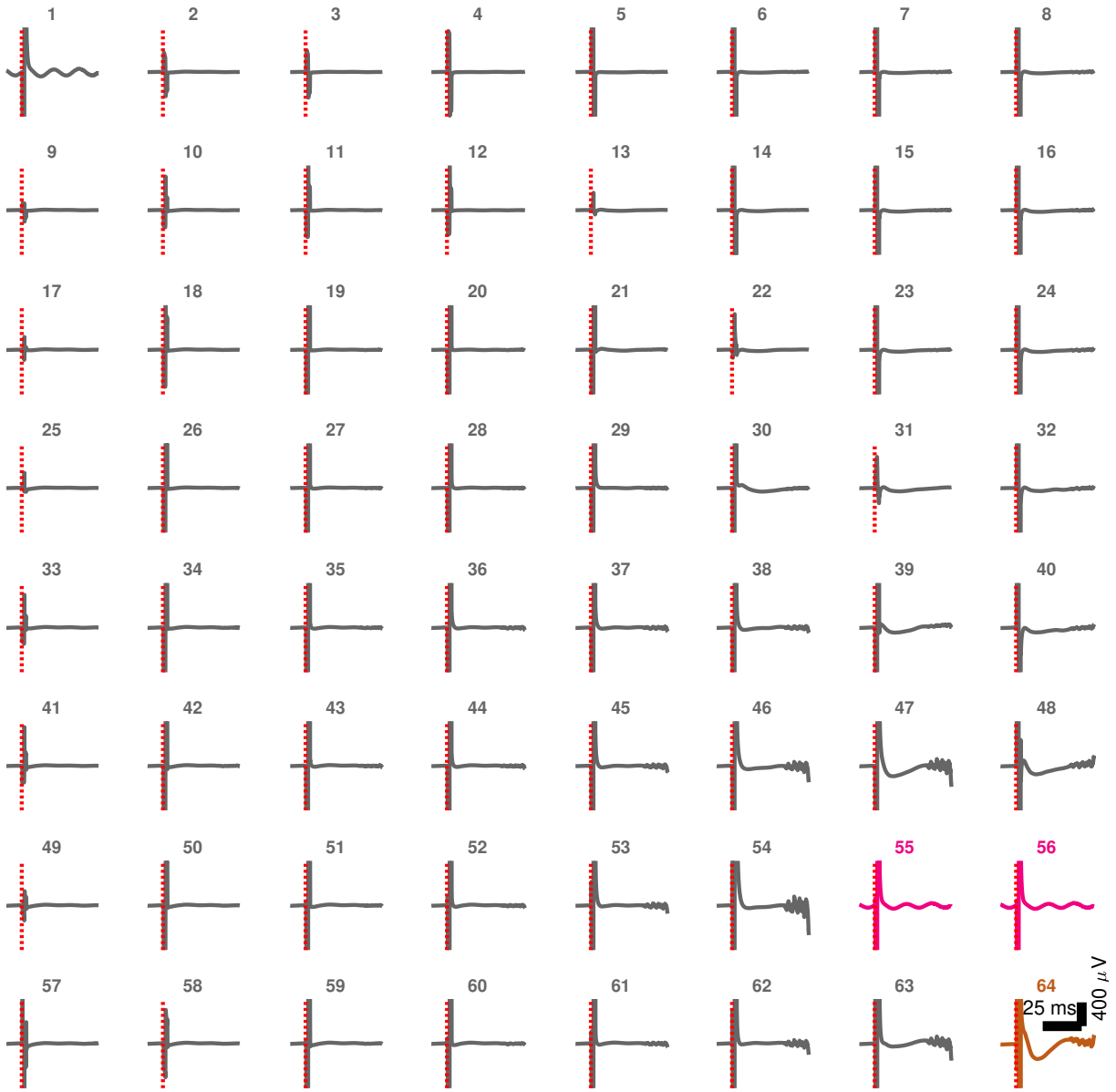

Figure E.5: Map of CEPs across cortex for subject 2. Pink channels indicate the stimulation channels, while gold indicates the trigger channel. Note the complex and variable morphologies across the cortex, with primarily local responses. The scale bar in the lower right applies to all subplots within the image. We are unable to simultaneously record and stimulate from the stimulation channels, so any signal visualized there should be disregarded.

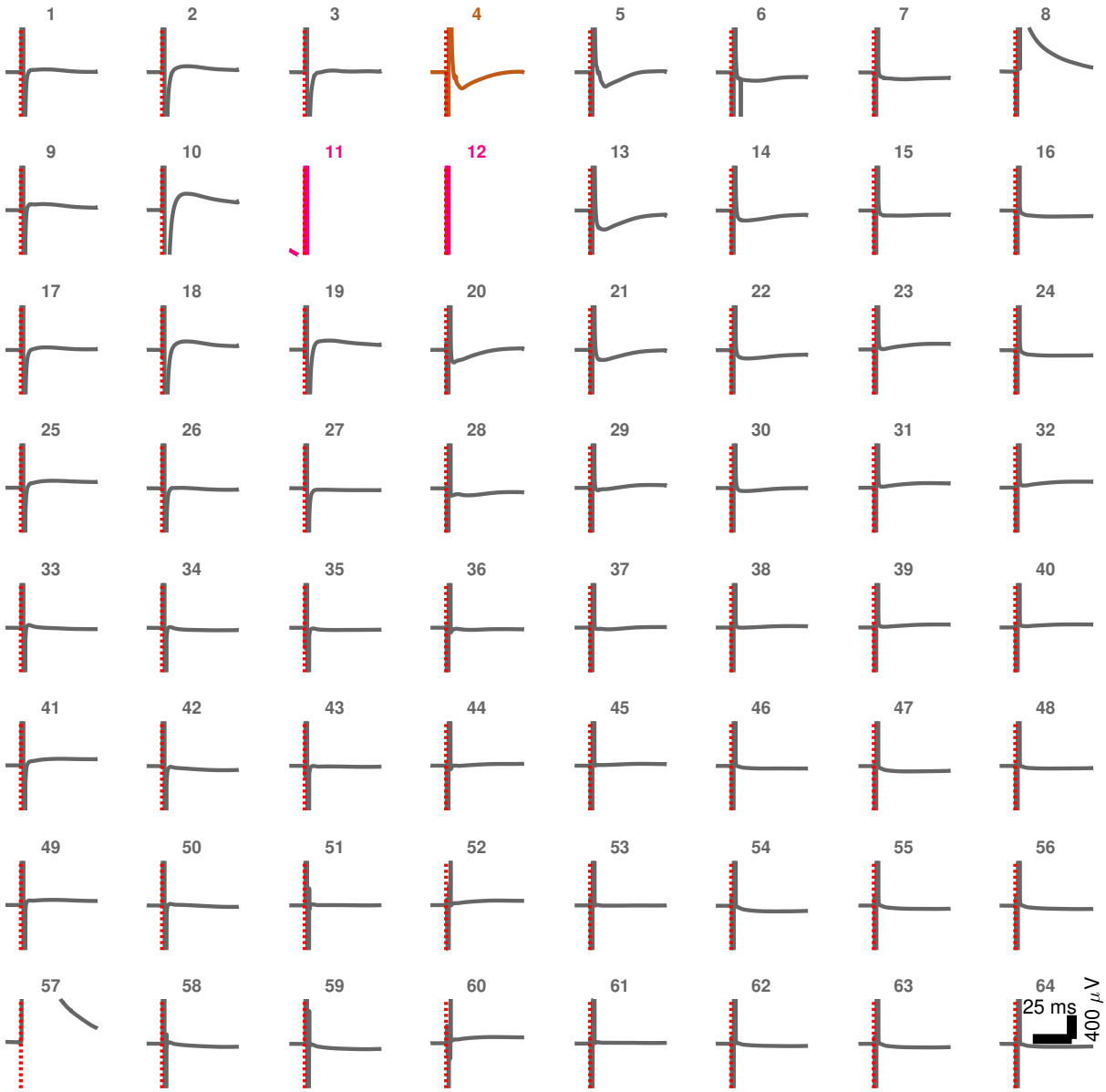

Figure E.6: Map of CEPs across cortex for subject 3. Pink channels indicate the stimulation channels, while gold indicates the trigger channel. Note the complex and variable morphologies across the cortex, with primarily local responses. The scale bar in the lower right applies to all subplots within the image. We are unable to simultaneously record and stimulate from the stimulation channels, so any signal visualized there should be disregarded.

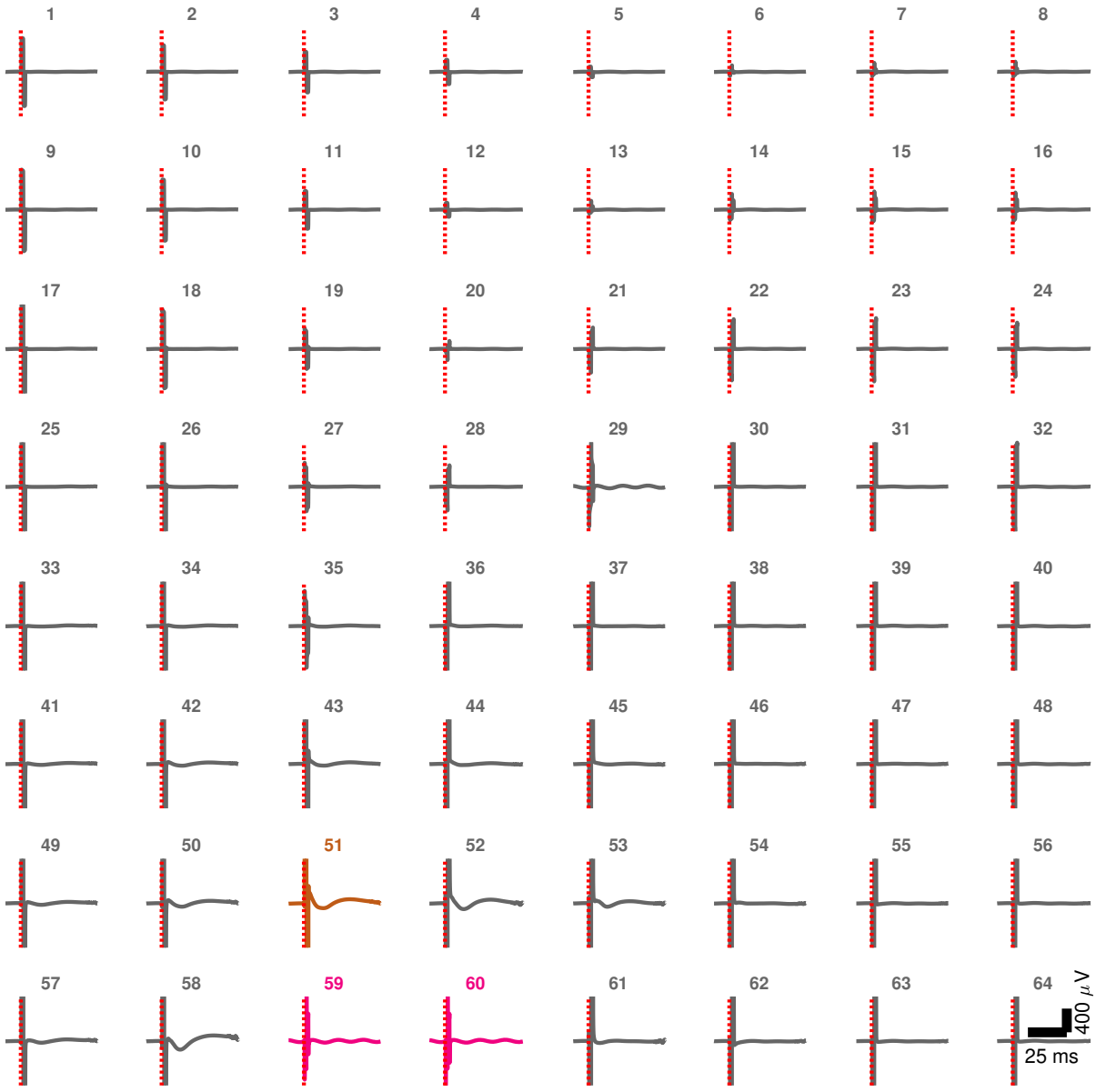

Figure E.7: Map of CEPs across cortex for subject 4. Pink channels indicate the stimulation channels, while gold indicates the trigger channel. Note the complex and variable morphologies across the cortex, with primarily local responses. The scale bar in the lower right applies to all subplots within the image. We are unable to simultaneously record and stimulate from the stimulation channels, so any signal visualized there should be disregarded.

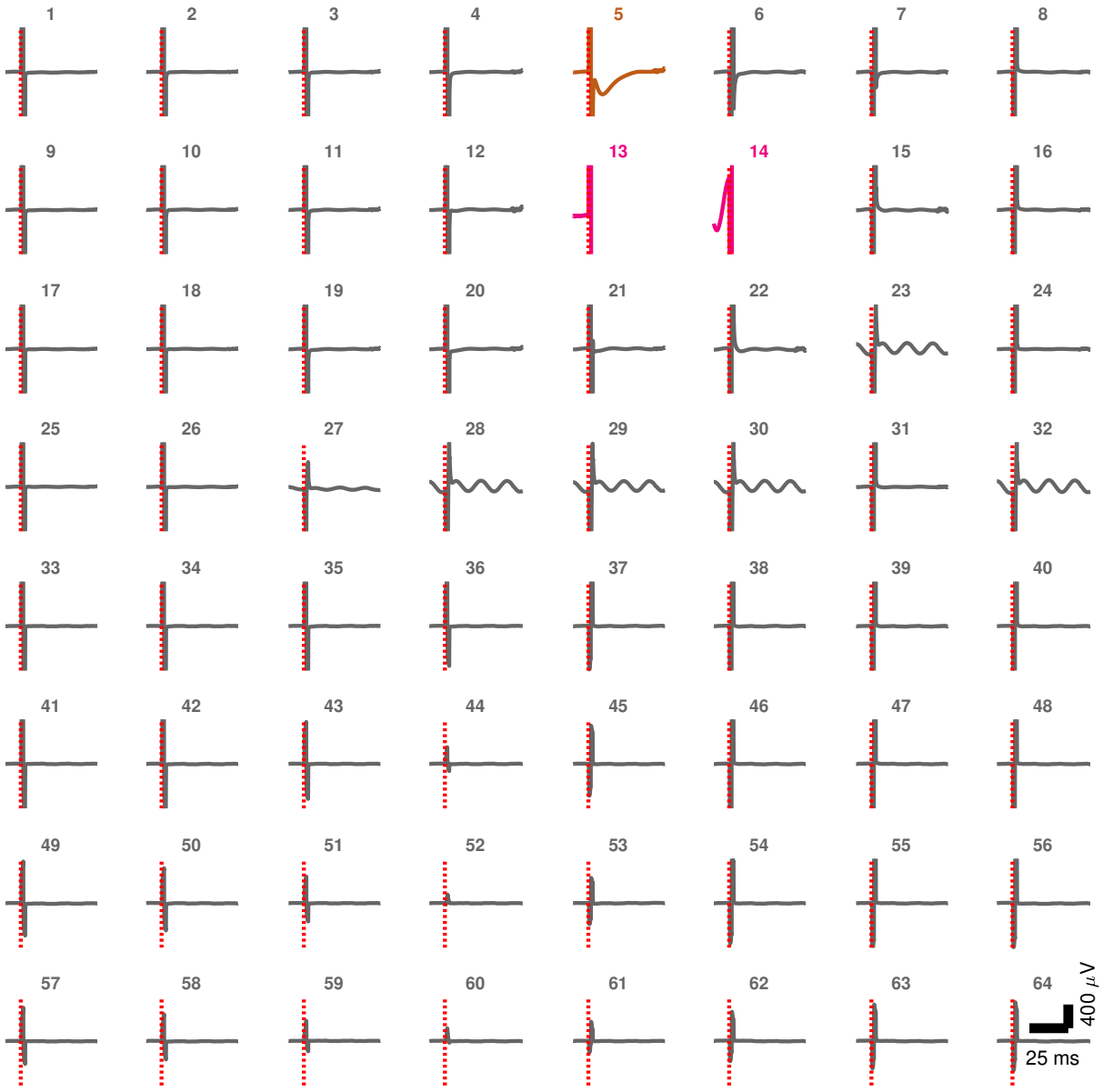

Figure E.8: Map of CEPs across cortex for subject 5. Pink channels indicate the stimulation channels, while gold indicates the trigger channel. Note the complex and variable morphologies across the cortex, with primarily local responses. The scale bar in the lower right applies to all subplots within the image. We are unable to simultaneously record and stimulate from the stimulation channels, so any signal visualized there should be disregarded.

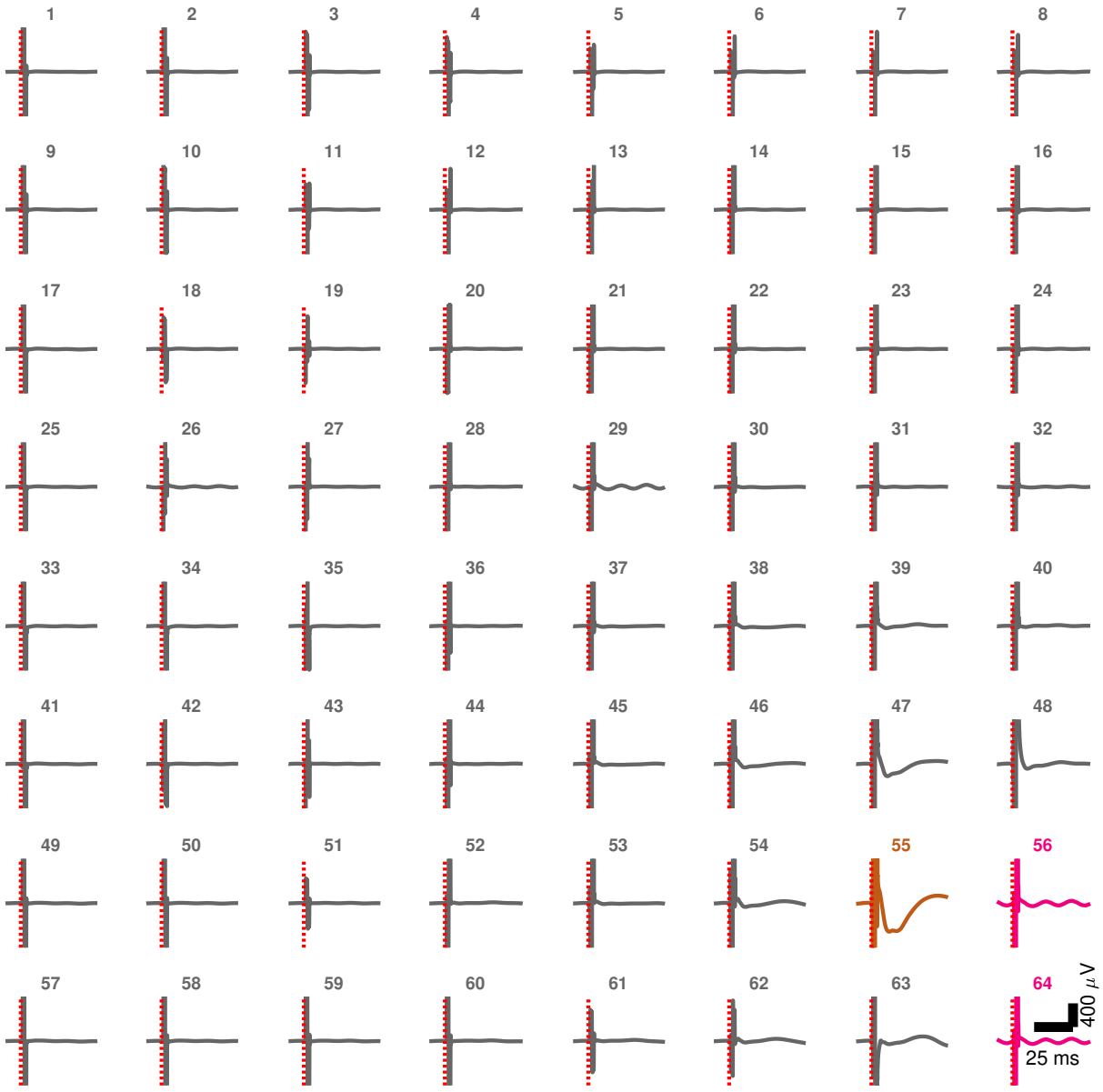

Figure E.9: Map of CEPs across cortex for subject 6. Pink channels indicate the stimulation channels, while gold indicates the trigger channel. Note the complex and variable morphologies across the cortex, with primarily local responses. The scale bar in the lower right applies to all subplots within the image. We are unable to simultaneously record and stimulate from the stimulation channels, so any signal visualized there should be disregarded.

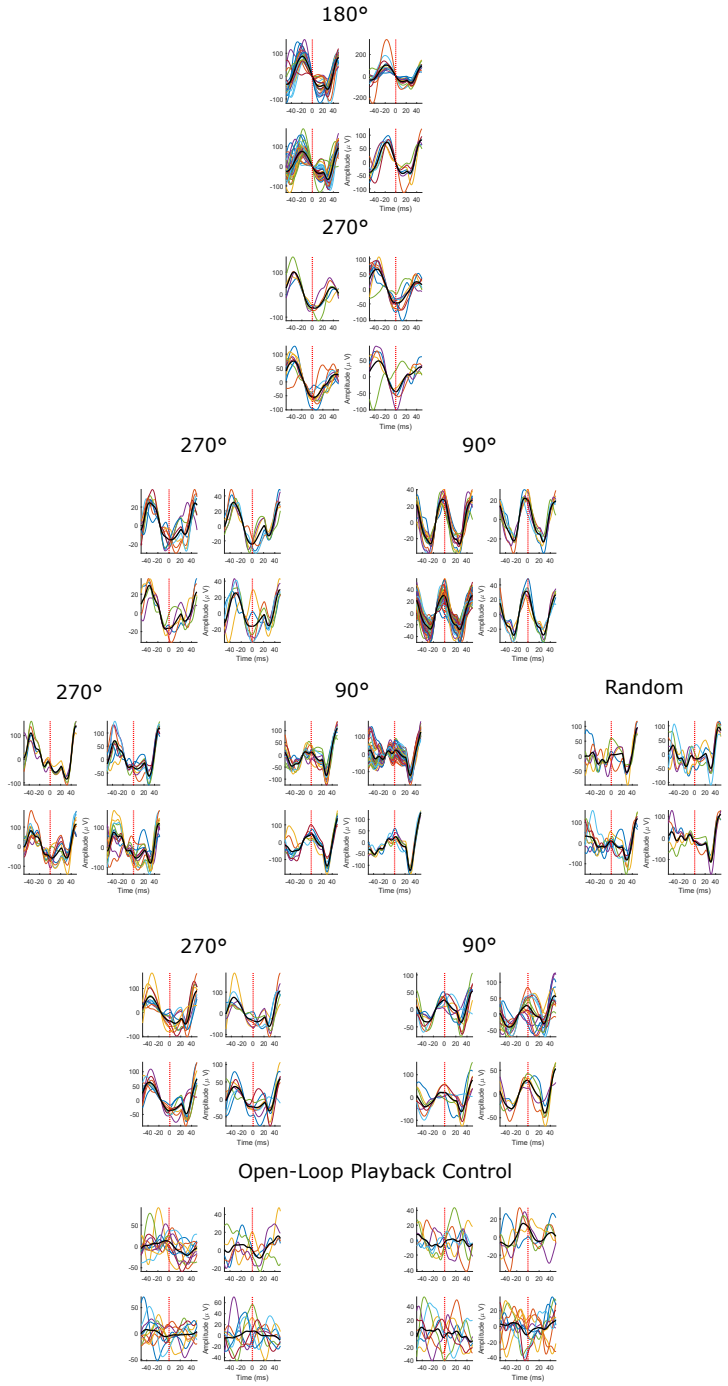

Figure E.10: Randomly selected real-time filtered conditioning trains. For each subject and condition where the beta-filtered channel was continuously recorded, we randomly sub-selected 4 beta bursts with greater than 5 conditioning stimuli delivered to assess the degree of retriggering in our experiment. Time 0, as well as the red line, indicates the time of stimulus delivery. Individual colored lines indicate trials within a beta-burst, while the thicker black line indicates the average waveform at the time.

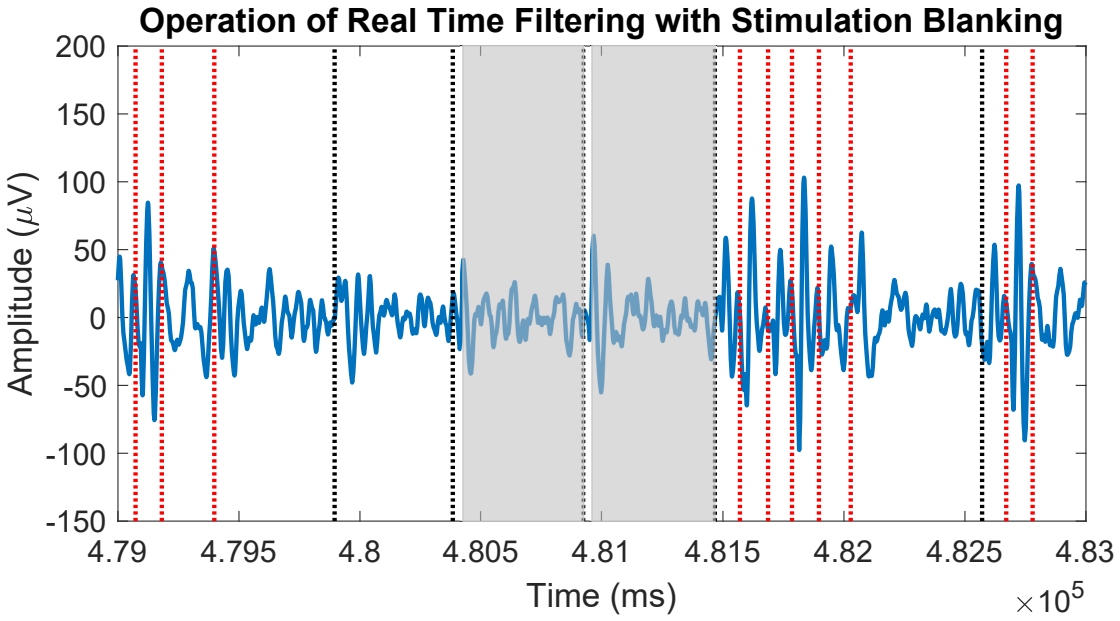

Figure E.11: Example of real time beta filtering, stimulation, and blanking. The red lines indicate time of delivery for the conditioning pulses, and the black lines indicate test pulses. Test pulses that were $\leq$500 ms after the end of a beta burst were considered probe pulses for that beta burst condition, and pulses greater than 2 seconds away from the end of a beta burst were baseline pulses. The shaded regions represent the null condition, where the beta RMS was exceeded, but no stimuli were delivered

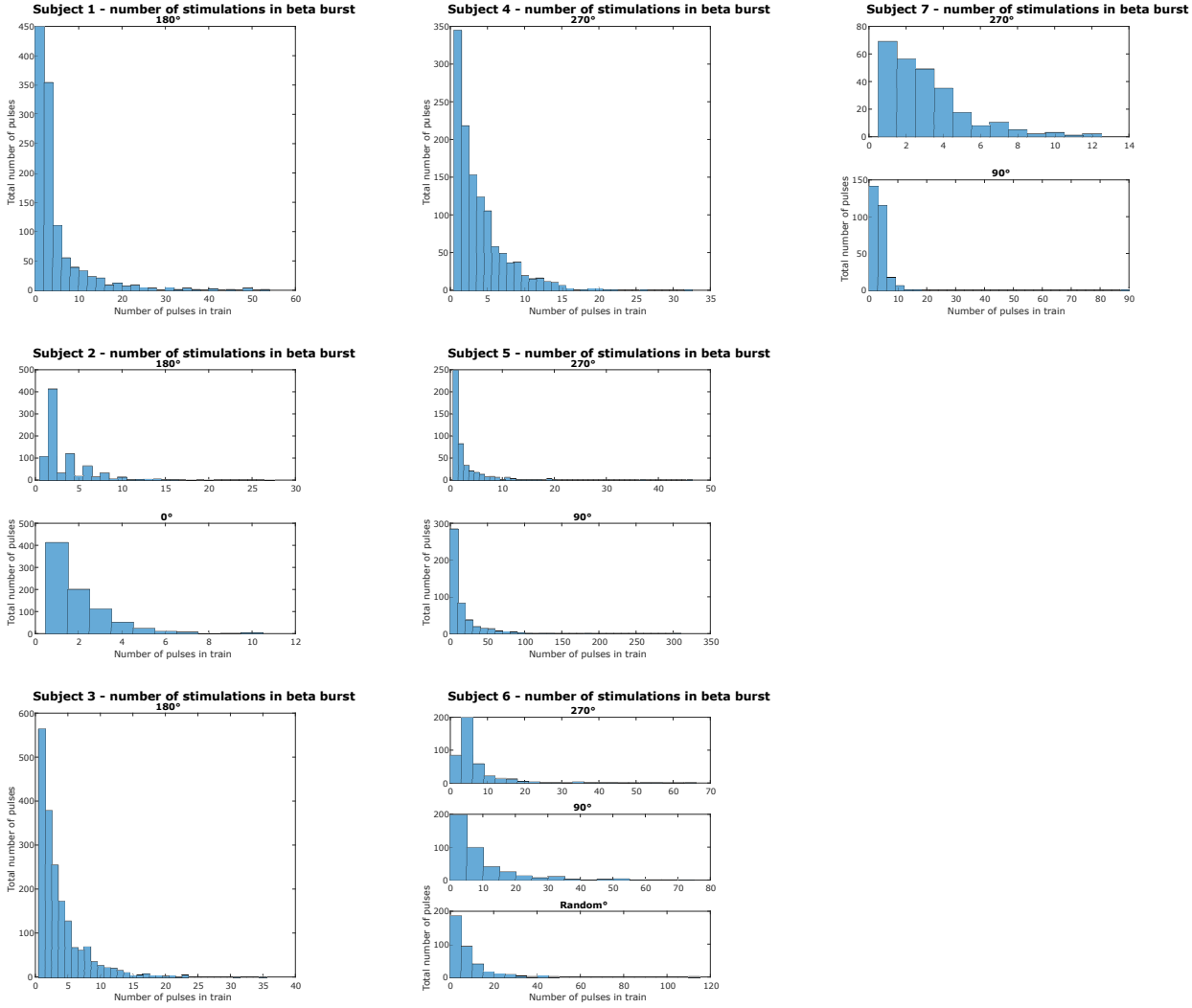

Figure E.12: Histogram of the number of conditioning stimuli delivered in a given beta burst across stimulation conditions and subjects. Subjects that had more than one test condition were subdivided by conditioning paradigm used.

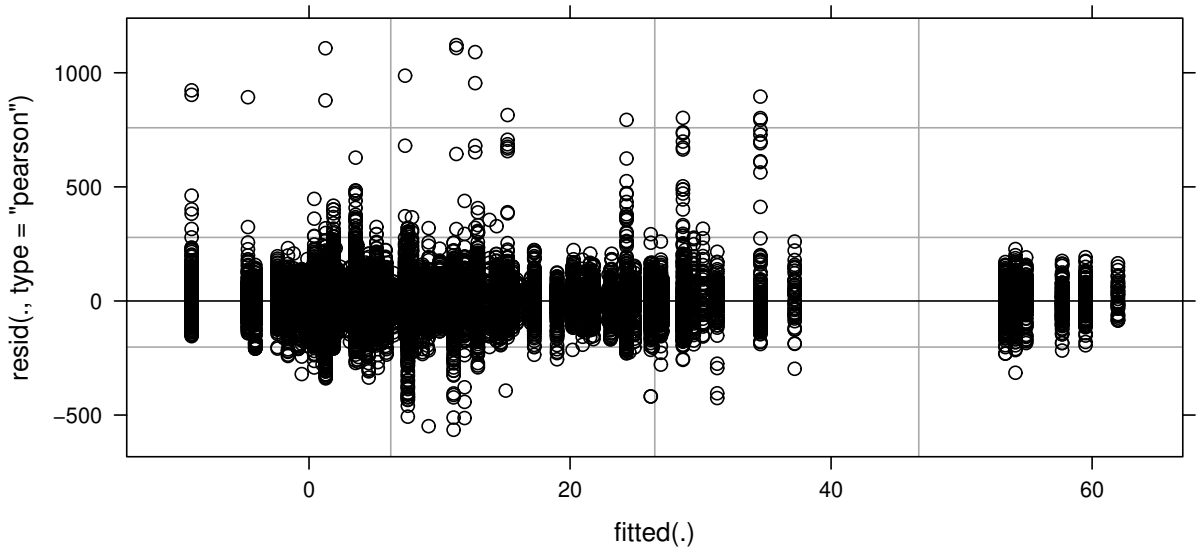

Figure E.13: Across subject linear mixed model residual plot. Plot of the residuals for the linear mixed model for all of the subjects.

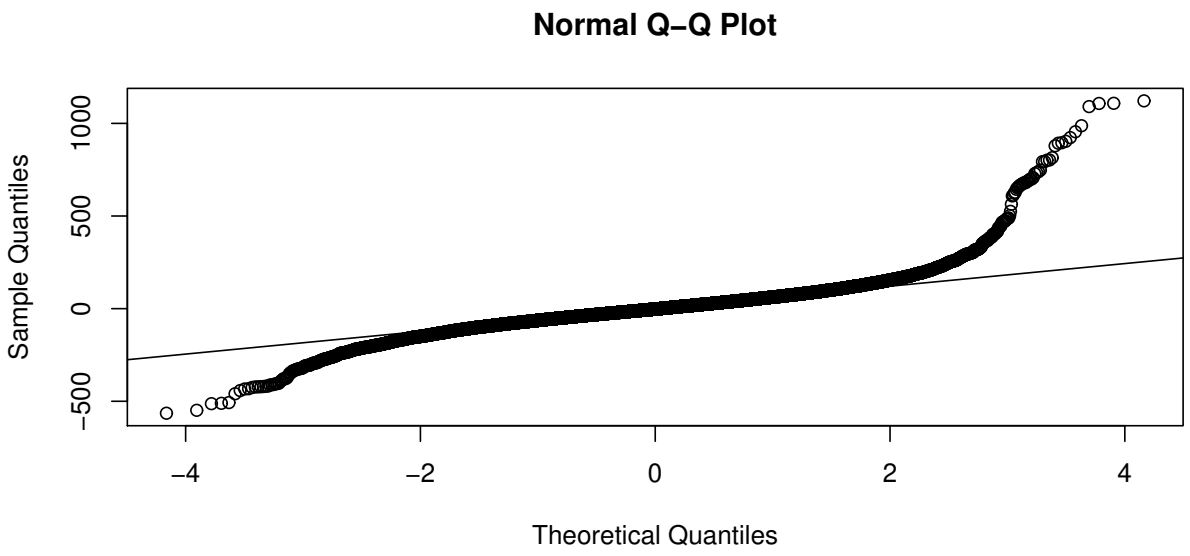

Figure E.14: Quantile-quantile/normality plot. Quantile-quantile (QQ)/normality plot illustrating the theoretical quartiles and sample quartiles for the data following the linear mixed model fit for all of the subjects.

Appendix F

PAIRED PULSE STIMULATION APPENDIX

Predictor	Numerator Df	Denominator DF	Sum Square Error	Mean Square Error	F Value	Pr(>F)
Stimulation Level	3	16532	40612918	13537639	792.87	$< 2.2e-16$
Condition	3	16534	1560763	520254	30.47	$< 2.2e-16$
Channel Location	1	16536	91354963	91354963	5350.47	$< 2.2e-16$
Disease	1	11	176	176	0.0103	0.921

Scaled Residuals				
Min	First Quartile	Median	Third Quartile	Max
-3.46	-0.53	-0.069	0.45	6.20

Predictor	Estimates	Confidence Interval	p-value
Stim Level Intercept	196.49	105.88 – 287.11	< 0.001
Stim Level - Linear	101.10	97.03 – 105.16	< 0.001
Stim Level - Quadratic	-8.37	-12.37 – -4.36	< 0.001
Stim Level - Cubic	0.52	-3.43 – 4.46	0.797
A/B 25	-21.18	-27.49 – -14.86	< 0.001
A/B 200	15.33	9.99 – 20.68	< 0.001
A/A 200	3.75	-4.05 – 11.54	0.346
Parkinson's	9.77	-178.81 – 193.38	0.921
Channel Location	199.90	194.54 – 205.25	< 0.001

Random Effects

σ^2	17074.20
τ_{00}	21332.62
ICC	0.56

Observations	16551
Marginal R^2 */ Conditional* R^2	0.204/0.646

contrast	estimate	SE	df	t.ratio	p.value
base - A/B 25	21.18	3.22	16534.43	6.58	$< .0001$
base - A/B 200	-15.33	2.73	16532.80	-5.62	$< .0001$
base - A/A 200	-3.75	3.98	16532.62	-0.94	0.782
A/B 25 - A/B 200	-36.51	3.83	16535.84	-9.53	$< .0001$
A/B 25 - A/A 200	-24.92	4.83	16534.48	-5.16	$< .0001$
A/B 200 - A/A 200	11.59	4.45	1652.45	2.60	0.046

Table F.1: Model fit for the effect of different conditioning paradigms across subjects. ANOVA results on the linear model fit. Following confirmation of statistically significant main effects, we proceeded to do post hoc testing for each of the individual stimulation levels and conditioning types. We did pairwise comparisons with a Tukey correction between the different estimated marginal means to demonstrate the significance of different conditioning paradigms. The Marginal R^2 represents the variance explained by the fixed effects, while the Conditional R^2 represents the variance explained by both the fixed and random effects. σ^2 represents the within-group variance, τ_{00} represents the deviance from the expected mean between the different groups, while ICC represents the intraclass correlation coefficient.

Predictor	Df	Sum Square Error	Mean Square Error	F Value	Pr(>F)
Stimulation Level	3	902626	300875	196.74	$< 2.2e-16$
Condition	2	428936	214468	140.17	$< 2.2e-16$
Residuals	818	1251583	1530		

Scaled Residuals				
Min	First Quartile	Median	Third Quartile	Max
-101.643	-27.249	-3.256	24.191	240.394

Predictor	Estimates	Confidence Interval	p-value
Stim Level Intercept	94.47	90.56 – 98.39	< 0.001
Stim Level - Linear	68.86	63.39 – 74.43	< 0.001
Stim Level - Quadratic	-10.47	-15.84 – -5.11	< 0.001
Stim Level - Cubic	1.62	-3.63 – 6.88	0.545
A/B 200 5 min	26.37	19.73 – 33.01	< 0.001
A/B 200 15 min	53.94	47.58 – 60.29	< 0.001

Observations 824
R^2/ *adjusted* R^2 0.515/0.513

Contrast	Estimate	SE	df	t.ratio	p.value
base - A/B 200 5 min	-15.26	3.67	818	-4.531	< 0.0001
base - A/B 200 15 min	-61.88	3.22	818	-19.19	< 0.0001
A/B 200 (5 min - 15 min)	-46.62	3.73	818	-12.509	< 0.0001

Table F.2: Model fit for the length of paired pulse conditioning. ANOVA results on the linear model fit. Following confirmation of statistically significant main effects, we proceeded to do post hoc testing for each of the individual stimulation levels and conditioning types. We did pairwise comparisons between the different estimated marginal means to demonstrate the significance of different conditioning paradigms

Predictor	Numerator Df	Denominator DF	Sum Square Error	Mean Square Error	F Value	Pr(>F)
Stimulation	3	2337	18910360	6303453	862.84	$< 2.2e-16$
Level Condition	1	2338	9568	9568	1.31	0.2526

Scaled Residuals				
Min	First Quartile	Median	Third Quartile	Max
-4.2344	-0.5650	-0.0938	0.4350	8.6339

Predictor	Estimates	Confidence Interval	p-value
Stim Level Intercept	246.78	170.80 – 314.76	0.086
Stim Level - Linear	178.31	171.39 – 185.23	< 0.001
Stim Level - Quadratic	-19.05	-25.98 – - 12.13	< 0.001
Stim Level - Cubic	11.31	4.38 – 8.23	0.545
Awake	5.01	-3.57 – 13.60	0.253

Random Effects

σ^2	7305.50
τ_{00}	2375.15
ICC	0.25
Observations	2344
Marginal R^2 */ Conditional* R^2	0.455/0.589

Table F.3: Model fit for the level of sedation effect on EP magnitude within one subject. ANOVA results on the linear model fit. The key result is that we fail to reject the null hypothesis that there is no statistically significant difference between the differing arousal states of the patient. The random effect for this subject was the particular channel analyzed, as there were two conditioning pairs which elicited EPs in this subject. The Marginal R^2 represents the variance explained by the fixed effects, while the Conditional R^2 represents the variance explained by both the fixed and random effects. σ^2 represents the within-group variance, τ_{00} represents the deviance from the expected mean between the different groups, while ICC represents the intraclass correlation coefficient.

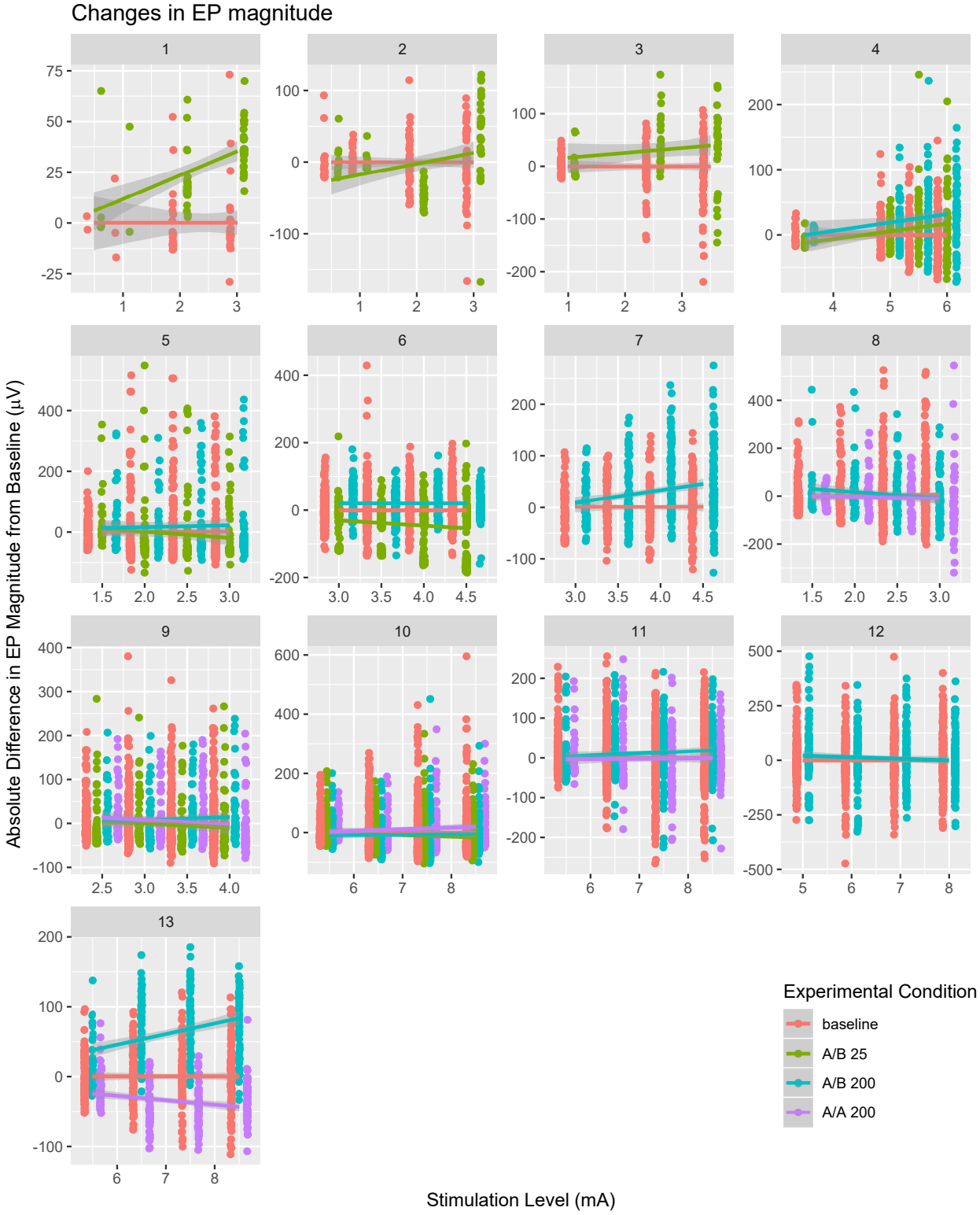

Figure F.1: Individual subject and channel peak-to-peak values for various stimulation amplitudes. The different colors indicate which experimental conditions are being considered (baseline, A/B 25, A/B 200, or A/A 200). The differences from baseline are computed from

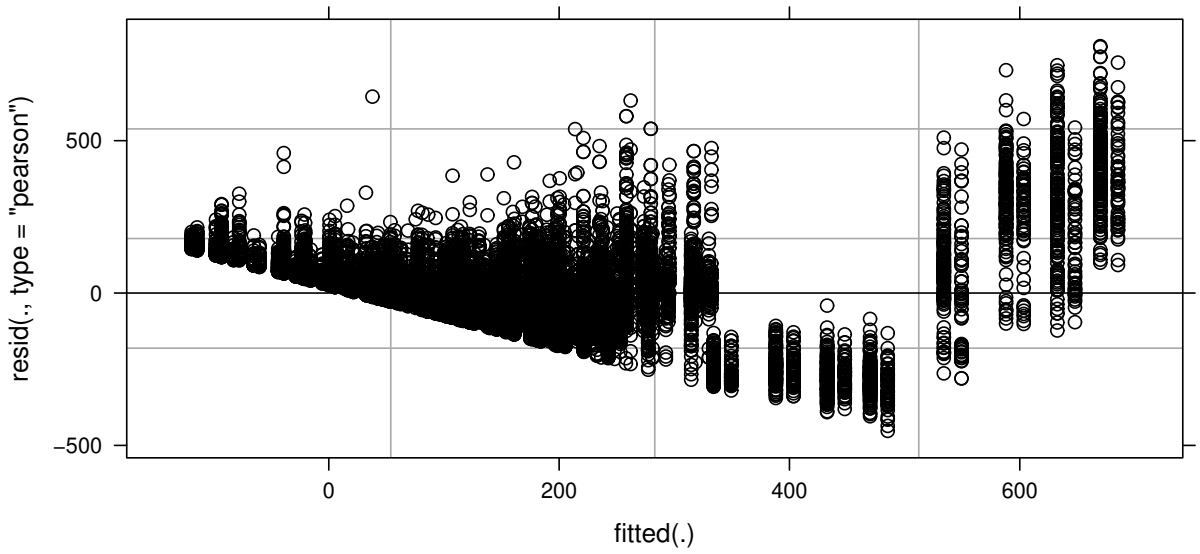

Figure F.2: Quantile-quantile plot for linear mixed model for all subjects. In order to assess the fit of our model, we visualized the quantile-quantile plot following our linear mixed model fit

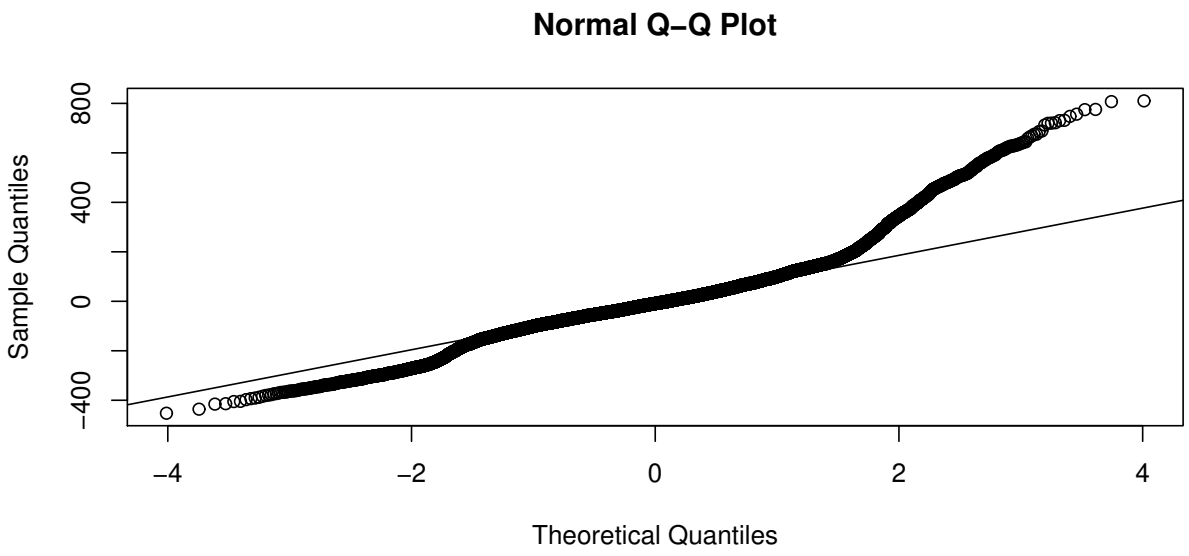

Figure F.3: Quantile-quantile plot for linear mixed model for all subjects. In order to assess the fit of our model, we visualized the quantile-quantile plot following our linear mixed model fit

F.1 Additional Publications and Presentations

F.1.1 Publications

Kogan M, Caldwell DJ, Hakimian S, Weaver KE, Ko AL, Ojemann JG, "Differentiation of Epileptic Regions from Voluntary High-Gamma Activation via Interictal Cross-Frequency Windowed Power-Power Correlation". Journal of Neurosurgery, 2019, May, 1–11. https://doi.org/10.3171/2

Caldwell DJ*, Wu J*, Casimo K, Ojemann JG, Rao RPN, "Interactive Web Application for Exploring Matrices of Brain Connectivity", Int. IEEE/EMBS Conf. Neural Eng. NER, pp. 42–45, 2017 , doi:10.1109/NER.2017.8008287, *These authors contributed equally

Wu J, Casimo K, Caldwell DJ, Rao RPN, Ojemann JG, "Electrocorticographic Dynamics Predict Visually Guided Motor Imagery of Grasp Shaping ",Int. IEEE/EMBS Conf. Neural Eng. NER, pp. 199-202, 2017, doi:10.1109/NER.2017.8008325